1990

# Circular Cylinder In Axial Flow

Stephen P. Sawchuk

# CIRCULAR CYLINDER IN AXIAL FLOW

by

Stephen P. Sawchuk

Department of Applied Mathematics

Submitted in partial fulfilment

of the requirements for the degree of

Doctor of Philosophy

Faculty of Graduate Studies

University of Western Ontario

London, Ontario

August 1990

ISBN 0-315-59114-5

## ABSTRACT

The boundary layer formed on the outer surface of a semi infinite circular cylinder in steady axial incompressible flow is studied in this thesis. Governing equations are solved using local similarity techniques and a nonsimilar numerical approach.

Two obvious similarity transformations can be used to obtain solutions for this problem, but they do not yield the same results, since the flow is essentially nonsimilar. In the extreme case that the radius of the cylinder is much larger than the boundary layer thickness, only one of the transformations leads to the correct solution, i.e., the Blasius solution. The other transformation yields an axial velocity profile which is deceptively close to the Blasius. This is also strongly suggested by comparing the series expansions of axial velocity profiles from each transformation. Solutions obtained by using either transformation merge at downstream locations.

Since the use of a single similarity variable does not solve the problem in its full range, an overall numerical solution is obtained by applying Keller's Box method with primitive variables and similarity coordinates. Similarity coordinates scale the axial and radial coordinates such that boundary layer growth does not appear explicitly as we move downstream. Thus, the numerical mesh does not need to be enlarged and this leads to increased efficiency in computation. Results are obtained in the range that start with the Blasius solution and proceed far downstream.

A local similarity method, which is very efficient, using primitive variables with similarity coordinates is also applied to obtain solutions that are valid over a wide range of the flow.

Results obtained by these methods compare well with previously obtained analytical and numerical solutions, but they extend considerably the range of solution.

## ACKNOWLEDGEMENTS

I am deeply indebted to Dr. M. Zamir who has guided me through this major task. The kindness and support that was given is very much appreciated and will always be remembered. Many thanks to Dr. P. J. Sullivan who generously allowed me access to his office and computer. I also thank Dr. R. W. Derksen and Dr. S. E. Camilletti for enlightening conversations on this topic.

TABLE OF CONTENTS

LIST OF TABLES

## LIST OF FIGURES

## LIST OF APPENDICES

## NOMENCLATURE

$a$ - cylinder radius

$Ei(-x) = \int_{-\infty}^{x} \frac{e^{-t}}{t} dt$ - exponential integral

$EI(-x) = \int_{-\infty}^{x} \frac{Ei(-t)}{t} dt$ - integral of exponential integral

$f_i$ - transformed stream function

$f(\eta_B)$ - Blasius stream function

$f(\eta_J, \xi)$ - two dimensional stream function

$f(\eta_C, \xi_C)$ - two dimensional stream function

$F(\eta)$ - transformed stream function

$G(\eta_1)$ - transformed stream function

$h_j$ - cross-stream coordinate step size

$H(s)$ - transformed stream function

$k_n$ - stream-wise step size

$L$ - characteristic length

$P = \frac{u^*}{U}$ - nondimensional axial velocity

$P^*$ - dimensional pressure

$Q = \frac{v^*}{U}$ - nondimensional radial velocity

$r^*$ - dimensional radial coordinate, measured from cylinder axis

$R = \frac{Ua}{\nu}$ - Reynolds number based on a

$R_c = \frac{Ua^2}{4\nu x^*}$ - stream-wise asymptotic expansion parameter

$R_L = \frac{UL}{\nu}$ - Reynolds number based on $L$

$s = \sqrt{\frac{U}{\nu x^*}} r^*$ - transformed similarity coordinate

$s_0 = \sqrt{\frac{U}{\nu x^*}} a$ - transformed stream-wise parameter

$s_1 = \sqrt{\frac{U}{\nu x^*}} y^*$ - transformed similarity coordinate

$s_i(\zeta)$ - transformed stream function of order i

$u^*$ - dimensional axial velocity

$U$ - mainstream velocity

$v^*$ - dimensional radial velocity

$x^*$ - dimensional axial coordinate

$y^* = r^* - a$ - dimensional radial coordinate, measured from cylinder surface

$\alpha_B = f''(0)$ - shooting parameter

$\alpha_F = F''(\eta_0)$ - shooting parameter

$\alpha_G = G''(0)$ - shooting parameter

$\alpha_H = H''(s_0)$ - shooting parameter

$\beta = \ln\left(\frac{4\nu x^*}{Ua^2}\right)$ - stream-wise asymptotic expansion parameter

$\gamma = .57721 = \ln c$ - Euler's constant

$\delta$ - boundary layer thickness

$\Delta = \frac{1}{a\sqrt{a}}\sqrt{\frac{U}{\nu x^*}}\int_a^{\infty}\left(1-\frac{u^*}{U}\right)r^* dr^*$ - displacement thickness

$\zeta = \frac{\frac{y^*}{a}\left(\frac{y^*}{a}+2\right)}{2\xi_x}$ - transformed cross-stream coordinate

$\eta = \sqrt{\frac{U}{2\nu x^*}}r^*$ - similarity coordinate based on $r$

$\eta_0 = \sqrt{\frac{Ua^2}{2\nu x^*}}$ - value of $\eta$ at $r = a$

$\eta_1 = \sqrt{\frac{U}{2\nu x^*}}y^*$ - similarity coordinate based on $y$

$\eta_\infty$ - value of $\eta$ at the boundary layer edge

$(\eta_1)_\infty$ - value of $\eta_1$ at boundary layer edge

$\eta_B = \sqrt{\frac{U}{2\nu x^*}}y^*$ - Blasius similarity coordinate

$\eta_C = \frac{\rho U}{2\sqrt{2\xi_C}}\frac{r^{*2}-a^2}{2a}$ - cross-stream coordinate

$\eta_J = \frac{r^{*2}-a^2}{a^2\xi}$ - cross-stream coordinate

$\eta_L = \sqrt{\frac{UL^2}{2\nu x^*}}$ - Blasius stream-wise parameter

$\eta_S = \frac{Ur^{*2}}{2\nu x^*}$ - transformed cross-stream coordinate

$\Theta = \frac{1}{a\sqrt{a}}\sqrt{\frac{U}{\nu x^*}}\int_a^{\infty}\frac{u^*}{U}\left(1-\frac{u^*}{U}\right)r^*dr^*$ - momentum thickness

$\Lambda = \sqrt{2}\eta$ - transformed similarity coordinate

$\mu$ - dynamic viscosity

$\nu$ - kinematic viscosity

$\tau = \mu\frac{\partial u^*}{\partial r^*}$ - shear stress

$\tau_0 = \mu\left(\frac{\partial u^*}{\partial r^*}\right)_{r^*=a}$ - skin-friction

$\psi$ - stream function

$X = \sqrt{2}F$ - transformed stream function

$\xi = \frac{4}{a}\sqrt{\frac{\nu x^*}{U}}$ - transformed stream-wise coordinate

$\xi_C = \rho\mu U x^*$ - stream-wise coordinate

$\xi_u = \frac{\xi}{2\sqrt{2}}$ - transformed stream-wise coordinate

$\xi_G = \frac{Ur^{*2}}{4\nu x}$ - transformed cross-stream coordinate

# 1 PRELIMINARY CONSIDERATIONS

## 1.1 INTRODUCTION

The boundary layer formed on the outer surface of a semi-infinite circular cylinder in steady laminar axial incompressible flow is studied in this thesis. The parameter $\lambda = \delta/a$, where $\delta$ is the boundary layer thickness and '$a$' the radius of the cylinder is important in describing this problem. When $\lambda$ is small the boundary layer thickness is small with respect to the radius of the cylinder. This shall be referred to as the Blasius limit of the problem because in this extreme the cylinder can be treated as a flat plate. When $\lambda$ is large the boundary layer thickness is large with respect to the radius of the cylinder. This shall be referred to as the needle limit because in this extreme the flow situation can be treated as that over a very thin needle or wire.

An overall exact solution of this problem in the full range of $\lambda$ does not exist at present, only parts of the solution have been obtained so far, with emphasis on skin friction, displacement and momentum thickness. Seban and Bond (1953) and Kelly (1954) constructed a second order series expansion about the Blasius limit. Glauert and Lighthill (1955) constructed an asymptotic expansion about the needle limit which was calculated to second order. Skin friction was obtained to third order due to the ingenuity of their method. Stewartson (1955) independently obtained an asymptotic expansion similar to that of Glauert and Lighthill (1955). An approximate full range solution was constructed by Glauert and Lighthill which bridged the series expansion of Seban and Bond (1953) and Kelly (1954) to their asymptotic expansion

by an approximate Pohlhausen expansion which covered the middle range of $\lambda$. The full range solution was an amalgamation of different solutions about different ranges of $\lambda$ and was only approximate. Sawchuk (1985) obtained a series expansion about the Blasius limit, similar to that of Seban and Bond (1953) and Kelly (1954), calculated to third order, but could be extended to higher orders. Jaffe and Okamura (1968), Cebeci (1970), and Cebeci and Smith (1974) obtained accurate solutions for a wide range of $\lambda$, to the point at which Glauert and Lighthill (1955) deemed their asymptotic solution to be accurate. This procedure was adequate for the skin-friction coefficient and for such integral quantities as the displacement thickness. However, the same point was not far enough in order to merge into the asymptotic solution as far as velocity profiles are concerned. Velocity profiles in these papers are not emphasized and often not shown. The values of the skin-friction coefficient obtained by the asymptotic solution are not accurate in the middle range of $\lambda$ because the difference that is tolerated between them and with the coefficients obtained by the numerical solutions is too large. Thus, in the middle range of $\lambda$ and beyond, an accurate solution does not exist. An extensive review of previous solutions and methods of solution is presented and some of the results are compared with those obtained by the methods in this thesis.

This thesis presents an exact full range solution using one method that starts at the Blasius limit and goes beyond the point that previous authors have gone in approaching the needle limit and, thus, merge more closely to the asymptotic solution. It will be referred to as the "overall" solution. The emphasis in this solution is on velocity profiles, since velocity profiles of the existing asymptotic solution are not accurate for a wide range of $\lambda$. The profiles obtained by this method will eventually merge with

merge with those of the asymptotic solution for very large $\lambda$, where the asynptotic velocities are more accurate. Because of the complexities of the governing equations, the required solution must necessarily be numerical. However, since a single similarity variable does not cover the entire range of the problem, careful analytical considerations must precede the solution. The method uses primitive variables and similarity coordinates which scale the boundary layer region and compensates for the growth of the boundary layer as one moves downstream towards the needle limit with little or no loss of accuracy. Previous solutions did not have these features.

'Quasi-similar' solutions are also presented, which attempt to cover the entire range of the problem, but are only valid for large $\lambda$. They are based on similarity methods and have led to the use of similarity coordinates in the "overall" solution. In fact, two transformations which lead to valid 'quasi-similar' solutions are shown to differ both numerically and analytically. These solutions in the middle range of $\lambda$ are questionable on physical grounds. In the Blasius limit, one transformation leads to a deceptive boundary layer solution and both numerical and analytical arguments show that it creates terms that are one order of magnitude larger than is expected.

Another method is presented which is very efficient numerically, but limited in the range of $\lambda$. It employs primitive variables and similarity coordinates, but has a local similarity constraint. The solutions obtained are quite accurate for large $\lambda$.

In summary, the "overall" solution which we present covers the entire range of the problem. It agrees well with the Blasius limit, the needle limit, and with previous solutions obtained in between. In principle, this solution could be taken as far as one wishes towards the needle limit. In contrast, the 'quasi-similar' or local similarity

solutions could be used only for large $\lambda$, where they are very accurate. Local similarity solutions yield more accurate velocity profiles than can be obtained by asymptotic solutions.

## 1.2 GOVERNING EQUATIONS

The boundary layer equations governing the laminar incompressible flow over a semi-infinite circular cylinder were first derived by Sowerby and Cooke (1953). They will be referred to as Cooke's equations and are given by :

$$u^*\frac{\partial u^*}{\partial x^*}+v^*\frac{\partial u^*}{\partial r^*}=\nu\left(\frac{\partial^2 u^*}{\partial r^{*2}}+\frac{1}{r^*}\frac{\partial u^*}{\partial r^*}\right), \tag{1.2.1}$$

$$\frac{\partial u^*}{\partial x^*}+\frac{\partial v^*}{\partial r^*}+\frac{v^*}{r^*}=0, \tag{1.2.2}$$

with $u^*=v^*=0$ at $r^*=a$ and $u\to U$ as $r^*\to\infty$,

where starred (*) quantities are dimensional. The equations are an approximation to the corresponding dimensional form of the Navier-Stokes equations,

$$u^*\frac{\partial u^*}{\partial x^*}+v^*\frac{\partial u^*}{\partial r}=\nu\left(\frac{1}{r^*}\frac{\partial(r^*\partial u^*/\partial r^*)}{\partial r^*}+\frac{\partial^2 u^*}{\partial x^{*2}}\right)-\frac{\partial P^*}{\partial x^*}, \tag{1.2.3}$$

$$u^*\frac{\partial v^*}{\partial x^*}+v^*\frac{\partial v^*}{\partial r^*}=\nu\left(\frac{1}{r^*}\frac{\partial(r^*\partial v^*/\partial r^*)}{\partial r^*}-\frac{v^*}{r^{*2}}+\frac{\partial^2 v^*}{\partial x^{*2}}\right)-\frac{\partial P^*}{\partial r^*}, \tag{1.2.4}$$

$$\frac{1}{r^*}\frac{\partial(r^*u^*)}{\partial x^*}+\frac{\partial v^*}{\partial r^*}+\frac{v^*}{r^*}=0, \tag{1.2.5}$$

and were derived by assuming that $r^*=O(\delta)$, where $\delta$ is the boundary layer thickness.

Since $r^* = a + y^*$, where y* is measured radially from the surface of the cylinder, then clearly $y^* = O(\delta)$. Hence, '$a$' must be at most $O(\delta)$. Along with the above assumptions of Cooke, we take x* and u* to be O(1).

Then, $\frac{\partial}{\partial r^*} \sim \frac{1}{\delta}$ and $\frac{\partial (r^* u^*)}{\partial x^*} \sim \delta$.

Applying this to the equation of continuity in the form :

$$\frac{\partial (r^* u^*)}{\partial x^*} + \frac{\partial (r^* v^*)}{\partial r^*} = 0,$$

while insisting all terms be of the same order gives :

$\frac{\partial (r^* v^*)}{\partial r^*} \sim \delta$, which in turn gives : $v^* \sim \delta$.

The individual terms on the left hand side of the momentum equation yield the relations :

$u^* \frac{\partial u^*}{\partial x^*} \sim 1$ and $v^* \frac{\partial u^*}{\partial r^*} \sim 1$.

The magnitude of the largest inertial term must match the highest ordered derivative viscous term. This gives the following relation :

$\frac{\nu}{r^*} \frac{\partial \left( r^* \frac{\partial u^*}{\partial r^*} \right)}{\partial r^*} \sim 1$. Thus, $\nu = O(\delta^2)$, since $\frac{1}{r^*} \frac{\partial \left( r^* \frac{\partial u^*}{\partial r^*} \right)}{\partial r^*} \sim \frac{1}{\delta^2}$, and $\nu \frac{\partial^2 u^*}{\partial x^{*2}} \sim \delta^2$.

The individual terms in the momentum equation in the radial direction behave as follows :

$u^* \frac{\partial v^*}{\partial x^*} \sim \delta$, $v^* \frac{\partial v^*}{\partial r^*} \sim \delta$, $\frac{\nu}{r^*} \frac{\partial \left( r^* \frac{\partial v^*}{\partial r^*} \right)}{\partial r^*} \sim \delta$, $\nu \frac{\partial^2 v^*}{\partial x^{*2}} \sim \delta^3$, and $\nu \frac{v^*}{r^{*2}} \sim \delta$.

Note, $\frac{\partial P^*}{\partial r^*}$ is at most $O(\delta)$, which asserts that the pressure gradient is negligible across the boundary layer. Applying Bernouli's equation with constant U gives rise to zero pressure gradient. Neglecting terms $O(\delta)$ and higher leaves the desired equations 1.1.1-2.

The nondimensional form of Cooke's equations is :

$$u\frac{\partial u}{\partial x}+v\frac{\partial u}{\partial r}=\frac{1}{R}\left(\frac{\partial^2 u}{\partial r^2}+\frac{1}{r}\frac{\partial u}{\partial r}\right), \tag{1.2.6}$$

$$\frac{\partial u}{\partial x}+\frac{\partial v}{\partial r}+\frac{v}{r}=0, \tag{1.2.7}$$

with $u=v=0$ at $r=1$ and $u\to 1$ as $r\to\infty$,

where $x=\frac{x^*}{a}$ and $r=\frac{r^*}{a}$ are the dimensionless axial and radial coordinates respectively, $u=\frac{u^*(r^*,x^*)}{U}$ and $v=\frac{v^*(r^*,x^*)}{U}$ are the corresponding velocity components, $R=\frac{Ua}{\nu}$, and U is the free stream velocity, ν is the kinematic viscosity and '$a$' is the radius of the cylinder (see Figure 1.2.1).

## 1.3 BACKGROUND

Seban and Bond (1953) and Kelly (1954) used a series expansion about the Blasius limit of the problem. A series expansion that is similar is derived by Sawchuk (1985) which has been extended one order with possible extension to all orders.

We introduce the parameter $\xi=4\sqrt{\nu x/Ua}$, which will also be useful in describing the problem.

When $\xi$ is small (or $\lambda$ is small), a series expansion using the parameter

$$\xi_x = \sqrt{\frac{2\nu x}{Ua}} = \frac{\xi}{2\sqrt{2}},$$

is taken about $\xi_x = 0$ for the stream function

$$\psi = \sum_{i=0}^{\infty} \xi_x^{i+1} s_i(\zeta), \tag{1.3.1}$$

where $\zeta = \frac{y(y+2)}{2\xi_x}$.

The corresponding velocity components are:

$$u = \sum_{i=0}^{\infty} \xi_x^i s_i' \text{ and } \sqrt{2xR}\, v = \sum_{i=0}^{\infty} \xi_x^{i+1} [\zeta s_i' - (i+1) s_i]. \tag{1.3.2}$$

Substituting into the governing equations and equating coefficients of like powers of $\xi_x$ to zero gives rise to the general kth order equation:

$$s_k''' + 2s_{k-1}'' + 4\zeta s_{k-1}''' + 4\zeta^2 s_{k-2}''' + 4\zeta s_{k-2}'' + \sum_{i=0}^{k} [(k+1-i) s_i'' s_{k-i} - (k-i) s_i' s_{k-i}']$$

$$+2\zeta \sum_{i=0}^{k-1} [(k-i) s_i'' s_{k-i-1} - (k-i-1) s_i' s_{k-i-1}'] = 0, \tag{1.3.3}$$

where the boundary conditions are

$$s_i'(0) = s(0) = 0, \lim_{\zeta \to \infty} s_o'(\zeta) = 1 \text{ and } \lim_{\zeta \to \infty} s_i'(\zeta) = 0,$$

where $i > 0$ in the latter and prime (') denotes differentiation with respect to $\zeta$. Terms with negative subscripts are taken to be zero.

The first equation to solve with k = 0 is :

$$s_0''' + s_0 s_0'' = 0, \tag{1.3.4}$$

i.e., the Blasius differential equation. All subsequent equations are linear and can be taken to any order desired. In this case, third order results were obtained for velocity, displacement thickness, and skin friction. A standard fourth order Runge-Kutta method with shooting was used to obtain the results.

The displacement thickness is given by:

$$\Delta = \sqrt{2}\left[\lim_{\zeta\to\infty}(\zeta - s_0(\zeta)) - \xi_{sr}s_1(\infty) - \xi_{sr}^2 s_2(\infty) - \xi_{sr}^3 s_3(\infty) + \ldots\right],$$

i.e.,

$$\Delta = \sqrt{2}[1.217 + .0358\xi_{sr} + .5943\xi_{sr}^2 - 1.639\xi_{sr}^3 + \ldots]. \tag{1.3.5}$$

The nondimensional skin friction is given by

$$\frac{a}{\mu U}\tau_0 = \left[\frac{\partial u}{\partial y}\right]_{y=0} = \sum_{i=0}^{\infty} \xi_{sr}^{i-1} s_i''(0)$$

which to third order is

$$\xi_{sr}\frac{a}{\mu U}\tau_0 = .4696 + .6943\xi_{sr} - .4643\xi_{sr}^2 + .8125\xi_{sr}^3. \tag{1.3.6}$$

The axial velocity and radial velocity parameter are plotted for $\xi = 2\sqrt{2}\,\xi_{sr} = .283$ in Figure 1.3.1 and the skin friction and displacement thickness are plotted in Figure 1.3.2. The solution begins to deteriorate at approximately $\xi = 0.1$.

When $\xi$ is large (or $\lambda$ is large) Glauert and Lighthill (1955) obtained an asymptotic solution using the stream function

$$\psi \sim \nu x^*\left[f_0(\xi_{sG}) + \frac{f_1(\xi_{sG})}{\beta} + \frac{f_2(\xi_{sG})}{\beta^2} + \ldots\right], \tag{1.3.7}$$

where

$$\xi_G \equiv \frac{Ur^{*2}}{4\nu x^*}, \quad \beta \equiv \ln\left(\frac{4\nu x^*}{Ua^2}\right). \tag{1.3.8}$$

Note that $\beta = \ln\left(\frac{\xi^2}{4}\right)$.

This series produces one nonlinear and n - 1 linear ordinary differential equations

$$\xi_G f_0''' + f_0'' + \frac{1}{2} f_0 f_0'' = 0, \tag{1.3.9}$$

$$\xi_G f_n''' + f_n'' + \frac{1}{2}\sum_{m=0}^{n} f_m f_{n-m}'' - \frac{1}{2}\sum_{m=1}^{n-1} m(f_m f_{n-m-1}'' - f_m' f_{n-m-1}') = 0. \tag{1.3.10}$$

after equating coefficients of like powers of beta. The axial and radial velocity components are respectively given by

$$u = \frac{1}{2}\left[f_0' + \frac{f_1'}{\beta} + \frac{f_2'}{\beta^2} + O(\beta^{-3})\right] \tag{1.3.11}$$

and

$$\sqrt{\frac{2\nu x^*}{U}}\frac{R}{a} v = \frac{1}{\sqrt{2\xi_G}}\left(\xi_G f'_0 - f_0 + \frac{\xi_G f'_1 - f_1}{\beta} + \frac{\xi_G f'_2 - f_2 + f_1}{\beta^2} + O(\beta^{-3})\ldots\right) \tag{1.3.12}$$

with the boundary conditions $f_n = 0$ at $\xi_G = e^{-\beta}$ for all n and each separate $f_n'$ satisfies

$$f_n' \sim a_n + b_n \ln(\xi_G) \text{ as } \xi_G \to 0, \tag{1.3.13}$$

where

$$b_0 = 0, \quad a_0 = 2, \quad b_1 = 2, \quad a_1 = 2\gamma, \quad b_2 = 2\gamma \text{ and } b_n = a_{n-1}, \text{ for } n = 1, 2, \ldots. \tag{1.3.14}$$

Glauert and Lighthill solve for the constants :

$$a_2 = b_3 = 2\gamma^2 - \frac{1}{2}\pi^2 - 4\ln 2, \tag{1.3.15}$$

They obtained the terms :

$$f_0 = 2\xi_G,\ f_0' = 2,\ f_0'' = 0,$$

$$f_1 = 2\xi_G Ei(-\xi_G) + 2e^{-\xi_G} - 2,\ f_1' = 2Ei(-\xi_G),\ f_1'' = 2\frac{e^{-\xi_G}}{\xi_G},$$

$$f_2' = \left(2e^{-\xi_G} + 4\ln\xi_G + 2 + 6\gamma - Ei(-\xi_G)\right)Ei(-\xi_G) - 4Ei(-2\xi_G) - 6EI(-\xi_G),$$

and

$$f_2'' = -2Ei(-\xi_G)\left[e^{-\xi_G} + \frac{e^{-\xi_G}}{\xi_G} + \frac{1}{\xi_G}\right] + 2\frac{e^{-\xi_G}}{\xi_G}\left(2\ln\xi_G + 1 + 3\gamma - e^{-\xi_G}\right). \tag{1.3.16}$$

In Appendix A we integrate $f_2'$ with respect to $\xi_G$ and obtain $f_2$ given by :

$$f_2 = \left[4\xi_G\ln\xi_G + (4+6\gamma)\xi_G - 4 - 4e^{-\xi_G} - \xi_G Ei(-\xi_G)\right]Ei(-\xi_G) + 4(1-\xi_G)Ei(-2\xi_G)$$

$$+\left(4\ln\xi_G + 4 + 6\gamma - 2e^{-\xi_G}\right)e^{-\xi_G} - 6\xi_G EI(-\xi_G) - 4\ln 2 - 2\gamma - 2. \tag{1.3.17}$$

The error in the axial velocity component is $O(1/\beta^3)$ away from the wall and $(\gamma^2 - 2\ln 2 - \pi^2/4)/\beta^2$ at the wall. Theoretically, the error at the wall should be eliminated by the next term in the series and it would have exactly the value quoted above but of opposite sign, since the velocity at the wall must be zero by the no-slip condition. Hence, the value of the velocity at the surface of the cylinder is actually the error as the results indicate. It is questionable as to how far reaching the effect this error has in the solution and at what point away from the surface does the smaller error apply.

We obtain the radial velocity component and estimate its error. Away from the wall the error estimate is $O(1/\beta^3)$. At the surface, the radial velocity should be zero due to the no-slip condition. However, it turns out to be zero with the error given by :

$$\sqrt{2}(2\gamma-1)\frac{e^{-\beta/2}}{\beta^2}, \text{ as } \beta\to\infty \text{ or as } \xi_G\to 0. \tag{1.3.18}$$

The error estimate above is the highest order neglected term in the expansion, i.e.,

$$\frac{R\xi}{2\sqrt{2}}\nu=\frac{1}{\sqrt{2\xi_G}}[\frac{2(1-\{1-\xi_G+O(\xi_G^2)\})}{\beta}+\frac{1}{\beta^2}(\{\ln\xi_G+\gamma-\xi_G$$

$$+\frac{\xi_G^2}{4}+O(\xi_G^3)\}\left(4+2\xi_G\left\{1-\xi_G+\frac{\xi_G^2}{2}+O(\xi_G^3)\right\}+4\right)-4\{\ln(2\xi_G)+\gamma-2\xi_G+\xi_G^2+O(\xi_G^3)\}$$

$$-(4\ln\xi_G+2+6\gamma)\left\{1-\xi_G+\frac{\xi_G^2}{2}+O(\xi_G^3)\right\}+2\{1-2\xi_G+2\xi_G^2+O(\xi_G^3)\}+4\ln 2+2\gamma)+O\left(\frac{1}{\beta^3}\right)]$$

$$\text{as } \xi_G\to 0, \tag{1.3.19}$$

which reduces to

$$\frac{R\xi}{2\sqrt{2}}\nu=\frac{1}{\sqrt{2\xi_G}}[\frac{2\xi_G-\xi_G^2+O(\xi_G^3)}{\beta}+\frac{1}{\beta^2}(2\xi_G\ln\xi_G+2(2\gamma-1)\xi_G-2\xi_G^2\ln\xi_G$$

$$+3(1-\gamma)\xi_G^2+O(\xi_G^3\ln\xi_G))+O\left(\frac{1}{\beta^3}\right)] \tag{1.3.20}$$

and at $\xi_G=e^{-\beta}$ gives :

$$\frac{R\xi}{2\sqrt{2}}\nu=\frac{e^{-3\beta/2}}{\sqrt{2}\beta}+\sqrt{2}(2\gamma-1)\frac{e^{-\beta/2}}{\beta^2}+\ldots, \tag{1.3.21}$$

the second of which is the leading error term. The error away from the surface is $O(1/\beta^3)$. Near the surface, as $\beta\to\infty$, the error estimate is $O(e^{-\beta/2}/\beta^2)$. If $f_3'(\xi_G)$ were available for the third order term in the expansion for $R\xi\nu/2\sqrt{2}$, then we expect the above error estimate to cancel at $\xi_G=e^{-\beta}$ with $\xi_G\ln\xi_G$ and $\xi_G$-terms that would exist in this third order term. This would yield $O(e^{-\beta}/\beta^3)$ as the error estimate at the

surface.

The skin friction is given by :

$$\tau_0 = \left[\frac{\mu U \xi_G}{a} \sum_{n=0}^{\infty} \frac{f''_n}{\beta^n}\right]_{\xi_G = e^{-\beta}} \sim \frac{\mu U}{a} \sum_{n=0}^{\infty} \frac{b_n}{\beta^n}.$$

$$\text{i.e., } \frac{a}{\mu U}\tau_0 \sim \frac{2}{\beta} + \frac{2\gamma}{\beta^2} + \frac{2\gamma^2 - \frac{1}{2}\pi^2 - 4\ln 2}{\beta^3} + O\left(\frac{1}{\beta^4}\right), \tag{1.3.22}$$

where $\xi_G f_n'' \sim b_n$, with an error of $O(e^{-\beta})$, since at $\xi_G = e^{-\beta}$,

$f_0'' = 0$ and $\xi_G f_0'' = 0$,

$$\xi_G f_1'' = 2\{1 - \xi_G + O(\xi_G^2)\} = 2\{1 - e^{-\beta} + O(e^{-2\beta})\},$$

$$\xi_G f_2'' = (2 + 6\gamma)\{1 - \xi_G + O(\xi_G^2)\} - 2\xi_G\{1 - \xi_G + O(\xi_G^2)\}\{\ln \xi_G + \gamma - \xi_G + O(\xi_G^2)\}$$

$$-2\{1 - 2\xi_G + O(\xi_G^2)\} - 2\{1 - \xi_G + O(\xi_G^2)\}\{\ln \xi_G + \gamma - \xi_G + O(\xi_G^2)\}$$

$$+4\{\ln \xi_G + \gamma - \xi_G + O(\xi_G^2)\} + 4\ln \xi_G\{1 - \xi_G + O(\xi_G^2)\} - 6\{\ln \xi_G + \gamma - \xi_G + O(\xi_G^2)\},$$

which reduces to :

$$\xi_G f_2'' = -4\xi_G \ln \xi_G + 6(1 - \gamma)\xi_G + O(\xi_G^2 \ln \xi_G) = 4\beta e^{-\beta} + 6(1 - \gamma)e^{-\beta} + \ldots. \tag{1.3.23}$$

Assembling the series for the shear stress yields :

$$\tau = \frac{\mu U}{a}\left[\left(f_0'' + \frac{f_1''}{\beta} + \frac{f_2''}{\beta^2} + O\left(\frac{1}{\beta^3}\right)\right)\right] \tag{1.3.24}$$

and at $\xi_G = e^{-\beta}$ gives:

$$\tau_0 = \frac{\mu U}{a}\left[\frac{2}{\beta}+\frac{2\gamma}{\beta^2}+\frac{2e^{-\beta}}{\beta}+\frac{6(1-\gamma)e^{-\beta}}{\beta^2}+O\left(\frac{1}{\beta^3}\right)\right]$$

$$= \frac{\mu U}{a}\left[\frac{2}{\beta}+\frac{2\gamma}{\beta^2}+\frac{2e^{-\beta}}{\beta} \text{ or } O\left(\frac{1}{\beta^3}\right)\right], \tag{1.3.25}$$

where the latter two terms are the error estimate, whichever is larger for the given value of $\beta$. One of the advantages of this asymptotic m ..d is the acquisition of the constant $b_3$, which gives the fourth term, i.e.,

$$\tau_0 = \frac{\mu U}{a}\left[\frac{2}{\beta}+\frac{2\gamma}{\beta^2}+\frac{2\gamma^2-\frac{\pi^2}{2}-4\ln 2}{\beta^3}+\frac{2e^{-\beta}}{\beta} \text{ or } O\left(\frac{1}{\beta^4}\right)\right], \tag{1.3.26}$$

and hence the new choice in error estimate.

It is expected that if $f_3''$ were available that the leading error term in,

$$\lim_{\xi_G \to e^{-\beta} \to 0} \xi_G f_3'' = b_3 \tag{1.3.27}$$

would be $O(e^{-\beta}/\beta^2)$, which would be due to a term containing $\xi_G \ln \xi_G$ and this is smaller than $O(e^{-\beta}/\beta)$, in the limit.

We calculate that for $\beta > 8.6$ or $\xi > 148$, the fourth order error term given in (1.3.26) becomes greater. Hence, some care must be taken for small values of $\beta$. The shear stress, uses the skin-friction expansion at the surface and thus, the corresponding error estimate. Away from the surface the error estimate is $O(1/\beta^3)$.

The displacement area is given by

$$\frac{\Delta'}{\pi a^2} = e^{\beta} \lim_{\xi_G \to -\infty}\left(\xi_G - \frac{1}{2}\sum_{n=0}^{\infty}\frac{f_n}{\beta^n}\right) = e^{\beta}\sum_{n=1}^{\infty}\frac{-\frac{1}{2}f_n(\infty)}{\beta^n} = e^{\beta}\left(\frac{1}{\beta}+\frac{1+\gamma+2\ln 2}{\beta^2}+\ldots\right), \tag{1.3.28}$$

with an error of $O(e^{\beta}/\beta^3)$.

To demonstrate, velocity profiles are displayed at various values of $\beta$ in Figures 1.3.3 and 1.3.4. Notice the negative values of u near the surface of the cylinder. Radial velocity parameters are plotted in Figures 1.3.5 and 1.3.6. Shear stress profiles are plotted in Figure 1.3.7 and tabulated in Table 1.3.1 respectively. One can see that the skin-friction parameter grows without bound for increasing $\beta, \lambda$ or $\xi$, while the shear stresses decay more rapidly away from the wall to the boundary layer edge.

The question of how far does the asymptotic solution apply is very important, i.e., when does it break down? The solution as it stands to second order (with a third order skin friction expression) seems to give reasonable results to a wide range of $\beta$. However, velocity profiles especially near the surface of the cylinder break down at lower values of $\beta$. In fact, negative axial velocities are still evident near the surface of the cylinder at values of $\beta \approx 12.42$ or $\xi \approx 1000$. The point downstream at which the velocity profiles are very inaccurate should be the tentative cut off for the region of validity for this solution. More terms could be added to the expansion in order to make the solution more accurate, however, this may or may not enhance the velocity profiles at smaller values of $\beta$. To obtain these extra terms would involve much numerical integration of various exponential integrals. This could prove to be very time consuming and even futile because some integrals arise which are asymptotically complicated.

The error estimates given in most cases are the highest order neglected terms in the asymptotic expansion. They do not represent the actual error because the coefficients of these terms are usually unknown. In the above expansions, some of the coefficients of the leading error terms for calculations about the surface of the cylinder have been obtained to get a better handle on the error. However, this still does not represent the

actual error. In the case of skin friction, two error estimates are given, i.e., each for a different range of $\beta$. Other solutions, which are not asymptotic, attempting to match with the asymptotic solution are only expected to approach the asymptotic values and not match them exactly. It is clear, however, that as $\beta \to \infty$, that the asymptotic solution becomes more accurate.

The above solutions do not cover the entire range of the problem. The range of the Pohlhausen solution in the paper by Glauert and Lighthill (1955) fills the gap between the region of validity of the series expansion and the asymptotic solution, but the solution itself is only approximate. As is demonstrated, the velocity profiles obtained by the asymptotic solution are not accurate near the surface of the cylinder. Also, the general accuracy of the solution is questionable, because the error estimates are vague.

Stewartson (1955) obtains essentially the same asymptotic series as Glauert and Lighthill (1955). Therefore, only some of the details of this asymptotic series to be used later for comparison purposes will be discussed.

The expression of the skin-friction coefficient obtained by Stewartson (1955) is given by :

$$\frac{\xi}{2\mu U}\frac{a}{}\tau_0 = 4R_c^{1/2}\Big[\frac{\{1/\eta_s - 1/2 + O(\eta_s)\}}{\ln(1/cR_c)} + \frac{\{-\ln(\eta_s c/2) + 3/2 + O(\eta_s)\}}{(\ln(1/cR_c))^2}$$

$$+\frac{\{-1/\eta_s(2\ln 2 + \pi^2/4) - 1/2(\ln(\eta_s c/2))^2 - \ln(\eta_s c/2) + O(1)\}}{(\ln(1/cR_c))^3} + \frac{\{D_4/\eta_s + O(\ln(\eta_s))\}}{(\ln(1/cR_c))^4}$$

$$+ \ \ldots \ + \frac{\{1/\eta_s + O(1)\}}{2R_c(\ln(1/cR_c))^2}\Big]_{(\eta_s = 2R_c)^2} \qquad (1.3.29)$$

where $\ln(1/cR_c) = -\ln R_c - \gamma$, $R_c = 4/\xi^2$, $\gamma$ is Euler's constant, and $\eta_S = 2R_c(r^*)^2$ is small, and the constant $D_4$ is undetermined.

Evaluating (1.3.29) at the surface of the cylinder, $\eta_S = 2R_c$, gives :[1]

$$\frac{\xi}{2}\frac{a}{\mu U}\tau_0 = 4R_c^{1/2}\left[\frac{1}{2R_c\ln(1/cR_c)} - \frac{\left(2ln2 + \frac{\pi^2}{4}\right)}{2R_c(\ln(1/cR_c))^3} + \frac{7}{2(\ln(1/cR_c))^2} + O\left(\frac{1}{R_c(\ln(1/cR_c))^4}\right)\right] \tag{1.3.30}$$

where we have obtained the order term and $\pi^2/4 + 2\ln 2 \approx 3.854$. The order term in (1.3.30) is of higher order than the third term in (1.3.30). The former is the leading term which is neglected from the series and will be used as the error estimate in the asymptotic expansion.

The numerical accuracy in expansion 1.3.30 is vague because the error estimate which should demonstrate the accuracy in the series is only the order of the leading neglected term. Hence, the margin of error in the series could be significantly effected, especially for larger values of $R_c$ or smaller values of $\xi$. This uncertainty in the accuracy necessitates obtaining a more accurate solution, at least to the point at which the uncertainty in accuracy is appropriately reduced, i.e., for large values of $\xi$.

---

1 There appears to be a typographical error in the paper by Stewartson (1955) in the third term in (1.3.30). We assume the correct version is as presented above.

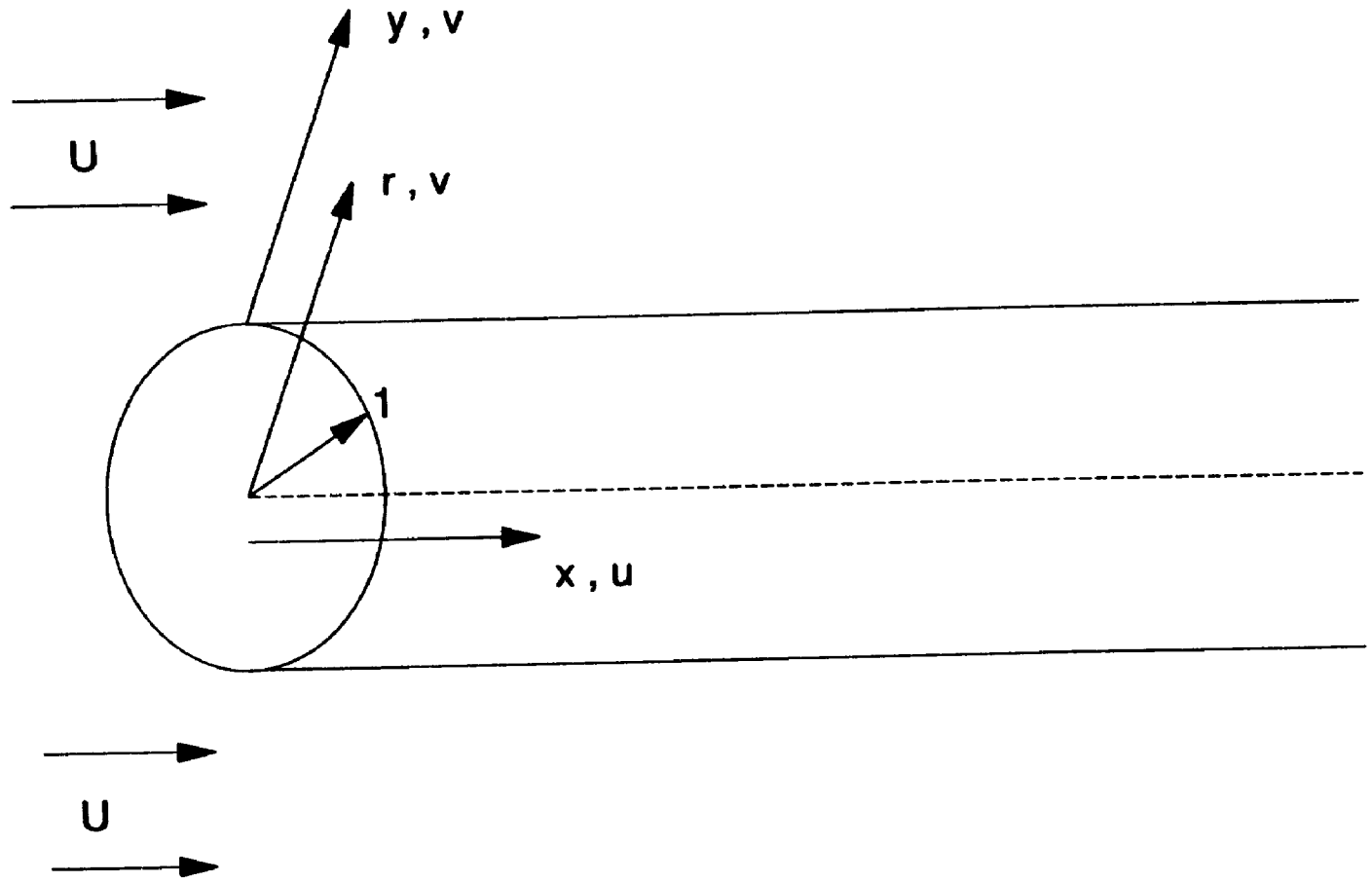


Figure 1.2.1 Basic Configuration of Circular Cylinder
In Axial Incompressible Flow.

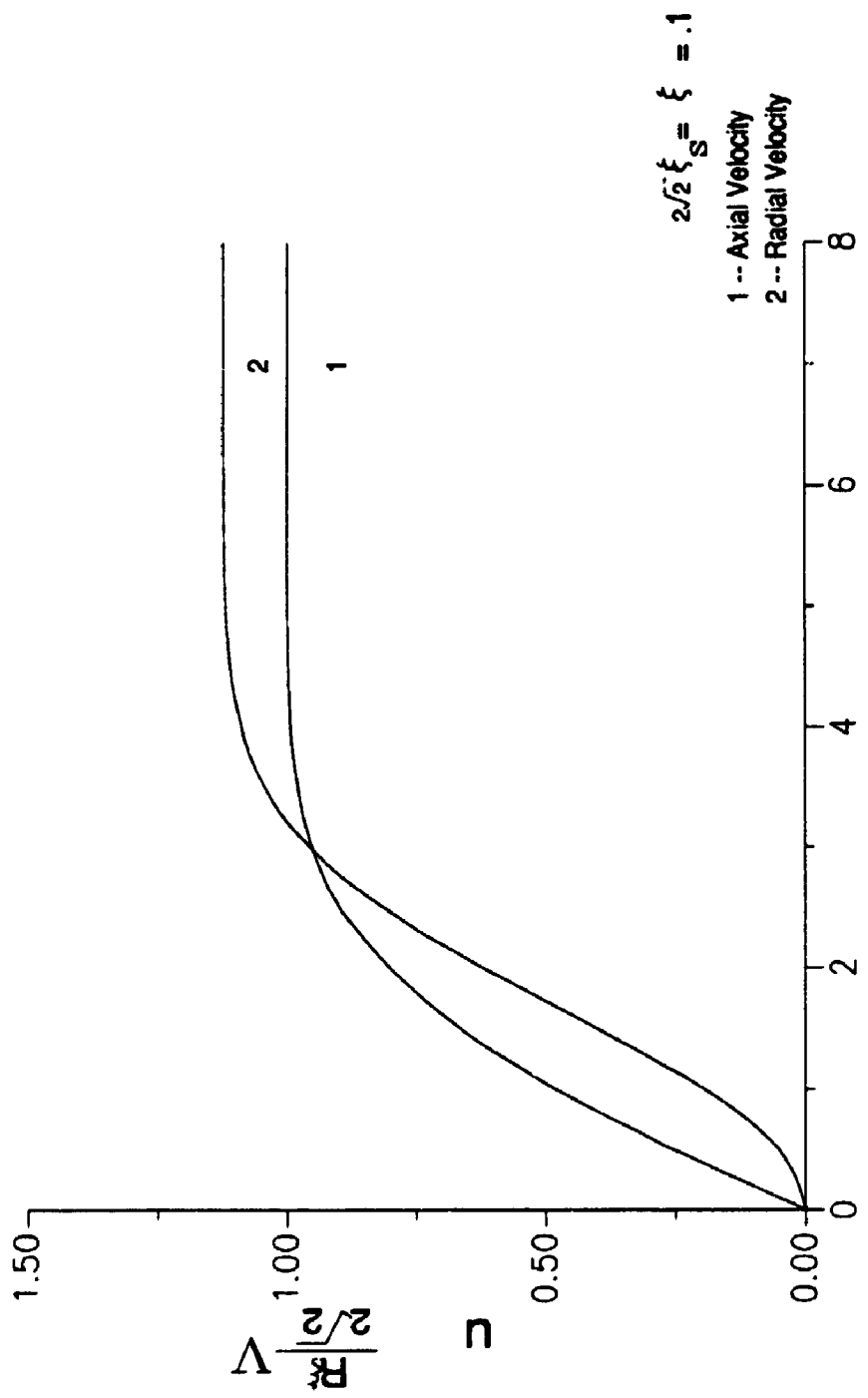


Figure 1.3.1 Axial and Radial Velocity Profiles From Series Expansion

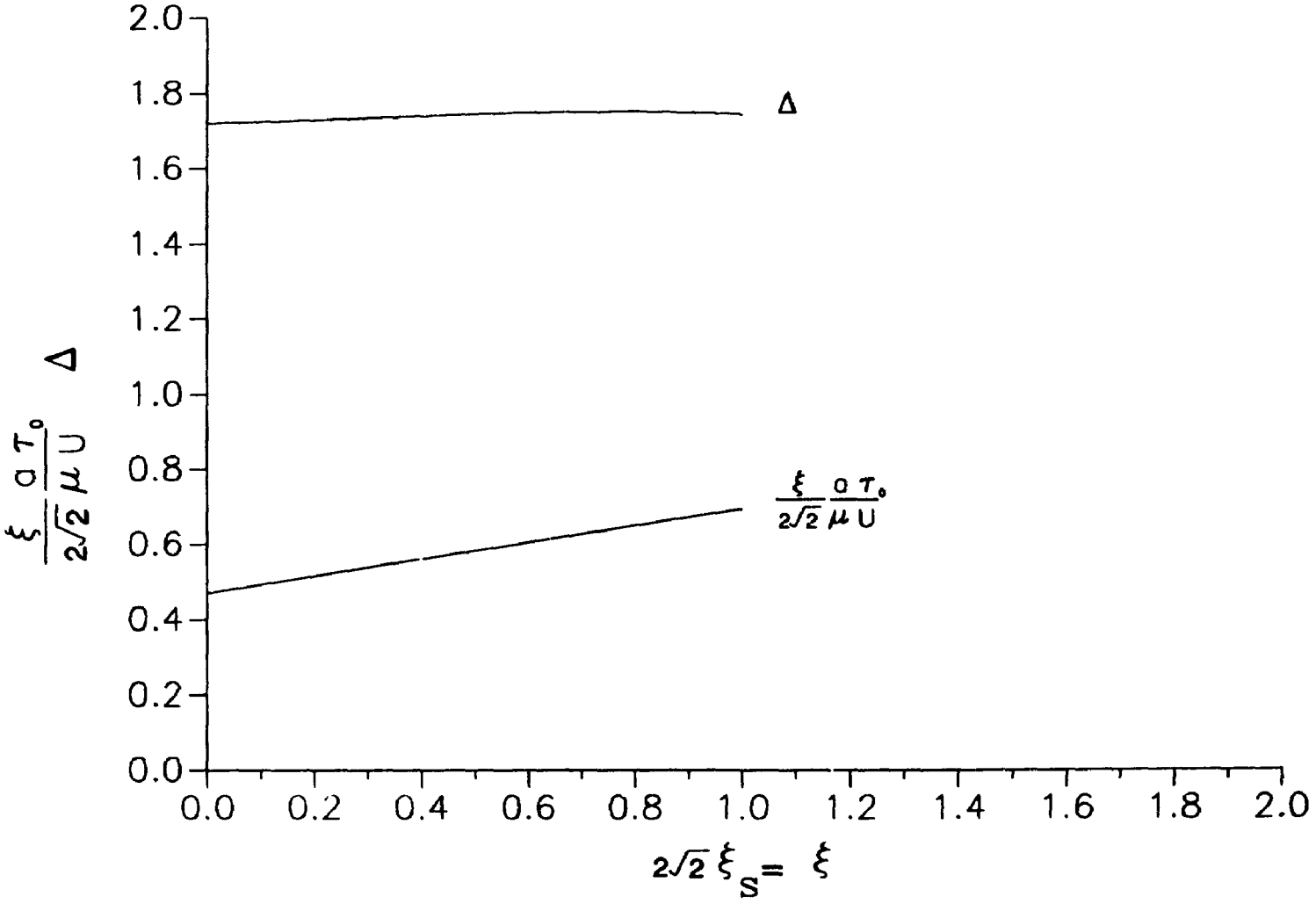


Figure 1.3.2 Skin-Friction Parameter and Displacement Thickness From Series Expansion.

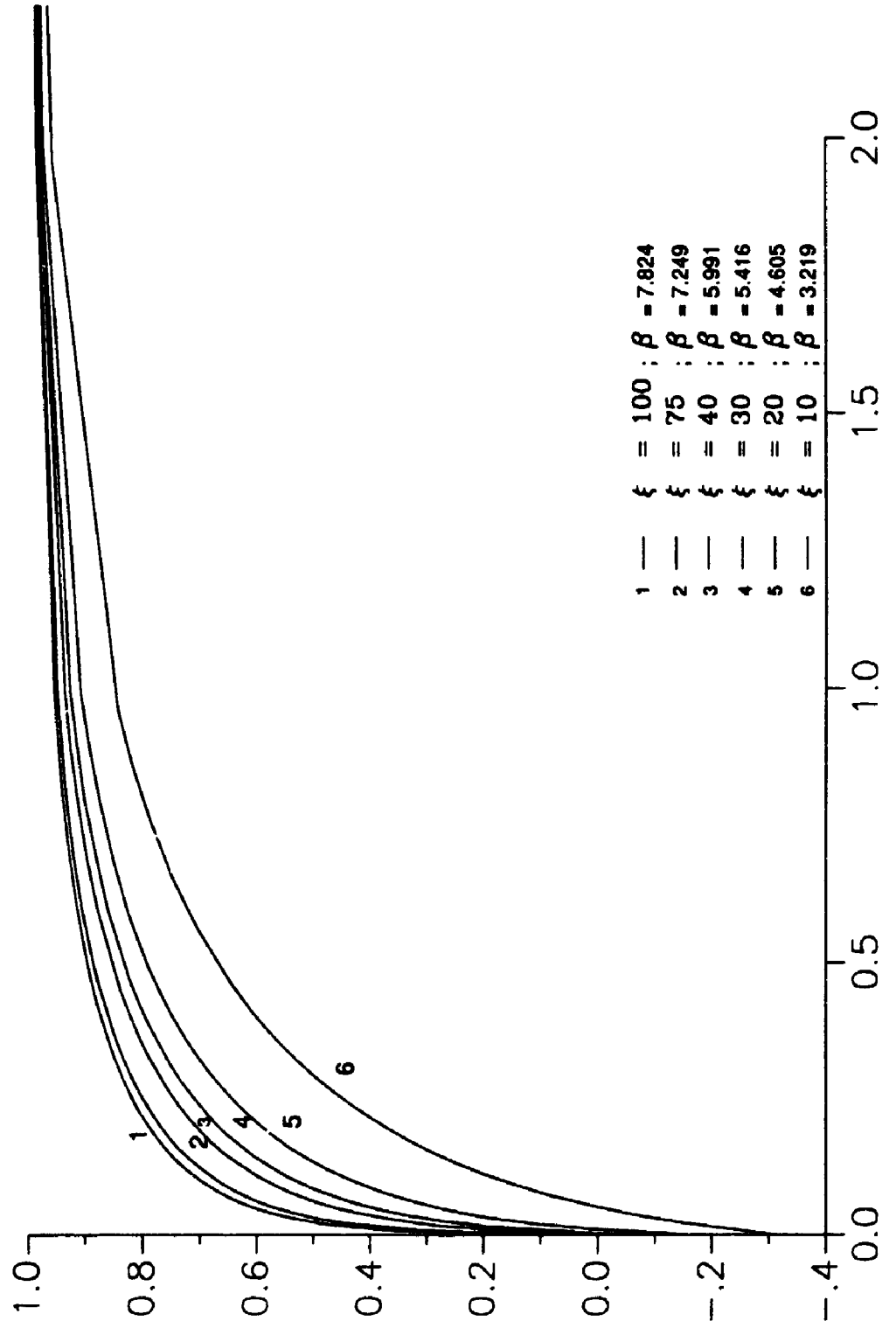


**Figure 1.3.3 Axial Velocity Profile From Asymptotic Solution.**

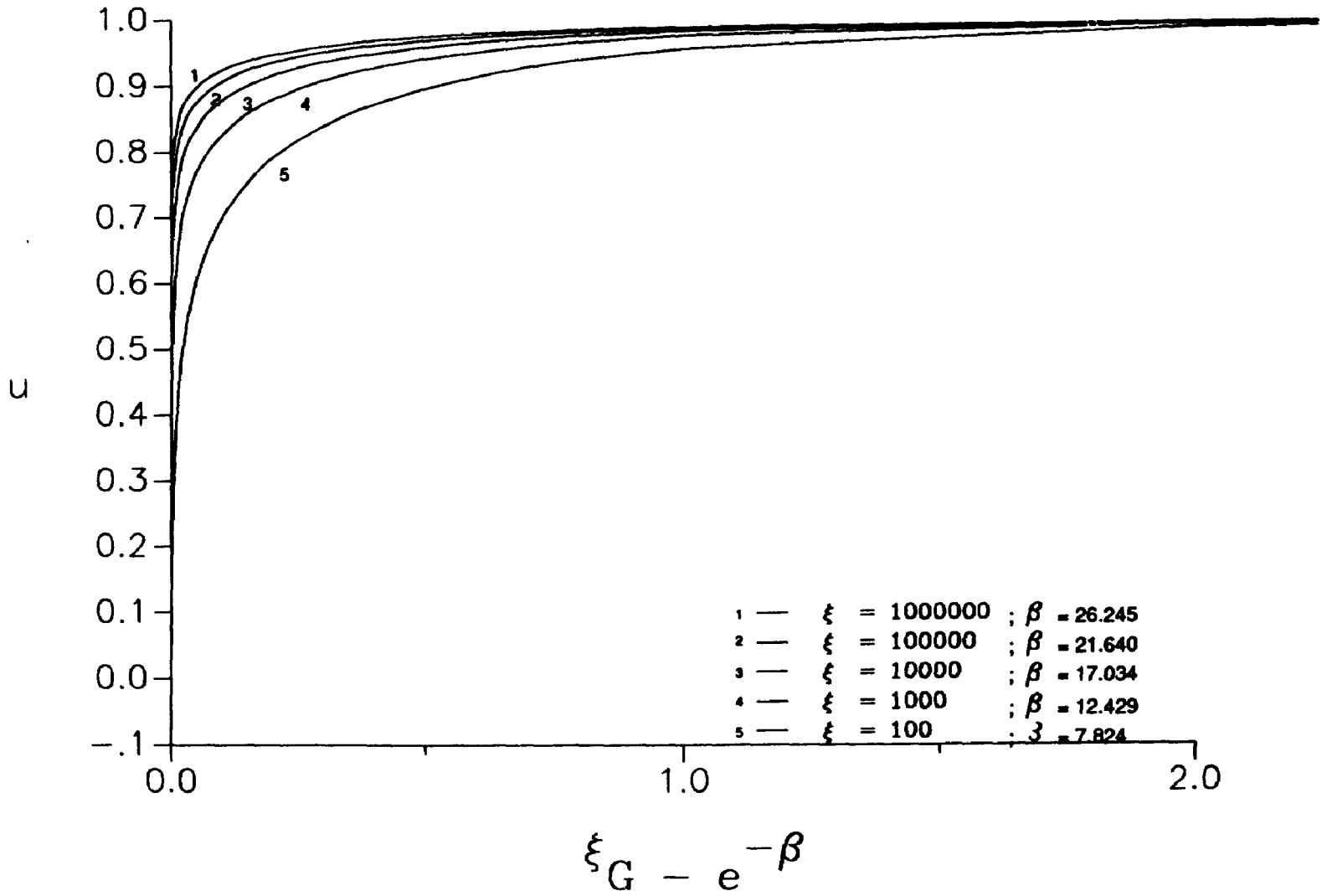


**Figure 1.3.4** Axial Velocity Profile From Asymptotic Solution.

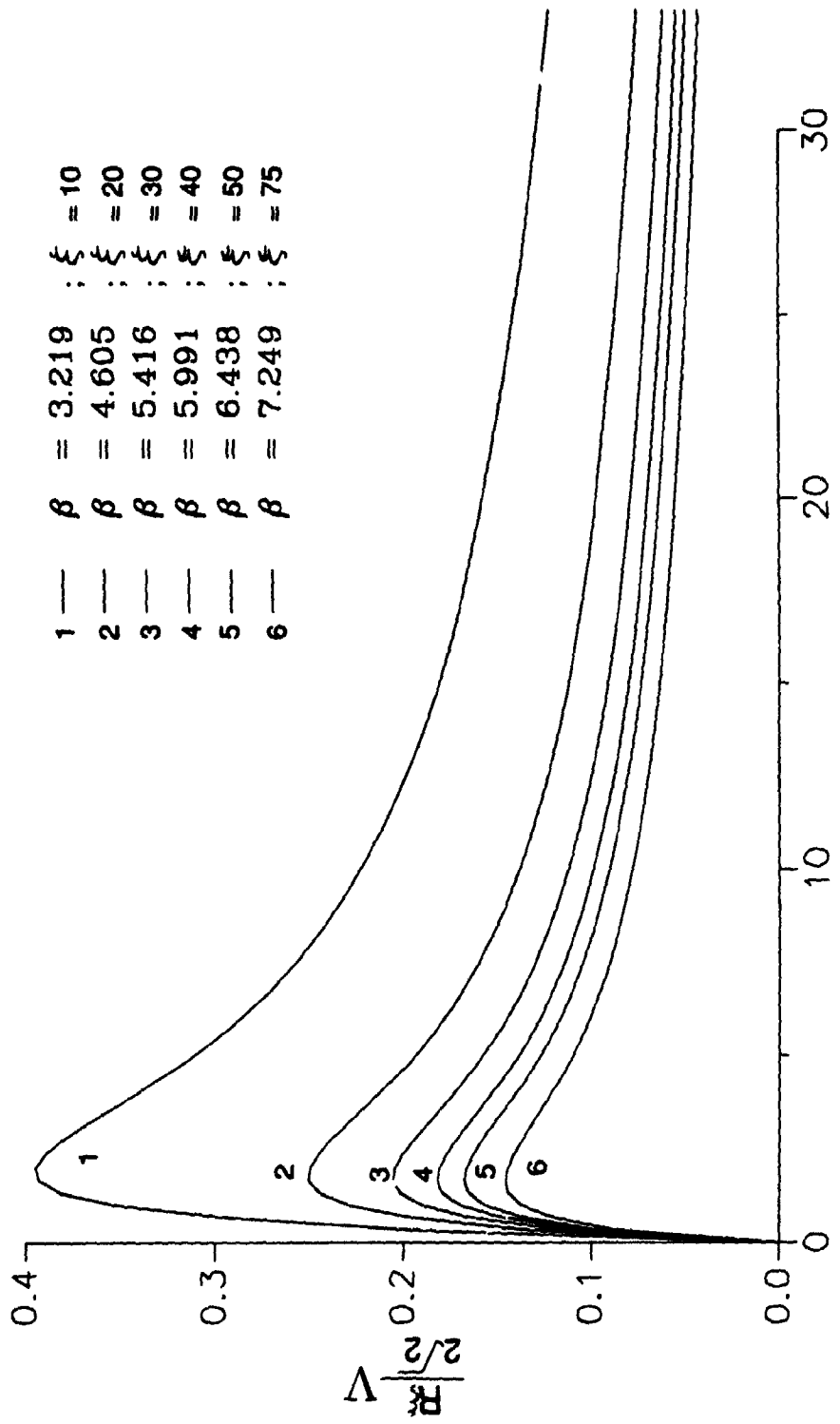


Figure 1.3.5 Radial Velocity Parameter Profile From Asymptotic Solution.

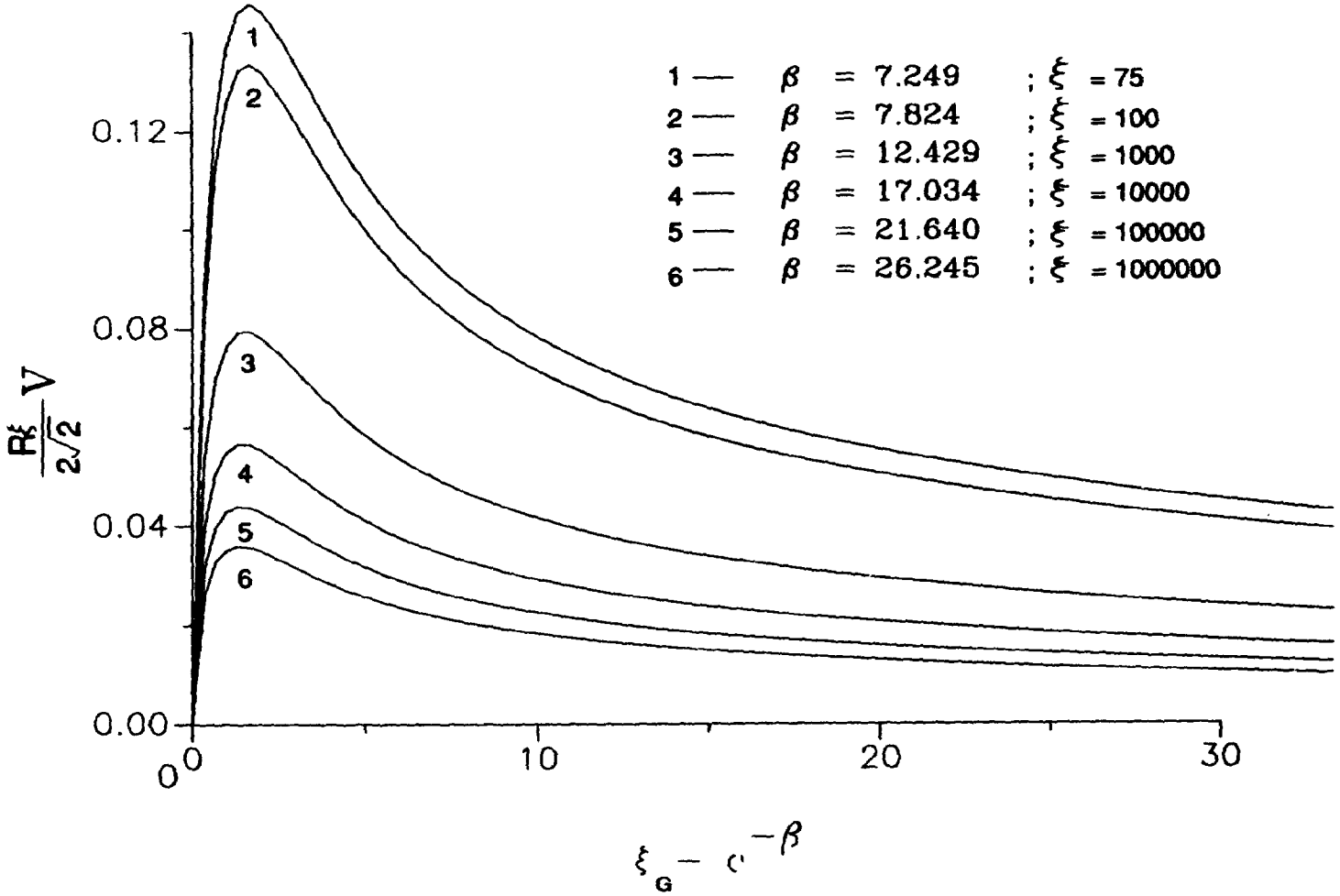


Figure 1.3.6 Radial Velocity Parameter Profile From Asymptotic Solution.

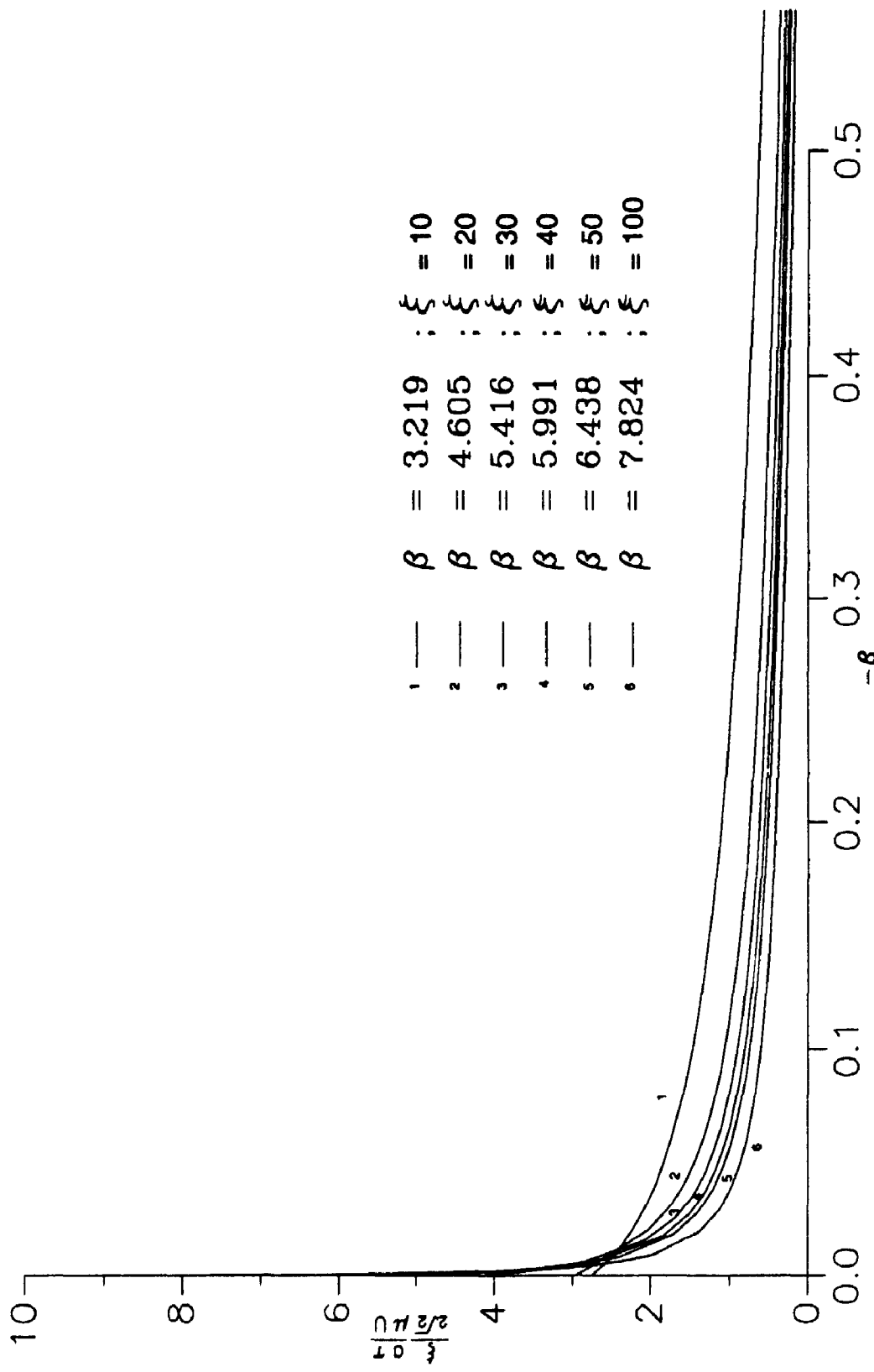


**Figure 1.3.7 Shear Stress Profile From Asymptotic Solution.**

Table 1.3.1 Shear Stress Profile From Asymptotic Solution.

| $\xi_G$ | $\beta$ = 12.429 | $\beta$ =17.034 | $\beta$ =21.639 | $\beta$ =26.245 |
|---|---|---|---|---|
| Surface | 58.2362 | 424.1351 | 3330.2535 | 27397.6727 |
| 0.001 | 3.7659 | 2.7140 | 2.1211 | 1.7407 |
| 0.002 | 2.6628 | 1.9185 | 1.4992 | 1.2302 |
| 0.003 | 2.1740 | 1.5660 | 1.2235 | 1.0039 |
| 0.004 | 1.8825 | 1.3557 | 1.0591 | 0.8689 |
| 0.005 | 1.6834 | 1.2120 | 0.9468 | 0.7767 |
| 0.006 | 1.5364 | 1.1060 | 0.8638 | 0.7086 |
| 0.007 | 1.4221 | 1.0235 | 0.7993 | 0.6556 |
| 0.008 | 1.3299 | 0.9569 | 0.7472 | 0.6129 |
| 0.009 | 1.2535 | 0.9018 | 0.7041 | 0.5774 |
| 0.010 | 1.1888 | 0.8551 | 0.6676 | 0.5474 |
| 0.050 | 0.5219 | 0.3733 | 0.2905 | 0.2377 |
| 0.100 | 0.3580 | 0.2548 | 0.1977 | 0.1614 |
| 0.200 | 0.2360 | 0.1667 | 0.1287 | 0.1048 |
| 0.300 | 0.1784 | 0.1253 | 0.0964 | 0.0783 |
| 0.400 | 0.1425 | 0.0996 | 0.0764 | 0.0620 |
| 0.500 | 0.1172 | 0.0816 | 0.0625 | 0.0506 |
| 1.000 | 0.0533 | 0.0366 | 0.0278 | 0.0223 |
| 2.000 | 0.0148 | 0.0100 | 0.0075 | 0.0060 |
| 3.000 | 0.0046 | 0.0031 | 0.0023 | 0.0018 |
| 4.000 | 0.0015 | 0.0010 | 0.0007 | 0.0006 |
| 5.000 | 0.0005 | 0.0003 | 0.0002 | 0.0002 |
| 10.000 | 0.0000 | 0.0000 | 0.0000 | 0.0000 |
| 50.000 | 0.0000 | 0.0000 | 0.0000 | 0.0000 |

# 2 SIMILARITY SOLUTIONS

## 2.1 PRELIMINARY

There are two obvious similarity transformations which may be applied to governing equations 1.2.6 and 1.2.7, and which we consider in details in this chapter. Unexpectedly, each transformation yields results that differ with each other. The extreme case of $\lambda = 0$ or $\xi = 0$, i.e, the Blasius limit is studied and the solutions from each transformation can be analytically shown to differ. One transformation yields the Blasius solution, while the other produces a deceptive solution.

If Cooke's equations 1.2.1 and 1.2.2 are written as

$$u^*(x^*,r^*)\frac{\partial u^*(x^*,r^*)}{\partial x^*}+v^*(x^*,r^*)\frac{\partial u^*(x^*,r^*)}{\partial r^*}=\nu\left(\frac{\partial^2 u^*(x^*,r^*)}{\partial r^{*2}}+\frac{1}{r^*}\frac{\partial u^*(x^*,r^*)}{\partial r^*}\right) \tag{2.1.1}$$

$$\frac{\partial u^*(x^*,r^*)}{\partial x^*}+\frac{\partial v^*(x^*,r^*)}{\partial r^*}+\frac{v^*(x^*,r^*)}{r^*}=0, \tag{2.1.2}$$

it may be expected that as $a \to \infty$ the two dimensional boundary layer equations of Prandtl can be obtained. This limit corresponds to the case $\xi = 0$ or $\lambda = 0$. In this limit $r^* \to \infty$, which hastily implies that

$$\frac{1}{r^*}\frac{\partial u^*}{\partial r^*} \to 0 \text{ and } \frac{v^*}{r^*} \to 0,$$

and leave the two dimensional boundary layer equations. However, since u*, v*, and their derivatives depend on r*, it is not clear that this limiting process does actually yield the two dimensional boundary layer equations.

On the other hand, if we now consider u = u(x,y) and v = v(x,y), Cooke's equations would read

$$u(x,y)\frac{\partial u(x,y)}{\partial x}+v(x,y)\frac{\partial u(x,y)}{\partial y}=\frac{1}{R}\left(\frac{\partial^2 u(x,y)}{\partial y^2}+\frac{1}{1+y}\frac{\partial u(x,y)}{\partial y}\right), \tag{2.1.3}$$

$$\frac{\partial u(x,y)}{\partial x}+\frac{\partial v(x,y)}{\partial y}+\frac{v(x,y)}{1+y}=0, \tag{2.1.4}$$

where

$$\frac{\partial}{\partial r}=\frac{\partial}{\partial y}. \tag{2.1.3}$$

The behavior of each individual term is still ambiguous in the limit '$a$' $\rightarrow \infty$ because of the dependence of y upon '$a$'. Therefore, it is important to analyze the behavior of the velocity components and their derivatives more closely to see how they behave in the limit as $a \rightarrow \infty$.

Introducing the nondimensional stream function

$$\psi(x,r)=\frac{\psi^*(x^*,r^*)}{Ua^2} \tag{2.1.5}$$

such that

$$u=\frac{1}{r}\frac{\partial \psi}{\partial r} \text{ and } v=-\frac{1}{r}\frac{\partial \psi}{\partial x}. \tag{2.1.6}$$

Cooke's equations 1.2.6 and 1.2.7 take the form

$$(1+y)\left(\frac{\partial\psi}{\partial y}\frac{\partial^2\psi}{\partial x\partial y}-\frac{\partial\psi}{\partial x}\frac{\partial^2\psi}{\partial y^2}\right)+\frac{\partial\psi}{\partial x}\frac{\partial\psi}{\partial y}=\frac{(1+y)^2}{R}\frac{\partial}{\partial y}\left(\frac{1}{(1+y)}\frac{\partial}{\partial y}\left((1+y)\frac{\partial\psi}{\partial y}\right)\right) \qquad (2.1.7)$$

We now use these equations to examine closely the two types of transformations and their results.

## 2.2 SIMILARITY BASED ON r

One transformation, based on the radial coordinate r, hereafter referred to as the r-based transformation, is :

$$\psi(x,r)=\frac{\eta}{\eta_0^{\,2}}F(\eta), \qquad (2.2.1)$$

where

$$\eta=\eta_0 r\,,\ \eta_0=\sqrt{\frac{Ua}{2\nu x}},\ \frac{1}{2x}=\frac{\eta_0^{\,2}}{R},\ \text{and clearly } \psi\equiv\psi(\eta,\eta_0). \qquad (2.2.2)$$

The velocity components are :

$$u=\frac{F(\eta)}{\eta}+F'(\eta)\ \text{ and }\ v=\frac{\eta_0}{R}(\eta F'(\eta)-F(\eta)). \qquad (2.2.3)$$

Clearly, $u=u(\eta)$ and $v=v(\eta,\eta_0)$ explicitly.

The individual terms in Cooke's equations 1.2.6-7 are given by

$$\frac{\partial u}{\partial x}=-\frac{\eta_0^{\,2}\eta}{R}\left\{F''+\frac{F'}{\eta}-\frac{F}{\eta^2}\right\}, \qquad (2.2.4)$$

$$u\frac{\partial u}{\partial x}=-\frac{\eta_0^2}{R}\left\{\eta F^{I}F^{II}+F^{I}F^{I}+FF^{II}-\frac{FF}{\eta^2}\right\}, \tag{2.2.5}$$

$$v\frac{\partial u}{\partial r}=\frac{\eta_0^2}{R}\left\{\eta F^{I}F^{II}+F^{I}F^{I}-2\frac{FF^{I}}{\eta}-FF^{II}+\frac{FF}{\eta^2}\right\}, \tag{2.2.6}$$

$$\frac{1}{R}\frac{\partial^2 u}{\partial r^2}=\frac{\eta_0^2}{R}\left\{F^{III}+\frac{F^{II}}{\eta}-2\frac{F^{I}}{\eta^2}+2\frac{F}{\eta^3}\right\}, \tag{2.2.7}$$

$$\frac{\partial v}{\partial r}=\frac{\eta_0^2}{R}\eta F^{II}, \tag{2.2.8}$$

$$\frac{1}{rR}\frac{\partial u}{\partial r}=\frac{\eta_0^2}{R}\left\{\frac{F^{II}}{\eta}+\frac{F^{I}}{\eta^2}-\frac{F}{\eta^3}\right\}, \tag{2.2.9}$$

$$\frac{v}{r}=\frac{\eta_0^2}{R}\left\{F^{I}-\frac{F}{\eta}\right\}, \tag{2.2.10}$$

and the terms neglected due to boundary layer approximation from the nondimensional Navier-Stokes Equations, i.e.,

$$u\frac{\partial u}{\partial x}+v\frac{\partial u}{\partial r}=\frac{1}{R}\left(\frac{1}{r}\frac{\partial(r\partial u/\partial r)}{\partial r}+\frac{\partial^2 u}{\partial x^2}\right)-\frac{\partial P}{\partial x}, \tag{2.2.11}$$

$$u\frac{\partial v}{\partial x}+v\frac{\partial v}{\partial r}=\frac{1}{R}\left(\frac{1}{r}\frac{\partial(r\partial v/\partial r)}{\partial r}-\frac{v}{r^2}+\frac{\partial^2 v}{\partial x^2}\right)-\frac{\partial P}{\partial r}, \tag{2.2.12}$$

$$\frac{1}{r}\frac{\partial(ru)}{\partial x}+\frac{\partial v}{\partial r}+\frac{v}{r}=0, \tag{2.2.13}$$

are given by :

$$\frac{1}{R}\frac{\partial^2 u}{\partial x^2}=\frac{\eta_0^4}{R^3}\left\{\eta^2 F^{III}+4\eta F^{II}+F^{I}-\frac{F}{\eta}\right\}, \tag{2.2.14}$$

$$u\frac{\partial v}{\partial x}=\frac{\eta_0^3}{R^2}\left\{-\eta^2 F^{I}F^{II}-\eta F^{I}F^{I}-\eta F F^{II}+\frac{FF}{\eta}\right\}, \tag{2.2.15}$$

$$v\frac{\partial v}{\partial r}=\frac{\eta_0^3}{R^2}\eta F^{II}\{\eta F^{I}-F\}, \tag{2.2.16}$$

$$\frac{1}{R}\frac{\partial^2 v}{\partial x^2}=\frac{\eta_0^5}{R^4}\{\eta^3 F^{III}+6\eta^2 F^{II}+3\eta F^{I}-3F\}, \tag{2.2.17}$$

$$\frac{1}{R}\frac{\partial^2 v}{\partial r^2}=\frac{\eta_0^3}{R^2}\{\eta F^{III}+F^{II}\}, \tag{2.2.18}$$

$$\frac{v}{Rr^2}=\frac{\eta_0^3}{R^2}\frac{1}{\eta}\left\{F^{I}-\frac{F}{\eta}\right\}, \tag{2.2.19}$$

$$\frac{1}{Rr}\frac{\partial v}{\partial r}=\frac{\eta_0^3}{R^2}F^{II}, \tag{2.2.20}$$

where

$$\frac{\partial \eta}{\partial x}=-\frac{\eta}{2x},\ \frac{\partial^2 \eta}{\partial x^2}=\frac{3\eta}{4x^2},\ \frac{\partial \eta_0}{\partial x}=-\frac{\eta_0}{2x},\ \frac{\partial^2 \eta_0}{\partial x^2}=\frac{3\eta_0}{4x^2},$$

$$\frac{\partial \eta}{\partial r}=\eta_0,\ \frac{\partial^2 \eta}{\partial r^2}=0,\ \frac{\partial \eta_0}{\partial r}=0,\ \frac{\partial^2 \eta_0}{\partial r^2}=0. \tag{2.2.21}$$

Substitution of 2.2.1 into governing equations 1.1.6-7 gives, finally,

$$\eta^3 F''' + 2\eta^2 F'' - \eta F' + F - 2\eta FF + 2\eta^2 FF' + 2\eta^3 FF'' = 0, \tag{2.2.22}$$

At $\eta = \eta_0$ the no-slip boundary conditions give :

$$F(\eta_0) = F'(\eta_0) = 0 \text{ and } \frac{F(\eta)}{\eta} + F'(\eta) \to 1 \text{ as } \eta \to \infty. \tag{2.2.23}$$

The displacement thickness in terms of the r-based transformation is:

$$\Delta = \sqrt{\frac{U}{\nu x}} \int_1^\infty (1-u) r\,dr = \frac{\sqrt{2}}{\eta_0} \int_{\eta_0}^{\eta_\infty} \left(1 - \frac{F}{\eta} - F'\right) \eta\, d\eta. \tag{2.2.24}$$

$$\therefore \quad \Delta = \frac{\sqrt{2}}{\eta_0} \left( \frac{\eta_\infty^2 - \eta_0^2}{2} - \eta_\infty F(\eta_\infty) \right). \tag{2.2.25}$$

The momentum thickness in terms of the r-based transformation is:

$$\Theta = \sqrt{\frac{U}{\nu x}} \int_1^\infty u(1-u) r\,dr = \frac{\sqrt{2}}{\eta_0} \int_{\eta_0}^{\eta_\infty} \left(\frac{F}{\eta} + F'\right) \left(1 - \frac{F}{\eta} - F'\right) \eta\, d\eta. \tag{2.2.26}$$

$$\therefore \quad \Theta = \frac{\sqrt{2}}{\eta_0} \left( \eta_\infty F(\eta_\infty) - \frac{F^2(\eta_\infty)}{2} - \eta_\infty F(\eta_\infty) F'(\eta_\infty) - \int_{\eta_0}^{\eta_\infty} \frac{F^2}{\eta} d\eta + \int_{\eta_0}^{\eta_\infty} \eta F F'' d\eta \right). \tag{2.2.27}$$

The shear stress is given by:

$$\frac{1}{\eta_0} \frac{a}{\mu U} \tau = \frac{1}{\eta_0} \frac{\partial u}{\partial r} = \frac{\partial u}{\partial \eta} = F'' + \frac{F'}{\eta} - \frac{F}{\eta^2}, \tag{2.2.28}$$

while skin friction is the above evaluated at $\eta_0$, i.e.,

$$\frac{1}{\eta_0}\frac{a}{\mu U}\tau_0 = \frac{1}{\eta_0}\left(\frac{\partial u}{\partial r}\right)_{r=1} = \left(\frac{\partial u}{\partial \eta}\right)_{\eta=\eta_0} = F''(\eta_0) \tag{2.2.29}$$

Recall that $F(\eta_0) = F'(\eta_0) = 0$.

## 2.3 SIMILARITY BASED ON y

The other transformation based on y, hereafter referred to as the y-based transformation is

$$\psi(x,y) = \frac{\eta_1 + \eta_0}{\eta_0^2} G(\eta_1), \tag{2.3.1}$$

where

$$\eta_1 = \eta_0 y \text{ and } \eta = \eta_1 + \eta_0. \tag{2.3.2}$$

The velocity components are given by :

$$u = \frac{G(\eta_1)}{\eta_1 + \eta_0} + G'(\eta_1) \text{ and } v = \frac{\eta_0}{R}(\eta_1 G'(\eta_1) - G(\eta_1)) \tag{2.3.3}$$

Clearly, $u = u(\eta_1, \eta_0)$ and $v = v(\eta_1, \eta_0)$ explicitly.

The individual terms in Cooke's equations, 1.2.6-7, are given by

$$\frac{\partial u}{\partial x} = \frac{\eta_0^2}{R}\left\{-\eta_1 G'' - \frac{\eta_1}{(\eta_1+\eta_0)}G' + \frac{G}{(\eta_1+\eta_0)}\right\}, \tag{2.3.4}$$

$$u\frac{\partial u}{\partial x} = \frac{\eta_0^2}{R}\left\{-\eta_1 G'G'' - \frac{\eta_1}{(\eta_1+\eta_0)}G'G' - \frac{\eta_1}{(\eta_1+\eta_0)}GG'' + \frac{\eta_0}{(\eta_1+\eta_0)^2}GG' + \frac{GG}{(\eta_1+\eta_0)^2}\right\}, \tag{2.3.5}$$

$$\nu\frac{\partial u}{\partial y}=\frac{\eta_0^2}{R}\left\{\eta_1 G^I G^{II}+\frac{\eta_1}{(\eta_1+\eta_0)}G^I G^I-\frac{(2\eta_1+\eta_0)}{(\eta_1+\eta_0)^2}GG^I-GG^{II}+\frac{GG}{(\eta_1+\eta_0)^2}\right\},$$

(2.3.6)

$$\frac{1}{R}\frac{\partial^2 u}{\partial y^2}=\frac{\eta_0^2}{R}\left\{G^{III}+\frac{G^{II}}{(\eta_1+\eta_0)}-2\frac{G^I}{(\eta_1+\eta_0)^2}+2\frac{G}{(\eta_1+\eta_0)^3}\right\},\tag{2.3.7}$$

$$\frac{\partial v}{\partial y}=\frac{\eta_0^2}{R}\eta_1 G^{II},\tag{2.3.8}$$

$$\frac{v}{(1+y)}=\frac{\eta_0^2}{R(\eta_1+\eta_0)}\{\eta_1 G^I-G\},\tag{2.3.9}$$

and the terms neglected in the Navier-Stokes Equations, (2.2.11-13), are given by :

$$\frac{1}{R}\frac{\partial^2 u}{\partial x^2}=\frac{\eta_0^4}{R^3}\left\{\eta_1^2 G^{III}+\eta_1\frac{(4\eta_1+3\eta_0)}{(\eta_1+\eta_0)}G^{II}+\frac{\eta_1}{(\eta_1+\eta_0)}G^I-\frac{G}{(\eta_1+\eta_0)}\right\},$$

(2.3.10)

$$u\frac{\partial v}{\partial x}=\frac{\eta_0^3}{R^2}\left\{-\eta_1^2 G^I G^{II}-\eta_1 G^I G^I-\frac{\eta_1^2}{(\eta_1+\eta_0)}GG^{II}+\frac{GG}{(\eta_1+\eta_0)}+\frac{\eta_0}{(\eta_1+\eta_0)}GG^I\right\},$$

(2.3.11)

$$\nu\frac{\partial v}{\partial y}=\frac{\eta_0^3}{R^2}\eta_1 G^{II}\{\eta_1 G^I-G\},\tag{2.3.12}$$

$$\frac{1}{R}\frac{\partial^2 v}{\partial x^2}=\frac{\eta_0^5}{R^4}\{\eta_1^3 G^{III}+6\eta_1^2 G^{II}+3\eta_1 G^I-3G\},\tag{2.3.13}$$

$$\frac{1}{R}\frac{\partial^2 v}{\partial y^2}=\frac{\eta_0^3}{R^2}\{\eta_1 G^{III}+G^{II}\}, \tag{2.3.14}$$

$$\frac{1}{R(1+y)}\frac{\partial v}{\partial y}=\frac{\eta_0^3}{R^2}\frac{\eta_1}{(\eta_1+\eta_0)}G^{II}, \tag{2.3.15}$$

$$\frac{v}{R(1+y)^2}=\frac{\eta_0^3}{R^2(\eta_1+\eta_0)^2}\{\eta_1 G^{I}-G\}, \tag{2.3.16}$$

where

$$\frac{\partial \eta_1}{\partial x}=-\frac{\eta_1}{2x}, \frac{\partial^2 \eta_1}{\partial x^2}=\frac{3\eta_1}{4x^2},$$

$$\frac{\partial \eta_1}{\partial y}=\eta_0, \frac{\partial^2 \eta_1}{\partial y^2}=0, \frac{\partial \eta_0}{\partial y}=0, \text{ and } \frac{\partial^2 \eta_0}{\partial y^2}=0. \tag{2.3.17}$$

Substitution of transformation 2.3.1 into governing equations I.1.1-2 gives, finally, :

$$(\eta_1+\eta_0)^3 G^{III}+2(\eta_1+\eta_0)^2 G^{II}-(\eta_1+\eta_0)G^{I}+G-2(\eta_1+\eta_0)GG$$

$$+2\eta_1(\eta_1+\eta_0)GG^{I}+(2\eta_1+\eta_0)(\eta_1+\eta_0)^2 GG^{II}=0, \tag{2.3.18}$$

At $\eta_1=0$ the no-slip boundary conditions give :

$$G(0)=G^{I}(0)=0 \text{ and } \frac{G(\eta_1)}{\eta_1+\eta_0}+G^{I}(\eta_1)\to 1 \text{ as } \eta_1\to\infty. \tag{2.3.19}$$

The displacement thickness in terms of the y-based transformation is:

$$\Delta = \sqrt{\frac{U}{\nu x}} \int_0^{\infty} (1-u)(1+y)dy = \frac{\sqrt{2}}{\eta_0} \int_0^{\eta_{1\infty}} \left(1 - \frac{G}{\eta_1+\eta_0} - G'\right)(\eta_1+\eta_0)d\eta_1. \tag{2.3.20}$$

$$\therefore \quad \Delta = \frac{\sqrt{2}}{\eta_0}\left(\eta_{1\infty}\eta_0 + \frac{\eta_{1\infty}^2}{2} - (\eta_0+\eta_{1\infty})G(\eta_{1\infty})\right). \tag{2.3.21}$$

The momentum thickness in terms of the y-based transformation is:

$$\Theta = \sqrt{\frac{U}{\nu x}} \int_0^{\infty} u(1-u)(1+y)dy = \frac{\sqrt{2}}{\eta_0} \int_0^{\eta_{1\infty}} (G + (\eta_1+\eta_0)G' - \frac{G^2}{(\eta_1+\eta_0)} - 2GG'$$

$$-(\eta_1+\eta_0)G'G')d\eta_1. \tag{2.3.22}$$

$$\therefore \quad \Theta = \frac{\sqrt{2}}{\eta_0}((\eta_{1\infty}+\eta_0)G(\eta_{1\infty}) - \frac{G^2(\eta_{1\infty})}{2} - (\eta_{1\infty}+\eta_0)G(\eta_{1\infty})G'(\eta_{1\infty}) - \int_0^{\eta_{1\infty}} \frac{G^2}{\eta_1+\eta_0} d\eta_1$$

$$+ \int_0^{\eta_{1\infty}} (\eta_1+\eta_0)GG''d\eta_1). \tag{2.3.23}$$

The shear stress is given by:

$$\frac{1}{\eta_0}\frac{a}{\mu U}\tau = \frac{1}{\eta_0}\frac{\partial u}{\partial y} = \frac{\partial u}{\partial \eta_1} = G'' + \frac{G'}{\eta_1+\eta_0} - \frac{G}{(\eta_1+\eta_0)^2}, \tag{2.3.24}$$

while skin friction is the above evaluated at 0, i.e.,

$$\frac{1}{\eta_0}\frac{a}{\mu U}\tau_0 = \frac{1}{\eta_0}\left(\frac{\partial u}{\partial y}\right)_{y=0} = \left(\frac{\partial u}{\partial \eta_1}\right)_{\eta_1=0} = G''(0) \tag{2.3.25}$$

Recall that $G(0) = G'(0) = 0$.

## 2.4 NUMERICAL-SIMILARITY SOLUTIONS

We solve the resulting ordinary differential equations, 2.2.22 and 2.3.18, numerically using a fourth order Runge-Kutta shooting method. In this section, the equations that are used in the numerical scheme are derived, the application of the numerical procedure is discussed, and the results are presented, discussed, and compared.

For the r-based transformation, we set

$$F'(\eta) = Z(\eta) \text{ and } Z'(\eta) = S(\eta). \tag{2.4.1}$$

Then, equation 2.2.22 is converted into the three first order ordinary differential equations,

$$F' = Z \text{ with } F(\eta_0) = 0,\ Z' = S \text{ with } Z(\eta_0) = 0 \tag{2.4.2}$$

and

$$\eta^3 S' + 2\eta^2 S - \eta Z + F - 2\eta FF + 2\eta^2 FZ + 2\eta^3 FS = 0, \tag{2.4.3}$$

with $S(\eta_0) = \alpha_F$.

For the y-based transformation, we set

$$G'(\eta_1) = Z(\eta_1) \text{ and } Z'(\eta_1) = S(\eta_1). \tag{2.4.4}$$

Then, equation 2.3.18 is converted into the three first order ordinary differential equations,

$$G' = Z \text{ with } G(0) = 0,\ Z' = S \text{ with } Z(0) = 0 \tag{2.4.5}$$

and

$$(\eta_1+\eta_0)^3 S' + 2(\eta_1+\eta_0)^2 S - (\eta_1+\eta_0)Z + G$$

$$-2(\eta_1+\eta_0)GG + 2\eta_1(\eta_1+\eta_0)GZ + (2\eta_1+\eta_0)(\eta_1+\eta_0)^2 GS = 0 \qquad (2.4.6)$$

with $S(0) = \alpha_G$.

Note that the $\alpha$'s are the initial shooting values for the second derivatives.

A Newton-Raphson procedure with over-relaxation is employed in conjunction with the Runge-Kutta scheme. The function $\kappa = 1 - Z(\eta_\infty)$, is used to aid in computation. It is a function of the asymptotic axial velocity near the boundary layer edge and of the varying estimates of the first derivative of the velocity at the wall, i.e., $\alpha$. Two reasonably close estimates of $\alpha$ are used to begin the procedure and then the numerical routine carries on to convergence such that the iterates of $\alpha$ and the requirement that $\kappa = 0$ satisfy a prescribed tolerance.

For example, given $\alpha^{i-1}$ and $\alpha^i$, $\alpha^{i+1}$ is obtained using the Newton formula given by :

$$\alpha^{i+1} = \alpha^i - \frac{\kappa(\alpha^i)}{d\kappa/d\alpha}. \qquad (2.4.7)$$

The derivative of $\kappa$ with respect to $\alpha$ is approximated by :

$$\frac{\Delta\kappa}{\Delta\alpha} = \frac{\kappa(\alpha^{i+1}) - \kappa(\alpha^i)}{\alpha^{i+1} - \alpha^i} \qquad (2.4.8)$$

After each new iterate of $\alpha$ is obtained, convergence is tested by making sure that

$\kappa \leq$ tolerance and that $|\alpha^{i+1} - \alpha^i| \leq$ tolerance. (2.4.9)

To accelerate convergence, over-relaxation is employed to reduces the number of iterations. The criterion to ensure over-relaxation is that if $\alpha_{i+1}$ satisfies $|\alpha^{i+1} - \alpha^{i}| < .02\alpha^{i}$ then the new iterate is increased according to :

$$\alpha^{i+1} = 1.19\alpha^{i}. \tag{2.4.10}$$

Otherwise, we use the original Newton iterate from equation 2.4.7.

In using the shooting method, caution must be taken to check that a particular solution is converging and consistent. In the boundary layer case, this is done by varying the step sizes and the prescribed value of the boundary layer edge to ensure that the nondimensional axial velocity asymptotes unity near the boundary layer edge, that negative velocities do not appear, that the shear stresses near the boundary layer edge asymptote zero and that the skin-friction coefficient, as well as all other calculated values, settle to a consistent value. Negative velocities usually indicate step sizes that are too large. The gradual numerical asymptoting of either the axial velocity to unity or the shear stress to zero is usually a good indicator of a stable numerical solution and a reliable test to ensure that the prescribed value for the boundary layer edge is appropriate.

It must be stressed that the solutions obtained from both transformations are nonsimilar, in general, due to the finite non-zero value of $\eta_0$, which depends on x and which appears in the boundary conditions. However, a 'quasi-similar' solution has been obtained in which solutions at fixed $\eta_0$ are pieced together to form an overall solution (Sawchuk 1985).

Solutions are obtained for a wide range of $\xi$ or $\eta_0$. In principle, 'quasi-similar' solutions could be obtained for all values of $\xi$. However, larger values of $\xi$ require smaller step sizes in order to obtain consistent results and ,thus, more computer storage is necessary.

Near $\xi = 0$, i.e., the Blasius limit, the step size can be as large as 0.1 in $\Delta\eta$. Moving downstream, the step size gradually decreases to $10^{-6}$ at $\xi = 10^6$.

The special case of similarity at $\xi = 0$ or $\eta_0 = \infty$ is obtained numerically by prescribing a large value of $\eta_0$. At the prescribed value of $\eta_0 \geq 1000$, the numerical solutions that are obtained have already settled to consistent values, i.e., larger values of $\eta_0$ would yield the same solution.

The integrals within the displacement and momentum thickness expressions are evaluated using Simpson's rule.

The numerical solutions stemming from the r-based transformation are obtained without any difficulty. Once the appropriate step size is established, the prescribed value of the boundary layer edge is easily obtained because the numerical solution using the r-based transformation asymptotes the appropriate outer boundary conditions very gradually. Even if the prescribed distance to integrate is larger than need be, the asymptotic process begins numerically at the same point in the cross-stream direction as it would for a smaller estimate. The skin friction and integral parameters converge to consistent values at larger estimates of the boundary layer edge.

Generally, there are no difficulties in obtaining the numerical results using the y-based transformation. In the range $0.05 \leq \xi < 40$ or $0.071 < \eta_0 < 57$, consistent solutions were not obtainable. Variation of the step size or of the prescribed boundary layer edge would not yield consistent results in this range.

Velocity profiles from the 'quasi-similar' solution for each transformation are plotted for various $\xi = 2\sqrt{2}/\eta_0$ in Figures 2.4.4, 2.4.5, 2.4.9 and 2.4.10. Velocity and shear stress profiles of one transformation are compared to those of the other transformation in Figures 2.4.1-3, 2.4.6-8, and 2.4.11-13. Similarly, the skin-friction coefficient, displacement and momentum thickness are tabulated for comparison with regards to each transformation in Tables 2.4.1-3.

It is important to notice that the axial velocities of the two transformations differ with each other in the Blasius limit at $\xi = 0$ or $\eta_0 \to \infty$. One would expect that solutions from either transformation would yield the same result and that this result would be consistent with the Blasius limit. The numerical values from the axial velocity profiles suggest that the y-based transformation does, in fact, yield the Blasius profile, while the r-based transformation yields a solution deceptively close to the Blasius, i.e., one that is shifted by a factor of $\sqrt{2}$ in the independent variable $\eta - \eta_0$.

The radial velocity parameter obtained with each transformation for $\xi \to 0$ or $\eta_0 \to \infty$ also differs significantly with respect to each transformation. The numerical values obtained from the y-based transformation are consistent with the radial velocity component obtained from the Blasius differential equation, whereas, the values obtained

from the r-based transformation are very large and on the same scale as the value chosen for the fixed $\eta_0$, i.e., of the order $10^6$. At $\xi = 0.05$ or $\eta_0 \approx 56.6$, a large difference can be seen in the radial velocity parameters in Figure 2.4.6.

Significant differences are evident between the coefficients of skin-friction from the two transformations in the lower range of $\xi$ in Table 2.4.1. Percentage differences start at approximately 41% at $\xi \approx 0$ and at $\xi = 40$ reduce from 4.0 % to 0.0002% at $\xi = 10^6$.

Momentum thickness also differs significantly with respect to each transformation. Here, percentage differences begin at 21%, jump to 41 % at $\xi = 40$ and steadily decrease to 0.01 % at $\xi = 10^6$. The difference is still quite high at $\xi = 500$, where it is 10%. Comparing values of displacement thickness shows that large differences occur near $\xi = 0$, but that they decrease as $\xi$ increases. At $\xi = 10^3$, the difference is 5% reducing to 0.01 % at $\xi = 10^6$.

Therefore, the numerical results would suggest that as $\xi$ increases or $\eta_0$ decreases the solutions from both transformations merge. Note, that comparisons are not made in the range $0.05 \leq \xi \leq 40$ because of the difficulties encountered with the numerical solution of the y-based transformation.

## 2.5 ANALYTICAL RELATIONSHIP BETWEEN THE TWO SIMILARITY TRANSFORMATIONS

In general, we expect that the similarity transformations based on r and y should yield the same solutions. This, however, is not the case as the solutions presented previously suggest. In the limit as $a \to \infty$ or $\eta_0 \to \infty$, the y-based transformation

yields the Blasius while the r-based transformation yields a solution which is not the Blasius. To study this difference more closely a relationship is sought between F and G in the limit as $\eta_0 \to \infty$.

The asymptotic boundary condition, $\frac{F(\eta)}{\eta} + F'(\eta) \to 1$ as $\eta \to \infty$, (2.5.1)

suggests that, if $F = O(\eta)$, then $F \sim \frac{\eta}{2}$ and $F' \sim 1/2$. (2.5.2a)

Let us assume along with (2.5.2a) that

$\lim_{\eta \to \infty} F'' = O(1)$ and $\lim_{\eta \to \infty} F''' = O(1)$. (2.5.2b)

Evaluating equation 2.2.22 in the limit as $\eta_0 \to \infty$ or $\eta \to \infty$, since $\eta = \eta_1 + \eta_0$, with the assumptions 2.5.2a and 2.5.2b yields :

$$F''' + 2FF'' - 2\frac{FF}{\eta^2} + 2\frac{FF'}{\eta} = 0. \tag{2.5.3}$$

Similarly, in the limit as $\eta_0 \to \infty$, equation 2.3.18 becomes :

$$G''' + GG'' = 0, \tag{2.5.4a}$$

with $\lim_{\eta_1 \to \infty} G' = 1$, and $\lim_{\eta_1 \to \infty} \frac{G(\eta_1)}{(\eta_1 + \eta_0)} = 0$. (2.5.4b)

Hence, a direct scaling of similarity transformations and similarity variables does not appear to be possible.

The numerical results suggest that as $\eta_0 \to \infty$, and as we approach the boundary layer edge, i.e., $\eta \to \infty$, that $F(\eta) \sim (\eta - \eta_0) = \eta_1 \neq \eta$.

On the other hand, if in the limit

$\eta_0 \to \infty$, we assume that as $\eta \to \infty$, that $F \sim \eta - \eta_0 = \eta_1$ and $F' \sim 1$, the asymptotic boundary condition 2.5.1 is satisfied, while (2.2.22) becomes

$$F''' + 2FF'' = 0. \tag{2.5.5}$$

An appropriate scaling of variables is chosen such that equation 2.5.5 is transformed to (2.5.4a), while satisfying the boundary conditions. Setting

$$F = A\mathrm{X} \text{ and } \eta = \bar{\omega}\Lambda, \tag{2.5.6}$$

where A and $\bar{\omega}$ are constant, then equation 2.5.5 becomes

$$\mathrm{X}''' + 2A\bar{\omega}\mathrm{X}\mathrm{X}'' = 0 \text{ and comparing with 2.5.4 implies that } 2A\bar{\omega} = 1. \tag{2.5.7}$$

The asymptotic boundary condition, (2.5.1), is rewritten as :

$$\lim_{\Lambda \to \infty}\left(\frac{\mathrm{X}}{\Lambda} + \mathrm{X}'\right) = \frac{\bar{\omega}}{A}. \tag{2.5.8}$$

Comparing (2.5.8) with the asymptotic limit in (2.5.4) implies that

$$\frac{\mathrm{X}}{\Lambda} \to 0, \text{ while } \mathrm{X}' \sim \frac{\bar{\omega}}{A}. \tag{2.5.9}$$

From (2.5.7) and (2.5.9), we have : $A = \bar{\omega} = \frac{1}{\sqrt{2}}$ (2.5.10)

Now, (2.5.5) has been transformed into (2.5.4a) by a suitable transformation and careful assumptions, i.e.,

$$F = \frac{\mathrm{X}}{\sqrt{2}} \text{ and } \eta = \frac{\Lambda}{\sqrt{2}} \text{ and that } \lim_{\eta \to \infty} \frac{F}{\eta} = 0, \tag{2.5.11}$$

but, a direct mathematical relationship between F and G is not possible because $F \equiv F(\eta)$ and $G \equiv G(\eta_1)$. Therefore, an alternative approach is used to further investigate the differences between the r-based and y-based transformations, in the Blasius limit.

## 2.6 COMPARISON WITH THE BLASIUS

It is important to compare the limiting case as $\eta_0 \to \infty$ of the above solutions with the Blasius solution for flow past a semi-infinite flat plate to shed more light on the inconsistencies encountered between the above solutions in the Blasius limit.

The nondimensional governing equations are :

$$u_B(x,y)\frac{\partial u_B(x,y)}{\partial x}+v_B(x,y)\frac{\partial u_B(x,y)}{\partial y}=\frac{1}{R_L}\frac{\partial^2 u_B(x,y)}{\partial y^2}, \tag{2.6.1}$$

$$\frac{\partial u_B(x,y)}{\partial x}+\frac{\partial v_B(x,y)}{\partial y}=0, \tag{2.6.2}$$

where all quantities are nondimensionalized as

$$u_B=\frac{u_B^*}{U},\ v_B=\frac{v_B^*}{U},\ y=\frac{y^*}{L},\ x=\frac{x^*}{L},\ R_L=\frac{UL}{\nu},$$

and L is a characteristic length.

Defining $\psi(x,y)$ such that

$$u_B(x,y)=\frac{\partial \psi}{\partial y},\quad v_B=-\frac{\partial \psi}{\partial x} \tag{2.6.3}$$

and using

$$\psi = \frac{f(\eta_B)}{\eta_L}, \text{ where } \eta_B = \eta_L y \text{ and } \eta_L = \sqrt{\frac{UL}{2\nu x}}, \text{ yields :} \tag{2.6.4}$$

$$u_B = f' \text{ and } v_B = \frac{\eta_L}{R_L}(\eta_B f' - f), \tag{2.6.5}$$

Individual terms of the two dimensional boundary layer equations in terms of f are given by :

$$u_B \frac{\partial u_B}{\partial x_B} = -\frac{\eta_L^2}{R_L}\eta_B f' f'', \; v_B \frac{\partial u_B}{\partial y_B} = \frac{\eta_L^2}{R_L} f''\{\eta_B f' - f\}, \; \frac{1}{R_L}\frac{\partial^2 u_B}{\partial y_B^2} = \frac{\eta_L^2}{R_L} f''', \tag{2.6.6}$$

$$\frac{\partial u_B}{\partial x_B} = -\frac{\eta_L^2}{R_L}\eta_B f'' \text{ and } \frac{\partial v_B}{\partial y_B} = \frac{\eta_L^2}{R_L}\eta_B f'', \tag{2.6.7}$$

and individual terms neglected from the Navier-Stokes Equations for the flat plate problem are given by :

$$\frac{1}{R_L}\frac{\partial^2 u_B}{\partial x_B^2} = \frac{\eta_L^4}{R_L^3}\{\eta_B^2 f''' + 3\eta_B f''\}. \tag{2.6.8}$$

$$u_B \frac{\partial v_B}{\partial x_B} = \frac{\eta_L^3}{R_L^2} f'\{-\eta_B^2 f'' - \eta_B f' + f\}, \tag{2.6.9}$$

$$v_B \frac{\partial v_B}{\partial y_B} = \frac{\eta_L^3}{R_L^2}\eta_B f''\{\eta_B f' - f\}, \tag{2.6.10}$$

$$\frac{1}{R_L}\frac{\partial^2 v_B}{\partial x_B^2} = \frac{\eta_L^5}{R_L^4}\{\eta_B^3 f''' + 6\eta_B^2 f'' + 3\eta_B f' - 3f\}, \tag{2.6.11}$$

$$\frac{1}{R_L}\frac{\partial^2 v_B}{\partial y_B^2} = \frac{\eta_L^3}{R_L^2}\{\eta_B f''' + f''\}, \tag{2.6.12}$$

where

$$\frac{\partial \eta_B}{\partial x_B} = -\frac{\eta_B}{2x_B}, \quad \frac{\partial^2 \eta_B}{\partial x_B^2} = \frac{3\eta_B}{4x_B^2}, \quad \frac{\partial \eta_L}{\partial x_B} = -\frac{\eta_L}{2x_B},$$

$$\frac{\partial^2 \eta_L}{\partial x_B^2} = \frac{3\eta_L}{4x_B^2}, \quad \frac{\partial \eta_B}{\partial y_B} = \eta_L, \quad \frac{\partial^2 \eta_B}{\partial y_B^2} = 0,$$

$$\frac{\partial \eta_L}{\partial y_B} = 0 \text{ and } \frac{\partial^2 \eta_L}{\partial y_B^2} = 0. \tag{2.6.13}$$

The differential equation obtained from the transformation 2.6.4 is :

$$f''' + ff'' = 0, \tag{2.6.14}$$

i.e., the Blasius Differential Equation with the boundary conditions :

$f(0) = f'(0) = 0$ and $f'(\eta_B) \to 1$ as $\eta_B \to \infty$.

Another similarity transformation based on r which is related to the previous r-based transformation by a shift of $\sqrt{2}$ in the independent variable is introduced. This transformation follows directly from the transformation 2.5.11, which transforms (2.5.5) into (2.5.4a) in the previous section. Solutions obtained using this transformation are exactly the same as that of the previous r-based transformation.

The solution obtained using this transformation is compared to the solution obtained using the y-based transformation in order to emphasize the differences between the two, in the Blasius limit.

The similarity transformation is

$$\psi = \frac{s}{s_0^2} H(s), \tag{2.6.15}$$

$$\text{where } s = s_0 r = \sqrt{2}\eta \text{ and } s_0 = \sqrt{\frac{Ua}{2\nu x}} = \sqrt{2}\eta_0. \tag{2.6.16}$$

The velocity components are

$$u = \frac{H(s)}{s} + H'(s) \text{ and } v = \frac{s_0}{2R}(sH'(s) - H(s)), \tag{2.6.17}$$

Clearly, $u = u(s)$ and $v = v(s, s_0)$.

Applying (2.6.15) to the governing equations 1.2.6-7 yields

$$s^3 H''' + 2s^2 H'' - sH' + H - sHH + s^2 HH' + s^3 HH'' = 0, \tag{2.6.18}$$

with boundary conditions

$$H(s_0) = H'(s_0) = 0 \text{ and } \frac{H(s)}{s} + H'(s) \to 1 \text{ as } s \to \infty. \tag{2.6.19}$$

Equation 2.6.18 has been solved numerically using a 4rth order Runge-Kutta shooting method for fixed $s_0$. Similarity breaks down, here, because the boundary conditions lead

to the implicit functional dependence of H on $s_0$, which depends on x. A 'quasi-similar' solution is obtained for fixed $s_0$. The relationship between the two r-based transformations is presented in Appendix D.

## 2.7 TAYLOR SERIES ABOUT THE SURFACE

The results from each transformation in the limit as $a \to \infty$ are investigated via Taylor series expansions and compared with that of the Blasius. The shift in the independent variable of $\sqrt{2}$ in the solution obtained from the r-based transformation can be viewed on a rigorous level. Results from both transformations are valid mathematically and numerically, but the r-based transformation is questionable on physical grounds.

A Taylor Series expansion of 11th order is obtained for F and its derivatives about $\eta = \eta_0$ from equation 2.2.22. Similarly, an expansion for G and its derivatives about $\eta_1 = 0$ are obtained from equation 2.3.18. The expansions are performed about the surface of the cylinder and are of the form :

$$F(\eta) = F_0 + \eta_1 F_0^{I} + \frac{\eta_1^2}{2!} F_0^{II} + \frac{\eta_1^3}{3!} F_0^{III} + ..., \tag{2.7.1}$$

where the subscript '0' indicates F evaluated at $\eta_0$, i.e., $F_0 \equiv F(\eta_0)$ or G evaluated at 0, i.e., $G_0 \equiv G(0)$ and the superscripts indicate differentiation with respect to the corresponding arguments.

To obtain the coefficients in the expansions, viz,

$F_0, F_0^I, \ldots, F_0^X, F_0^{XI},$

the corresponding ordinary differential equations must be differentiated with respect to function arguments 8 times. Then, each set of 9 equations, starting with the original, are evaluated at the surface of the cylinder to obtain the corresponding coefficients. The current equation being evaluated uses previously obtained coefficients. Note that all equations will use $F_0$ and $F_0^I$ or $G_0$ and $G_0^I$ obtained from the no-slip boundary condition.

The 8 ordinary differential equations obtained by differentiation along with the corresponding coefficients in the series expansions obtained from the r-based and y-based transformations are presented in Appendix B and C respectively.

To obtain the Taylor Series expansions for the velocity components and the individual terms in governing equations 1.2.6-7, the expansions of F, G and their derivatives are used along with the expansions of

$1/\eta,\ \ 1/\eta^2,$ , and $1/\eta^3$ about $\eta = \eta_0$ or $\eta_1 = 0$.

The latter expansions are given by :

$$\frac{1}{\eta} = \frac{1}{\eta_0} \sum_{i=0}^{\infty} \left( -\frac{\eta_1}{\eta_0} \right)^i, \quad \frac{1}{\eta^2} = \frac{1}{\eta_0^2} \sum_{i=0}^{\infty} (i+1) \left( -\frac{\eta_1}{\eta_0} \right)^i,$$

$$\frac{1}{\eta^3} = \frac{1}{\eta_0^3} \sum_{i=0}^{\infty} \frac{(i+1)(i+2)}{2} \left( -\frac{\eta_1}{\eta_0} \right)^i. \qquad (2.7.2)$$

From the series expansions obtained for F and its derivatives the series expansions of the velocity components are given by :

$$u = \alpha_F \eta_1 - \frac{\alpha_F}{2\eta_0}\eta_1^2 + 2\frac{\alpha_F}{\eta_0^2}\frac{\eta_1^3}{3!} - \left(3!\frac{\alpha_F}{\eta_0^3} + 2\alpha_F^2\right)\frac{\eta_1^4}{4!} + \left(4!\frac{\alpha_F}{\eta_0^4} + 12\frac{\alpha_F^2}{\eta_0}\right)\frac{\eta_1^5}{5!}$$

$$-\left(5!\frac{\alpha_F}{\eta_0^5} + 74\frac{\alpha_F^2}{\eta_0^2}\right)\frac{\eta_1^6}{6!} + \left(6!\frac{\alpha_F}{\eta_0^6} + 510\frac{\alpha_F^2}{\eta_0^3} + 44\alpha_F^3\right)\frac{\eta_1^7}{7!} - (7!\frac{\alpha_F}{\eta_1^7} + 3954\frac{\alpha_F^2}{\eta_0^4}$$

$$+616\frac{\alpha_F^3}{\eta_0})\frac{\eta_1^8}{8!} + \left(8!\frac{\alpha_F}{\eta_0^8} + 34272\frac{\alpha_F^2}{\eta_0^5} + 7256\frac{\alpha_F^3}{\eta_0^2}\right)\frac{\eta_1^9}{9!} - (9!\frac{\alpha_F}{\eta_0^9} + 329328\frac{\alpha_F^2}{\eta_0^6}$$

$$+85032\frac{\alpha_F^3}{\eta_0^3} + 3000\alpha_F^4)\frac{\eta_1^{10}}{10!} + O(\eta_1^{11}), \qquad (2.7.3)$$

$$v = \frac{1}{R}\{\eta_0^2\alpha_F\eta_1 - \eta_0\frac{\alpha_F}{2}\eta_1^2 + 3\alpha_F\frac{\eta_1^3}{3!} - \left(12\frac{\alpha_F}{\eta_0} + 2\eta_0^2\alpha_F^2\right)\frac{\eta_1^4}{4!} + \left(60\frac{\alpha_F}{\eta_0^2} + 6\eta_0\alpha_F^2\right)\frac{\eta_1^5}{5!}$$

$$-\left(360\frac{\alpha_F}{\eta_0^3} + 30\alpha_F^2\right)\frac{\eta_1^6}{6!} + \left(2520\frac{\alpha_F}{\eta_0^4} + 192\frac{\alpha_F^2}{\eta_0} + 44\eta_0^2\alpha_F^3\right)\frac{\eta_1^7}{7!} - (20160\frac{\alpha_F}{\eta_0^5} + 1458\frac{\alpha_F^2}{\eta_0^2}$$

$$+352\eta_0\alpha_F^3)\frac{\eta_1^8}{8!} + \left(181440\frac{\alpha_F}{\eta_0^6} + 12690\frac{\alpha_F^2}{\eta_0^3} + 3032\alpha_F^3\right)\frac{\eta_1^9}{9!} - (1814400\frac{\alpha_F}{\eta_0^7} + 124020\frac{\alpha_F^2}{\eta_0^4}$$

$$+29096\frac{\alpha_F^3}{\eta_0} + 3000\eta_0^2\alpha_F^4)\frac{\eta_1^{10}}{10!} + O(\eta_1^{11})\}, \qquad (2.7.4)$$

Resulting expansions for individual terms from the governing equations, 1.2.6-7, and neglected individual terms from the Navier-Stokes equations, 1.2-3-5, are presented in Appendix B. The series expansions for individual terms of the momentum equation 1.2.6 are in equations B.19-22. Those for the individual terms from continuity equation 1.2.7 are in equations B.23-25. Those for the individual

terms neglected from Navier-Stokes equations 1.2.3-5 are in equations B.26-32.

Series expansions of the velocity components for G are given by :

$$u = \alpha_G \eta_1 - \frac{\alpha_G}{2\eta_0}\eta_1^2 + 2\frac{\alpha_G}{\eta_0^2}\frac{\eta_1^3}{3!} - \left(3!\frac{\alpha_G}{\eta_0^3} + \alpha_G^2\right)\frac{\eta_1^4}{4!} + \left(4!\frac{\alpha_G}{\eta_0^4} + 6\frac{\alpha_G^2}{\eta_0}\right)\frac{\eta_1^5}{5!}$$

$$-\left(5!\frac{\alpha_G}{\eta_0^5} + 43\frac{\alpha_G^2}{\eta_0^2}\right)\frac{\eta_1^6}{6!} + \left(6!\frac{\alpha_G}{\eta_0^6} + 361\frac{\alpha_G^2}{\eta_0^3} + 11\alpha_G^3\right)\frac{\eta_1^7}{7!} - (7!\frac{\alpha_G}{\eta_0^7} + 3414\frac{\alpha_G^2}{\eta_0^4}$$

$$+109\frac{\alpha_G^3}{\eta_0})\frac{\eta_1^8}{8!} + \left(8!\frac{\alpha_G}{\eta_0^8} + 35604\frac{\alpha_G^2}{\eta_0^5} + 998\frac{\alpha_G^3}{\eta_0^2}\right)\frac{\eta_1^9}{9!} - (9!\frac{\alpha_G}{\eta_0^9} + 404712\frac{\alpha_G^2}{\eta_0^6}$$

$$+9364\frac{\alpha_G^3}{\eta_0^3} + 375\alpha_G^4)\frac{\eta_1^{10}}{10!} + O(\eta_1^{11}\}, \qquad (2.7.5)$$

$$v = \frac{1}{R}\{\eta_0\alpha_G\frac{\eta_1^2}{2} - 4\frac{\alpha_G}{2}\frac{\eta_1^3}{3!} + 21\frac{\alpha_G}{\eta_0}\frac{\eta_1^4}{4!} - \left(132\frac{\alpha_G}{\eta_0^2} + 4\eta_0\alpha_G^2\right)\frac{\eta_1^5}{5!} + \left(960\frac{\alpha_G}{\eta_0^3} + 35\alpha_G^2\right)\frac{\eta_1^6}{6!}$$

$$-\left(7920\frac{\alpha_G}{\eta_0^4} + 336\frac{\alpha_G^2}{\eta_0}\right)\frac{\eta_1^7}{7!} + \left(73080\frac{\alpha_G}{\eta_0^5} + 3556\frac{\alpha_G^2}{\eta_0^2} + 77\eta_0^2\alpha_G^3\right)\frac{\eta_1^8}{8!} - (745920\frac{\alpha_G}{\eta_0^6}$$

$$+40784\frac{\alpha_G^2}{\eta_0^3} + 960\alpha_G^3)\frac{\eta_1^9}{9!} + \left(8346240\frac{\alpha_G}{\eta_0^7} + 502722\frac{\alpha_G^2}{\eta_0^4} + 10953\frac{\alpha_G^3}{\eta_0}\right)\frac{\eta_1^{10}}{10!} - (101606400\frac{\alpha_G}{\eta_0^8}$$

$$+6631100\frac{\alpha_G^2}{\eta_0^5} + 127710\frac{\alpha_G^3}{\eta_0^2} + 3750\eta_0\alpha_G^4)\frac{\eta_1^{11}}{11!} + O(\eta_1^{12}\}, \qquad (2.7.6)$$

Resulting expansions for individual terms from the governing equations, 1.2.6-7, and neglected individual terms from the Navier-Stokes equations, 1.2-3-5, are presented in Appendix C. The series expansions for individual terms of the

momentum equation 1.2.6 are in equations C.19-22. Those for the individual terms from continuity equation 1.2.7 are in equations C.23-25. Those for the individual terms neglected from Navier-Stokes equations 1.2.3-5 are in equations C.26-32.

Using the same method as in the previous sections, the Blasius function, f, is expanded in a Taylor Series about $\eta_B = 0$ (see Weyl (1942)). The expansion is:

$$f = \alpha_B \frac{\eta_B^2}{2} - \alpha_B^2 \frac{\eta_B^5}{5!} + 11\alpha_B^3 \frac{\eta_B^8}{8!} - 375\alpha_B^4 \frac{\eta_B^{11}}{11!} + O(\eta_B^{14}), \tag{2.7.7}$$

$$\text{as } \eta_B \to 0 \text{ and }, \alpha_B \equiv f''(0) \equiv f_0'' = .46960 \text{ (see Rosenhead 1963)} \tag{2.7.8}$$

Clearly,

$$u_B = \alpha_B \eta_B - \alpha_B^2 \frac{\eta_B^4}{4!} + 11\alpha_B^3 \frac{\eta_B^7}{7!} - 375\alpha_B^4 \frac{\eta_B^{10}}{10!} + O(\eta_B^{13}), \tag{2.7.9}$$

and

$$v_B = \frac{\eta_L}{R_L}\left\{\alpha_B \frac{\eta_B^2}{2} - 4\alpha_B^2 \frac{\eta_B^5}{5!} + 77\alpha_B^3 \frac{\eta_B^8}{8!} - 3750\alpha_B^4 \frac{\eta_B^{11}}{11!} + O(\eta_B^{11})\right\},$$

$$\text{as } \eta_B \to 0. \tag{2.7.10}$$

Resulting expansions for individual terms from the two dimensional boundary layer equations and neglected individual terms from the two dimensional Navier-Stokes equations are presented in Appendix D. The series expansions for individual terms of the momentum equation are in equations D.28-30. Those for the individual terms from continuity equation are in equations D.31-32. Those for the individual terms neglected from Navier-Stokes equations are in equations D.33-37.

Series expansion of individual terms and velocity components for the r-based transformation involving H is presented in Appendix D. The axial and radial components of velocity are given by equations D.19 and D.20. Individual terms of the momentum equation are given by equations D.21-23. Individual terms from the continuity equations are given by equations D.24-26.

## 2.8 COMPARISON OF SERIES EXPANSIONS

The Taylor series expansions for F and G differ from each other as do their numerical solutions as seen in section 2.4 and 2.7 and in appendices B and C. While, the corresponding coefficients of each expansion are of the same order in $\eta_0$, a relationship linking one expansion to the another does not exist. In this section, we compare corresponding series expansions from the two r-based transformations, the y-based transformation and the Blasius problem itself, in the Blasius limit.

As $\eta_0 \to \infty$, the axial velocity expansion, (2.7.3), from the r-based transformation yields :

$$u = \alpha_F \eta_1 - 2\alpha_F^2 \frac{\eta_1^4}{4!} + 44\alpha_F^3 \frac{\eta_1^7}{7!} - 3000\alpha_F^4 \frac{\eta_1^{10}}{10!} + O(\eta_1^{13}),$$

for small $\eta_1$. (2.8.1)

Numerical results suggest that $\lim_{\eta_0 \to \infty} \alpha_F = \sqrt{2}\alpha_G$, so that (2.8.1) can be written as

$$u = \alpha_G(\sqrt{2}\eta_1) - \alpha_G^2\frac{(\sqrt{2}\eta_1)^4}{4!} + 11\alpha_G^3\frac{(\sqrt{2}\eta_1)^7}{7!} - 375\alpha_G^4\frac{(\sqrt{2}\eta_1)^{10}}{10!} + O(\eta_1^{13})$$

for small $\eta_1$. (2.8.2)

Similarly, in the limit as $\eta_0 \to \infty$ or $s_0 \to \infty$ the expansion of the axial velocity component from the r-based transformation involving H, given in Appendix D in equation D.19, becomes :

$$u = \alpha_H s_1 - \alpha_H^2\frac{s_1^4}{4!} + 11\alpha_H^3\frac{s_1^7}{7!} - 375\alpha_H\frac{s_1^{10}}{10!} + O(s_1^{13}),$$

for small $s_1 = s - s_0 = \sqrt{2}\eta_1$, (2.8.3)

Numerical results suggest that $\lim_{\eta_0, s_0 \to \infty} \alpha_H = \alpha_G$ indicating that (2.8.3) can be written as:

$$u = \alpha_G s_1 - \alpha_G^2\frac{s_1^4}{4!} + 11\alpha_G^3\frac{s_1^7}{7!} - 375\alpha_G\frac{s_1^{10}}{10!} + O(s_1^{13}),$$

for small $s_1$. (2.8.4)

In the limit as $\eta_0 \to \infty$, the axial velocity component from the y-based transformation, (2.7.5), becomes:

$$u = \alpha_G\eta_1 - \alpha_G^2\frac{\eta_1^4}{4!} + 11\alpha_G^3\frac{\eta_1^7}{7!} - 375\alpha_G\frac{\eta_1^{10}}{10!} + O(s_1^{13}),$$

for small $\eta_1$. (2.8.5)

Numerical results suggest that $\lim_{\eta_0 \to \infty} \alpha_G = \alpha_B$. Note, that in the Blasius limit

$\eta_0$ corresponds to $\eta_L$, $R$ corresponds to $R_L$, $u \to u_B$, and $v \to v_B$.

The coefficients of the powers of $\eta_1$ in (2.8.5) are identical to the coefficients of the powers of $\sqrt{2}\eta_1$ in (2.8.2) and to the coefficients of the powers of $s_1$ in (2.8.4). These coefficients are identical to those in (2.7.9) after substituting $\alpha_G = \alpha_B$. Thus, the series expansion from the y-based transformation, (2.8.5), matches exactly with the Blasius expansion (2.7.9). Both series expansions from the r-based transformations, (2.8.2) and (2.8.4), indicate a shift in the independent variable of $\sqrt{2}$, which is misleading close to the Blasius expansion 2.7.9.

Comparing series expansions of the radial velocity component in the limit as $\eta_0 \to \infty$ requires matching the highest order terms in $\eta_0$ from each transformation with that of the Blasius. In the limit as $\eta_0 \to \infty$ the expansion, (2.7.4), from the r-based transformation yields :

$$v = \frac{\eta_0^2}{R}\left\{\alpha_F\eta_1 - 2\alpha_F^2\frac{\eta_1^4}{4!} + 44\alpha_F^3\frac{\eta_1^7}{7!} + O(\eta_1^{10})\right\}, \text{ for small } \eta_1 \tag{2.8.6}$$

while the expansion, 2.7.6, from the y-based transformation yields :

$$v = \frac{\eta_0}{R}\left\{\alpha_G\frac{\eta_1^2}{2} - 4\alpha_G^2\frac{\eta_1^5}{5!} + 77\alpha_G^3\frac{\eta_1^8}{8!} + O(\eta_1^{11})\right\}, \text{ fro small } \eta_1. \tag{2.8.7}$$

Comparing (2.8.7) with the Blasius (2.7.10) shows an exact match, while (2.8.6) and (2.7.10) indicate no correspondence at all. In fact, (2.8.6) is an order of $\eta_0$ higher than

in the correct (2.8.7). Significantly large values of the radial velocity component can be seen in the numerical results, as was pointed out in section 2.4. It is interesting to compare (2.8.6) with (2.8.1) in the limit as $\eta_0 \to \infty$ because the axial and radial velocities from the r-based transformations are the same but for a factor of $\eta_0^2/R$.

In the limit as $\eta_0 \to \infty$,, the series expansions of all individual terms in the governing equations from the r-based transformations, equations B.19-25, do not match with those of the Blasius, equations D.28-32. However, the series expansions from the y-based transformation, equations C.19-25, are identical. The numerical solutions obtained in section 2.4 suggest the same unexpected results.

## 2.9 OBTAINING THE TWO DIMENSIONAL BOUNDARY LAYER EQUATIONS

To further explain the difference between the two similarity transfo.mations in the limit as $\eta_0 \to \infty$,, it is necessary to obtain Prandtl's two dimensional boundary layer equations from either the Navier-Stokes equations, 1.2.3-5, or Cooke's equations, 1.2.1-2. Then the order of magnitude of each individual terms from the analysis of these equations will be compared with the orders of magnitude of the same individual terms produced by the similarity transformations in the next section.

Assuming

$$r^* = a + y^* \sim 1,\ x^* \sim 1,\ y^* \sim \delta, \text{ and } u^* \sim 1, \tag{2.9.1}$$

gives rise to

$$a \sim 1, \quad \delta r = \delta y \sim \delta. \quad \frac{\partial u}{\partial x} \sim 1. \tag{2.9.2}$$

Applying these relations to the equation of continuity gives :

$$\frac{\partial (r^* u^*)}{\partial x^*} \sim 1 \text{ and, thus, } \frac{\partial (r^* v^*)}{\partial r^*} \sim 1, \tag{2.9.3}$$

$$\text{which yields, } v^* \sim \delta, \frac{v^*}{r^*} \sim \delta, \text{ and } \frac{\partial v^*}{\partial r^*} \sim 1. \tag{2.9.4}$$

The individual terms on the right hand side of the momentum equation, 1.2.3, give :

$$u^* \frac{\partial u^*}{\partial x^*} \sim 1, \; v^* \frac{\partial u^*}{\partial r^*} \sim 1. \tag{2.9.5}$$

Matching the largest inertial term with the highest order derivative viscous term

$$\text{implies } \frac{\nu}{r^*} \frac{\partial \left( r^* \frac{\partial u^*}{\partial r^*} \right)}{\partial r^*} \sim 1. \text{ Hence, } \nu \sim \delta^2 \text{ since } \frac{1}{r^*} \frac{\partial \left( r^* \frac{\partial u^*}{\partial r^*} \right)}{\partial r^*} \sim \frac{1}{\delta^2}. \tag{2.9.6}$$

Remaining terms from the two momentum equations 1.2.3-4 have the following relations :

$$\nu \frac{\partial^2 u^*}{\partial x^{*2}} \sim \delta^2, \; u^* \frac{\partial v^*}{\partial x} \sim \delta, \; \nu \frac{\partial^2 v^*}{\partial x^{*2}} \sim \delta^3, \; v^* \frac{\partial v^*}{\partial r^*} \sim \delta,$$

$$\nu \frac{\partial \left( r^* \frac{\partial v^*}{\partial r^*} \right)}{\partial r^*} \sim \delta, \text{ and } \nu \frac{v^*}{r^{*2}} \sim \delta^3. \tag{2.9.7}$$

Note, that the individual terms can be split into two pieces, i.e.,

$$\frac{\nu}{r^*}\frac{\partial\left(r^*\frac{\partial u^*}{\partial r^*}\right)}{\partial r^*}=\nu\frac{\partial^2 u^*}{\partial r^{*2}}+\frac{\nu}{r^*}\frac{\partial u^*}{\partial r^*}=O(1)+O(\delta)\text{ respectively} \tag{2.9.8}$$

and

$$\frac{\partial(r^*v^*)}{\partial r^*}=\frac{\partial v^*}{\partial r^*}+\frac{v^*}{r^*}=O(1)+O(\delta)\text{ respectively.} \tag{2.9.9}$$

The magnitude of individual terms in the Navier-Stokes equations, I.2.3-5, respectively correspond to

$$O(1)+O(1)=O(1)+O(\delta^2)-\frac{\partial P}{\partial x^*}, \tag{2.9.10a}$$

$$O(\delta)+O(\delta)=O(\delta)+O(\delta^3)+O(\delta^3)-\frac{\partial P}{\partial r^*}, \tag{2.9.10b}$$

$$O(1)+O(1)+O(\delta)=0, \tag{2.9.10c}$$

where $\frac{\partial P^*}{\partial r^*}$ is at most $O(\delta)$.

This leaves P as a function of x* only. Hence, applying Bernouli's equation with U constant gives $\partial P/\partial x^*=0$.

Retaining the terms in the Navier-Stokes equations that are O(1) only gives the remaining two dimensional boundary layer equations, i.e.,

$$u^*\frac{\partial u^*}{\partial x^*}+v^*\frac{\partial u^*}{\partial y^*}=\nu\frac{\partial^2 u^*}{\partial y^{*2}}, \tag{2.9.11}$$

$$\frac{\partial u^*}{\partial x^*}+\frac{\partial v^*}{\partial y^*}=0, \tag{2.9.11b),}$$

## 2.10 ORDER ANALYSIS ON SIMILARITY SOLUTIONS

Now that the behavior of the individual terms from both the Navier-Stokes and Cooke's equations is established in the Blasius limit, the behavior of the corresponding terms obtained using the two similarity transformations can be compared.

From the basic assumptions in (2.9.1), one can see that:

$$\eta_L \sim \frac{1}{\delta}, \text{ and } \eta_B = \eta_L \frac{y^*}{L} \sim 1, \tag{2.10.1}$$

where $L \sim 1$, $R_L \sim \frac{1}{\delta^2}$ and $f(\eta_B) \sim 1$, as well as its derivatives.

As $\eta_0 \to \infty$, all individual terms obtained from the y-based transformation in Sections 2.3 and expansions C.2.7 correspond exactly to the terms in the Blasius in section 2.9, where

$$\eta_0 \sim \frac{1}{\delta}, \quad \eta_1 = \eta_0 \frac{y^*}{a} \sim 1, \text{ and } G(\eta_1) \sim 1 \text{ as well as its derivatives.} \tag{2.10.2}$$

However, the order analysis of terms obtained from the r-based transformation in Section 2.2 and from equations B.19-25 does not agree with that of Section 2.9. Individual terms from Navier-Stokes equations, (1.2.3-5), obtained from the r-based transformation give the following relations :

$$v^* \sim 1, \quad u^* \frac{\partial u^*}{\partial x^*} \sim \frac{1}{\delta}, \quad v^* \frac{\partial u^*}{\partial r^*} \sim \frac{1}{\delta}, \quad \frac{1}{R} \frac{\partial^2 u^*}{\partial x^{*2}} \sim 1,$$

$$\frac{\partial u^*}{\partial x^*} \sim \frac{1}{\delta}, \quad \frac{\partial v^*}{\partial r^*} \sim \frac{1}{\delta}, \text{ and } \frac{v^*}{r^*} \sim 1. \tag{2.10.3}$$

Note that $U = O(1)$ and $F(\eta) \sim 1$, as well as its derivatives.

In a true boundary layer, the axial velocity component should be O(1), while the radial velocity component should be O(δ). However, this is not the case, here. In fact, the independent variable

$$\eta = \eta_0 \frac{r^*}{a} = O\left(\frac{1}{\delta}\right) O(1) = O\left(\frac{1}{\delta}\right) \neq O(1). \tag{2.10.4}$$

This suggest that η is large for small δ and this presents a problem.

Solutions obtained using the r-based similarity transformations do not give the Blasius in the limit $\eta_0 \to \infty$. This is evident from comparisons with the Blasius solutions from three different approaches, i.e., comparing with the numerical solutions, the series expansions, and with the order of magnitude arguments.

If we retain the individual terms from either the Navier-Stokes equations, 1.2.3-5, or Cooke's equations, 1.2.1-2, that are transformed using the r-based transformations and are O(1) or higher according to the order of magnitude analysis, more than just the two dimensional boundary layer equations, (2.9.11-12), will remain. Unexpectedly, terms of $O(1/\delta)$ remain. Examining the series expansions, B.19 and B.20 for the nonlinear terms in the momentum equation, i.e., $u^*\partial u^*/\partial x^*$ and $v^*\partial u/\partial r^*$ and the individual terms (B.23) and (B.24) in the continuity equations, i.e.,

equations, i.e., $\partial u^*/\partial x^*$ and $\partial v^*/\partial r^*$, shows that the terms $O(1/\delta)$ or equivalently $O(\eta_0^3/R)$ do cancel leaving terms of the following magnitudes in Cooke's equations (see equations I.1.1-2 for the corresponding terms) :

$$O(1)+O(1)=O(1)+O(\delta), \tag{2.10.6a}$$

$$O(1)+O(1)+O(1)=0. \tag{2.10.6b}$$

In the Blasius limit, the following individual terms neglected by boundary layer approximation from the Navier-Stokes equations, i.e.,

$$\frac{1}{R}\frac{\partial^2 u}{\partial x^2}=O(1),\ u\frac{\partial v}{\partial x}=O\left(\frac{1}{\delta}\right),\ v\frac{\partial v}{\partial r}=O\left(\frac{1}{\delta}\right),\ \frac{1}{R}\frac{\partial^2 v}{\partial x^2}=O(1),\text{ and }\frac{1}{R}\frac{\partial^2 v}{\partial r^2}=O(1),$$

have the following magnitudes, according to the order of magnitude analysis :

$O(\delta^2)$, $O(\delta)$, $O(\delta^2)$, $O(\delta^3)$, and $O(\delta^3)$ respectively,

Discounting these terms, the individual terms $v^*/r^* \sim 1$ still remain in the continuity equation. The latter are not present in the two dimensional boundary layer equations.

Series expansions of all individual terms in Cooke's equations, 1.2.1-2, cancel to any order since they are based on these equations, however, individual terms should reflect the corresponding orders of magnitude obtained in Section 2.8 which deals with order of magnitude analysis applied to governing equations 1.2.1-2 or the corresponding Navier-Stokes.

Similarity transformations on the boundary layer equations should preserve orders of magnitude throughout the entire Navier-Stokes equations, not just the boundary layer equations themselves, i. e. , a neglected term from the Navier-Stokes equation

due to boundary layer approximation which is $O(\delta)$ must have the similarity transformation reflect that order of magnitude for that individual term even though the term is neglected. The r-based similarity transformations do not adhere to this concept, since higher order individual terms are produced which do not preserve the correct orders of magnitude to obtain the Blasius limit as $\eta_0 \to \infty$.

A finite axial velocity profile is obtained which is very near the Blasius in the limit as $\eta_0 \to \infty$ and this is very misleading. However, the highest order terms in the differential equations ($O(1/\delta)$) cancelled in order to produce the finite u. This cancellation can be seen term for term in the series expansions B.19 and B.20.

This natural and seemingly innocent similarity transformation does not yield correct physical results in the limit as $\eta_0 \to \infty$, as we have shown in this chapter, due to the implicit functional dependence of $\Gamma$ on $\eta_0$ and hence, x (Sawchuk 1985). This dependence brings about higher order terms associated with $\eta_0$ in individual terms in equation 2.1.7 that contain a derivative with respect to x. These higher order terms do not arise in the y-based similarity transformation because this implicit functional dependence on $\eta_0$ does not exist. This difference can be traced to using r or $y + 1$ as opposed to y in the similarity variable. A good example of this is in the radial velocity components of each transformation. For the r-based transformation

$$v(x,r) = \frac{\eta_0}{R}\{(\eta_1 + \eta_0)F'(\eta) - F(\eta)\}, \tag{2.10.6}$$

and the y-based transformation

$$v(x,y)=\frac{\eta_0}{R}\{\eta_1 G'(\eta_1)-G(\eta_1)\}, \tag{2.10.7}$$

It is clear that in the former

$v=v(\eta,\eta_0)=O(\eta_0^2)$ and in the latter that $v=v(\eta_1,\eta_0)=O(\eta_0)$. The higher order term is created by the r-based transformation which is not consistent with the order analysis leading to the Blasius.

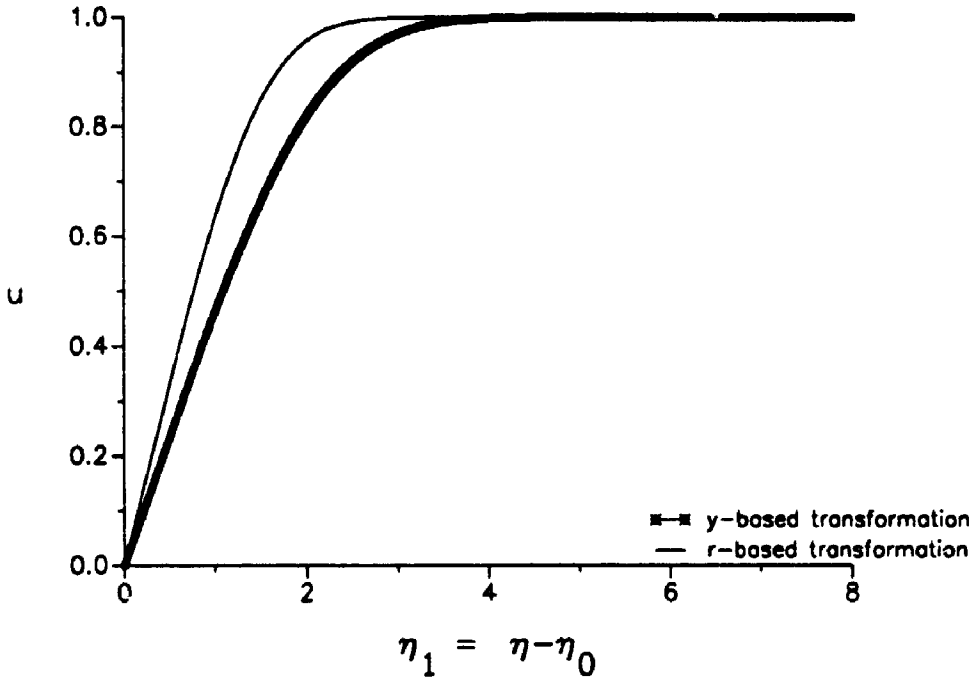


Figure 2.4.1 Comparison of axial velocity obtained from r-based vs. y-based transformations at $\xi = 0$.

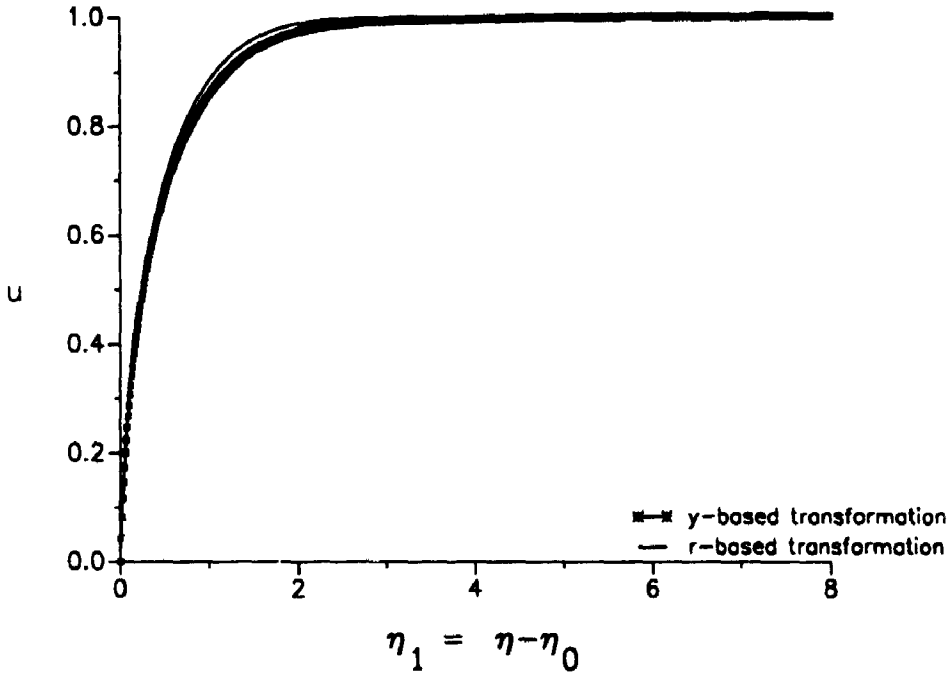


Figure 2.1.2 Comparison of axial velocity obtained from r-based vs. y-based transformations at $\xi = 40$.

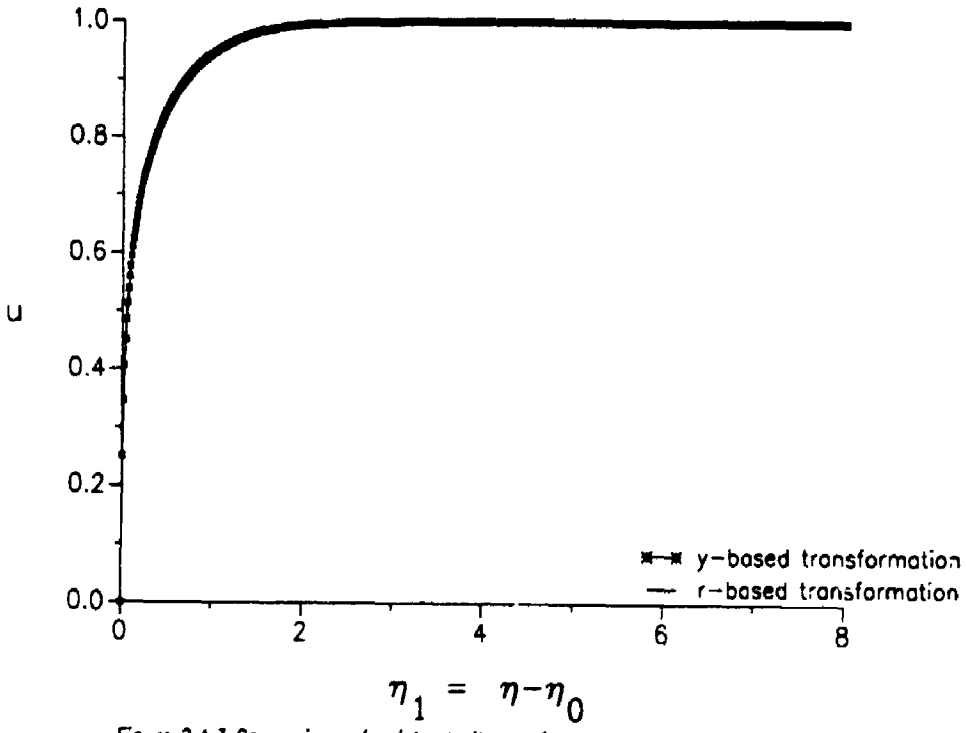


Figure 2.4.3 Comparison of axial velocity obtained from r-based vs. y-based transformations at $\xi = 1000$.

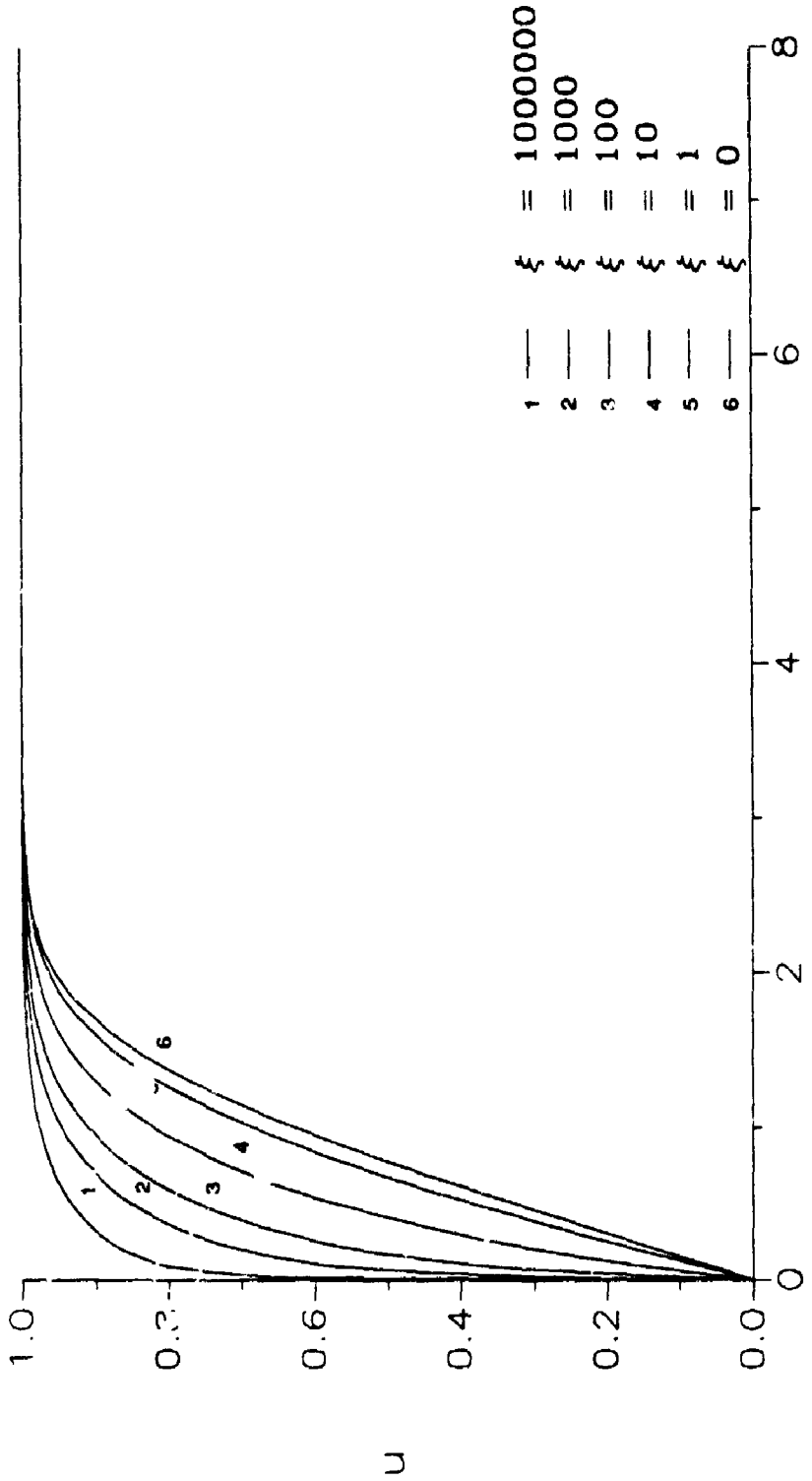


Figure 2.4.4 Axia velocity obtained from r-based transformation.

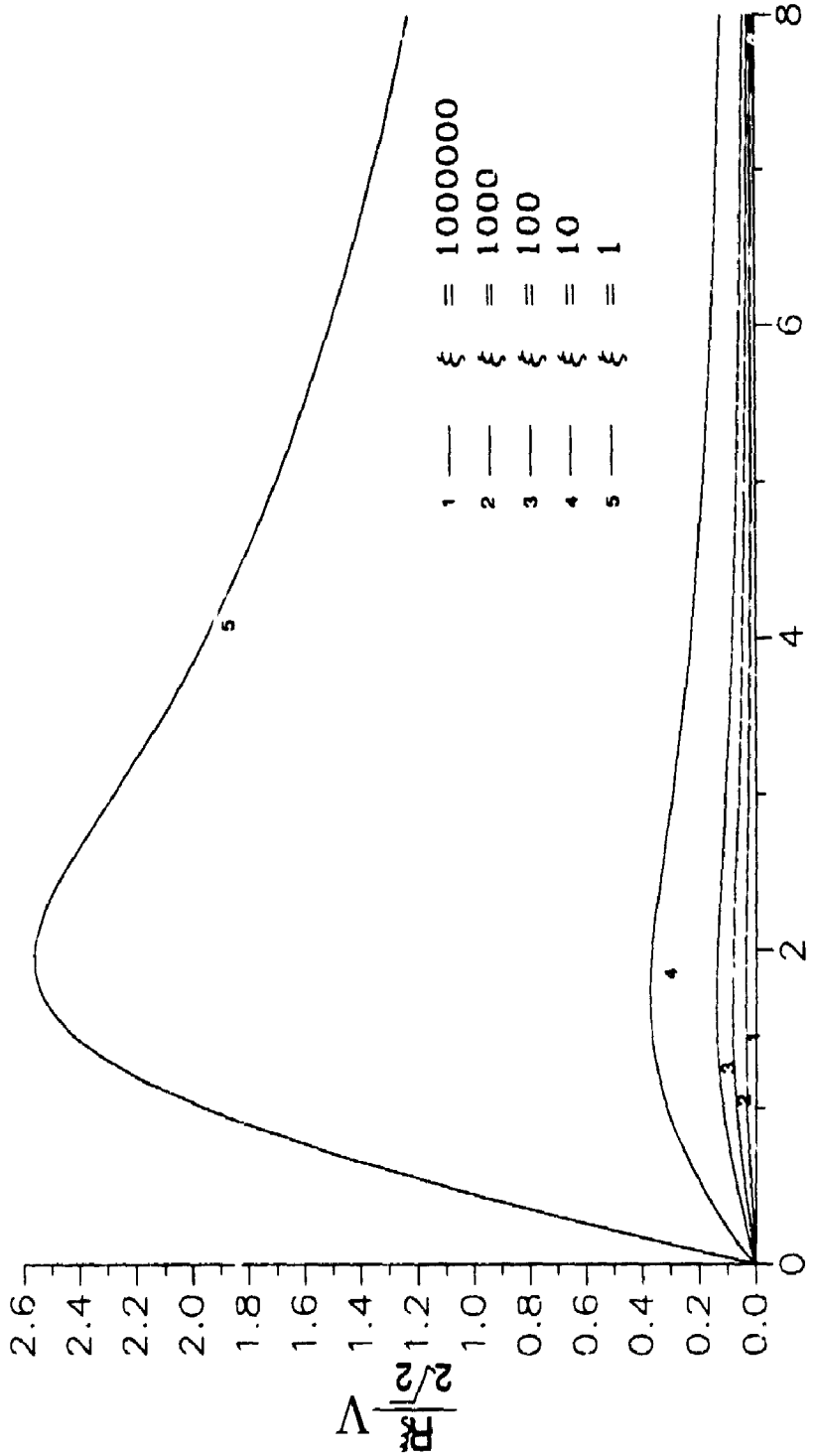


**Figure 2.4.5 Radial velocity parameter obtained through r-based transformation.**

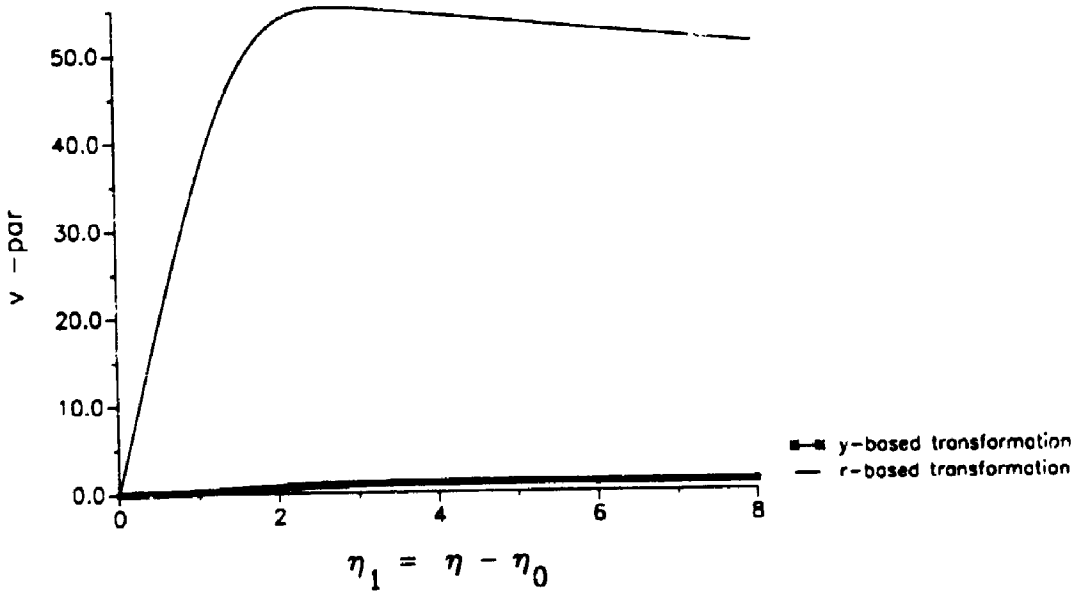


Figure 2.4.6 Comparison of radial velocity parameter (v–par) obtained from $r$–based vs. $y$–based transformations at $\xi = 0.05$.

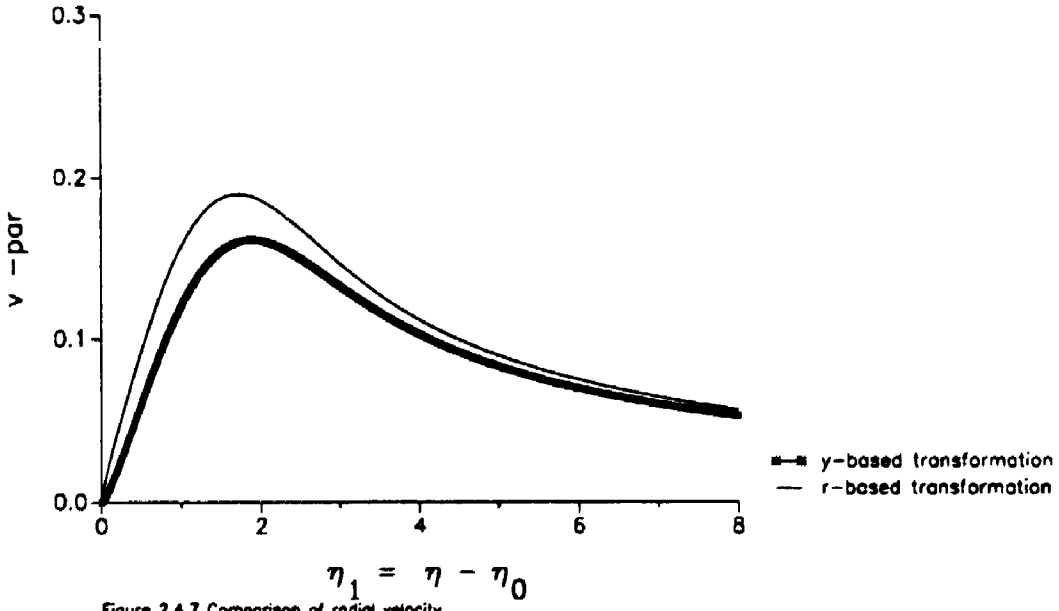


Figure 2.4.7 Comparison of radial velocity parameter (v-par) obtained from r-based vs. y-based transformations at $\xi = 40$.

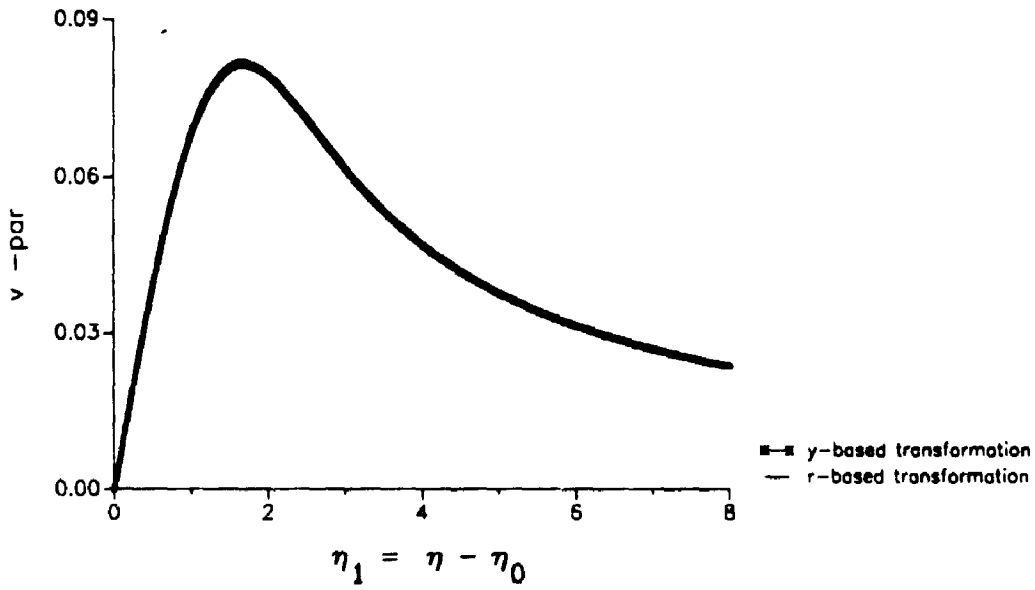


Figure 2.4.8 Comparison of radial velocity parameter (v-par) obtained from r-based vs. y-based transformations at $\xi$ = 1000.

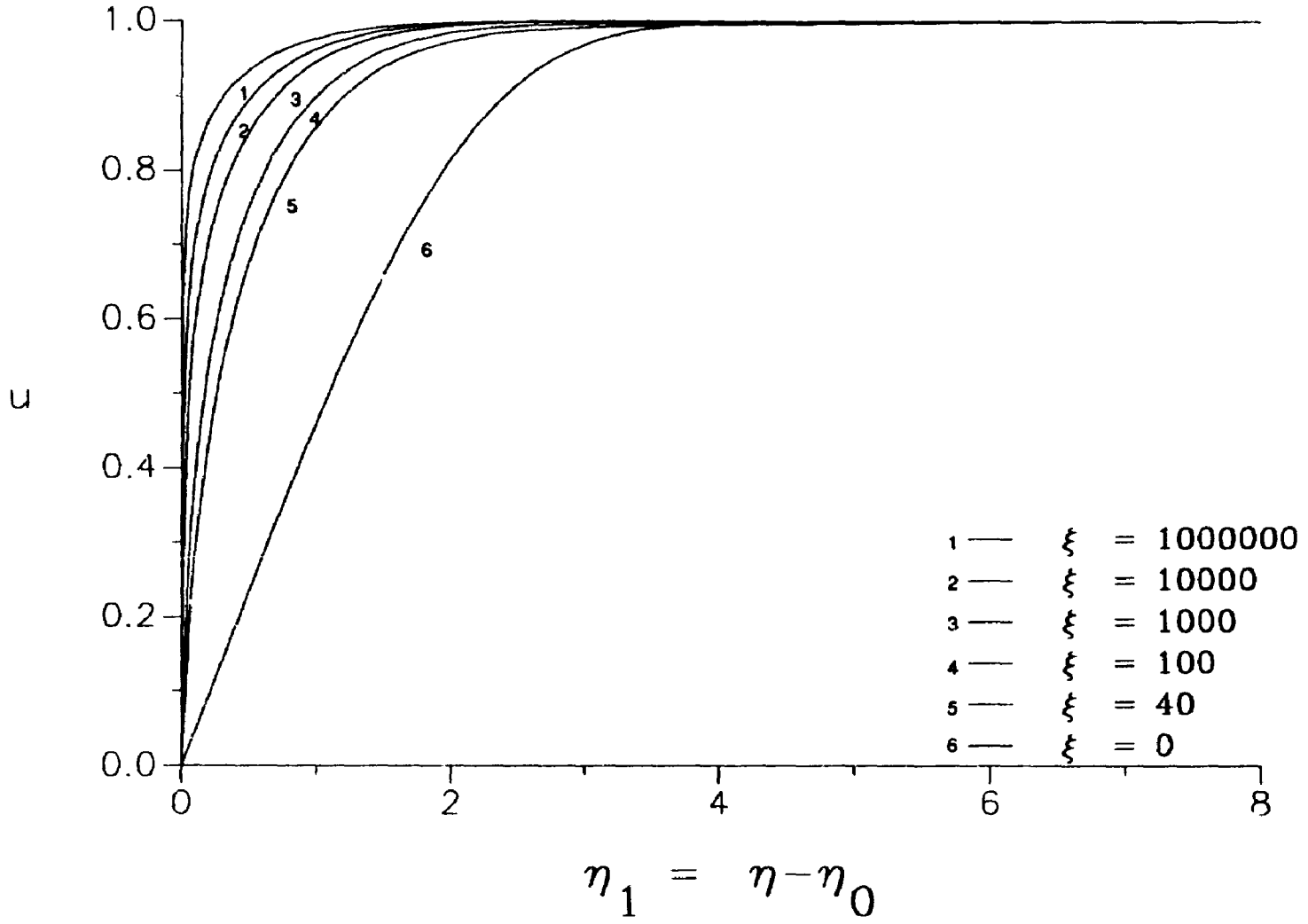


Figure 2.4.9 Axial velocity obtained by y-based transformation from 'quasi'-similar solution.

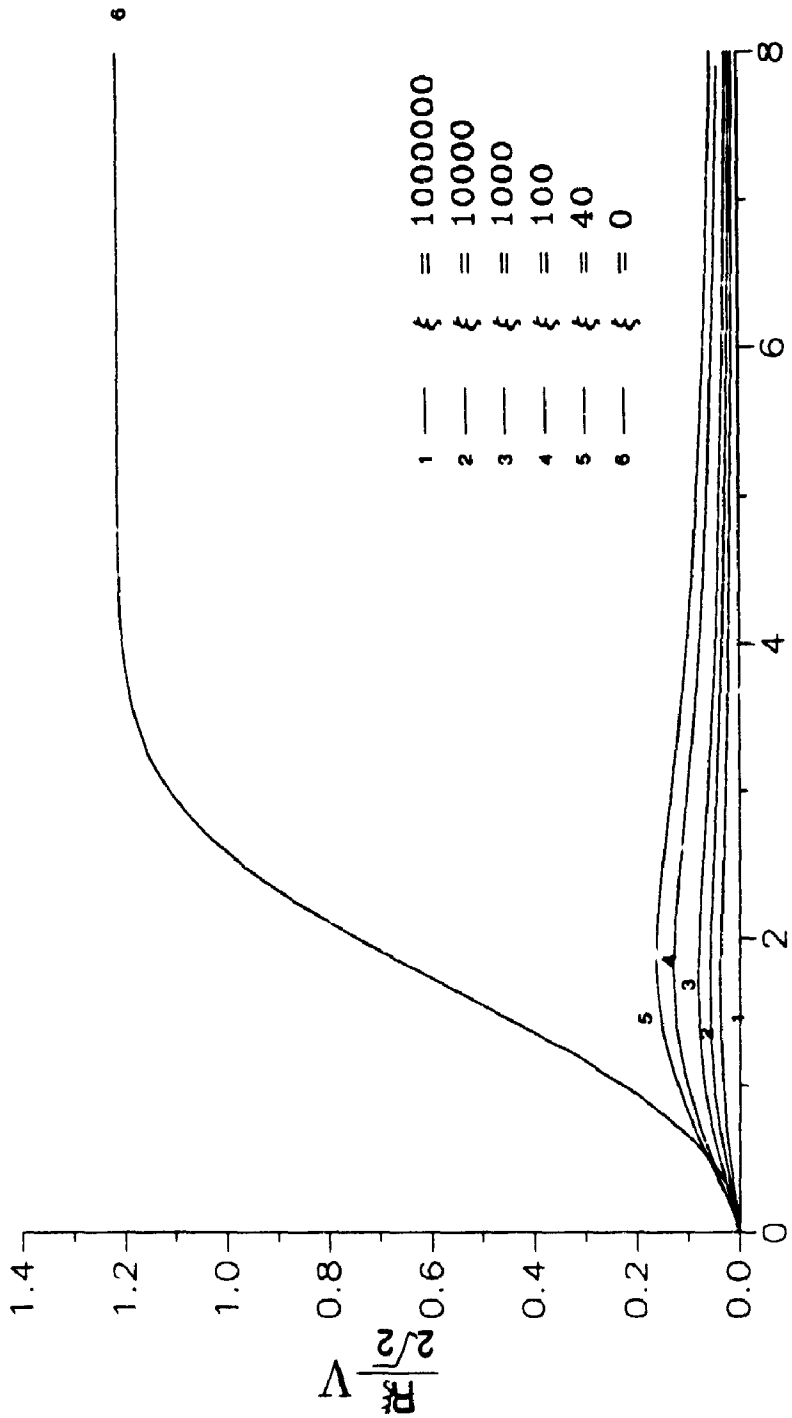


**Figure 2.4.10 Radial velocity parameter obtained by y-based transformation from 'quasi'-similar solution.**

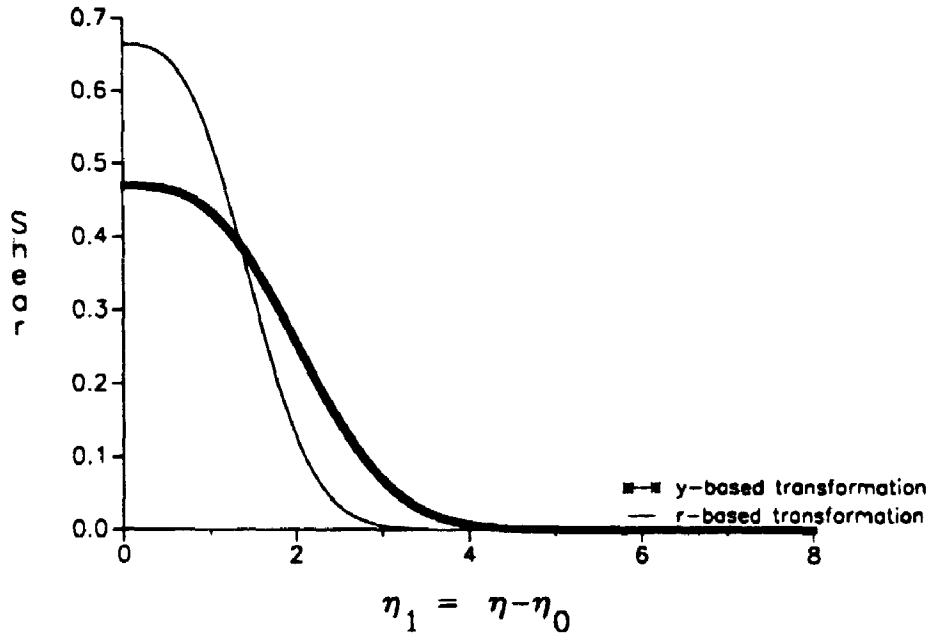


Figure 2.4.11 Comparison of shear stress parameter obtained from r-based vs. y-based transformations at $\xi = 0$

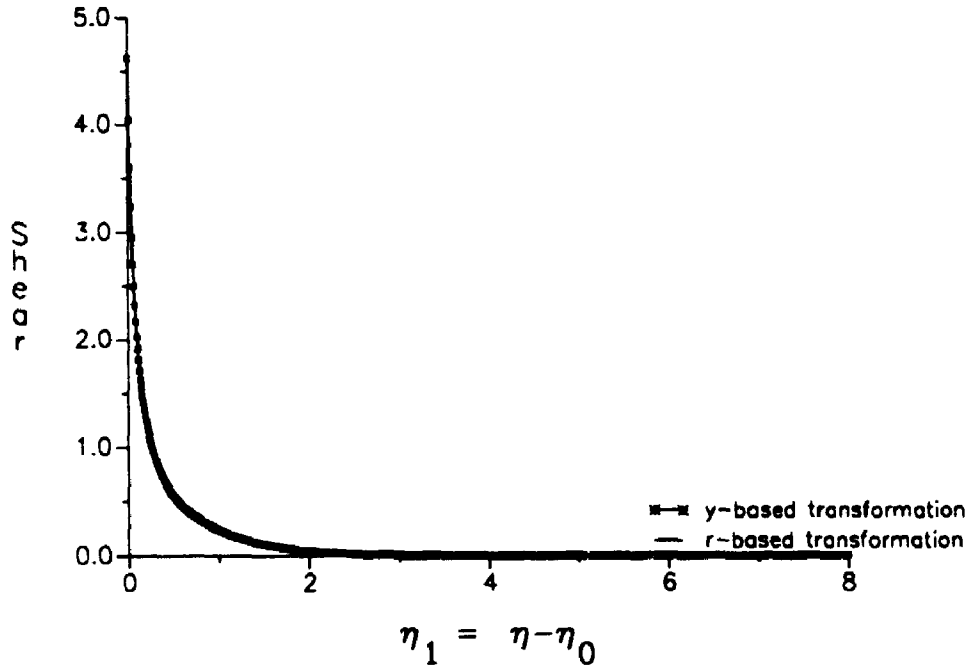


Figure 2.4.12 Comparison of shear stress parameter obtained from r-based vs. y-based transformations at $\xi = 40$.

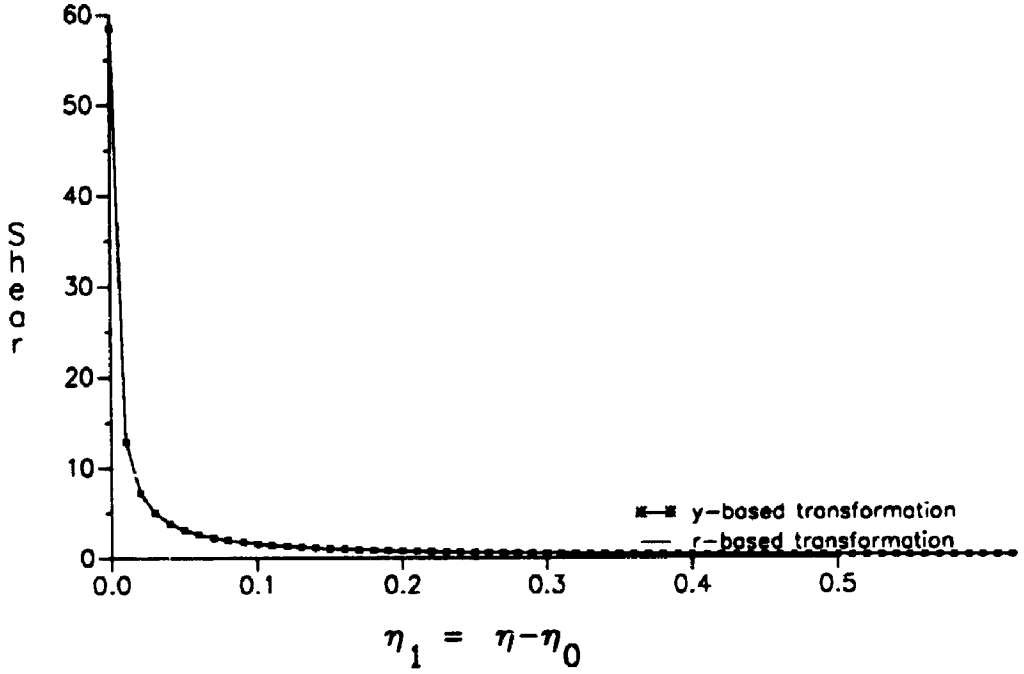


Figure 2.4.13 Comparison of shear stress parameter obtained from r-based vs. y-based transformations at $\xi = 1000$.

| | $\frac{\xi}{2\sqrt{2}} \frac{a\tau_o}{\mu U}$ | |
|---|---|---|
| $\xi$ | r - based | y-based |
| 0.000 | 0.66411443 | 0.46959000 |
| 0.050 | 0.67415925 | 0.43501037 |
| 40.000 | 4.80335419 | 4.61898253 |
| 100.000 | 9.30769200 | 9.32413583 |
| 500.000 | 33.04048158 | 32.91289622 |
| 1000.000 | 58.64608517 | 58.52907237 |
| 10000.000 | 425.93454100 | 425.84324282 |
| 100000.000 | 3340.58524616 | 3340.51059659 |
| 1000000.000 | 27459.72133193 | 27459.65827909 |

Table 2.4.1 Comparison of skin-friction coefficient obtained from r-based and y-based transformation 'quasi'-similar solutions.

| | $\Delta$ | |
|---|---|---|
| $\xi$ | r - based | y-based |
| 0.000 | 1.21678323 | 1.72093588 |
| 0.050 | 1.22294359 | 2.19165879 |
| 40.000 | 4.49925919 | 7.08996600 |
| 100.000 | 8.14726118 | 10.77160556 |
| 500.000 | 27.01557998 | 29.67987473 |
| 1000.000 | 47.09254461 | 49.76898040 |
| 10000.000 | 329.43904642 | 332.14308058 |
| 100000.000 | 2530.90289097 | 2533.62338454 |
| 1000000.000 | 20537.55444739 | 20540.28578380 |

Table 2.4.2 Comparison of displacement thickness between the r-based transformation vs. the y-based transformation.

| | $\theta$ | |
|---|---|---|
| $\xi$ | r - based | y-based |
| 0.000 | 0.46960228 | 0.66423656 |
| 0.050 | 0.47659754 | 0.99619155 |
| 40.000 | 3.39513927 | 5.76176508 |
| 100.000 | 6.54808174 | 9.02945454 |
| 500.000 | 23.34647029 | 25.89978784 |
| 1000.000 | 41.43569916 | 44.03105948 |
| 10000.000 | 301.14786449 | 303.79952157 |
| 100000.000 | 2361.38641532 | 2364.37149780 |
| 1000000.000 | 19413.08034811 | 19416.08736250 |

Table 2.4.3 Comparison of momentum thickness obtained by r-based vs. y-based transformation from 'quasi'-similar solutions.

# 3 PAST NUMERICAL SOLUTIONS

## 3.1 PRELIMINARY

Since the similarity solutions do not cover the full range of the flow along a circular cylinder, in this chapter, we consider numerical solutions. A brief sketch of earlier numerical solutions is presented in this chapter followed by present numerical solutions in the next.

Jaffe and Okamura (1968) use a shooting method, Cebeci, Wogulis and Partin (1968) and Cebeci (1970) use an implicit finite difference method outlined in Smith and Cebeci (1968). More recently, the Keller's Box method is used by Cebeci and Smith (1974). In all cases a stream function formulation with stretched coordinates is used. The full range of the problem is not covered, since the solution extending the furthest from past numerical results, only envelopes the range, $\xi = 0$ to $\xi \approx 64$. Also, velocity profiles are not emphasized. The asymptotic solutions of Glauert and Lighthill (1955) and Stewartson (1955) only adequately cover the latter parts of this range with regards to the skin-friction coefficient and displacement thickness. Velocity profiles near the surface of the cylinder are inaccurate here, as well as, for values of $\xi$ beyond this range. The range of existing numerical solutions should be extended to give a more accurate and complete picture of the flow.

## 3.2 METHOD OF JAFFE AND OKAMURA

Jaffe and Okamura (1968) proposed a solution to the problem which we briefly outline in order to compare with present solutions outlined in the next chapter.

With the variable $\eta_J = \frac{r^{*2} - a^2}{a^2 \xi}$ and the transformation

$$\psi = \sqrt{\frac{U \nu x^*}{a}} f = \frac{U}{4} \xi f(\eta_J, \xi), \tag{3.2.2}$$

[1]Cooke's equations, 1.2.6-7, are reduced to

$$((1 + \xi \eta_J) f'')' + f f'' = \xi \left( f' \frac{\partial f'}{\partial \xi} - f'' \frac{\partial f}{\partial \xi} \right). \tag{3.2.3}$$

The velocity components are given by

$$u = \frac{f'}{2} \text{ and } \frac{R\xi}{2\sqrt{2}} v = \frac{1}{\sqrt{2(1 + \xi \eta_J)}} (\eta_J f' - f - \xi f_\xi). \tag{3.2.4}$$

with the boundary conditions

$$f(0, \xi) = f'(0, \xi) = 0 \text{ and } f'(\eta_\infty, \xi) = 2. \tag{3.2.5}$$

A least squares fit is used to obtain the derivatives in the stream-wise direction. The velocity field is divided up into n stations. At n = 0 or $\xi = 0$ the derivatives vanish so that there is no need to approximate them. At n = 1, the two point backward difference equation, which is accurate to first order with respect to $\Delta\xi$ is given by :

$$\frac{f_1 - f_0}{\xi_1} = \frac{\partial f_1}{\partial \xi}. \tag{3.2.6}$$

---

1 There appears to be a misprint in the paper by Jaffe and Okamura (1968) in equation 3.2.3, in which f and $\psi$ are switched. We assume that the corrected version is as printed here.

At n = 2, the three point linear least squares fit is used, i.e. $\frac{\partial f_2}{\partial \xi} = \frac{|A_2|}{|D_2|}$, (3.2.7)

where $|D_2| \equiv \det\begin{bmatrix} 3 & \sum_i \xi^i \\ \sum_i \xi^i & \sum_i (\xi^i)^2 \end{bmatrix}$ and $|A_2| \equiv \det\begin{bmatrix} 3 & \sum_i f_i \\ \sum_i \xi^i & \sum_i \xi^i f_i \end{bmatrix}$

At $n \geq 3$, the four point quadratic least squares fit is used, i.e.

$$\frac{\partial f_n}{\partial \xi} = \frac{(|A_n| + 2|B_n|\xi)}{|D_n|}, \tag{3.2.8}$$

where $|D_n| \equiv \det\begin{bmatrix} 4 & \sum_i \xi & \sum_i (\xi^i)^2 \\ \sum_i \xi^i & \sum_i (\xi^i)^2 & \sum_i (\xi^i)^3 \\ \sum_i (\xi^i)^2 & \sum_i (\xi^i)^3 & \sum_i (\xi^i)^4 \end{bmatrix}$, $|A_n| \equiv \det\begin{bmatrix} 4 & \sum_i f_i & \sum_i (\xi^i)^2 \\ \sum_i \xi^i & \sum_i \xi^i f_i & \sum_i (\xi^i)^3 \\ \sum_i (\xi^i)^2 & \sum_i (\xi^i)^2 f_i & \sum_i (\xi^i)^4 \end{bmatrix}$,

and

$$|B_n| \equiv \det\begin{bmatrix} 4 & \sum_i \xi^i & \sum_i f_i \\ \sum_i \xi^i & \sum_i (\xi^i)^2 & \sum_i \xi^i f_i \\ \sum_i (\xi^i)^2 & \sum_i (\xi^i)^3 & \sum_i (\xi^i)^2 f_i \end{bmatrix}.$$

In the above expressions, f is replaced by $f'$ to obtain the approximation for the cross derivative in (3.2.3).[2]

The resulting equations are solved using a Runge-Kutta shooting method in the cross-stream direction. The Runge-Kutta shooting method that is used is assumed to be the standard fourth order method. The numerical convergence is tested by solving

2 There appears to be a misprint with the previous two determinants for equation 3.2.8 in the paper of Jaffe and Okamura (1968). We assume the corrected versions to be as printed in this paper.

at twice the number of stations in the stream-wise direction using one half the value of the original step size. For most results, accuracy is quoted to 3 and sometimes 4 decimal places. Ultimately, the skin friction coefficient, displacement and momentum thickness are given in the range $\xi = 0$ to $\xi = 40$.

The reason that the numerical results were obtained only to $\xi = 40$ is not given. Glauert and Lighthill (1955) mention that the limit of reliability of the asymptotic series solution for the skin-friction is "probably" near this point. Therefore, a reason for stopping the numerical method at this point in $\xi$ could be because it was felt that the asymptotic series already covered the range beyond. The increase in numerical error could be another reason. Another possiblity could be that using stretched coordinates brings about a further complication at this point. As one moves downstream, the numerical grid using stretched coordinates must be enlarged in order to satisfy the asymptotic conditions at the boundary layer edge because of the growth of the boundary layer. Thus, the authors could have stopped the procedure at $\xi = 40$ because the boundary layer thickness is quite large there and to keep increasing the grid further complicates the numerical method. Using this method requires much computer storage due to the least square approach which uses solutions at 4 previous stations in general. This fact, together with the need for a growing numerical grid and the subsequent care that must be taken in shooting may have also prevented the further advancement of the solution.

The range covered by the numerical solutions should overlap with that of the asymptotic solution in order to properly match ,i.e., numerical solutions should go beyond $\xi = 40$. Since velocity profiles near the surface of the cylinder obtained from the asymptotic solution are not reliable at this point, numerical solutions must go fur-

further in $\xi$ to obtain profiles that are reliable so that a proper comparison can be made with the asymptotic solution. This would give a more complete and accurate picture of the flow.

## 3.3 METHOD OF CEBECI

Cebeci (1970) used an implicit finite difference method to obtain the solution of equations 1.2.1-2 in the range $\xi \approx 0$ to $\xi \approx 64$. This solution extends the range of the series solution covered by Seban and Bond (1953) and Kelly (1954) and by the asymptotic solution of Stewartson (1955). The emphasis in this work is on turbulent flows, which involve many more details.

The transformation, $\psi = \sqrt{2\xi_c} f(\xi_c, \eta_c)$ with stretched coordinates

$$\xi_c = \rho\mu U x^* \text{ and } \eta_c = \frac{\rho U}{2\sqrt{2\xi_c}} \frac{r^{*2} - a^2}{2a}. \tag{3.3.1}$$

is substituted into governing equations 1.2.6-7 and gives

$$\left(\left(1 + \sqrt{\frac{8\nu x}{Ua}}\right) f''\right)' + ff'' = 2\xi_c \left(f' \frac{\partial f'}{\partial \xi_c} - f'' \frac{\partial f}{\partial \xi_c}\right). \tag{3.3.2}$$

with the boundary conditions $f(\xi_c, 0) = 0$, $f'(\xi_c, 0) = 0$, and $f'(\xi_c, \infty) = 1$. (3.3.3)

The coordinates are obtained from using a combination of the Mangler transformation, as given by Probstein-Elliott (1956), and the Levy-Lees (1959) transformation, i.e.,

$$d\bar{x} = \left(\frac{a}{L}\right)^2 dx^* = a\,dx \text{ and } d\bar{y} = \frac{(a + y^*)}{L} dy^* = (1 + y)a\,dy \tag{3.3.4}$$

and

$$d\xi_C = \rho\mu U d\bar{x} \text{ and } d\eta_C = \frac{\rho U}{\sqrt{2\xi_C}} d\bar{y}, \tag{3.3.5}$$

respectively. Note, $L = a$ is the characteristic length.

Transformation 3.3.5 is used to stretch both coordinates and remove a possible singularity at $\bar{x} = 0$ for flows dealing with sharp tipped bodies. Using of similarity variables can also remove this singularity (see Blottner (1975)).

These stretched coordinates remove a large variation in boundary layer thickness along the surface in most similar and nonsimilar flows. However, the variation is not removed in the flow along a semi-infinite circular cylinder. At $\xi \approx 64$, the boundary layer thickness is about 100, whereas near $\xi \approx 0$ it has the value of 6 (see Cebeci and Smith (1974)).

The stream function is translated by $\phi = f - \eta_C$, (3.3.6)

The stream function is translated by $\phi = f - \eta_C$ and after discretization equation 3.3.2 becomes

$$\left(\left(1 + \sqrt{\frac{8vx}{Ua}}\right)\phi''\right)' + (\phi + \eta_C)\phi'' = 2\xi_C((\phi' + 1)(A_1\phi' + A_2\phi_{n-1}' + A_3\phi_{n-2}'$$

$$-\phi''(A_1\phi + A_2\phi_{n-1} + A_3\phi_{n-2})), \tag{3.3.7}$$

where $\phi$'s without a subscript are evaluated at station n. The coefficients $A_1, A_2$ and $A_3$ are known at the current station including the quantities with subscripts n - 1 and n - 2 from the previous 2 stations. This reduces the problem to that of solving a nonlinear ordinary differential equation at station n.

At $\xi_C = 0$, stream-wise derivatives vanish and at $\xi_C = (\xi_C)_1$ a two point formula replaces the three point formula. At all other $\xi_C$, the three point formula takes over.

Linearizing the discretized equation is done by assigning the value of the previous iterate to each nonlinear factor, while all other values are at the current iterate value, i.e.,

$$\left(\left(1+\sqrt{\frac{8\nu x}{Ua}}\right)\phi''\right)'+(\phi_0+\eta_C)\phi''=2\xi_C((\phi_0'+1)(A_1\phi'+A_2\phi_{n-1}'+A_3\phi_{n-2}'$$

$$-\phi_0''(A_1\phi+A_2\phi_{n-1}+A_3\phi_{n-2})), \tag{3.3.8}$$

where the subscript 0 indicates the previous iterate.

The dependent variables $\phi$ and $\phi'$ are replaced by the perturbations $\delta\phi=\phi-\phi_0$ and $\delta\phi'=\phi'-\phi_0'$ etc.. This is used, in order to reduce round off error. The difference molecule seen in Figure 3.3.1 uses seven points, i.e., three in the stream-wise direction and five in the cross-stream direction. Cebeci and Smith (1968) use a variable grid which incorporates shorter steps near the wall and larger steps near the boundary layer edge. In the numerical procedure a Choleski decomposition is used to solve the resulting equations at each step of $(\xi_C)_n$.

## 3.4 METHOD OF CEBECI AND SMITH

Cebeci and Smith (1974) use the Keller's Box method to solve within the same range of $\xi$ as Cebeci (1970). The stream function and coordinates, equations 3.3.1, used in Cebeci (1970), which lead to equation 3.3.2 are the same.

They substitute $u_C=f'$ and $v_C=u_C'$, into equation 3.3.2 to obtain :

$$\left(\left(1+\sqrt{\frac{8\nu x}{Ua}}\eta_C\right)v_C\right)'=-fv_C+2\xi_C\left(u_C\frac{\partial u_C}{\partial\xi_C}-v_C\frac{\partial f}{\partial\xi_C}\right), \tag{3.4.1}$$

with the boundary conditions

$$f(\xi_C,0)=0,\ u_C(\xi_C,0)=0 \text{ and } u_C(\xi_C,\infty)=1. \tag{3.4.2}$$

The equations used to substitute for the derivatives of f are discretized over the box in Figure 3.4.1a, where central differences are taken in the cross-stream direction. Here, the discretization occurs at n instead of the midpoint $n-1/2$ because derivatives in $\xi_C$ do not occur and formulae remain second order while remaining simple algebraically.

Momentum equation 3.3.1 is discretized over the center of the box in Figure 3.4.1b, where central differences and averages are taken in both stream-wise and cross-stream directions.

The resulting difference equations are :

$$\frac{(f_j^n - f_{j-1}^n)}{h_j} = \frac{1}{2}((u)_j^n + (u)_{j-1}^n), \tag{3.4.3}$$

$$\frac{((u)_j^n - (u)_{j-1}^n)}{h_j} = \frac{1}{2}((v)_j^n + (v)_{j-1}^n), \tag{3.4.4}$$

$$\frac{\left(1+\sqrt{\frac{8vx}{U_e}}\eta\right)_j^n v_j^n - \left(1+\sqrt{\frac{8vx}{U_e}}\eta\right)_{j-1}^n v_{j-1}^n}{h_j} + \left(1+\frac{1}{k_n}(\xi_n+\xi_{n-1})\right)(f_j^n + f_{j-1}^n)\frac{(v_j^n + v_{j-1}^n)}{4}$$

$$-\frac{(\xi_n+\xi_{n-1})}{4k_n}(u_j^n + u_{j-1}^n)^2 + \frac{(\xi_n+\xi_{n-1})}{2k_n}((f_j^n + f_{j-1}^n)(v_j^{n-1} + v_{j-1}^{n-1}) - (f_j^{n-1} + f_{j-1}^{n-1})(v_j^n + v_{j-1}^n))$$

$$= -\frac{\left(1+\sqrt{\frac{8vx}{U_e}}\eta\right)_j^{n-1} v_j^{n-1} - \left(1+\sqrt{\frac{8vx}{U_e}}\eta\right)_{j-1}^{n-1} v_{j-1}^{n-1}}{h_j} + \left(\frac{1}{k_n}(\xi_n+\xi_{n-1}) - 1\right)(f_j^{n-1}$$

$$+f_{j-1}^{n-1})\frac{(v_j^{n-1} + v_{j-1}^{n-1})}{4} - \frac{(\xi_n+\xi_{n-1})}{4k_n}(u_j^{n-1} + u_{j-1}^{n-1})^2, \tag{3.4.5}$$

where the subscript C is dropped for simplicity.

The boundary conditions are given by $f_0^n = 0$, $u_0^n = 0$ and $u_j^n = 1$. (3.4.6)

Newton's method is used such that the dependent variables in (3.4.3-5) are replaced by the perturbations,

$$\delta f_j^{(i)} = f_j^{(i+1)} - f_j^{(i)}, \quad \delta u_j^{(i)} = u_j^{(i+1)} - u_j^{(i)} \text{ and } \delta v_j^{(i)} = v_j^{(i+1)} - v_j^{(i)},$$

second order terms in $\delta$ are neglected and a system of equations in the perturbation quantities arise which form a block tridiagonal structure and are solved with a block tridiagonal scheme. The degree of accuracy in this solution is not that clear, but it is assumed that Richardson extrapolation is used.

At $\xi_C = 0$ the transformed governing equations, (3.4.1), and difference equations, (3.4.3-5), do not contain $\xi_C$-dependent terms. An initial estimate or a previously derived solution is used to start the procedure.

A linear velocity profile is used to start the procedure, i.e., $u_C = a + b\eta_C$. Integrating and using the boundary conditions 3.4.7 gives the initial iterates:

$$f^{(0)} = \frac{\eta_C^2}{2\eta_\infty}, \quad u_C^{(0)} = \frac{\eta_C}{\eta_\infty}, \quad v_C^{(0)} = \frac{1}{\eta_\infty}. \tag{3.4.8}$$

Starting at a prescribed $(\xi_C)_n$ involves starting the procedure with a previously obtained profile or estimate or using a solution obtained by other means.

The growth of the boundary layer as one moves downstream necessitates the need to extend the computational grid. To carry this out, the skin-friction parameter, $v_C$, is tested at $\eta_\infty$ to see if $| v_C | \leq \varepsilon$, where $\varepsilon = 10^{-4}$, for example. If this condition is satisfied, then there is no need to increase the size of the grid. If not, then $\eta_\infty$ is extended such that

$$(\eta_\infty)_{n+1} = (\eta_\infty)_n + \Delta\eta_\infty,$$

where $\Delta\eta$ is a constant numerical step size.

Values of the dependent variables are assigned in the newly created region according to :

$$(u_C)_j^n \equiv 1,\ (v_C)_j^n \equiv 0,\ f_j^n \equiv (\eta_C)_j - \eta_{\infty}((\xi_C)_n) + f_{j-1}^n,\ \text{for } (\eta_{\infty})_n \le (\eta_C)_j \le (\eta_{\infty})_{n+1}. \quad (3.4.8)$$

The equation for the extended values of f, in (3.4.8), are obtained by integrating the equation :

$u_C = f'$, with $u_C = 1$.

Results are compared to the asymptotic solution by Stewartson (1955), the series expansion obtained by Seban and Bond (1953) and Kelly (1954), and with the previous numerical solution by Cebeci (1970).

The local skin-friction coefficient obtained by Cebeci and Smith (1974) agrees well with that of Cebeci (1970).

In order to compare the local skin-friction coefficient obtained by the asymptotic expansion of Stewartson (1955), Cebeci and Smith (1974) used two terms of the series in equation 1.3.30, i.e.,

$$\frac{\xi}{2}\frac{a}{\mu U}\tau_0 = \frac{2}{R_c^{1/2}}\left(\frac{1}{\ln(1/cR_c)} - \frac{3.854}{(\ln(1/cR_c))^3} + \dots\right) \quad (3.4.1)$$

The 'extra' leading term given by Stewartson (1955), i.e., $7/(2(\ln(1/cR_c))^2)$ is neglected. However, this term makes a significant difference in the numerical values obtained from the asymptotic expansion 1.3.30, especially for smaller values of $\xi$.

Table 3.4.1 compares the skin-friction coefficients of Cebeci (1970), Cebeci and Smith (1974), calculated values from the first two terms of Stewartson's (1955) series, the proper leading error estimate in the series and the lower order term given by

Stewartson (1955) which we refer to as the 'extra' term. Both numerical solutions begin to match with the asymptotic series 3.4.1 for larger values of $\xi$. The leading term neglected in (1.3.30), i.e., $O(1/R_c(\ln(1/cR_c))^4)$, appears to affect the truncated series in the first decimal place and its importance diminishes for increasing $\xi$. It does not account for the difference between the asymptotic and numerical solutions. Thus, the estimate may be too small.

Cebeci and Smith (1974) claim that it "appears" as though the asymptotic series is valid for $\xi > 14$. However, as we have already pointed out, accuracy of the asymptotic series for lower values of $\xi$ is questionable. The match with the numerical solutions with respect to skin-friction may be adequate, but not accurate. Although, it is not expected that the numerical solutions compare exactly with the series solution, since the series is asymptotic, a better match is expected for larger values of $\xi$. Thus, the numerical solutions should cover a larger range in $\xi$.

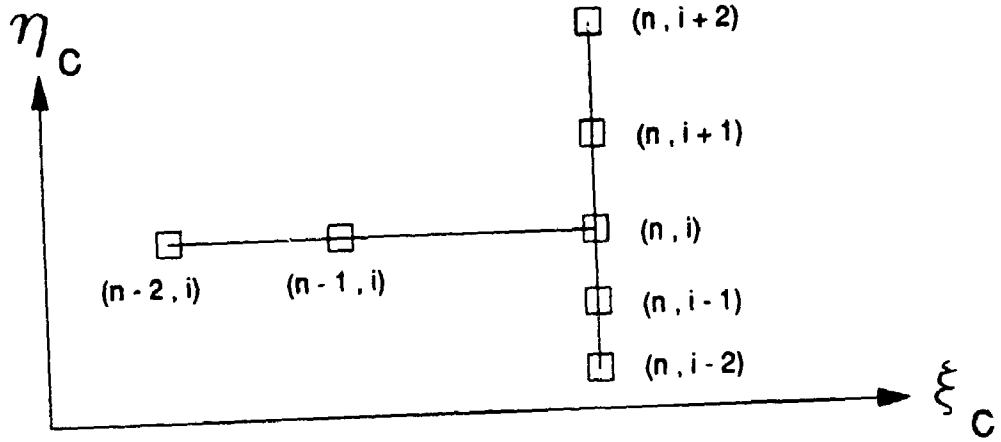


Figure 3.3.1 Discretization molecule for Cebeci (1968) and Cebeci (1970).

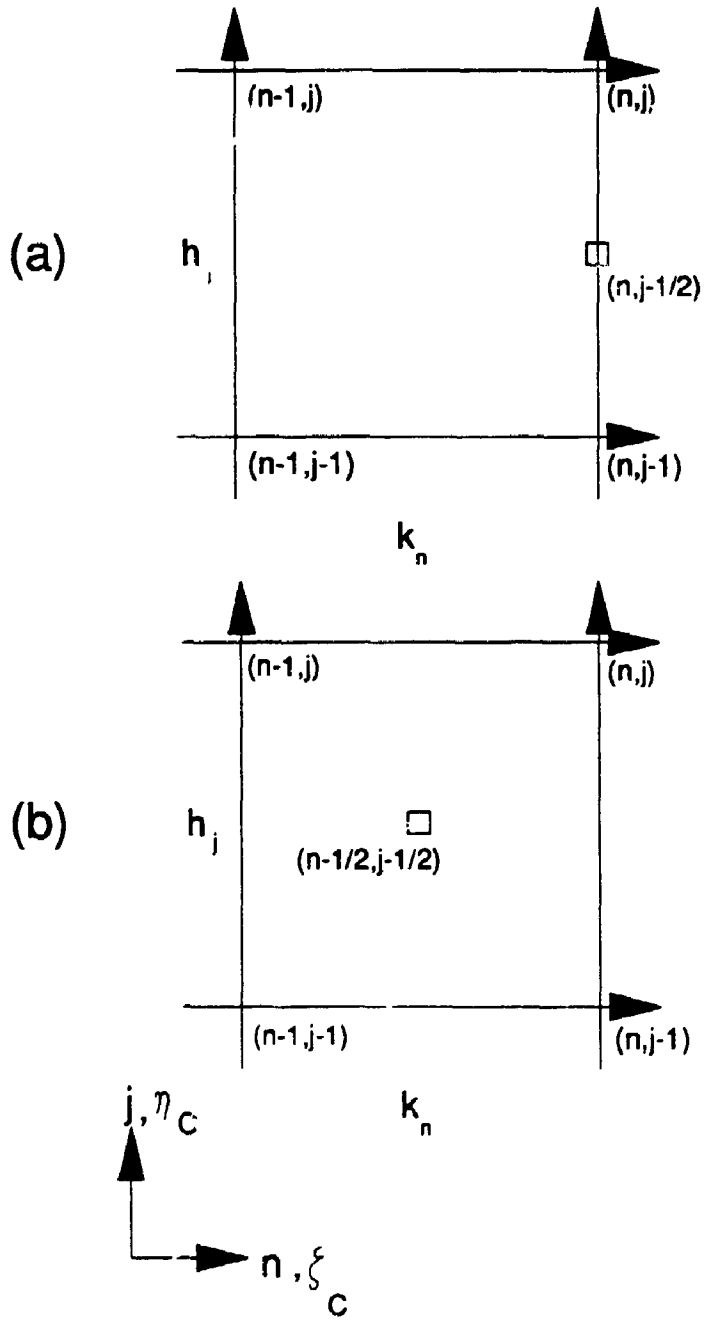


Figure 3.4.1 Box used in numerical grid for Keller Box method for (a) equations 3.4.1 and (b) momentum equation 3.4.2.

| | $\frac{\xi a}{2\sqrt{2}\mu U}\tau_0$ | | | | |
|---|---|---|---|---|---|
| $\xi$ | CS (1974) | C (1970) | S (1955) | Leading Error | Extra Term |
| 8.058 | 2.327 | 2.312 | 0.769 | 0.168 | 0.711 |
| 12.751 | 3.052 | 3.015 | 2.469 | 0.066 | 0.224 |
| 14.249 | 3.269 | 3.254 | 2.792 | 0.057 | 0.175 |
| 20.151 | 4.081 | 4.066 | 3.808 | 0.038 | 0.085 |
| 28.484 | 5.150 | 5.126 | 4.983 | 0.028 | 0.044 |
| 63.725 | 9.123 | 9.086 | 9.077 | 0.020 | 0.011 |

Table 3.4.1 Comparison of skin-friction coefficient obtained from Stewartson (1955) (S), Cebeci (1970) (C), and Cebeci and Smith (1974) (CS). The leading error is the error estimate from the order term in equation 1.4.2 and the extra term is the 3rd. term included from the same equation.

# 4 PRESENT NUMERICAL SOLUTIONS

## 4.1 PRELIMINARY

The numerical approach presented in this chapter uses Keller's Box method, but with a primitive variable and a similarity coordinate formulation. These features, which have not been used on this problem previously, were inspired by the similarity methods in Chapter 2. An accurate numerical solution in the full range of the problem is obtained and compared with previous numerical solutions.

On using primitive variables, we refer to Keller (1978) who mentions, "there is no great need in introducing a stream function when employing the Box scheme, but tradition and bad habits are difficult to overcome." It appears as though the Keller's Box scheme using primitive variables has not been applied to momentum equations in boundary layer flow problems, in general.

By using similarity coordinates, we find that the growth of the boundary layer as we move downstream is compensated for, i.e., the physical coordinates are scaled such that the value for the edge of the boundary layer which is used numerically remains constant. In fact, the computational grid is compressed to the extent that the boundary layer thickness appears to shrink, as we move downstream

On the other hand, the boundary layer thickness increases rapidly using stretched coordinates. The numerical use of stretched coordinates tends to give better accuracy near the surface of the cylinder for larger values of $\lambda$, where sharp variations in shear and velocity profiles are present. However, the loss of accuracy using similarity coordinates is small and may be minimized.

Similarity coordinates have, in the past, been used extensively in solving two dimensional boundary layer problems and some axially-symmetric problems. They have not been used numerically to solve flow problems whose governing equations involve the transverse curvature term, i.e., the y-term in parenthesis in $\partial[(1+y)\partial u/\partial y]/\partial y$, is the transverse curvature term.

Keller and Cebeci (1978) appear to choose the stretched coordinates for numerical solutions to axially-symmetric problems without any hesitation. However, Keller's Box scheme has been used with similarity-type coordinates (see Keller (1978)), but these are used in two dimensional problems and not axially-symmetric problems. Keller and Cebeci (1971) mention that "to treat axially-symmetric flows, the variable transformation needs to be modified slightly." This statement is made after a two dimensional plane laminar boundary layer problem is set up with similarity-type coordinates which are a consequence of the Levy-Lees (1959) transformation. The former statement implies that the variable transformation would be different, i.e., the Levy-Lees (1959) transformation would still be used, but, it would yield stretched coordinates for axially-symmetric problems (see equation 3.3.4 and 3.3.5). Stretched coordinates are used by Jaffe and Okamura (1968), Cebeci, Wogulis, and Partin

(1968), Cebeci (1970), and Cebeci and Smith (1974) in dealing with the boundary layer formed along the outer surface of a semi-infinite circular cylinder in incompressible laminar flow. Others have used the Levy-Lees (1959) transformation for other axially-symmetric boundary layer problems Thus, it appears that when dealing with any axially-symmetric boundary layer problems, stretched coordinates are the coordinates of choice, while similarity coordinates appear to be reserved for two-dimensional problems. This is reinforced by Blottner (1975), who reviews many numerical methods for two-dimensional and axially-symmetric boundary layer flows. Blottner mentions that the use of similarity variables keeps the boundary layer thickness uniform for many flow situations, but that it is most common to use the Levy-Lees (1956) transformations. Problems dealt with within Blottner (1975) use the latter. Although, the paper deals with general compressible two-dimensional or axially-symmetric boundary layer equations, the axially-symmetric case does not involve a transverse curvature factor.

The numerical solution we obtain covers the range of $\xi$ from 0 to 1000 with the possibility of being extended to any value of $\xi$. The range of some previous numerical solutions could possibly be extended, but they stop at the point where the asymptotic solutions appear to be valid with respect to the skin-friction coefficient. Even though the asymptotic solutions appear to be valid at a specified value of $\xi$, the accuracy in matching with past numerical solutions is not known.

We have also obtained a solution using the Keller's Box method with primitive variables but using stretched coordinates. The solution can be readily compared to that of previous authors, since essentially the same coordinates are used, and it also serves as a comparison to the present solution, which is obtained using similarity coordinates. It also covers the range of $\xi$ from 0 to 1000, but it demonstrates the growth of the boundary layer as we move downstream.

## 4.2 METHOD USING PRIMITIVE VARIABLES AND SIMILARITY COORDINATES

The Keller's Box method with primitive variables using similarity coordinates is used to solve the governing equations 1.2.6-7. The method is accurate and efficient in solving a system of partial differential equations that are parabolic (see Keller and Cebeci (1972b)). The method employs a non-uniform grid, is easy to program, stable, accurate to second order, and can be made more accurate with the use of Richardson extrapolation.

Transforming the coordinate system from (x,r) to ($\eta_1$, $\xi$) using :

$$\eta_1 = \left(\frac{Ua}{2\nu x}\right)^{1/2} y \text{ gives : } \frac{\partial}{\partial r} = \frac{2\sqrt{2}}{\xi}\frac{\partial}{\partial \eta_1}, \frac{\partial^2}{\partial r^2} = \frac{8}{\xi^2}\frac{\partial^2}{\partial \eta_1^2},$$

and

$$\frac{\partial}{\partial x} = -\frac{8\eta_1}{R\xi^2}\frac{\partial}{\partial \eta_1} + \frac{8}{R\xi}\frac{\partial}{\partial \xi}.$$

Applying this transformation to the governing equations 1.2.6-7 yields

$$(H\overline{R})_{\eta_1} + \tilde{Q}\overline{R} = \xi HPP_{\xi}, \tag{4.2.1}$$

$$\tilde{Q}_{\eta_1} - (2H-1)P = \xi HP_{\xi}, \tag{4.2.2}$$

where

$$\overline{R} = P_{\eta_1}, \tag{4.2.3}$$

and $P = u$, $Q = v$, $\tilde{Q} = H\left(\eta_1 P - \frac{\overline{R}\xi}{2\sqrt{2}}Q\right)$, and $H = 1 + \frac{\xi}{2\sqrt{2}}\eta_1$.

The boundary conditions become:

$P = \tilde{Q} = Q = 0$ at $\eta_1 = 0$ and $P \to 1$ as $\eta_1 \to \infty$.

The discretization of equations 4.2.1-2 over the box in Figure 4.2.1b gives :

$$H^j\overline{R}^j - H^{j-1}\overline{R}^{j-1} + \frac{h_j}{4}(\tilde{Q}^j + \tilde{Q}^{j-1})(\overline{R}^j + \overline{R}^{j-1}) - \xi_{n-1/2}H^{j-1/2}_{n-1/2}\frac{h_j}{4k_n}(P^j + P^{j-1})^2 = H^{j-1}_{n-1}\overline{R}^{j-1}_{n-1}$$

$$-H^j_{n-1}\overline{R}^j_{n-1} - \frac{h_j}{4}(\tilde{Q}^j_{n-1} + \tilde{Q}^{j-1}_{n-1})\left(\overline{R}^j_{n-1} + \overline{R}^{j-1}_{n-1}\right) - \xi_{n-1/2}H^{j-1/2}_{n-1/2}\frac{h_j}{4k_n}(P^j_{n-1} + P^{j-1}_{n-1})^2. \tag{4.2.4}$$

and

$$\tilde{Q}^j - \tilde{Q}^{j-1} - \frac{h_j}{2}\left\{\left(H^j_n + H^{j-1}_n - 1 + \frac{(\xi_n + \xi_{n-1})}{4k_n}(H^j_n + H^{j-1}_n + H^j_{n-1} + H^{j-1}_{n-1})\right\}(P^j + P^{j-1})\right.$$

$$= \frac{h_j}{2}\left\{H^j_{n-1} + H^{j-1}_{n-1} - 1 - \frac{(\xi_n + \xi_{n-1})}{4k_n}(H^j_n + H^{j-1}_n + H^j_{n-1} + H^{j-1}_{n-1})\right\}(P^j_{n-1} + P^{j-1}_{n-1}) + \tilde{Q}^{j-1}_{n-1} - \tilde{Q}^j_{n-1},$$

(4.2.5)

where

$$H_n^j = 1 + \frac{\xi_n}{2\sqrt{2}}\eta_1^j, \text{ etc. and } H_{n-1/2}^{j-1/2} = \frac{1}{4}(H_n^j + H_n^{j-1} + H_{n-1}^j + H_{n-1}^{j-1}) = 1 + \frac{\xi_{n-1/2}}{2\sqrt{2}}\eta_1^{j-1/2}.$$

Discretizing 4.2.3 at $\xi_n$ over the box in Figure 4.2.1a gives

$$P^j - P^{j-1} - \frac{h_j}{2}(\overline{R}^j + \overline{R}^{j-1}) = 0. \tag{4.2.6}$$

Note that any $t_{m-1/2} = \frac{1}{2}(t_m + t_{m-1})$ or $t^{m-1/2} = \frac{1}{2}(t^m + t^{m-1})$.

The boundary conditions in discretized form are given by :

$$P_n^0 = 0, \; P_n^j = 1 \text{ and } \tilde{Q}_n^0 = 0. \tag{4.2.7}$$

Keller and Cebeci (1971), Keller (1975), Keller (1978), and others state that this method is accurate to second order. Individual terms in the momentum equation, (4.2.1), and the continuity equation, (4.2.2), are discretized over the box centered at (j-1/2,n-1/2) (see Figure 4.2.1). Keller (1975) states that product terms or nonlinear terms can either be discretized as "a product of averages or average of products." The errors would still be second order, provided that the discretization is accurately centered, i.e., "symmetric centering must be maintained" (see Keller and Cebeci (1972a)). Keller (1978) states that any weighted averages with total weight unity of discretized product variables is acceptable. When the proper centering is maintained there is no serious effect on accuracy or stability. The choice of discretization with minimal arithmetic is ideal.

For this analysis, product terms such as $\bar{Q}\bar{R}$ and $(2H-1)P$ on the left hand side of the momentum and the continuity equations, i.e., (4.2.1 and 4.2.2), are first averaged in the n-direction and then each separate factor of the product is averaged in the j-direction. To illustrate this, consider the product from (4.2.1), viz,

$$(\bar{Q}\bar{R})^{j-1/2}_{n-1/2} = (\bar{Q}^{j-1/2}\bar{R}^{j-1/2})_{n-1/2}. \tag{4.2.8}$$

In a series expansion about $\xi_{n-1/2}$,

$$(\bar{Q}^{j-1/2}\bar{R}^{j-1/2})_n = (\bar{Q}\bar{R})^{j-1/2}_{n-1/2} + \frac{k_n}{2}\{(\bar{Q}\bar{R})_\xi\}^{j-1/2}_{n-1/2} + \frac{k_n^2}{8}\{(\bar{Q}\bar{R})_{\xi\xi}\}^{j-1/2}_{n-1/2} + \ldots, \tag{4.2.9}$$

$$(\bar{Q}^{j-1/2}\bar{R}^{j-1/2})_{n-1} = (\bar{Q}\bar{R})^{j-1/2}_{n-1/2} - \frac{k_n}{2}\{(\bar{Q}\bar{R})_\xi)\}^{j-1/2}_{n-1/2} + \frac{k_n^2}{8}\{(\bar{Q}\bar{R})_{\xi\xi}\}^{j-1/2}_{n-1/2} + \ldots, \tag{4.2.10}$$

Adding and rearranging the above two expressions yields :

$$(\bar{Q}\bar{R})^{j-1/2}_{n-1/2} = \frac{1}{2}\left((\bar{Q}^{j-1/2}\bar{R}^{j-1/2})_n + (\bar{Q}^{j-1/2}\bar{R}^{j-1/2})_{n-1}\right) - \frac{k_n^2}{8}\{(\bar{Q}\bar{R})_{\xi\xi}\}^{j-1/2}_{n-1/2} + \ldots \tag{4.2.11}$$

Expanding the first term on the right hand side of (4.2.11) about $(\eta_1^{j-1/2}, \xi_n)$ gives :

$$(\bar{Q}\bar{R})^{j-1/2}_n = \left(\bar{Q}^{j-1/2}_n \bar{R}^{j-1/2}_n\right) = \left(\frac{\bar{Q}^j_n + \bar{Q}^{j-1}_n}{2} - \frac{h_j^2}{8}(\bar{Q}_{\eta_1\eta_1})^{j-1/2}_n + \ldots\right)\left(\frac{\bar{R}^j_n + \bar{R}^{j-1}_n}{2}\right.$$

$$\left. - \frac{h_j^2}{8}\left(\bar{R}_{\eta_1\eta_1}\right)^{j-1/2}_n + \ldots\right) = \bar{Q}^{j-1/2}_n \bar{R}^{j-1/2}_n + O(h_j^2). \tag{4.2.12}$$

Similarly for the second term $(\bar{Q}\bar{R})^{j-1/2}_{n-1}$

in (4.2.11), we get the same expression as in (4.2.12), except that the subscript n is replaced by n - 1.

Hence, (4.2.11) can be rewritten as

$$(\bar{Q}\bar{R})^{j-1/2}_{n-1/2} = \frac{1}{2}\bar{Q}^{j-1/2}_{n}\bar{R}^{j-1/2}_{n} + \frac{1}{2}\bar{Q}^{j-1/2}_{n-1}\bar{R}^{j-1/2}_{n-1} + O(h_j^2 + k_n^2). \tag{4.2.13}$$

The product term in continuity equation 4.2.2, i.e.,

$$\{(2H-1)\bar{R}\}^{j-1/2}_{n-1/2}, \tag{4.2.14}$$

is discretized in the same manner as the term $\bar{Q}\bar{R}$ is above, where, $\bar{Q}$ is replaced by $(2H-1)$. The term $(\bar{Q}_{\eta_1})^{j-1/2}_{n-1/2}$ in (4.2.2) requires the series expansions of each of $\bar{Q}^{j}_{n}$, $\bar{Q}^{j-1}_{n}$, $\bar{Q}^{j-1}_{n-1}$ and $\bar{Q}^{j}_{n-1}$ about, $(\eta_1^{j-1/2}, \xi_{n-1/2})$, which are presented in Appendix G. Combining and rearranging these expansions yields :

$$(\bar{Q}_{\eta_1})^{j-1/2}_{n-1/2} = \frac{\bar{Q}^{j}_{n} + \bar{Q}^{j}_{n-1} - \bar{Q}^{j-1}_{n} - \bar{Q}^{j-1}_{n-1}}{2h_j} - \frac{h_j^2}{24}(\bar{Q}_{\eta_1\eta_1\eta_1})^{j-1/2}_{n-1/2} - \frac{k_n^2}{12}(\bar{Q}_{\eta_1\xi\xi})^{j-1/2}_{n-1/2} + \ldots, \tag{4.2.15}$$

Similarly, $(H\bar{R})_{\eta_1}$ from (4.2.1) becomes

$$\left((H\bar{R})_{\eta_1}\right)^{j-1/2}_{n-1/2} = \frac{H^{j}_{n}\bar{R}^{j}_{n} + H^{j}_{n-1}\bar{R}^{j}_{n-1} - H^{j-1}_{n}\bar{R}^{j-1}_{n} - H^{j-1}_{n-1}\bar{R}^{j-1}_{n-1}}{2h_j} - \frac{h_j^2}{24}\left((H\bar{P})_{\eta_1\eta_1\eta_1}\right)^{j-1/2}_{n-1/2} - \frac{k_n^2}{12}\left((H\bar{R})_{\eta_1\xi\xi}\right)^{j-1/2}_{n-1/2} + \ldots.$$

(4.2.16)

The products on the right hand side of the momentum and continuity equations 4.2.1 and 4.2.2, have each factor averaged separately in both directions of j and n. By using series expansions similar to those in Appendix G, the term $\xi HPP_\xi$ from (4.2.1) becomes :

$$\xi_{n-1/2}H^{j-1/2}_{n-1/2}\left(P^{j-1/2}_{n-1/2}-\frac{h_j^2}{8}(P_{\eta_1\eta_1})^{j-1/2}_{n-1/2}-\frac{k_n^2}{8}(P_{\xi\xi})^{j-1/2}_{n-1/2}+\ldots\right)\left(\frac{P^{j-1/2}_n-P^{j-1/2}_{n-1}}{k_n}-\frac{h_j^2k_n}{12}(P_{\eta_1\eta_1\xi})^{j-1/2}_{n-1/2}\right.$$

$$\left.-\frac{k_n^2}{24}(P_{\xi\xi\xi})^{j-1/2}_{n-1/2}+\ldots\right)=\frac{(\xi_n+\xi_{n-1})}{2}\frac{(H^j_n+H^{j-1}_n+H^j_{n-1}+H^{j-1}_{n-1})}{4}\left(\frac{P^j_n+P^{j-1}_n+P^j_{n-1}+P^{j-1}_{n-1}}{4}\right.$$

$$\left.-\frac{h_j^2}{8}(P_{\eta_1\eta_1})^{j-1/2}_{n-1/2}-\frac{k_n^2}{8}(P_{\xi\xi})^{j-1/2}_{n-1/2}+\ldots\right)\left(\frac{P^j_n+P^{j-1}_n-P^j_{n-1}-P^{j-1}_{n-1}}{2k_n}-\frac{h_j^2}{12}(P_{\eta_1\eta_1\xi})^{j-1/2}_{n-1/2}\right.$$

$$\left.-\frac{k_n^2}{24}(P_{\xi\xi\xi})^{j-1/2}_{n-1/2}+\ldots\right)=\frac{(\xi_n+\xi_{n-1})}{2}\frac{(H^j_n+H^{j-1}_n+H^j_{n-1}+H^{j-1}_{n-1})}{4}\left\{\frac{(P^j_n+P^{j-1}_n)^2}{8k_n}\right.$$

$$\left.-\frac{(P^j_{n-1}+P^{j-1}_{n-1})^2}{8k_n}\right\}+O(h_j^2+k_n^2). \qquad (4.2.17)$$

Similar treatment is given to the term $\xi HP_\xi$, in continuity equation 4.2.2.

Individual terms in equation 4.2.3 are averaged over $(\eta_1^{j-1/2},\xi_n)$, because there is no need to average in the n direction since derivatives with respect to $\xi$ are non-existent here. Averaging in the n-direction would complicate the discretized equations more than necessary. However, according to Keller (1975), there is no reason why averaging in the n-direction could not be applied. In either case, the desired second order accuracy is obtained (see Keller (1975)).

The differences in using a stream function formulation as in Cebeci and Smith (1974) as opposed to a primitive variable formulation are obvious when we compare the discretized equations of each approach. The stream function formulation involves two equations used for substitution, i.e., $u_C = f'$ and $v_C = u_C'$, which require the centering to be done at the edge of the box in Figure 4.2.1a. The remaining equation 3.4.1 is discretized at the center of the box. On the other hand, the primitive variable formulation involves only one equation for substituting, i.e., (4.2.3), which requires the centering be carried out at the edge of the box. The remaining two equations, (4.2.1) and (4.2.2), require the discretization to be done in the middle of the box to maintain the desired second order accuracy.

## 4.3 SOLUTIONS TO THE DISCRETIZED EQUATIONS

Taking $(\tilde{Q}^j_{n-1}, \overline{R}^j_{n-1}, P^j_{n-1})$to be known quantities for $0 \le j \le J$, the resulting system of equations (4.2.4-7) is one of 3 J + 3 unknowns, i.e.,

$(\tilde{Q}^j_n, \overline{R}^j_n, P^j_n)$, for $j = 0, 1, 2, \ldots, J$.

Using Newton's method to solve this system, rewriting the unknowns by dropping the subscript n, and introducing the ith iterates gives :

$\left(\tilde{Q}^j_{(i)}, \overline{R}^j_{(i)}, P^j_{(i)}\right)$, $i = 0, 1, 2, \ldots$

with the following initial values:

$$P^0_{(0)}=0,\quad \bar{R}^0_{(0)}=\bar{R}^0_{n-1},\quad \tilde{Q}^0_{(0)}=0,\quad P^j_{(0)}=P^j_{n-1},\quad \bar{R}^j_{(0)}=\bar{R}^j_{n-1},\quad \tilde{Q}^j_{(0)}=\tilde{Q}^j_{n-1},$$

for $1 \le j \le J-1$,

and $P^J_{(0)}=1$, $\bar{R}^J_{(0)}=\bar{R}^J_{n-1}$ and $\tilde{Q}^J_{(0)}=\tilde{Q}^J_{n-1}$.

We introduce the higher iterates, namely,

$$\tilde{Q}^j_{(i+1)}=\tilde{Q}^j_{(i)}+\delta\tilde{Q}^j_{(i)},\ \bar{R}^j_{(i+1)}=\bar{R}^j_{(i)}+\delta\bar{R}^j_{(i)},\ \text{and}\ P^j_{(i+1)}=P^j_{(i)}+\delta P^j_{(i)}, \tag{4.3.1}$$

which are substituted into equations 4.2.4-6. The quadratic terms in the perturbative quantities $\left(\delta\tilde{Q}^j_{(i)},\ \delta\bar{R}^j_{(i)},\ \delta P^j_{(i)}\right)$ are neglected..

The discretized equations 4.2.4-6, then, become:

$$\delta\tilde{Q}^j_{(i)}-\delta\tilde{Q}^{j-1}_{(i)}+FAC^j(\delta P^j_{(i)}+\delta P^{j-1}_{(i)})=m^j_{(i)}, \tag{4.3.2}$$

$$\beta^j\delta\bar{R}^j+\theta^j\delta\tilde{Q}^j+\gamma^j\delta P^j+\beta^j\delta\bar{R}^{j-1}+\theta^j\delta\tilde{Q}^{j-1}+\gamma^j\delta P^{j-1}=t^j, \tag{4.3.3}$$

and

$$\delta P^j_{(i)}-\delta P^{j-1}_{(i)}-\frac{h_j}{2}\left(\delta\bar{R}^j_{(i)}+\delta\bar{R}^{j-1}_{(i)}\right)=l^j_{(i)}, \tag{4.3.4}$$

where

$$m^j\equiv\tilde{Q}^{j-1}-\tilde{Q}^j-FAC^j(P^j+P^{j-1})+\tilde{Q}^{j-1}_{n-1}-\tilde{Q}^j_{n-1}$$

$$+\frac{h_j}{2}\left\{H^j_{n-1}+H^{j-1}_{n-1}-1-\frac{(\xi_n+\xi_{n-1})}{4k_n}(H^j_n+H^{j-1}_n+H^j_{n-1}+H^{j-1}_{n-1})\right\}(P^j_{n-1}+P^{j-1}_{n-1}),$$

$$t^j \equiv S^j_{n-1} + H^{j-1}\overline{R}^{j-1} - H^j\overline{R}^j - \frac{h_j}{4}(\bar{Q}^j + \bar{Q}^{j-1})(\overline{R}^j + \overline{R}^{j-1}) + \xi_{n-1/2}H^{j-1/2}_{n-1/2}\frac{h_j}{4k_n}(P^j + P^{j-1})^2,$$

$$l^j \equiv P^{j-1} - P^j + \frac{h_j}{2}(\overline{R}^j + \overline{R}^{j-1}), \tag{4.3.5}$$

$$S^j_{n-1} \equiv H^{j-1}_{n-1}\overline{R}^{j-1}_{n-1} - H^j_{n-1}\overline{R}^j_{n-1} - \frac{h_j}{4}(\bar{Q}^j_{n-1} + \bar{Q}^{j-1}_{n-1})\left(\overline{R}^j_{n-1} + \overline{R}^{j-1}_{n-1}\right) - \xi_{n-1/2}H^{j-1/2}_{n-1/2}\frac{h_j}{4k_n}(P^j_{n-1} + P^{j-1}_{n-1})^2,$$

$$\beta^j \equiv H^j + \frac{h_j}{4}(\bar{Q}^j + \bar{Q}^{j-1}),$$

$$\theta^j \equiv \frac{h_j}{4}(\overline{R}^j + \overline{R}^{j-1}),$$

$$\gamma^j \equiv -\xi_{n-1/2}H^{j-1/2}_{n-1/2}\frac{h_j}{2k_n}(P^j + P^{j-1}),$$

$$\tilde{\beta}^j \equiv -H^{j-1} + \frac{h_j}{4}(\bar{Q}^j + \bar{Q}^{j-1}),$$

and

$$FAC^j \equiv -\frac{h_j}{2}\left\{H^j_n + H^{j-1}_n - 1 + \frac{(\xi_n + \xi_{n-1})}{4k_n}(H^j_n + H^j_{n-1} + H^{j-1}_n + H^{j-1}_{n-1})\right\}.$$

The boundary conditions are given by :

$$\delta\bar{Q}^0_{(i)} = \delta P^0_{(i)} = \delta P^j_{(i)} = 0 \quad i = 0, 1, \ldots. \tag{4.3.6}$$

According to Keller (1978), solving for the perturbative quantities directly over solving for the absolute quantities during iteration is advantages in reducing cancellation errors.

Equations 4.3.2-4 can be rewritten as:

$$\overline{F}^j_{(i)}\delta^j_{(i)} - \overline{G}^j_{(i)}\delta^{j-1}_{(i)} = s^j_{(i)}, \quad j = 1,2,3,\ldots,J \text{, where} \tag{4.3.7}$$

$$\delta^j_{(i)} \equiv \begin{bmatrix} \delta\tilde{Q}^j_{(i)} \\ \delta\overline{R}^j_{(i)} \\ \delta P^j_{(i)} \end{bmatrix}, \qquad s^j_{(i)} \equiv \begin{bmatrix} m^j_{(i)} \\ t^j_{(i)} \\ l^j_{(i)} \end{bmatrix}, \tag{4.3.8}$$

and

$$\overline{F}^j_{(i)} \equiv \begin{bmatrix} 1 & 0 & FAC^j \\ \theta^j & \beta^j & \gamma^j \\ 0 & -\dfrac{h_j}{2} & 1 \end{bmatrix}, \qquad \overline{G}^j_{(i)} \equiv \begin{bmatrix} 1 & 0 & -FAC^j \\ -\theta^j & -\beta^j & -\gamma^j \\ 0 & \dfrac{h_j}{2} & 1 \end{bmatrix}.$$

This linear system is set up into a block tridiagonal structure. From (4.3.6), $\delta\tilde{Q}^0_{(i)} = \delta P^0_{(i)} = 0$, so that at j = 1, (4.3.7) becomes:

$$\delta\tilde{Q}^1 + FAC^1\delta P^1 = m^1,$$

$$\theta^1\delta\tilde{Q}^1 + \beta^1\delta\overline{R}^1 + \gamma^1\delta P^1 + \tilde{\beta}^1\delta\overline{R}^0 = t^1,$$

and

$$-\frac{h_1}{2}\delta\overline{R}^1 + \delta P^1 - \frac{h_1}{2}\delta\overline{R}^0 = l^1.$$

In matrix notation,

$$[E^1_{(i)}]\begin{bmatrix} \delta\overline{R}^0 \\ \delta\tilde{Q}^1 \\ \delta\overline{R}^1 \\ \delta P^1 \end{bmatrix} = \begin{bmatrix} m^1_{(i)} \\ t^1_{(i)} \\ l^1_{(i)} \end{bmatrix},$$

where

$$[E^1_{(i)}] \equiv \begin{bmatrix} 0 & 1 & 0 & FAC^1 \\ \beta^1_{(i)} & \theta^1_{(i)} & \beta^1_{(i)} & \gamma^1_{(i)} \\ -\frac{h_1}{2} & 0 & -\frac{h_1}{2} & 1 \end{bmatrix}.$$

Similarly at j = J, recalling that $\delta P^J = 0$,

$$[E^J_{(i)}] \begin{bmatrix} \delta^{J-1} \\ \delta\bar{Q}^J \\ \delta\bar{R}^J \end{bmatrix} = \begin{bmatrix} m^J_{(i)} \\ t^J_{(i)} \\ l^J_{(i)} \end{bmatrix},$$

where

$$[E^J_{(i)}] \equiv \begin{bmatrix} -1 & 0 & FAC^J & 1 & 0 \\ \theta^J_{(i)} & \beta^J_{(i)} & \gamma^J_{(i)} & \theta^J_{(i)} & \beta^J_{(i)} \\ 0 & -\frac{h_J}{2} & -1 & 0 & -\frac{h_J}{2} \end{bmatrix}.$$

The complete block tridiagonal system can be reduced to:

$$\begin{bmatrix} [E_{(i)}^1] & & & & \\ & -\overline{G}_{(i)}^2\overline{F}_{(i)}^2 & & 0 & \\ & & -\overline{G}_{(i)}^3\overline{F}_{(i)}^3 & & \\ & & & \ddots & \\ 0 & & & -\overline{G}_{(i)}^{J-1}\overline{F}_{(i)}^{J-1} & \\ & & & & [E_{(i)}^J] \end{bmatrix} \begin{bmatrix} \begin{bmatrix} \delta\overline{R}^0 \\ \delta^1 \end{bmatrix} \\ \delta^2 \\ \delta^3 \\ \vdots \\ \begin{bmatrix} \delta^{J-1} \\ \delta\bar{Q}^J \\ \delta\overline{R}^J \end{bmatrix} \end{bmatrix} = \begin{bmatrix} s_{(i)}^1 \\ s_{(i)}^2 \\ s_{(i)}^3 \\ \vdots \\ s_{(i)}^{J-1} \\ s_{(i)}^J \end{bmatrix} \quad (4.3.9)$$

or

$$\overline{A}_{(i)} z^j = s_{(i)}^j, \quad (4.3.10)$$

where $\overline{A}_{(i)}$ is the coefficient matrix in (4.3.9) and

$$z^1 \equiv \begin{bmatrix} \delta\overline{R}^0 \\ \delta\bar{Q}^1 \\ \delta\overline{R}^1 \end{bmatrix}, \quad z^j \equiv \begin{bmatrix} \delta P^{j-1} \\ \delta\bar{Q}^j \\ \delta\overline{R}^j \end{bmatrix}, 2 \le j \le J. \quad (4.3.11)$$

The coefficient matrix $\overline{A}_{(i)}$ is of order 3 J + 3 and the vectors $z^j$ and $s_{(i)}^j$ have that dimension. Decomposing $\overline{A}_{(i)}$ into $3 \times 3$ blocks, i. e.,

$$\overline{A}_{(i)} = \begin{bmatrix} A^1_{(i)} & C^1_{(i)} & & & & & & & \\ B^2_{(i)} & A^2_{(i)} & C^2_{(i)} & & & & & & \\ & \cdot & \cdot & \cdot & & & 0 & & \\ & & \cdot & \cdot & \cdot & & & & \\ & & & B^j_{(i)} & A^j_{(i)} & C^j_{(i)} & & & \\ & & & & \cdot & \cdot & \cdot & & \\ & & 0 & & \cdot & \cdot & \cdot & & \\ & & & & & & B^{J-1}_{(i)} & A^{J-1}_{(i)} & C^{J-1}_{(i)} \\ & & & & & & & B^J_{(i)} & A^J_{(i)} \end{bmatrix}, \qquad (4.3.11\,a)$$

where

$$A^1_{(i)} \equiv \begin{bmatrix} 0 & 1 & 0 \\ \tilde{\beta}^1_{(i)} & \theta^1_{(i)} & \beta^1_{(i)} \\ -\frac{h_1}{2} & 0 & -\frac{h_1}{2} \end{bmatrix}, \quad C^j_{(i)} \equiv \begin{bmatrix} FAC^j & 0 & 0 \\ \gamma^j_{(i)} & 0 & 0 \\ 1 & 0 & 0 \end{bmatrix},$$

$$1 \le j \le J-1, \quad (4.3.12\,a)$$

and

$$B^j_{(i)} \equiv \begin{bmatrix} 0 & -1 & 0 \\ 0 & \theta^j_{(i)} & \tilde{\beta}^j_{(i)} \\ 0 & 0 & -\frac{h_j}{2} \end{bmatrix}, \quad A^j_{(i)} \equiv \begin{bmatrix} FAC^j & 1 & 0 \\ \gamma^j_{(i)} & \theta^j_{(i)} & \beta^j_{(i)} \\ -1 & 0 & -\frac{h_j}{2} \end{bmatrix}.$$

$$2 \le j \le J \quad (4.3.12\,b)$$

The block tridiagonal factorization procedure to solve this system of equations is outlined in Appendix E.

## 4.4 GENERAL ITERATION STEP

At $\xi = 0$, terms on the right hand sides of equations 4.2.1 and 4.2.2 vanish, which reduce to the equations that give the Blasius solution. Since there is no previous step in $\xi$, all terms in the discretized equations 4.3.2-5 with subscript n - 1 vanish. Individual terms in equations 4.3.2-5 with factors of $\xi$ vanish, while $H = 1$.

At this point an initial profile is needed to begin the iteration procedure. A linear profile in $\eta_1$ is used, which satisfies the boundary conditions, i.e.,

$$P = \frac{\eta_1}{(\eta_1)_\infty}. \tag{4.4.1}$$

Differentiating (4.4.1) with respect to $\eta_1$ gives the initial profile for $\overline{R}$, i.e.,

$$\overline{R} = \frac{1}{(\eta_1)_\infty}. \tag{4.4.2}$$

Inserting (4.4.1) into (4.2.2), keeping in mind that $\xi = 0$ and $H = 1$, and then integrating with respect to $\eta_1$ gives $\bar{Q}$, viz,

$$\bar{Q} = \frac{\eta_1^2}{2(\eta_1)_\infty}. \tag{4.4.3}$$

Beginning calculations at the point where $\xi > 0$, involves starting the procedure with a known solution or using a previous solution, obtained by this or some other method, to be used as the initial iterate. An appropriate estimate of the solution may also be used as is done above for the case $\xi = 0$.

When iterations begin at a particular step in $\xi$, the initial iterate is the solution at the previous step, i.e.,

$$\left(\left(\tilde{Q}_n^j\right)_{(0)}, \left(\overline{R}_n^j\right)_{(0)}, \left(P_n^j\right)_{(0)}\right) = \left(\tilde{Q}_{n-1}^j, \overline{R}_{n-1}^j, P_{n-1}^j\right). \tag{4.4.4}$$

If this solution is smooth the error in the initial guess is $O(k_n)$. But Newton's method converges quadratically, i.e.,

$$\delta^{i+1} = O(\{\delta^1\}^2), \tag{4.4.5}$$

where $\delta$ is the error in the Newton iteration scheme. Therefore, the initial error is $O(k_n)$ and after one iteration the error is $\delta^1 = O(k_n^2)$. This is in keeping with second order accuracy.

Iterations start with a given initial profile and provided the next step in $\xi$ is $O(k_n)$, then the desired accuracy will be maintained. In applying the Keller's Box procedure, it is found that three iterations were carried out at each step in $\xi$, so that the error of the iteration is much lower than the second order truncation error. In fact, it is $O(k_n^8)$. Keller (1978) states that if the step size in the downstream direction is too large, or a different initial guess is used, or if there is a slight error in the computer coding that it is not uncommon for three or four iterations to occur.

At a general stage in calculation where $\xi > 0$, the right hand sides of discretized equations 4.2.4 and 4.2.5 are calculated only once for all iterations. During the

current iteration, the quantities $[m^j_{(i)},\ t^j_{(i)},\ l^j_{(i)}]$ are calculated from equations 4.3.5. Thus, the inhomogeneous terms $s^j_{(i)}$, as well as the coefficients in equations 4.3.2-4 are known in (4.3.8).

The matrix elements for $[A^j_{(i)},\ B^j_{(i)},\ C^j_{(i)}]$ are determined from 4.3.12.

The factorization in Appendix E, equation E.1 is now used. The quantities $d^1_{(i)},\ e^1_{(i)},\ g^1_{(i)}$ are calculated for j = 1 from (E.3) and $x^1_{(i)},\ y^1_{(i)},\ z^1_{(i)}$ from (E.12). Then the matrix elements of $\alpha^j_{(i)}$ are found from (E.4), $d^j_{(i)},\ e^j_{(i)},\ g^j_{(i)}$ from (E.5), and $x^j_{(i)},\ y^j_{(i)},\ z^j_{(i)}$ from (E.14) for j = 2. The last step is successively repeated for j = 3, 4, 5, ..., J.

The perturbation quantities $\delta^j_{(i)}$ are then calculated from (E.15-17). Those quantities are then added to the latest iterates according to (4.3.1) and the calculations are repeated until convergence is achieved. Then, the whole procedure is repeated at the next step in $\xi$.

The convergence criterion is given by :

$$\left|\left(\delta\overline{R}^0_n\right)_{(i)}\right| < \text{tolerance} = 10^{-6}. \tag{4.4.6}$$

In general, criterion 4.4.6 brings about three iterations at each step in $\xi$.

Another criterion is used to test the shear stress parameter at the boundary layer edge to see if the numerical grid needs to be enlarged in order to accommodate the growth of the boundary layer. This criterion is given by :

$$\left|\overline{R}(\xi_n, \eta_\infty)\right| < \text{tolerance} = 10^{-4}. \tag{4.4.7}$$

If (4.4.7) is satisfied, then the solution advances to the next step in $\xi$. Otherwise, the numerical grid must be extended and values of the dependent variables at the new grid points must be determined and implemented. However, because of the use of similarity coordinates, condition 4.4.7 was always satisfied. In fact, criterion 4.4.7 was always satisfied even after tightening the tolerance to a value of $10^{-6}$. The value for the edge of the boundary layer can remain constant with the use of similarity coordinates, once an appropriate value is obtained. A value is chosen such that it is minimal.

Approaching the edge of the boundary layer, as one moves downstream, shear stress parameters progressively decrease in value and the axial velocity profiles approach unity sooner. Thus, it appears as though the boundary layer thickness is decreasing in value as one moves downstream. This trend is consistent throughout the entire solution.

The solution at the needle limit is described by the velocity profile $P = 1$, everywhere, except for no-slip at the surface, $Q = 0$, and $(\xi a)/(2\sqrt{2}\mu U)\tau = 0$, except for an infinite skin friction coefficient. Although this actual solution can never be obtained numerically, the solutions we obtain using similarity coordinates as the needle limit is approached favourably demonstrate a trend towards the limiting solution.

With the advantage of compensating for boundary layer growth, similarity coordinates could be used to scale the growth of the boundary layer in turbulent flows.

Thus, it may be advantageous to use similarity coordinates over the Levy-Lees coordinates for axially-symmetric turbulent boundary layer problems as well, since the boundary layer grows very large using other coordinates.

## 4.5 RICHARDSON EXTRAPOLATION

Richardson extrapolation is applied to the results to increase the accuracy of the solution. An estimate of the truncation error which is a polynomial in even powers of the step sizes exists and begins with second order. This is demonstrated in the earlier error analysis in Section 4.2. An extrapolation is applied to improve accuracy by two orders of magnitude with each application. Also, Keller and Cebeci (1971), Keller (1975), and Keller (1978) state and show that the errors in the numerical solution have asymptotic expansions in powers of the squares of the mesh sizes so that Richardson extrapolation is justified.

In using Richardson extrapolation, three kinds of error are confronted. Firstly, round-off error is the error accumulated by rounding off values that are stored in a computer to a finite number of digits. Next, iteration error is the error due to iterations being terminated at a finite stage. Finally, truncation error is the error due to approximation using a finite number of terms in a series expansion.

It is assumed that an exact solution is available in order to use Richardson extrapolation. However, this is not true in practice due to round-off error, but round-off error can affect a value in the 14th or 15th decimal place with the use of double precision programming. According to Keller and Cebeci (1972b) round-off error is usually sev-

eral orders of magnitude less than the truncation error tolerated. Thus, an extrapolation will only increase the accuracy if the iteration errors are smaller than the truncation errors. We saw in Section 4.4 that the iteration error is six orders of magnitude smaller than the truncation error.

Three numerical solutions have been obtained using three different mesh sizes. When extrapolated, fourth order accuracy is obtained.

When applying Richardson extrapolation to the displacement and momentum thickness, the order of operation of numerical procedures performed on the integrals involved is very important. The displacement thickness involves an integral with a linear integrand. The integral may be numerically evaluated first and the result extrapolated or the integrand may be first extrapolated and the result integrated numerically. However, this is not the case for the momentum thickness because it involves an integrand which is non-linear. Here, the integrand must first be extrapolated and then the integral is evaluated numerically.

In the following, we demonstrate the need for the order of operations to occur. The factors used in extrapolation, which are the values obtained from combining the different mesh sizes of individual solutions for Richardson extrapolation, are obtained in Appendix F. Defining,

$$\Delta_1 \equiv \sqrt{\frac{Ua}{\nu x}} \int_1^{\infty} (1-u_1) r\,dr\,,\ \Delta_2 \equiv \sqrt{\frac{Ua}{\nu x}} \int_1^{\infty} (1-u_2) r\,dr,$$

$$\text{and } \Delta_3 \equiv \sqrt{\frac{Ua}{\nu x}} \int_1^{\infty} (1-u_3) r\,dr \tag{4.5.1}$$

and, in general, the factors $\alpha_1$, $\alpha_2$, and $\alpha_3$, where

$$\alpha_1 + \alpha_2 + \alpha_3 = 1, \tag{4.5.2}$$

we have

$$\alpha_1\Delta_1 + \alpha_2\Delta_2 + \alpha_3\Delta_3 = \Delta_E, \tag{4.5.3}$$

where $\Delta_E \equiv$ extrapolated displacement thickness obtained by extrapolating the displacement thickness calculated from three individual solutions.

We also define, $u_E \equiv \alpha_1 u_1 + \alpha_2 u_2 + \alpha_3 u_3$. (4.5.4)

Then,

$$\sqrt{\frac{Ua}{\nu x}} \int_1^{\infty} \{(\alpha_1+\alpha_2+\alpha_3) - u_E\} r\,dr = \sqrt{\frac{Ua}{\nu x}} \int_1^{\infty} \{\alpha_1+\alpha_2+\alpha_3 - \alpha_1 u_1 - \alpha_2 u_2 - \alpha_3 u_3\} r\,dr$$

$$= \sqrt{\frac{Ua}{\nu x}} \left\{ \alpha_1 \int_1^{\infty} (1-u_1) r\,dr + \alpha_2 \int_1^{\infty} (1-u_2) r\,dr + \alpha_3 \int_1^{\infty} (1-u_3) r\,dr \right\}$$

$$= \alpha_1\Delta_1 + \alpha_2\Delta_2 + \alpha_3\Delta_3 = \Delta_E. \tag{4.5.5}$$

Hence, the order of operation in numerically calculating the extrapolated displacement thickness is of no consequence.

Obtaining an extrapolated momentum thickness requires the numerical integration of the already extrapolated axial velocity profile within the integrand.

Defining

$$\Theta_1 = \sqrt{\frac{aU}{\nu x}} \int_1^{\infty} u_1(1-u_1) r\,dr,$$

$$\Theta_2 = \sqrt{\frac{aU}{\nu x}} \int_1^{\infty} u_2(1-u_2) r\,dr,$$

and

$$\Theta_3 = \sqrt{\frac{aU}{\nu x}} \int_1^{\infty} u_3(1-u_3) r\,dr. \tag{4.5.6}$$

and inserting $u_E$ into the expression for momentum thickness yields

$$\sqrt{\frac{Ua}{\nu x}} \int_1^{\infty} u_E(1-u_E) r\,dr = \sqrt{\frac{Ua}{\nu x}} \int_1^{\infty} (\alpha_1 u_1 + \alpha_2 u_2 + \alpha_3 u_3 - \alpha_1^2 u_1^2 - \alpha_2^2 u_2^2 - \alpha_3^2 u_3^2$$

$$-2\alpha_1\alpha_2 u_1 u_2 - 2\alpha_1\alpha_3 u_1 u_3 - 2\alpha_2\alpha_3 u_2 u_3) r\,dr \tag{4.5.7}$$

But,

$$\alpha_1\Theta_1 + \alpha_2\Theta_2 + \alpha_3\Theta_3 = \sqrt{\frac{Ua}{\nu x}} \int_1^{\infty} (a_1 u_1 - a_1 u_1^2 + a_2 u_2 - a_2 u_2^2 + a_3 u_3 - a_3 u_3^2) r\,dr. \tag{4.5.8}$$

Comparison of (4.5.7) to (4.5.8) shows that

$$\sqrt{\frac{Ua}{vx}}\int_1^{\infty} u_E(1-u_E)r\,dr \neq \alpha_1\Theta_1+\alpha_2\Theta_2+\alpha_3\Theta_3,$$

and that the extrapolated velocity is needed initially for the proper calculation. Three solutions, $u_1(h^1,k^1)$, $u_2(h^2,k^2)$ and $u_3(h^3,k^3)$, are obtained in the range, $\xi=0$ to $\xi=1000$, and are extrapolated using the formula in Appendix F. The derivation to obtain the formula for the fourth order solution is also presented in Appendix F. The same extrapolations apply to the three dependent variables, viz, P, $\tilde{Q}$, and $\overline{R}$.

Step sizes are small so that a very accurate solution is obtained and used for comparison later on. Step sizes are small throughout the entire range, especially in the cross stream direction, so that interpolations are not needed further down stream where rapid changes in profiles occur near the wall. An $\eta_\infty$ of 8 is settled upon after some experimentation. An ETA-10 Mainframe computer was used, which sustains 16 significant figures.

The mesh that is employed is given in Table 4.5.1.

For the range $\xi=0$ to $\xi=0.005$, the three solutions, i.e., $u_1(h^1,5k^3)$, $u_2(2h^1,k^3)$ and $u_3(h^1,k^3)$,combine, using equation F.5 from Appendix F, to give :

$$u_E=\frac{(33u_3-u_1-8u_2)}{24}-4C(h^1)^4-25D(k^3)^4. \qquad (4.5.9)$$

Assuming that the constants C and D are O(1), the solution is reliable to 8 decimal places.

For the range $\xi = 0.005$ to $\xi = 0.05$ the solutions given by :

$u_1(h^1, 9k^3)$, $u_2(2h^1, k^3)$ and $u_3(h^1, k^3)$, combine to give :

$$u_E = \frac{323u_3}{240} - \frac{u_1}{80} - \frac{u_2}{3} - 4C(h^1)^4 - 81D(k^3)^4. \tag{4.5.10}$$

In this range, the solution is reliable to at least 6 decimal places.

For the range $\xi = 0.05$ to $\xi = 0.1$ the solutions, given by :

$u_1(h^1, 10k^3)$, $u_2(2h^1, k^3)$ and $u_3(h^1, k^3)$, combine to give :

$$u_E = \frac{399u_3}{297} - \frac{u_1}{99} - \frac{u_2}{3} - 4C(h^1)^4 - 100D(k^3)^4. \tag{4.5.11}$$

The solution is reliable to at least 6 decimal places, again.

For $\xi = 0.1$ to $\xi = 1000.0$ the solutions given by :

$u_1(h^1, 2k^3)$, $u_2(2h^1, k^3)$ and $u_3(h^1, k^3)$, combine to give :

$$u_E = \frac{(5u_3 - u_1 - u_2)}{3} - 4C(h^1)^4 - 4D(k^3)^4. \tag{4.5.12}$$

Here, the solution is reliable to at least 4 decimal places.

At $\xi = 0$, step sizes in the downstream direction do not apply. Hence, $u_1$ and $u_3$ are identical. Combining solutions $u_1$ and $u_2$ gives :

$$u_E = \frac{(4u_1 - u_2)}{3} - 4C(h^1)^4. \tag{4.5.13}$$

Table 4.5.3 compares the values obtained for the skin-friction parameter of the three individual solutions with the extrapolated solution. Each individual solution appears to be accurate to at least 3 decimal places.

Final results of the extrapolated solution for the range $\xi = 0$ to $\xi = 1000$ will be presented in the final chapter.

Solutions have been obtained using a 386 personal computer, which will be referred to as PC, in an attempt to minimize expense and maximize efficiency of the method. Fewer discretized points are used creating larger mesh sizes to promote efficiency. Since the most rapid changes in the dependent variables occur near the wall, and since these changes become even sharper as one moves downstream, the highest concentration of discretized points within the numerical grid should be close to the wall. The most gradual changes occur near the boundary layer edge. As one moves downstream, these changes become even more gradual. Thus, the lowest concentration of points within the grid should be near the boundary layer edge.

In approaching the needle case, the numerical solution changes more gradually in the $\xi$-direction. Thus, progressively larger step sizes are used as $\xi$ becomes larger. To demonstrate this, later on a comparison is made between the solution obtained on the ETA-10 computer using the smaller mesh to solution obtained on the PC using the larger mesh.

The mesh employed is in Table 4.5.2.

For $\xi$ starting at 0 and going to 1000, three solutions given by : $u_1(2h^2, 2k^3)$, $u_2(h^2, 2k^3)$ and $u_3(2h^2, k^3)$, combine, using equation F.5 from Appendix F, to give :

$$u_E = \frac{(4u_3 - 5u_1 + 4u_2)}{3} - 36C(h^2)^4 - 36D(k^3)^4. \qquad (4.5.14)$$

The extrapolated skin-friction parameter is compared with the individual solutions obtained on the PC in Table 4.5.4. These results demonstrate more clearly the gain in accuracy obtained in applying Richardson extrapolation to the numerical solutions obtained on a coarse grid.

Comparisons of the solutions obtained on the ETA-10 with those obtained on the PC show excellent agreement. Table 4.5.5 compares the extrapolated skin-friction parameters. Table 4.5.6 and 4.5.7 compares momentum and displacement thickness. Tables 4.5.8-11 compares the velocity component and shear stress parameter profiles. The comparisons indicate that solutions obtained on the PC with a larger mesh agree very well with solutions obtained on the ETA-10. Hence, the large jumps in step sizes appear to be justifiable.

A comparison of skin-friction parameter obtained by Cebeci and Smith (1974), Cebeci (1968), and the method of this chapter in Figure 4.5.2. Agreement between all three methods is very good.

## 4.6 METHOD USING PRIMITIVE VARIABLES WITH STRETCHED COORDINATES

The Keller's Box method is now used with primitive variables, but with the stretched coordinates of Jaffe and Okamura (1968). A direct comparison of results of this section is made with results of Jaffe and Okamura (1968). This primitive variable approach has a different discretization to that of the stream function approach of Cebeci and Smith (1974). This has already been pointed out in Section 4.2.

Using the stretched coordinates of Jaffe and Okamura (1968), i.e.,

$$\eta_j = \frac{r^2 - 1}{\xi}, \text{ and } H = 1 + \xi\eta,$$

and $\xi$, we take the primitive variables, $P = u$ and $Q = v$, with the definition,

$$\tilde{Q} = 2\eta_j P - \frac{\overline{R}\xi}{2}\sqrt{H}\,Q,$$

and transform equations 1.2.6-7 using the relations :

$$\frac{\partial}{\partial r} = \frac{2}{\xi}\sqrt{1 + \xi\eta_j}\,\frac{\partial}{\partial \eta_j},$$

$$\frac{\partial^2}{\partial r^2} = \frac{2}{\xi}\frac{\partial}{\partial \eta_j} + 4\frac{(1 + \xi\eta_j)}{\xi^2}\frac{\partial^2}{\partial \eta_j^2},$$

and

$$\frac{\partial}{\partial x} = \frac{8}{\overline{R}\xi^2}\left(\xi\frac{\partial}{\partial \xi} - \eta_j\frac{\partial}{\partial \eta_j}\right).$$

The governing equations 1.2.6-7 are rewritten as :

$$(H\bar{R})_{\eta_J} + \tilde{Q}\bar{R} = 2\xi P P_{\xi} \tag{4.6.1}$$

and

$$\tilde{Q}_{\eta_J} - 2P = 2\xi P_{\xi}, \tag{4.6.2}$$

where $\bar{R} = P_{\eta_J}$, (4.6.3)

with the boundary conditions :

$$P = \tilde{Q} = Q = 0 \text{ at } \eta_J = 0 \text{ and } P \to 1 \text{ as } \eta_J \to \infty. \tag{4.6.4}$$

Discretizing (4.6.3) at the edge of box in Figure 4.2.1a gives :

$$P_n^j - P_n^{j-1} - \frac{h_j}{2}\left(\bar{R}_n^j + \bar{R}_n^{j-1}\right) = 0 \tag{4.6.5}$$

Discretizing (4.6.1) and (4.6.2) over the box centered at (j-1/2,n-1/2) in Figure 4.2.1b gives :

$$H_n^j \bar{R}_n^j - H_n^{j-1}\bar{R}_n^{j-1} + h_j \tilde{Q}_n^{j-1/2}\bar{R}_n^{j-1/2} - \frac{2h_j\xi_{n-1/2}}{k_n}(P_n^{j-1/2})^2 = S_{n-1}^j \tag{4.6.6}$$

and

$$\tilde{Q}_n^j - \tilde{Q}_n^{j-1} - h_j\left(1 + \frac{(\xi_n + \xi_{n-1})}{k_n}\right)(P_n^j + P_n^{j-1}) = \tilde{Q}_{n-1}^{j-1} - \tilde{Q}_{n-1}^j + h_j(1$$

$$-\frac{(\xi_n + \xi_{n-1})}{k_n})(P_{n-1}^j + P_{n-1}^{j-1}), \tag{4.6.7}$$

where

$$S_{n-1}^{j} \equiv H_{n-1}^{j-1}\overline{R}_{n-1}^{j-1} - H_{n-1}^{j}\overline{R}_{n-1}^{j} - h_j\bar{Q}_{n-1}^{j-1/2}\overline{R}_{n-1}^{j-1/2} - \frac{2h_j\xi_{n-1/2}}{k_n}(P_{n-1}^{j-1/2})^2$$

and $H_n^j \equiv 1 + \xi_n\eta_U^j$.

The boundary conditions become :

$$P_n^0 = 0, \quad P_n^J = 1, \text{ and } \bar{Q}_n^0 = 0. \tag{4.6.8}$$

The method is still second order. Note that $\eta_1$ is replaced by $\eta_J$ in Figure 4.5.1.

The discretization is performed in a similar way for equations 4.6.1-3 as it was for equations 4.2.1-3 in Section 4.5.

## 4.7 SOLUTIONS TO THE DISCRETIZED EQUATIONS

Discretized equations 4.6.5-7 are solved using Newton's method in the same way as the equations in section 4.2.4-6. The resulting equations are :

$$\delta\bar{Q}_{(i)}^{J} - \delta\bar{Q}_{(i)}^{J-1} + FAC_{(i)}^{J}(\delta P_{(i)}^{J} + \delta P_{(i)}^{J-1}) = m_{(i)}^{J} \tag{4.7.1}$$

$$\delta P_{(i)}^{J} - \delta P_{(i)}^{J-1} - \frac{h_J}{2}\left(\delta\overline{R}_{(i)}^{J} + \delta\overline{R}_{(i)}^{J-1}\right) = l_{(i)}^{J} \tag{4.7.2}$$

$$\beta_{(i)}^{J}\delta\overline{R}_{(i)}^{J} + \theta_{(i)}^{J}\delta\bar{Q}_{(i)}^{J} + \gamma_{(i)}^{J}\delta P_{(i)}^{J} + \tilde{\beta}_{(i)}^{J}\delta\overline{R}_{(i)}^{J-1} + \theta_{(i)}^{J}\delta\bar{Q}_{(i)}^{J-1} + \gamma_{(i)}^{J}\delta P_{(i)}^{J-1} = t_{(i)}^{J}, \tag{4.7.3}$$

where

$$t_{(i)}^{J} = S_{n-1}^{J} + \frac{2h_j\xi_{n-1/2}}{k_n}(P^{J-1/2})^2 - H_n^J\overline{R}^J + H_n^{J-1}\overline{R}^{J-1} - h_j\bar{Q}^{J-1/2}\overline{R}^{J-1/2},$$

$$m_{(i)}^{j} = \bar{Q}_{n-1}^{j-1} - \bar{Q}_{n-1}^{j} + h_j\left(1 - \frac{(\xi_{3n} + \xi_{3n-1})}{k_n}\right)(P_{n-1}^{j} + P_{n-1}^{j-1}) - \bar{Q}_{(i)}^{j} + \bar{Q}_{(i)}^{j-1} - FAC_{(i)}^{j}(P_{(i)}^{j} + P_{(i)}^{j-1}),$$

$$l_{(i)}^{j} = P_{(i)}^{j-1} - P_{(i)}^{j} + \frac{h_j}{2}\left(\overline{R}_{(i)}^{j} + \overline{R}_{(i)}^{j-1}\right), \tag{4.7.4}$$

$$\beta_{(i)}^{j} \equiv H_n^{j} + \frac{h_j}{2}\bar{Q}_{(i)}^{j-1/2},$$

$$\theta_{(i)}^{j} \equiv \frac{h_j}{2}\overline{R}_{(i)}^{j-1/2},$$

$$\gamma_{(i)}^{j} = -\frac{2h_j\xi_{3n-1/2}}{k_n}P_{(i)}^{j-1/2},$$

$$\tilde{\beta}_{(i)}^{j} = -H_n^{j-1} + \frac{h_j}{2}\bar{Q}_{(i)}^{j-1/2},$$

$$FAC_{(i)}^{j} \equiv -h_j\left(1 + \frac{(\xi_{3n} + \xi_{3n-1})}{k_n}\right).$$

with the boundary conditions :

$$\delta\bar{Q}_{(i)}^{0} = \delta P_{(i)}^{0} = \delta P_{(i)}^{J} = 0 \quad i = 0, 1, \ldots. \tag{4.7.5}$$

This system of equations is put into matrix and block matrix form in the same way as the system of equations in section 4.3. The block tridiagonal system which is obtained is the same as in section 4.3 using the same variable names and boundary conditions, except that the definitions of the matrix elements and variables, given above in 4.7.1-5, are different. Thus, the same block tridiagonal factorization procedure is also used.

## 4.8 GENERAL ITERATION STEP

The numerical procedure is the same as in section 4.4. The differences that are encountered are included in this section.

At $\xi = 0$, i.e., the Blasius limit, the initial profile start the iteration procedure, is a linear profile in $\eta_J$, which satisfies the boundary conditions, i.e.,

$$P = \frac{\eta_J}{(\eta_J)_\infty}. \tag{4.11.1}$$

Differentiating (4.8.1) with respect to $\eta_J$ gives the initial profile for $\overline{R}$, i.e.,

$$\overline{R} = \frac{1}{(\eta_J)_\infty}. \tag{4.11.2}$$

Substituting (4.8.1) into (4.6.2) with $\xi = 0$, and integrating with respect to $\eta_J$ gives :

$$\bar{Q} = \frac{\eta_J^2}{(\eta_J)_\infty}. \tag{4.11.3}$$

Again, when starting the numerical procedure at a value of $\xi > 0$, a known solution is used as the first iterate. This solution is either previously obtained or an estimate at that particular step in $\xi$ is used.

The general stage in calculation is exactly the same as in section 4.4. The convergence criterion is the same as condition 4.4.6 and it, still, brings about three iterations at each new step in $\xi$.

It is found that the boundary layer grows considerably as one moves downstream. This is due to using the stretched coordinates. Also, condition 4.4.7 that tests the shear stress parameter at the edge of the boundary layer to see whether the numerical grid needs to be enlarged in order to accommodate the growth of the boundary layer had to be adjusted. The reason for this is that the displacement and momentum thickness were found to be much too small at larger $\xi$-values when compared with the previously obtained solutions in sections 4.4 and 4.5 or with the solutions of Glauert and Lighthill (1955). However, the skin-friction coefficient and velocity profiles obtained compared very well to solutions obtained in sections 4.4 and 4.5.

In order to obtain the proper values of the integral quantities, two approaches were taken. First, the tolerance in condition 4.4.7 was tightened, i.e.,

$$|\bar{R}(\xi_m, \eta_\infty)| < \text{tolerance} = 10^{-6} \tag{4.8.1}$$

Note, that this is a much smaller value than that suggested by Cebeci and Smith (1974). Second, a new procedure is used. At each new step in $\xi$, the displacement and momentum thickness are calculated. A new calculation is performed at the same $\xi$-value, but with an enlarged numerical grid. Then, the former value of the displacement thickness is compared to the newer value. Similarly for the momentum thickness. This process is repeated until the comparison demonstrates convergence to 4 decimal places for both integral quantities. Then we move on to the next step in $\xi$.

The result of each approach obtained integral quantities that matched with those of the Glauert and Lighthill (1955) and with the previous solution in Sections 4.4 and

4.5. It was found that the skin-friction and axial velocity profiles matched more closely with previous solutions. Of course, both approaches lead to prolonged computer use because of repeated calculation at each step in $\xi$ in order to satisfy the new conditional criteria. It was noticed that the values for the boundary layer thickness were greatly increased over the values obtained using the previous criterion 4.4.7.

When the numerical grid needs to be enlarged, the dependent variables must be calculated and implemented into the extended region. The values of the dependent variables are calculated as follows:

$P(\xi_n, \eta_J^*) = 1,$

$\overline{R}(\xi_n, \eta_J^*) = \overline{R}(\xi_n, \eta_J),$

where

$h_j = \Delta\eta_J,\ \eta_{J_-} \le \eta_J^* \le \eta_{J_-}^*,$

$\eta_J^*$ is the dependent variable in the extended grid region,

$\eta_{J_-}$ is the previous boundary layer edge distance at $n-1$

and

$\eta_{J_-}^*$ is the new boundary layer edge distance at $n$.

Integrating equation 4.6.2 and recalling that at the edge of the boundary layer, $P = 1$ and $P_\xi = 0$, gives :

$$\bar{Q}(\xi_n, \eta_J^*) = 2\Delta\eta_J + \bar{Q}(\xi_n, \eta_J), \tag{4.11.5}$$

An $\eta_\infty = 6$ is used to begin the numerical procedure, but this soon increases as we move downstream.

## 4.9 RICHARDSON EXTRAPOLATION

Richardson extrapolation is applied to three numerical solutions obtained using three mesh sizes.

The solutions given as a function of mesh sizes are :

$u_1(2h^2, 2k^3)$, $u_2(h^2, 2k^3)$ and $u_3(2h^2, k^3)$, and are obtained for $\xi = 0$ to $\xi = 1000$. The mesh is relatively small so that a very accurate solution is obtained to compare with previous solutions and so that interpolations are avoided further down stream where closely spaced mesh points are needed to approximate the rapidly changing profiles near the wall.

The mesh employed is given in Figure 4.9.1.

Applying equation F.5 from Appendix F, to the three individual solutions yields :

$$u_E = \frac{(4u_3 - 5u_1 + 4u_2)}{3} - 36C(h^2)^4 - 36D(k^3)^4. \tag{4.9.1}$$

It is computationally more inconvenient to extrapolate the solutions with the growth of the numerical grid because each individual solution does not always reach a common $\eta_\infty$.).

Final results of the extrapolated solution for the range $\xi = 0$ to $\xi = 1000$ will be presented in the final chapter.

The skin-friction coefficient obtained by the individual solutions is compared to the extrapolated solution Table 4.9.2. Although the individual results are quite accurate, the extrapolated results appear to be more relevant for the larger values of $\xi$.

Table 4.9.3 compares the skin-friction obtained from the previous solution using similarity coordinates with the solution of this section using stretched coordinates. Agreement is excellent with the largest difference being less than 0.01 %.

Table 4.9.4 compares the displacement thickness obtained previously using similarity coordinates in section 4.5 to that obtained in this section and to that obtained by Jaffe and Okamura (1968). The solutions obtained in this chapter agree very well with each other with the largest difference being less than 0.6 %. The largest difference between either of the solutions obtained in this chapter to that of Jaffe and Okamura is less than .6 %.

The skin-friction coefficient obtained by the method of this section is compared to that of Jaffe and Okamura (1968). The agreement is excellent, with the largest difference being less than .2 %.

The momentum thickness obtained by the methods of this chapter are compared with that of Jaffe and Okamura (1968). Agreement is excellent between the three solutions. The largest difference between the solutions of this chapter is less than .2 %, while the largest difference between either of these solutions and the momentum

thickness obtained by Jaffe and Okamura is less than .6 %.

The Keller's Box method using similarity coordinates has an advantage over the method using stretched coordinates in that discretized points do not need to be added as we move downstream to accommodate the growing boundary layer. This is because boundary layer growth is scaled out using these coordinates and , therefore, there is no need for the numerical grid to be enlarged. However, the method using stretched coordinates has a slight advantage over the method using similarity coordinates because fewer points are needed to maintain similar accuracy near the wall. The further one moves downstream, more points need to be added near the wall to improve accuracy regardless of the coordinates being used. We feel that the efficiency of the Keller's Box method using either stretched coordinates or similarity coordinates is nearly the same, provided that an optimally spaced non-uniform grid is used in each case.

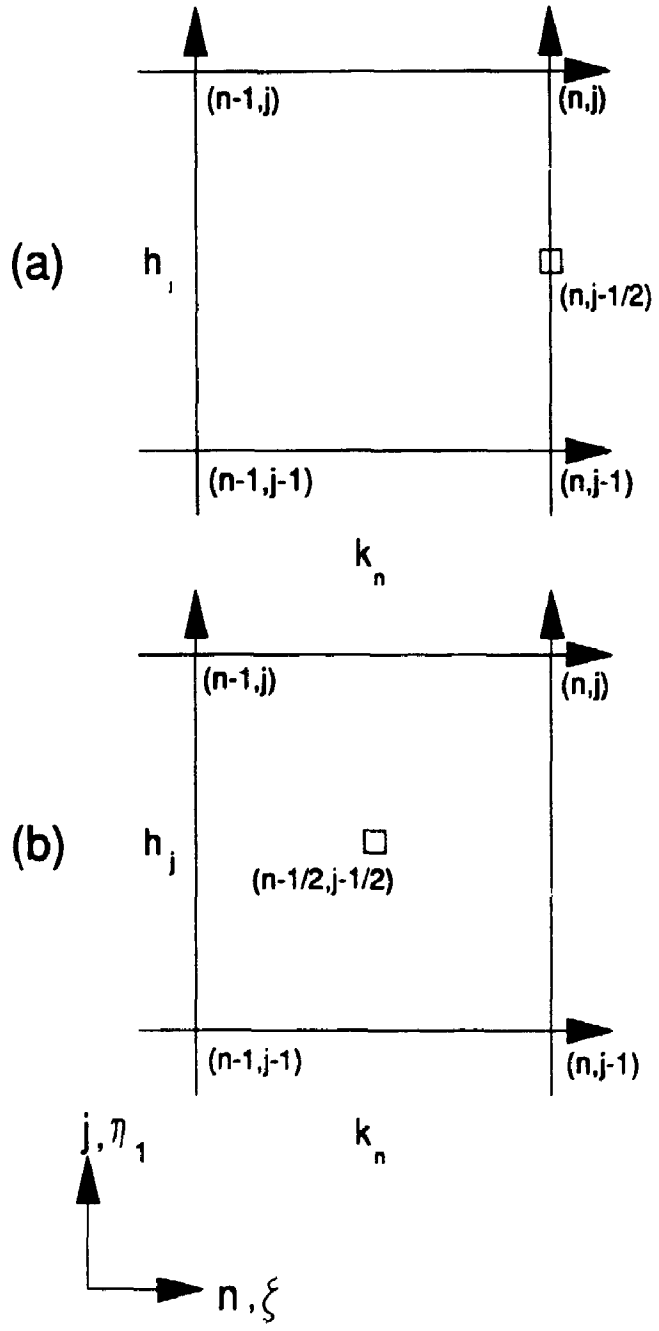


Figure 4.2.1 Box used for discretization in Keller Box method for (a) equation 4.2.3 and (b) momentum and continuity equations 4.2.1-2.

VARIABLE GRID

| Streamwise Direction | | Cross-stream Direction | |
|---|---|---|---|
| Interval | Step Size | Interval | Step Size |
| $0 \le \xi \le 0.005$ | $k^3 = 0.001$ | $0 \le \eta_1 \le 0.01$ | $h^1 = 10^{-5}$ |
| $0.005 \le \xi \le 0.1$ | $k^3 = 0.005$ | $0.01 \le \eta_1 \le 0.5$ | $h^1 = 10^{-4}$ |
| $0.1 \le \xi \le 1000.$ | $k^3 = 0.05$ | $0.5 \le \eta_1 \le 3.0$ | $h^1 = 10^{-3}$ |
| Table 4.5.1 Step sizes used to obtain the overall solution. | | $3.0 \le \eta_1 \le 8.0$ | $h^1 = 0.005$ |

| | $\frac{\xi}{2\sqrt{2}} \frac{a\,\tau_0}{\mu\,U}$ | | | |
|---|---|---|---|---|
| $\xi$ | MESH 1 | MESH2 | MESH3 | EXTRAPOLATED |
| 0.000 | 0.46960003 | 0.46960016 | 0.46960003 | 0.46959999 |
| 0.005 | 0.47082568 | 0.47082610 | 0.47082597 | 0.47082594 |
| 0.100 | 0.49357367 | 0.49360100 | 0.49360087 | 0.49360110 |
| 0.200 | 0.51657479 | 0.51661179 | 0.51661165 | 0.51662389 |
| 0.300 | 0.53874271 | 0.53879942 | 0.53879927 | 0.53881807 |
| 0.400 | 0.56021925 | 0.56026845 | 0.56026830 | 0.56028460 |
| 0.500 | 0.58105720 | 0.58110605 | 0.58110589 | 0.58112207 |
| 0.600 | 0.60134077 | 0.60138407 | 0.60138391 | 0.60139830 |
| 0.700 | 0.62112024 | 0.62116197 | 0.62116181 | 0.62117561 |
| 0.800 | 0.64045163 | 0.64048945 | 0.64048929 | 0.64050179 |
| 0.900 | 0.65937242 | 0 65940850 | 0.65940834 | 0.65942026 |
| 1.000 | 0.67792186 | 0.67795497 | 0.67795480 | 0.67796572 |
| 2.000 | 0.84813380 | 0.84815333 | 0.84815314 | 0.84815952 |
| 3.000 | 0.99998272 | 0.99999615 | 0.99999596 | 1.00000031 |
| 4.000 | 1.14037394 | 1.14038401 | 1.14038381 | 1.14038703 |
| 5.000 | 1.27269019 | 1.27269815 | 1.27269796 | 1.27270049 |
| 10.000 | 1.86278657 | 1.86279025 | 1.86279009 | 1.86279121 |
| 50.000 | 5.41314674 | 5.41314633 | 5.41314722 | 5.41314768 |
| 100.000 | 9.06272788 | 9.06272394 | 9.06272808 | 9.06272953 |
| 500.000 | 32.56930776 | 32.56924110 | 32.56930778 | 32.56933001 |
| 600.000 | 37.85724221 | 37.85715578 | 37.85724223 | 37.85727105 |
| 700.000 | 43.02335327 | 43.02324611 | 43.02335328 | 43.02338901 |
| 800.000 | 48.08928295 | 48.08915412 | 48.08928296 | 48.08932591 |
| 900.000 | 53.07057016 | 53.07041864 | 53.07057017 | 53.07062068 |
| 1000.000 | 57.97886422 | 57.97868892 | 57.97886423 | 57.97892267 |

Table 4.5.3 Comparison of skin-friction coefficient from individual solutions at different mesh sizes from the overall Keller Box method vs. the results from Richardson extrapolation. Results obtained on ETA-10.

VARIABLE GRID

| Streamwise Direction | | Cross-stream Direction | |
|---|---|---|---|
| Interval | Step Size | Interval | Step Size |
| $0 \le \xi \le 0.005$ | $k^3 = 2.5 \times 10^{-3}$ | $0 \le \eta_1 \le 10^{-4}$ | $h^2 = 5 \times 10^{-7}$ |
| $0.005 \le \xi \le 0.05$ | $k^3 = 2.25 \times 10^{-2}$ | $10^{-4} \le \eta_1 \le 10^{-3}$ | $h^2 = 2.25 \times 10^{-4}$ |
| $0.05 \le \xi \le 0.1$ | $k^3 = 0.025$ | $10^{-3} \le \eta_1 \le 10^{-2}$ | $h^2 = 2.25 \times 10^{-3}$ |
| $0.1 \le \xi \le 1.0$ | $k^3 = 0.05$ | $10^{-2} \le \eta_1 \le 0.05$ | $h^2 = 0.005$ |
| $1.0 \le \xi \le 5.0$ | $k^3 = 0.125$ | $0.05 \le \eta_1 \le 8.0$ | $h^2 = 0.025$ |
| $5.0 \le \xi \le 10.0$ | $k^3 = 0.25$ | | |
| $10 \le \xi \le 40$ | $k^3 = 0.5$ | | |
| $40 \le \xi \le 50$ | $k^3 = 1.0$ | | |
| $50 \le \xi \le 100$ | $k^3 = 2.5$ | | |
| $100 \le \xi \le 200$ | $k^3 = 5.0$ | | |
| $200 \le \xi \le 300$ | $k^3 = 10.0$ | | |
| $300 \le \xi \le 500$ | $k^3 = 25.0$ | | |
| $500 \le \xi \le 1000$ | $k^3 = 50.0$ | | |

Table 4.5.2 Step sizes used to obtain the overall solution on PC.

| | $\frac{\xi}{2\sqrt{2}} \frac{a\tau_0}{\mu U}$ | | | |
|---|---|---|---|---|
| $\xi$ | MESH 1 | MESH2 | MESH3 | EXTRAPOLATED |
| 0.000 | 0.4696229067 | 0.4696057179 | 0.4696229067 | 0.4695999883 |
| 0.005 | 0.4708486610 | 0.4708313945 | 0.4708488730 | 0.4708259217 |
| 0.100 | 0.4935985068 | 0.4935798440 | 0.4936198771 | 0.4936021168 |
| 0.200 | 0.5166013894 | 0.5165814077 | 0.5166359871 | 0.5166208774 |
| 0.300 | 0.5387708612 | 0.5387497102 | 0.5388263765 | 0.5388166803 |
| 0.400 | 0.5602488029 | 0.5602265971 | 0.5602972457 | 0.5602837856 |
| 0.500 | 0.5810879797 | 0.5810648531 | 0.5811362817 | 0.5811215469 |
| 0.6 | 0.6013724507 | 0.6013485003 | 0.6014155047 | 0.6013979222 |
| 0.700 | 0.6211530628 | 0.6211284066 | 0.6211944243 | 0.6211753365 |
| 0.800 | 0.6404852779 | 0.6404600034 | 0.6405227638 | 0.6405015598 |
| 0.900 | 0.6594067425 | 0.6593809582 | 0.6594425311 | 0.6594200816 |
| 1.000 | 0.6779567499 | 0.6779305370 | 0.6779895762 | 0.6779655678 |
| 2.000 | 0.8481041855 | 0.8480784827 | 0.8481715142 | 0.8481596867 |
| 3.000 | 0.9999470216 | 0.9999299109 | 1.0000041171 | 1.0000003347 |
| 4.000 | 1.1403261706 | 1.1403254169 | 1.1403725715 | 1.1403870335 |
| 5.000 | 1.2726184559 | 1.2726416916 | 1.2726567296 | 1.2727004684 |
| 10.000 | 1.8623976964 | 1.8626515439 | 1.8624388959 | 1.8627910924 |
| 50.000 | 5.4036951874 | 5.4107341094 | 5.4037323339 | 5.4131299454 |
| 100.000 | 9.0314015499 | 9.0547177805 | 9.0315028885 | 9.0626249755 |
| 500.000 | 32.1062730759 | 32.4482679292 | 32.1069316118 | 32.5631442615 |
| 600.000 | 37.2248170188 | 37.6902016220 | 37.2261273587 | 37.8470769429 |
| 700.000 | 42.2010274776 | 42.8048382324 | 42.2023133207 | 43.0078229415 |
| 800.000 | 47.0572153693 | 47.8131535603 | 47.0585321163 | 48.0668886200 |
| 900.000 | 51.8105655458 | 52.7311747458 | 51.8118043779 | 53.0396962553 |
| 1000.000 | 56.4740340989 | 57.5706779721 | 56.4752281461 | 57.9378179928 |

Table 4.5.4 Comparison of skin-friction coefficient of individual solutions obtained by overall Keller Box method vs.results of Richardson extrapolation. Solutions obtained on PC.

| | $\frac{\xi}{2\sqrt{2}}\frac{a\tau_o}{\mu U}$ | |
|---|---|---|
| $\xi$ | ETA-10 | PC |
| 0.000 | 0.46959999 | 0.46959999 |
| 0.005 | 0.47082594 | 0.47082592 |
| 0.100 | 0.49360110 | 0.49360212 |
| 0.200 | 0.51662389 | 0.51662088 |
| 0.300 | 0.53881807 | 0.53881668 |
| 0.400 | 0.56028460 | 0.56028379 |
| 0.500 | 0.58112207 | 0.58112155 |
| 0.600 | 0.60139830 | 0.60139792 |
| 0.700 | 0.62117561 | 0.62117534 |
| 0.800 | 0.64050179 | 0.64050156 |
| 0.900 | 0.65942026 | 0.65942008 |
| 1.000 | 0.67796572 | 0.67796557 |
| 2.000 | 0.84815952 | 0.84815969 |
| 3.000 | 1.00000031 | 1.00000033 |
| 4.000 | 1.14038703 | 1.14038703 |
| 5.000 | 1.27270049 | 1.27270047 |
| 10.000 | 1.86279121 | 1.86279109 |
| 20.000 | 2.87157226 | 2.87157108 |
| 30.000 | 3.77266300 | 3.77265889 |
| 40.000 | 4.61329320 | 4.61328376 |
| 50.000 | 5.41314768 | 5.41312995 |
| 100.000 | 9.06272953 | 9.06262498 |
| 500.000 | 32.56933001 | 32.56314426 |
| 600.000 | 37.85727105 | 37.84707694 |
| 700.000 | 43.02338901 | 43.00782294 |
| 800.000 | 48.08932591 | 48.06688862 |
| 900.000 | 53.07062068 | 53.03969626 |
| 1000.000 | 57.97892267 | 57.93781799 |

Table 4.5.5 Comparison of skin-friction coefficient obtained from overall Keller Box method using similarity coordinates solved on ETA-10 vs. PC.

| | θ | |
|---|---|---|
| ξ | ETA-10 | PC |
| 0.000 | 0.664114675 | 0.663330627 |
| 0.005 | 0.664981884 | 0.664195767 |
| 0.100 | 0.681211130 | 0.680386151 |
| 0.200 | 0.697821300 | 0.696964034 |
| 0.300 | 0.714014858 | 0.713118065 |
| 0.400 | 0.729826532 | 0.728893091 |
| 0.500 | 0.745294661 | 0.744326113 |
| 0.600 | 0.760450504 | 0.759447969 |
| 0.700 | 0.775321409 | 0.774285815 |
| 0.800 | 0.789930044 | 0.788862175 |
| 0.900 | 0.804296734 | 0.803197292 |
| 1.000 | 0.818438664 | 0.817308288 |
| 2.000 | 0.950202693 | 0.948787943 |
| 3.000 | 1.069630496 | 1.067961247 |
| 4.000 | 1.180870349 | 1.178964707 |
| 5.000 | 1.286121546 | 1.283991995 |
| 10.000 | 1.757145077 | 1.754001877 |
| 50.000 | 4.571826736 | 4.561979736 |
| 100.000 | 7.430662374 | 7.412944464 |
| 500.000 | 25.551887904 | 25.469602945 |
| 600.000 | 29.595753625 | 29.496484294 |
| 700.000 | 33.539813994 | 33.423009017 |
| 800.000 | 37.401987137 | 37.267048091 |
| 900.000 | 41.195111530 | 41.04[illegible]97520 |
| 1000.000 | 44.928790121 | 44.755623350 |

Table 4.5.7 Comparison of momentum thickness
obtained by overall Keller Box method using similarity coordinates
solved on ETA-10 vs. PC.
Percentage difference is less than 0.5 %.

| | △ | |
|---|---|---|
| ξ | ETA-10 | PC |
| 0.000 | 1.7208208642 | 1.7215845980 |
| 0.005 | 1.7209131931 | 1.7216789300 |
| 0.100 | 1.7235724599 | 1.7243726415 |
| 0.200 | 1.7279174598 | 1.7287702055 |
| 0.300 | 1.7335048030 | 1.7343880154 |
| 0.400 | 1.7400693492 | 1.7409858794 |
| 0.500 | 1.7474056019 | 1.7483556425 |
| 0.600 | 1.7553689550 | 1.7563521176 |
| 0.700 | 1.7638431161 | 1.7648588431 |
| 0.800 | 1.7727387723 | 1.7737864951 |
| 0.900 | 1.7819835872 | 1.7830627418 |
| 1.000 | 1.7915199730 | 1.7926300369 |
| 2.000 | 1.8956073833 | 1.8970038974 |
| 3.000 | 2.0050910637 | 2.0067476875 |
| 4.000 | 2.1145260576 | 2.1164266164 |
| 5.000 | 2.2223983811 | 2.2245320104 |
| 10.000 | 2.7320531449 | 2.7352655335 |
| 50.000 | 5.9438426511 | 5.9549414801 |
| 100.000 | 9.2126942597 | 9.2341085412 |
| 500.000 | 29.6022240549 | 29.7199153103 |
| 600.000 | 34.1076413974 | 34.2507403401 |
| 700.000 | 38.4922572948 | 38.6606099822 |
| 800.000 | 42.7779704042 | 42.9712592353 |
| 900.000 | 46.9804467879 | 47.1982400523 |
| 1000.000 | 51.1113918949 | 51.3531552105 |

Table 4.5.6 Comparison of displacement thickness obtained by overall Keller Box method using similarity coordinates solved on ETA-10 vs. PC.
Percentage difference is less than 0.5 %.

| $\xi = 0$ | U | | $\frac{R^*}{2\sqrt{2}}V$ | | $\frac{\xi}{2\sqrt{2}}\frac{\partial T}{\mu U}$ | |
|---|---|---|---|---|---|---|
| $\eta_1$ | ETA-10 | PC | ETA-10 | PC | ETA-10 | PC |
| 0.000 | 0.00000000 | 0.00000000 | 0.0000000000 | 0.0000000000 | 0.46959999 | 0.46959999 |
| 0.001 | 0.00046960 | 0.00046961 | 0.0000002396 | 0.0000002396 | 0.46959999 | 0.46959999 |
| 0.010 | 0.00469600 | 0.00469600 | 0.0000234800 | 0.0000234800 | 0.46959995 | 0.46959995 |
| 0.020 | 0.00939200 | 0.00939199 | 0.0000939200 | 0.0000939198 | 0.46959970 | 0.46959970 |
| 0.030 | 0.01408799 | 0.01408799 | 0.0002113197 | 0.0002113197 | 0.46959900 | 0.46959900 |
| 0.040 | 0.01878398 | 0.01878397 | 0.0003756792 | 0.0003756888 | 0.46959764 | 0.46959763 |
| 0.050 | 0.02347994 | 0.02347995 | 0.0005869970 | 0.0005869975 | 0.46959540 | 0.46959539 |
| 0.100 | 0.04695907 | 0.04695908 | 0.0023479270 | 0.0023479280 | 0.46956324 | 0.46956323 |
| 0.500 | 0.23422747 | 0.23422747 | 0.0584710450 | 0.0584710550 | 0.46503036 | 0.46503036 |
| 1.000 | 0.46063258 | 0.46063258 | 0.2276424900 | 0.2276424800 | 0.43437914 | 0.43437915 |
| 2.000 | 0.81669462 | 0.81669462 | 0.7465924100 | 0.7465924100 | 0.25566917 | 0.25566918 |
| 3.000 | 0.96905461 | 0.96905460 | 1.1115959200 | 1.1115958800 | 0.06771035 | 0.06771035 |
| 4.000 | 0.99777010 | 0.99777009 | 1.2071939400 | 1.2071938900 | 0.00687410 | 0.00687410 |
| 5.000 | 0.99993586 | 0.99993587 | 1.2164447800 | 1.2164448200 | 0.00025779 | 0.00025779 |
| 6.000 | 0.99999929 | 0.99999929 | 1.2167762200 | 1.2167762200 | 0.00000356 | 0.00000356 |
| 7.000 | 1.00000000 | 1.00000000 | 1.2167806200 | 1.2167806300 | 0.00000002 | 0.00000002 |
| 8.000 | 1.00000000 | 1.00000000 | 1.2167806200 | 1.2167806300 | 0.00000000 | 0.00000000 |

Table 4.5.8 Comparison of velocity and shear stress profiles between solutions obtained by the overall Keller Box method solved on ETA-10 vs. PC at $\xi = 0$.

| $\xi = 1$ | U | | $\frac{R\xi}{2\sqrt{2}}V$ | | $\frac{\xi}{2\sqrt{2}}\frac{a\tau}{\mu U}$ | |
|---|---|---|---|---|---|---|
| $\eta_1$ | ETA-10 | PC | ETA-10 | PC | ETA-10 | PC |
| 0.000 | 0.00000000 | 0.00000000 | 0.0000000000 | 0.0000000000 | 0.67796572 | 0.67796558 |
| 0.001 | 0.00067784 | 0.00067784 | 0.0000002480 | 0.0000002480 | 0.67772611 | 0.67772597 |
| 0.010 | 0.00676770 | 0.00676770 | 0.0000246691 | 0.0000246790 | 0.67557713 | 0.67557699 |
| 0.020 | 0.01351160 | 0.01351160 | 0.0000984566 | 0.0000984666 | 0.67320500 | 0.67320483 |
| 0.030 | 0.02023186 | 0.02023185 | 0.0002209896 | 0.0002209992 | 0.67084878 | 0.67084864 |
| 0.040 | 0.02692862 | 0.02692862 | 0.0003919647 | 0.0003919746 | 0.66850799 | 0.66850784 |
| 0.050 | 0.03360206 | 0.03360204 | 0.0006110219 | 0.0006110700 | 0.66618214 | 0.66618199 |
| 0.100 | 0.06662424 | 0.06662423 | 0.0024161910 | 0.0024162576 | 0.65475968 | 0.65475953 |
| 0.500 | 0.31133243 | 0.31133236 | 0.0552060933 | 0.0552075624 | 0.56978598 | 0.56978586 |
| 1.000 | 0.56880503 | 0.56880493 | 0.1941529597 | 0.1941570413 | 0.45683212 | 0.45683206 |
| 2.000 | 0.89207660 | 0.89207651 | 0.5122239663 | 0.5122313020 | 0.18965535 | 0.18965541 |
| 3.000 | 0.98799633 | 0.98799630 | 0.6084281283 | 0.6084353806 | 0.03187460 | 0.03187463 |
| 4.000 | 0.99947920 | 0.99947919 | 0.5509639994 | 0.5509703135 | 0.00188831 | 0.00188832 |
| 5.000 | 0.99999154 | 0.99999156 | 0.4824392483 | 0.4824448943 | 0.00003903 | 0.00003903 |
| 6.000 | 0.99999995 | 0.99999995 | 0.4278310932 | 0.4278360142 | 0.00000028 | 0.00000028 |
| 7.000 | 1.00000000 | 1.00000000 | 0.3843013995 | 0.3843058198 | 0.00000000 | 0.00000000 |
| 8.000 | 1.00000000 | 1.00000000 | 0.3488113511 | 0.3488153632 | 0.00000000 | 0.00000000 |

Table 4.5.9 Comparison of velocity and shear stress profiles obtained by overall Keller BOx method solved on ETA-10 vs. PC at $\xi = 1$.

| $\xi$ =10 | U | | $\frac{R\xi}{2\sqrt{2}}V$ | | $\frac{\xi}{2\sqrt{2}}\frac{\partial T}{\mu U}$ | |
|---|---|---|---|---|---|---|
| $\eta$ | ETA-10 | PC | ETA-10 | PC | ETA-10 | PC |
| 0.000 | 0.00000000 | 0.00000000 | 0.0000000000 | 0.0000000000 | 1.86279121 | 1.86279109 |
| 0.001 | 0.00185950 | 0.00185951 | 0.0000003847 | 0.0000003847 | 1.85622846 | 1.85622835 |
| 0.010 | 0.01830617 | 0.01830617 | 0.0000373822 | 0.0000373726 | 1.79918034 | 1.79918022 |
| 0.020 | 0.03599760 | 0.03599761 | 0.0001462209 | 0.0001462211 | 1.73976901 | 1.73976888 |
| 0.030 | 0.05311420 | 0.05311420 | 0.0003219919 | 0.0003220010 | 1.68415308 | 1.68415296 |
| 0.040 | 0.06969214 | 0.06969214 | 0.0005606290 | 0.0005606640 | 1.63197846 | 1.63197838 |
| 0.050 | 0.08576420 | 0.08576418 | 0.0008585449 | 0.0008585779 | 1.58293353 | 1.58293343 |
| 0.100 | 0.15949804 | 0.15949804 | 0.0031327329 | 0.0031329029 | 1.37602434 | 1.37602426 |
| 0.500 | 0.53440759 | 0.53440760 | 0.0487934735 | 0.0487956608 | 0.65932547 | 0.65932545 |
| 1.000 | 0.77698877 | 0.77698878 | 0.1319494007 | 0.1319525041 | 0.34955878 | 0.34955875 |
| 2.000 | 0.96634958 | 0.96634958 | 0.2379043387 | 0.2379071871 | 0.07629782 | 0.07629781 |
| 3.000 | 0.99774147 | 0.99774147 | 0.2181407918 | 0.2181429311 | 0.00711467 | 0.00711468 |
| 4.000 | 0.99993930 | 0.99993932 | 0.1727916490 | 0.1727933748 | 0.00024815 | 0.00024814 |
| 5.000 | 0.99999937 | 0.99999937 | 0.1402900121 | 0.1402913479 | 0.00000318 | 0.00000319 |
| 6.000 | 1.00000000 | 1.00000000 | 0.1179636954 | 0.1179648181 | 0.00000001 | 0.00000001 |
| 7.000 | 1.00000000 | 1.00000000 | 0.1017662166 | 0.1017671852 | 0.00000000 | 0.00000000 |
| 8.000 | 1.00000000 | 1.00000000 | 0.0894798289 | 0.0894806805 | 0.00000000 | 0.00000000 |

Table 4.5.10 Comparison of velocity and shear stress profiles obtained by the overall Keller Box method solved on the ETA-10 vs. PC at $\xi$ = 10.

| $\xi = 10^3$ | U | | $\frac{R\xi}{2\sqrt{2}} V$ | | $\frac{\xi}{2\sqrt{2}} \frac{\partial T}{\mu U}$ | |
|---|---|---|---|---|---|---|
| $\eta_1$ | ETA-10 | PC | ETA-10 | PC | ETA-10 | PC |
| 0.000 | 0.00000000 | 0.00000000 | 0.0000000000 | 0.0000000000 | 57.97892267 | 57.93781799 |
| 0.001 | 0.04964497 | 0.04961076 | 0.0000037953 | 0.0000038202 | 42.83460332 | 42.80423535 |
| 0.010 | 0.24794215 | 0.24825730 | 0.0001735761 | 0.0001645526 | 12.78323738 | 12.77417641 |
| 0.020 | 0.34245552 | 0.34282200 | 0.0004756130 | 0.0004624793 | 7.18344308 | 7.17835441 |
| 0.030 | 0.40202919 | 0.40237036 | 0.0008378663 | 0.0008230726 | 4.99510706 | 4.99157029 |
| 0.040 | 0.44563199 | 0.44594735 | 0.0012407894 | 0.0012241992 | 3.82858526 | 3.82587604 |
| 0.050 | 0.48003981 | 0.48033299 | 0.0016745299 | 0.0016560488 | 3.10359939 | 3.10140480 |
| 0.100 | 0.58919924 | 0.58944324 | 0.0041486026 | 0.0041211376 | 1.59291100 | 1.59179217 |
| 0.500 | 0.84528012 | 0.84535724 | 0.0295509563 | 0.0294764451 | 0.30543456 | 0.30524679 |
| 1.000 | 0.94133178 | 0.94135543 | 0.0586674713 | 0.0585771757 | 0.11649989 | 0.11644333 |
| 2.000 | 0.99396040 | 0.99396213 | 0.0755844844 | 0.0755101886 | 0.01582560 | 0.01582055 |
| 3.000 | 0.99970756 | 0.99970761 | 0.0603018280 | 0.0602486592 | 0.00100951 | 0.00100928 |
| 4.000 | 0.99999407 | 0.99999406 | 0.0459816779 | 0.0459415993 | 0.00002580 | 0.00002579 |
| 5.000 | 0.99999995 | 0.99999995 | 0.0368111349 | 0.0367791079 | 0.00000025 | 0.00000025 |
| 6.000 | 1.00000000 | 1.00000000 | 0.0306793439 | 0.0306523662 | 0.00000000 | 0.00000000 |
| 7.000 | 1.00000000 | 1.00000000 | 0.0262980789 | 0.0262752256 | 0.00000000 | 0.00000000 |
| 8.000 | 1.00000000 | 1.00000000 | 0.0230119654 | 0.0229919834 | 0.00000000 | 0.00000000 |

Table 4.5.11 Comparison of velocity and shear stress profiles obtained by overall Keller Box method solved on ETA-10 vs. PC at $\xi = 1000$.

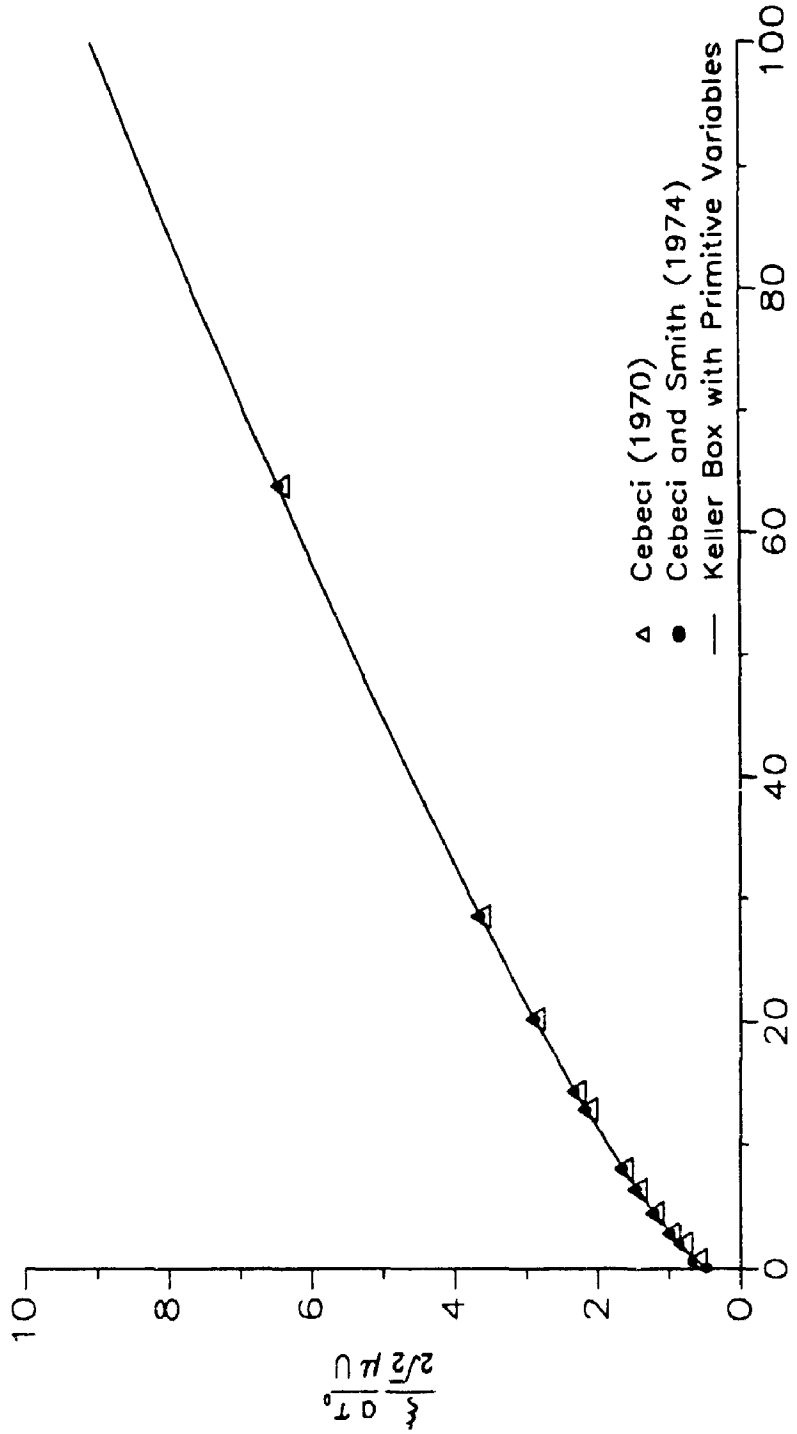


Figure 4.5.2 Comparison of skin-friction coefficient for the overall Keller Box method using similarity coordinates with the method of Cebeci (1970) and Cebeci and Smith (1974).

VARIABLE GRID

| Streamwise Direction | | Cross-stream Direction | |
|---|---|---|---|
| Interval | Step Size | Interval | Step Size |
| $0 \le \xi \le 0.005$ | $k^3 = 2.5 \times 10^{-3}$ | $0 \le \eta_j \le 0.05$ | $h^2 = 1.25 \times 10^{-4}$ |
| $0.005 \le \xi \le 0.05$ | $k^3 = 2.25 \times 10^{-2}$ | $0.05 \le \eta_j \le 8.0$ | $h^2 = 0.0125$ |
| $0.05 \le \xi \le 0.1$ | $k^3 = 0.025$ | $8.0 \le \eta_j \le 18.0$ | $h^2 = 0.025$ |
| $0.1 \le \xi \le 1.0$ | $k^3 = 0.05$ | $18.0 \le \eta_j \le 37.5$ | $h^2 = 0.075$ |
| $1.0 \le \xi \le 5.0$ | $k^3 = 0.125$ | $37.5 \le \eta_j \le 55.0$ | $h^2 = 0.175$ |
| $5.0 \le \xi \le 10.0$ | $k^3 = 0.25$ | $55.0 \le \eta_j \le 70.0$ | $h^2 = .375$ |
| $10 \le \xi \le 40$ | $k^3 = 0.5$ | $70.0 \le \eta_j \le 86.0$ | $h^2 = 0.8$ |
| $40 \le \xi \le 50$ | $k^3 = 1.0$ | $86.0 \le \eta_j$ | $h^2 = 1.0$ |
| $50 \le \xi \le 100$ | $k^3 = 2.5$ | | |
| $100 \le \xi \le 200$ | $k^3 = 5.0$ | | |
| $200 \le \xi \le 300$ | $k^3 = 10.0$ | | |
| $300 \le \xi \le 500$ | $k^3 = 25.0$ | | |
| $500 \le \xi \le 1000$ | $k^3 = 50.0$ | | |

Table 4.9.1 Step sizes used to obtain overall solution with PC using stretched coordinates.

| | $\frac{\xi}{2\sqrt{2}}\frac{a\tau_s}{\mu U}$ | | | |
|---|---|---|---|---|
| $\xi$ | MESH 1 | MESH2 | MESH3 | EXTRAPOLATED |
| 0.000 | 0.66417860 | 0.66413066 | 0.66417860 | 0.664114680 |
| 0.010 | 0.66591223 | 0.66586446 | 0.66591219 | 0.665848483 |
| 0.100 | 0.69813443 | 0.69809008 | 0.69811906 | 0.698054803 |
| 0.200 | 0.73068687 | 0.73064622 | 0.73068167 | 0.730625737 |
| 0.300 | 0.76210352 | 0.76206681 | 0.76205947 | 0.761995840 |
| 0.400 | 0.79245155 | 0.79241896 | 0.79241535 | 0.792359830 |
| 0.500 | 0.82190543 | 0.82187712 | 0.82187679 | 0.821829497 |
| 0.600 | 0.85057675 | 0.85055292 | 0.85054636 | 0.850504457 |
| 0.700 | 0.87853378 | 0.87851463 | 0.87850841 | 0.878474420 |
| 0.800 | 0.90585916 | 0.90584489 | 0.90583330 | 0.905805653 |
| 0.900 | 0.93260298 | 0.93259383 | 0.93258043 | 0.932560713 |
| 1.000 | 0.95882295 | 0.95881913 | 0.95880049 | 0.958787910 |
| 2.000 | 1.19948747 | 1.19954959 | 1.19941791 | 1.199477550 |
| 3.000 | 1.41411643 | 1.41426691 | 1.41404447 | 1.414221123 |
| 4.000 | 1.61252790 | 1.61278686 | 1.61246136 | 1.612784460 |
| 5.000 | 1.79950028 | 1.79988511 | 1.79944097 | 1.799934307 |
| 10.000 | 2.63312486 | 2.63431944 | 2.63305348 | 2.634622460 |
| 50.000 | 7.64480952 | 7.65387456 | 7.64529680 | 7.657545947 |
| 100.000 | 12.79508431 | 12.81217540 | 12.79534208 | 12.818216123 |
| 500.000 | 45.97890870 | 46.04134771 | 45.97773464 | 46.060595300 |
| 600.000 | 53.44373197 | 53.51707805 | 53.44181819 | 53.538975037 |
| 700.000 | 60.73542672 | 60.82017251 | 60.73283595 | 60.844966747 |
| 800.000 | 67.88386738 | 67.98067182 | 67.88116721 | 68.009339740 |
| 900.000 | 74.91135802 | 75.02102680 | 74.90865225 | 75.053975367 |
| 1000.000 | 81.83417017 | 81.95763243 | 81.83162767 | 81.995396517 |

Table 4.9.2 Comparison of skin-friction coefficient of individual Keller Box solutions using stretched coordinates with Richardson extrapolated results.

| | $\frac{\xi}{2\sqrt{2}}\frac{\sigma T_0}{\mu U}$ | |
|---|---|---|
| $\xi$ | SIMILARITY | STRETCHED |
| 0.000 | 0.46959999 | 0.46959999 |
| 0.050 | 0.48173322 | 0.48173567 |
| 0.100 | 0.49360110 | 0.49359928 |
| 0.200 | 0.51662389 | 0.51663041 |
| 0.300 | 0.53881807 | 0.53881243 |
| 0.400 | 0.56028460 | 0.56028301 |
| 0.500 | 0.58112207 | 0.58112121 |
| 0.600 | 0.60139830 | 0.60139747 |
| 0.700 | 0.62117561 | 0.62117522 |
| 0.800 | 0.64050179 | 0.64050132 |
| 0.900 | 0.65942026 | 0.65942000 |
| 1.000 | 0.67796572 | 0.67796543 |
| 2.000 | 0.84815952 | 0.84815871 |
| 3.000 | 1.00000031 | 1.00000535 |
| 4.000 | 1.14038703 | 1.14041083 |
| 5.000 | 1.27270049 | 1.27274575 |
| 10.000 | 1.86279121 | 1.86295941 |
| 50.000 | 5.41314768 | 5.41470267 |
| 100.000 | 9.06272953 | 9.06384754 |
| 500.000 | 32.56933001 | 32.56975928 |
| 600.000 | 37.85727105 | 37.85777231 |
| 700.000 | 43.02338901 | 43.02388859 |
| 800.000 | 48.08932591 | 48.08986531 |
| 900.000 | 53.07062068 | 53.07117494 |
| 1000.000 | 57.97892267 | 57.97950090 |

Table 4.9.3 Skin-friction coefficient obtained by overall Keller Box method using similarity coordinates vs stretched coordinates.

| | △ | | |
|---|---|---|---|
| ξ | SIMILARITY | STRETCHED | JO (1968) |
| 0.000 | 1.72082086 | 1.72078800 | 1.7208 |
| 0.005 | 1.72091319 | 1.72088000 | 1.721 |
| 0.050 | 1.72196839 | 1.72193300 | 1.722 |
| 0.100 | 1.72357246 | 1.72354100 | - |
| 0.200 | 1.72791746 | 1.72788000 | 1.728 |
| 0.300 | 1.73350480 | 1.73348100 | - |
| 0.400 | 1.74006935 | 1.74003500 | 1.740 |
| 0.500 | 1.74740560 | 1.74736800 | - |
| 0.600 | 1.75536896 | 1.75532900 | 1.755 |
| 0.700 | 1.76384312 | 1.76380000 | - |
| 0.800 | 1.77273877 | 1.77269300 | 1.773 |
| 0.900 | 1.78198359 | 1.78193500 | - |
| 1.000 | 1.79151997 | 1.79146800 | 1.792 |
| 2.000 | 1.89560738 | 1.89526000 | 1.896 |
| 3.000 | 2.00509106 | 2.00425900 | 2.005 |
| 4.000 | 2.11452606 | 2.11312000 | 2.115 |
| 5.000 | 2.22239838 | 2.22038100 | 2.222 |
| 10.000 | 2.73205314 | 2.72578200 | 2.731 |
| 20.000 | 3.63992185 | 3.62066300 | 3.637 |
| 30.000 | 4.45815149 | 4.43086900 | 4.449 |
| 40.000 | 5.22060547 | 5.19357700 | 5.185 |
| 50.000 | 5.94384265 | 5.92159700 | - |
| 100.000 | 9.21269426 | 9.19831600 | - |
| 500.000 | 29.60222405 | 29.56097000 | - |
| 600.000 | 34.10764140 | 34.06005000 | - |
| 700.000 | 38.49225729 | 38.43863000 | - |
| 800.000 | 42.77797040 | 42.71741000 | - |
| 900.000 | 46.98044679 | 46.91220000 | - |
| 1000.000 | 51.11139189 | 51.03465000 | - |

Table 4.9.4 Comparison of displacement thickness obtained by overall Keller Box method using similarity vs. stretched coordinates and vs. the solution obtained by Jaffe and Okamura (1968) (JO). Greatest difference is less than 0.7 %.

| | $\frac{\xi}{2\sqrt{2}} \frac{a \tau_o}{\mu U}$ | |
|---|---|---|
| $\xi$ | Overall (stretched) | JO (1968) |
| 0.000 | 0.664114680 | 0.6641 |
| 0.050 | 0.681277117 | 0.6813 |
| 0.100 | 0.698054803 | - |
| 0.200 | 0.730625737 | 0.7306 |
| 0.300 | 0.761995840 | - |
| 0.400 | 0.792359830 | 0.7924 |
| 0.500 | 0.821829497 | - |
| 0.600 | 0.850504457 | 0.8505 |
| 0.700 | 0.878474420 | - |
| 0.800 | 0.905805653 | 0.9058 |
| 0.900 | 0.932560713 | - |
| 1.000 | 0.958787910 | 0.9588 |
| 2.000 | 1.199477550 | 1.199 |
| 3.000 | 1.414221123 | 1.414 |
| 4.000 | 1.612784460 | 1.613 |
| 5.000 | 1.799934307 | 1.800 |
| 10.000 | 2.634622460 | 2.634 |
| 20.000 | 4.061734123 | 4.061 |
| 30.000 | 5.336718597 | 5.338 |
| 40.000 | 6.526130760 | 6.535 |
| 50.000 | 7.657545947 | - |
| 100.000 | 12.818216123 | - |
| 500.000 | 46.060595300 | - |
| 600.000 | 53.538975037 | - |
| 700.000 | 60.8449667[illegible] | - |
| 800.000 | 68.009339740 | - |
| 900.000 | 75.053975367 | - |
| 1000.000 | 81.995396517 | - |

Table 4.9.5 Comparison of skin-friction coefficient of overall Keller Box solution using stretched coordinates vs. solution of Jaffe and Okamura (1968) (JO). Greatest difference is less than 0.2 %.

| | θ | | |
|---|---|---|---|
| ξ | SIMILARITY | STRETCHED | J-O (1968) |
| 0.000 | 0.664114675 | 0.664114673 | 0.6641 |
| 0.005 | 0.664981884 | 0.664981912 | 0.6649 |
| 0.050 | 0.672726720 | 0.672727886 | 0.6727 |
| 0.100 | 0.681211130 | 0.681211470 | - |
| 0.200 | 0.697821300 | 0.697827250 | 0.6978 |
| 0.300 | 0.714014858 | 0.714019186 | - |
| 0.400 | 0.729826532 | 0.729828797 | 0.7298 |
| 0.500 | 0.745294661 | 0.745295973 | - |
| 0.600 | 0.760450504 | 0.760451368 | 0.7604 |
| 0.700 | 0.775321409 | 0.775321524 | - |
| 0.800 | 0.789930044 | 0.789929263 | 0.7899 |
| 0.900 | 0.804296734 | 0.804294283 | - |
| 1.000 | 0.818438664 | 0.818433749 | 0.8184 |
| 2.000 | 0.950202693 | 0.949914667 | 0.9503 |
| 3.000 | 1.069630496 | 1.068891456 | 1.070 |
| 4.000 | 1.180870349 | 1.179609214 | 1.181 |
| 5.000 | 1.286121546 | 1.284301786 | 1.286 |
| 10.000 | 1.757145077 | 1.751361252 | 1.756 |
| 20.000 | 2.561382612 | 2.543335039 | 2.557 |
| 30.000 | 3.276621764 | 3.251409848 | 3.270 |
| 40.000 | 3.941326847 | 3.916906600 | 3.921 |
| 50.000 | 4.571826736 | 4.552352551 | - |
| 100.000 | 7.430662374 | 7.418496068 | - |
| 500.000 | 25.551887904 | 25.515114817 | - |
| 600.000 | 29.595753625 | 29.553492470 | - |
| 700.000 | 33.539813994 | 33.492373426 | |
| 800.000 | 37.401987137 | 37.348487212 | - |
| 900.000 | 41.195111530 | 41.134807848 | - |
| 1000.000 | 44.928790121 | 44.860873234 | - |

Table 4.9.6 Comparison of momentum thickness obtained by overall Keller Box method using similarity vs. stretched coordinates vs. the solution of Jaffe and Okamura (1968) (JO). Greatest percentage difference is less than 0.5 %.

# 5 LOCAL SIMILARITY SOLUTION

## 5.1 PRELIMINARY

Although, in principle, the Keller's Box method described previously could be used to obtain solutions that more closely approach the needle limit, it is restricted by the limited storage capacity of computing systems. Of course, the need for increased computer capacity is because smaller step sizes, which foster more grid points, are required to obtain reasonable accuracy to better approximate the rapidly changing velocity and shear stress profiles near the surface of the cylinder for large values of $\xi$. This is regardless of the coordinates, variables or methods used. Thus, one must be aware that numerical interpolation schemes are needed at this point to estimate values of the dependent variables at the new discrete locations that are created when the numerical grid is subdivided.

For large distances downstream, the asymptotic solution of Glauert and Lighthill (1955) becomes more accurate due to the increase in value of the expansion parameter $\beta$. However, it was pointed out previously, that even at a $\xi$-value of 1000, velocity profiles are obtained which are inaccurate near the surface of the cylinder. Also, solving for higher order terms in the asymptotic expansion could be a difficult and tedious numerical task. Since the solution must be obtained numerically, a simple and efficient approach should be used. One of these approaches includes the "overall" Keller's Box procedure previously described. Another, is a method which is also efficient, but simpler to use in an attempt to solve the full range of the problem.

This method is related to the Keller's Box method and it yields accurate solutions near the needle limit. The simplicity of this method together with the accurate solutions it produces makes it a suitable substitute to the "overall" Keller's Box procedure at large enough $\xi$. In principle, it could completely overtake the asymptotic solution in its range of validity. This method and the results it produces are described in this chapter.

## 5.2 METHOD OF LOCAL SIMILARITY

Using the equations from the Keller's Box primitive variable formulation, i.e., equations 4.2.1-3, with similarity coordinates $\eta_1$ and $\xi$, but setting $P_\xi = 0$, as in a local similarity approach gives :

$$\overline{R} = P_{\eta_1}, \tag{5.2.1}$$

$$(H\overline{R})_{\eta_1} + \tilde{Q}\overline{R} = 0, \tag{5.2.2}$$

and

$$\tilde{Q}_{\eta_1} - (2H - 1)P = 0, \tag{5.2.3}$$

with the boundary conditions:

$$P(0) = \tilde{Q}(0) = 0 \text{ at } \eta_1 = 0 \text{ and } P(\infty) = 1. \tag{5.2.4}$$

Quantities $\tilde{Q}$ and H are defined as in section 4.2, i.e.

$$\tilde{Q} = H\left(\eta_1 P - \overline{R}\frac{\xi}{2\sqrt{2}}Q\right) \text{ and } H = 1 + \frac{\xi}{2\sqrt{2}}\eta_1.$$

and we note that P and $\tilde{Q}$ are explicit functions of $\eta_1$.

Alternatively, equations 5.2.1-3 may be obtained by transforming the governing equations 1.2.6-7, via

$$\frac{\partial}{\partial r}=\frac{2\sqrt{2}}{\xi}\frac{\partial}{\partial \eta_1},\ \frac{\partial^2}{\partial r^2}=\frac{8}{\xi^2}\frac{\partial^2}{\partial \eta_1^2},\ \text{and}\ \frac{\partial}{\partial x}=-\frac{8\eta_1}{\overline{R}\xi^2}\frac{\partial}{\partial \eta_1}.$$

This local similarity method which assumes that $P_\xi = 0$ is comparable to the methods used in Chapter 2 obtaining the 'quasi'-similar solutions. This is because, in each case, the dependent variables involved depend implicitly and not explicitly on $\xi$. Recall that $\xi = 2\sqrt{2}/\eta_0$.

The method of solution uses the Keller's Box technique with simplified equations 5.2.1-3. However, the discretization is employed over a line, as in Figure 5.2.1, and not a box because of this lack of functional dependence of P on $\xi$. Keller (1978) states that the Box scheme can be used on equations of similar boundary layer flows by setting the stream-wise variable to zero in the nonsimilar equations. Blottner (1975) explains that the assumption of local similarity, which neglects $\xi$-derivatives, can be used to obtain approximate solutions to some flows.

Discretization of equation 5.2.1 is the same as in section 4.2, given by equation 4.2.6. The discretized equations of 5.2.1-3 are given by :

$$P^j - P^{j-1} - \frac{h_j}{2}(\overline{R}^j + \overline{R}^{j-1}) = 0. \qquad (5.2.5)$$

$$H^j\overline{R}^j - H^{j-1}\overline{R}^{j-1} + h_j\tilde{Q}^{j-1/2}\overline{R}^{j-1/2} = 0, \qquad (5.2.6)$$

and

$$\tilde{Q}^j - \tilde{Q}^{j-1} - h_j(H^j + H^{j-1} - 1)P^{j-1/2} = 0. \qquad (5.2.7)$$

Central differences are used in approximation to obtain these discretized formulae above. Alternatively, (5.2.6) and (5.2.7) could be obtained by setting individual terms with subscripts (n - 1) and terms with $k_n$ in the denominator to zero in difference equations 4.2.4 and 4.2.5.

Series expansions used in discretization are the same as those used in section 4.2, except that individual terms in $\xi$ and $\xi$-derivatives are neglected.

The product terms in equations 5.2.5 and 5.2.6 are discretized in a similar manner as in (4.2.12) about $\eta_1^{j-1/2}$, i.e.,

$$(\bar{Q}\bar{R})^{j-1/2} = \bar{Q}^{j-1/2}\bar{R}^{j-1/2} = \left(\frac{\bar{Q}^j + \bar{Q}^{j-1}}{2} - \frac{h_j^2}{8}\bar{Q}^{j-1/2}_{\eta_1\eta_1} + \ldots\right)\left(\frac{\bar{R}^j + \bar{R}^{j-1}}{2} - \frac{h_j^2}{8}\bar{R}^{j-1/2}_{\eta_1\eta_1} + \ldots\right), \tag{5.2.8}$$

Hence, we take the product of averages. Similarly for the term, $(2H-1)P$, in (5.2.3), where (2H - 1) is treated as the factor $\bar{Q}$ is above.

The term $\bar{Q}_{\eta_1}$ is simply discretized in a central difference over $\eta_1^{j-1/2}$, which as in (4.2.15) gives :

$$\bar{Q}_{\eta_1} = \frac{\bar{Q}^j - \bar{Q}^{j-1}}{h_j} - \frac{h_j^2}{24}\bar{Q}^{j-1/2}_{\eta_1\eta_1\eta_1} + \ldots. \tag{5.2.9}$$

This is similar for the term $(H\bar{R})_{\eta_1}$ in 5.2.2, where (H R bar) is treated as one entity.

Applying Newton's method to equations 5.2.5-7 yields :

$$\beta^j \delta\bar{R}^j + \theta^j \delta\tilde{Q}^j + \tilde{\beta}^j \delta\bar{R}^{j-1} + \theta^j \delta\tilde{Q}^{j-1} = t^j, \tag{5.2.10}$$

$$\delta\tilde{Q}^j - \delta\tilde{Q}^{j-1} + FAC^j(\delta P^j + \delta P^{j-1}) = m^j, \tag{5.2.11}$$

and

$$\delta P^j_{(i)} - \delta P^{j-1}_{(i)} - \frac{h_j}{2}\left(\delta\bar{R}^j_{(i)} + \delta\bar{R}^{j-1}_{(i)}\right) = l^j_{(i)}, \tag{5.2.12}$$

where

$$\beta^j \equiv H^j + \frac{h_j}{2}\tilde{Q}^{j-1/2},$$

$$\tilde{\beta}^j \equiv H^{j-1} + \frac{h_j}{2}\tilde{Q}^{j-1/2},$$

$$\theta^j \equiv \frac{h_j}{2}\bar{R}^{j-1/2},$$

$$FAC^j \equiv -\frac{h_j}{2}(H^j + H^{j-1} - 1),$$

$$t^j \equiv H^{j-1}\bar{R}^{j-1} - H^j\bar{R}^j - h_j\tilde{Q}^{j-1/2}\bar{R}^{j-1/2},$$

$$l^j \equiv P^{j-1} - P^j + \frac{h_j}{2}(\bar{R}^j + \bar{R}^{j-1}), \tag{5.2.13}$$

and

$$m^j \equiv \tilde{Q}^{j-1} - \tilde{Q}^j + h_j(H^j + H^{j-1} - 1)P^{j-1/2}. \tag{5.2.11}$$

The coefficient $\gamma$ is non-existent, here, because the term $\xi HPP_\xi$ from equation 4.2.1, that produces it has been set to zero in (5.2.2) due to local similarity considerations.

Rewriting this linear system as :

$$\overline{F}^j \delta^j - \overline{G}^j \delta^{j-1} = s^j, \tag{5.2.14}$$

where

$$\overline{F}^j \equiv \begin{bmatrix} 1 & 0 & FAC^j \\ \theta^j & \beta^j & 0 \\ 0 & -\frac{h_j}{2} & 1 \end{bmatrix} \text{ and } \overline{G}^j \equiv \begin{bmatrix} 1 & 0 & -FAC^j \\ -\theta^j & -\beta^j & 0 \\ 0 & \frac{h_j}{2} & 1 \end{bmatrix}.$$

with the boundary conditions

$$\delta P^0 = \delta \bar{Q}^0 = \delta P^J = 0, \tag{5.2.15}$$

we see that the block tridiagonal structure can be maintained.

Thus, the complete block tridiagonal system can be reduced similarly to that in (4.3.9) or (4.3.10), except that the elements of the $3 \times 3$ matrices are different and definition 4.3.11 still holds, i.e.,

$$z^1 \equiv \begin{bmatrix} \delta \overline{R}^0 \\ \delta \bar{Q}^1 \\ \delta \overline{R}^1 \end{bmatrix}, \quad z^j \equiv \begin{bmatrix} \delta P^{j-1} \\ \delta \bar{Q}^j \\ \delta \overline{R}^j \end{bmatrix}, 2 \le j \le J. \tag{5.2.16}$$

The coefficient matrix $\overline{A}_{(i)}$ is of order 3 J + 3 and the vectors $z^j$ and $s^j_{(i)}$ have that dimension.

Decomposing the coefficient matrix, $\overline{A}_{(i)}$ into the $3 \times 3$ blocks gives :

$$\overline{A}_{(i)}=\begin{bmatrix} A^1_{(i)} & C^1_{(i)} & & & & & & & \\ B^2_{(i)} & A^2_{(i)} & C^2_{(i)} & & & & & & \\ & \cdot & \cdot & \cdot & & & 0 & & \\ & & \cdot & \cdot & \cdot & & & & \\ & & & B^J_{(i)} & A^J_{(i)} & C^J_{(i)} & & & \\ & & & & \cdot & \cdot & \cdot & & \\ & & 0 & & \cdot & \cdot & \cdot & & \\ & & & & & & B^{J-1}_{(i)} & A^{J-1}_{(i)} & C^{J-1}_{(i)} \\ & & & & & & & B^J_{(i)} & A^J_{(i)} \end{bmatrix},$$

where

$$A^1 \equiv \begin{bmatrix} 0 & 1 & 0 \\ \beta^1 & \theta^1 & \beta^1 \\ -\frac{h_1}{2} & 0 & -\frac{h_1}{2} \end{bmatrix}, \quad C^J \equiv \begin{bmatrix} FAC^J & 0 & 0 \\ 0 & 0 & 0 \\ 1 & 0 & 0 \end{bmatrix}, \tag{5.2.17 a}$$

$$B^J \equiv \begin{bmatrix} 0 & -1 & 0 \\ 0 & \theta^J & \beta^J \\ 0 & 0 & -\frac{h_J}{2} \end{bmatrix} \text{ and } A^J \equiv \begin{bmatrix} FAC^J & 1 & 0 \\ 0 & \theta^J & \beta^J \\ -1 & 0 & -\frac{h_J}{2} \end{bmatrix}. \tag{5.2.17 b}$$

At j = 1, the boundary conditions 5.2.15 gives :

$$[E^1_{(i)}]\begin{bmatrix} \delta\overline{R}^0 \\ \delta\bar{Q}^1 \\ \delta\overline{R}^1 \\ \delta P^1 \end{bmatrix} = \begin{bmatrix} m^1_{(i)} \\ t^1_{(i)} \\ l^1_{(i)} \end{bmatrix},$$

where

$$[E^1_{(i)}] \equiv \begin{bmatrix} 0 & 1 & 0 & FAC^J \\ \beta^1 & \theta^1 & \beta^1 & 0 \\ -\frac{h_1}{2} & 0 & -\frac{h_1}{2} & 1 \end{bmatrix}.$$

At j = J, (5.2.15) gives :

$$[E^J_{(i)}]\begin{bmatrix}\delta^{J-1}\\ \delta\bar{Q}^J\\ \delta\bar{R}^J\end{bmatrix}=\begin{bmatrix}m^J_{(i)}\\ t^J_{(i)}\\ l^J_{(i)}\end{bmatrix}$$

$$[E^J_{(i)}]=\begin{bmatrix}-1 & 0 & FAC^J & 1 & 0\\ \theta^J & \beta^J & 0 & \theta^J & \beta^J\\ 0 & -\frac{h_J}{2} & -1 & 0 & \frac{h_J}{2}\end{bmatrix}.$$

Appendix E may be consulted as to the solution of the block tridiagonal system, as was the case in Sections 4.3 and 4.7.

## 5.3 NUMERICAL SOLUTION

This method is very sensitive to the initial profiles that are used to begin the first iteration. An initial profile must be chosen that is appropriate in approximating the behavior of the velocity components and shear stresses at the location of the cylinder that we wish to solve, i.e., at the chosen value of $\xi$.

For example, near $\xi = 0$, the profile is essentially Blasius so that an initial profile that is exactly the Blasius or one close to it can be used. However, much farther down stream the velocity profile approaches the needle limit. In terms of similarity coordinates, we know from the previous solution in Chapter 4 that the axial velocity profile increases sharply to unity near the wall which makes u = 1 over most of the boundary layer region. Similarly, the shear stress profile decreases sharply to zero near the wall, such that it is equal to zero over most of the boundary layer region. Thus, the initial profiles that are chosen to begin the iteration should reflect this.

The initial axial velocity profiles which must satisfy the boundary conditions are estimated according to :

$$P = \frac{\eta_1}{\eta_\infty} \text{ for } 0 \le \eta_1 \le \eta_1^* \text{ and } P = 1 \text{ for } \eta_1^* \le \eta_1 \le \eta_\infty, \tag{5.3.1}$$

where the value of $\eta_1^*$ is obtained by trial and error and depends upon the value of $\xi$ which determines the point along the cylinder at which we seek a solution. Proceeding further downstream requires a smaller value of $\eta_1^*$.

Integrating (5.2.3) using (5.3.1) yields the initial profile for the radial velocity, i.e.,

$$\bar{Q} = \int_0^{\eta_1} \bar{Q}_{\eta_1} d\eta_1 = \int_0^{\eta_1} (2H - 1) P \, d\eta_1 = \int_0^{\eta_1} \left( 1 + \xi \frac{\eta_1}{\sqrt{2}} \right) P \, d\eta_1,$$

$$\text{which gives : } \bar{Q} = \frac{\eta_1^2}{\eta_\infty} \left( \frac{1}{2} + \xi \frac{\eta_1}{3\sqrt{2}} \right) \text{ for } 0 \le \eta_1 \le \eta_1^*, \tag{5.3.2 a}$$

$$\text{or } \bar{Q} = \eta_1 \left( 1 + \xi \frac{\eta_1}{2\sqrt{2}} \right) \text{ for } \eta_1^* \le \eta_1 \le \eta_\infty. \tag{5.3.2 b}$$

Differentiating equation 5.3.1 with respect to $\eta_1$ gives :

$$\bar{R} = \frac{1}{\eta_\infty} \text{ for } 0 \le \eta_1 \le \eta_1^* \text{ and } \bar{R} = 0 \text{ for } \eta_1^* \le \eta_1 \le \eta_\infty. \tag{5.3.3}$$

Trial and error and prior knowledge from the "overall" Keller's Box solution leads to setting $\bar{R}(0)$ to be a large value which depends on $\xi$ instead of using (5.3.3) there. For example, at $\xi = 1000$, $\bar{R}(0) = 50$ leads to a convergent solution.

In the case of an inappropriate estimate of an initial profile, divergence occurs in just a few iterations.

A value of $\eta_\infty = 8$ is used, while step sizes in $h_j$ are kept very small near the surface of the cylinder. This numerical approach has been quite successful for $\xi = 0$ to $\xi = 10^6$.

The remaining calculations that are performed are the same as described in section 4.4.

The convergence criterion used is the same as in (4.4.4). With the appropriate choice in initial profiles, only three to four iterations are required. The numerical grid does not need to be enlarged because the boundary layer growth is scaled down due to using similarity coordinates. However, if the grid needed to be increased, say if other coordinates are used, then we need only begin the entire procedure with a larger grid, since the method only solves at one station in $\xi$. In other words, the solution does not depend on any previous steps in $\xi$.

The local similarity Keller's Box approach is simpler and more efficient than the full Keller's Box approach because the solution is obtained only one station at a time in $\xi$ instead of at several stations. Computer storage is not required for solutions at a previous-step and the same number of iterations occur in a particular step as in the full Box scheme. The use of interpolation schemes further downstream which are needed to deal with rapidly changing profiles near the wall are not required. This is because the numerical grid need only be further subdivided in order to create the smaller step sizes required to obtain the needed accuracy. On the other hand, some experimentation is required in order to obtain the appropriate estimate of the initial profile. Successful estimates are more easily obtained if the general behavior of the boundary layer is known.

We apply Richardson extrapolation to two individual solutions obtained at different mesh sizes to produce a solution accurate to fourth order. Appendix F may be consulted as to the equations that lead up to the fourth order expression.

The mesh employed in the $\eta_1$-direction is in Table 5.3.1.

The solutions as a function of mesh sizes are given by $u_1(h^1)$ and $u_2(2h^1)$ and are obtained at a point of $\xi$ within the range $\xi = 0$ to $\xi = 10^6$. The extrapolated solutions are obtained using equation F.7 from Appendix F and are given by :

$$u_E = \frac{(4u_1 - u_2)}{3} - C h_1^4, \tag{5.3.4}$$

Extrapolation formulae are the same for all dependent variables, P, $\bar{Q}$, and $\overline{R}$. The largest step size of $h_j^1 = 0.01$ maintains accuracy up to 7 decimal places, where a 386 PC is used to carry out the computations.

The final results in terms of the velocity and shear stress profiles are presented in the next chapter.

Table 5.3.2 compares the individual skin-friction coefficient of each individual solution with the extrapolated result. Agreement is good to five digits for most of the steps, except at $\xi = 10^6$, where the extrapolation is more appropriate.

Comparisons are made with the solution obtained in this chapter to the "overall" Keller's Box solution. The skin-friction coefficient is compared in Table 5.3.3. We see that after the initial match at $\xi = 0$, the coefficient obtained by the local similarity approach deviates right after to a percentage difference of less than 5 % at $\xi = 1$ and $\xi = 10$. However, as $\xi$ increases the solutions begin to merge. Here, the percentage differences are less than 3 % at $\xi = 100$ and less than 2 % at $\xi = 1000$.

Comparison of velocity profiles between this local similarity approach and the "overall" Keller's Box method is demonstrated in Figures 5.3.1-4. We notice the agreement for large values of $\xi$. For $\xi > 100$, profiles begin to merge. At $\xi = 1000$, agreement is good.

This method is very successful where the needle limit is being approached. It is also very accurate right at the Blasius limit as it must be. It is worth noting that this method can take over where the y-based quasi-similar solution is not obtainable in the range from $\xi = .05$ to $\xi < 40$.

Comparison is made with the 'quasi'-similar solutions obtained in Chapter 2. Figure 5.3.5 shows that the skin-friction coefficients from each approach begin to merge at approximately $\xi = 55$. Figure 5.3.6 shows that the displacement thickness merges at approximately $\xi = 400$ and Figure 5.3.7 shows momentum thickness merging at approximately $\xi = 1000$. It appears as though the present solution of this chapter is in between the other two solutions.

The local similarity and 'quasi'-similar solutions appear to merge at approximately $\xi = 1000$ overall. The success in matching of the local similarity solution with the "overall" Keller's Box solution for $\xi \geq 100$ suggests that the local similarity Keller's Box method could proceed where the "overall" Keller's Box method stops, while obtaining accurate solutions. The efficiency of this method makes it even more attractive to use.

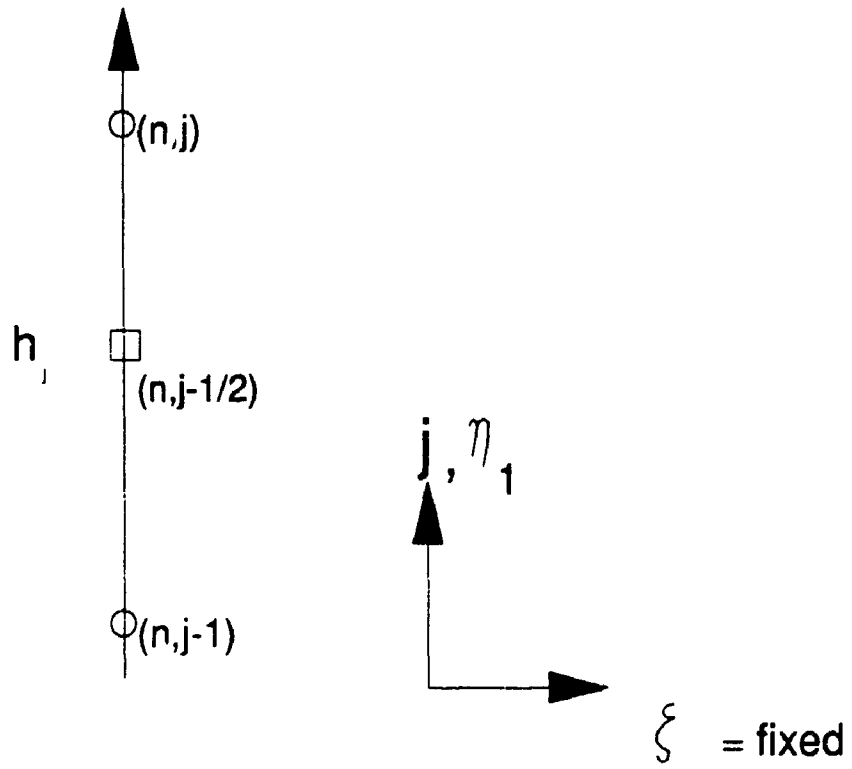


Figure 5.2.1 Numerical grid used for local similarity method.

| VARIABLE GRID | |
|---|---|
| Cross-stream Direction | |
| Interval | Step Size |
| $0 \le \eta_1 \le 0.001$ | $h^1 = 10^{-6}$ |
| $0.001 \le \eta_1 \le 0.01$ | $h^1 = 10^{-5}$ |
| $0.01 \le \eta_1 \le 0.1$ | $h^1 = 10^{-4}$ |
| $0.1 \le \eta_1 \le 1.0$ | $h^1 = 0.001$ |
| $1.0 \le \eta_1 \le 3.0$ | $h^1 = 0.005$ |
| $3.0 \le \eta_1 \le 8.0$ | $h^1 = 0.01$ |

Table 5.3.1 Step sizes used to obtain the local similarity solution to $\xi = 10^6$.

| $\xi$ | $\frac{\xi a}{2\sqrt{2}\mu U}\tau_0(h^1)$ | $\frac{\xi a}{2\sqrt{2}\mu U}\tau_0(2h^1)$ | $\frac{\xi a}{2\sqrt{2}\mu U}(\tau_E)_0$ |
|---|---|---|---|
| 0.00 | 0.46960053 | 0.46960216 | 0.46959999 |
| 0.05 | 0.48444469 | 0.48444638 | 0.48444413 |
| 1.00 | 0.70645536 | 0.70645773 | 0.70645408 |
| 10.00 | 1.94337665 | 1.94337848 | 1.94337604 |
| 40.00 | 4.75290311 | 4.75289554 | 4.75290563 |
| 100.00 | 9.26873687 | 9.26870751 | 9.26874666 |
| 500.00 | 33.01477236 | 33.01460300 | 33.01482881 |
| $10^3$ | 58.62421628 | 58.62387976 | 58.62432845 |
| $10^4$ | 425.92012776 | 425.91703296 | 425.92115936 |
| $10^5$ | 3339.56674292 | 3339.44768300 | 3339.60642956 |
| $10^6$ | 27436.37393986 | 27367.53194150 | 27451.32127265 |

Table 5.3.2 Comparison of skin-friction coefficients from the individual solutions at different mesh sizes to the extrapolated solution, $(\tau_E)_0$.

| $\xi$ | $\frac{\xi a}{2\sqrt{2}\mu U}\tau_0(h^1)$ Overall | $\frac{\xi a}{2\sqrt{2}\mu U}\tau_0$ Local Similarity | Percentage Difference |
|---|---|---|---|
| 0.00 | 0.46959999 | 0.46959999 | 0.0 |
| 0.05 | 0.48173322 | 0.48444413 | 0.6 |
| 1.00 | 0.67796572 | 0.70645408 | 4.2 |
| 10.00 | 1.86279121 | 1.94337604 | 4.3 |
| 100.00 | 9.06272953 | 9.26874666 | 2.3 |
| 500.00 | 32.56933001 | 33.01482881 | 1.4 |
| $10^3$ | 57.97892267 | 58.62432845 | 1.1 |

Table 5.3.3 Comparison of skin-friction coefficients from the overall Keller's Box solution with that of the local similarity Keller's Box solution. Percentage difference is included.

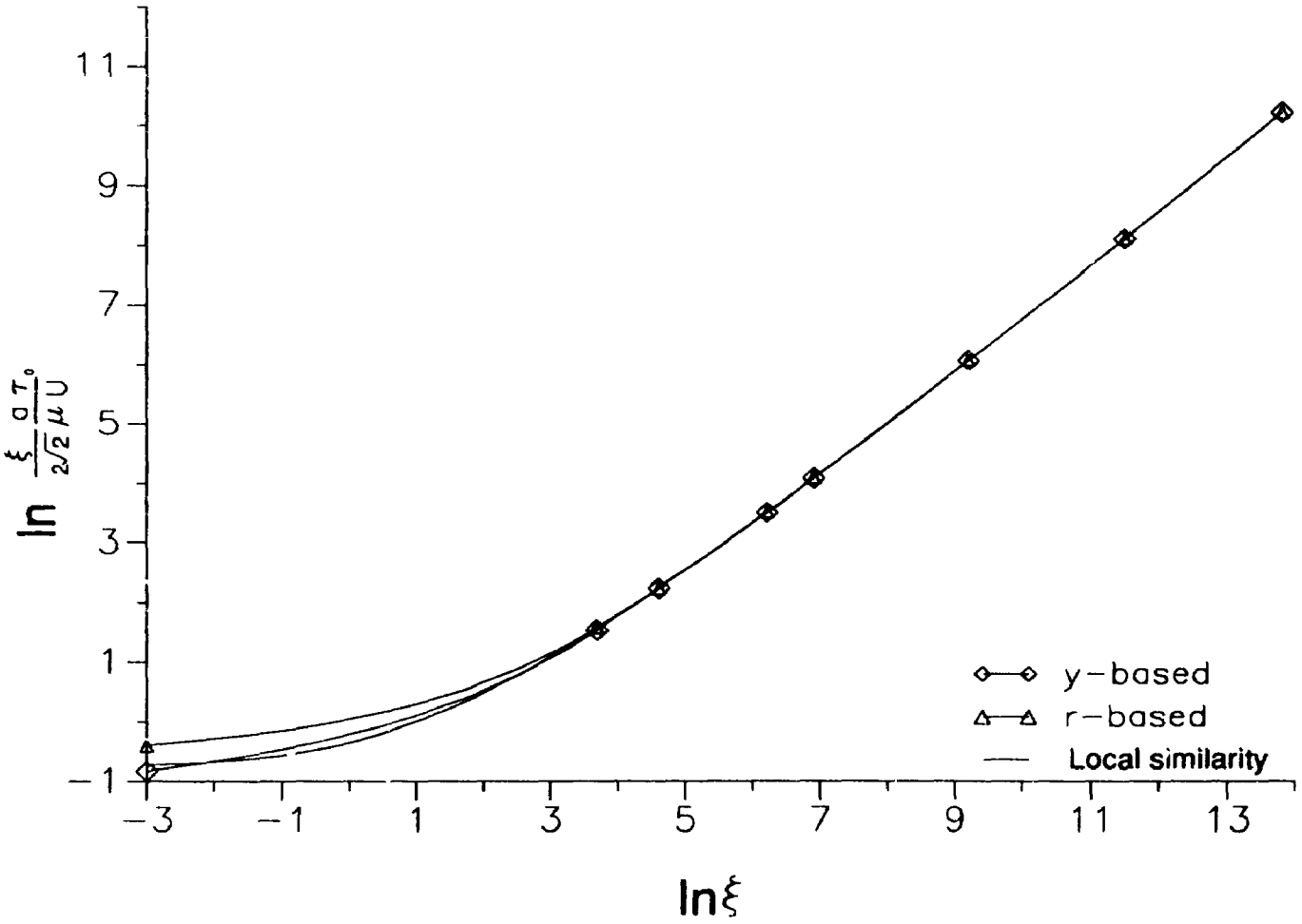


Figure 5.3.5 Comparison of skin-friction coefficient from local similarity Keller Box solution vs. r-based vs. y-based transformation 'quasi'-similar solutions.

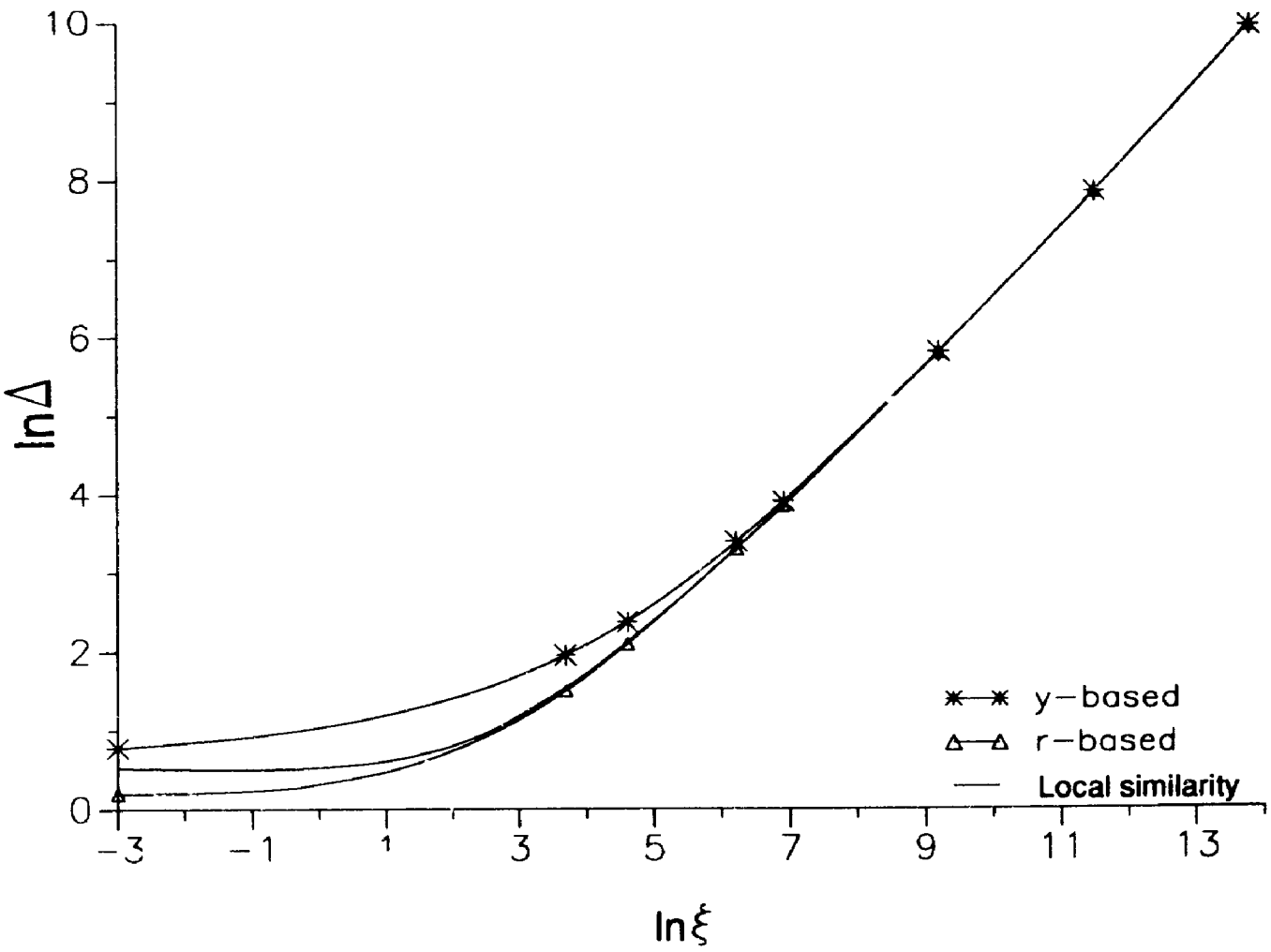


Figure 5.3.6 Comparison of displacement thickness of local similarity Keller Box solution vs. r-based transformation vs. y-based transformation 'quasi'-similar solutions.

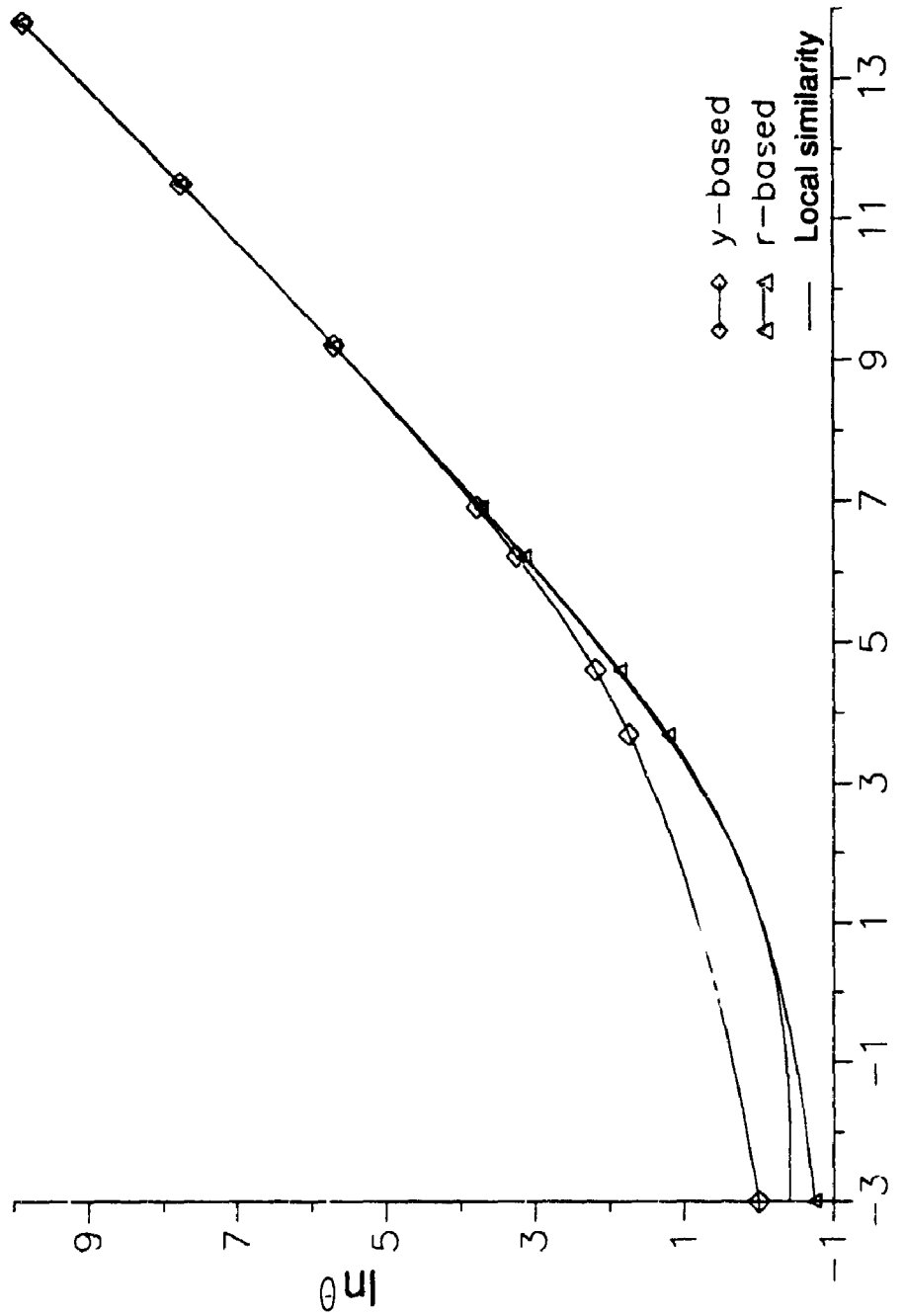


Figure 5.3.7 Comparison of momentum thickness obtained by local similarity Keller Box method vs. r-based vs. y-based transformations from the 'quasi'-similar solutions.

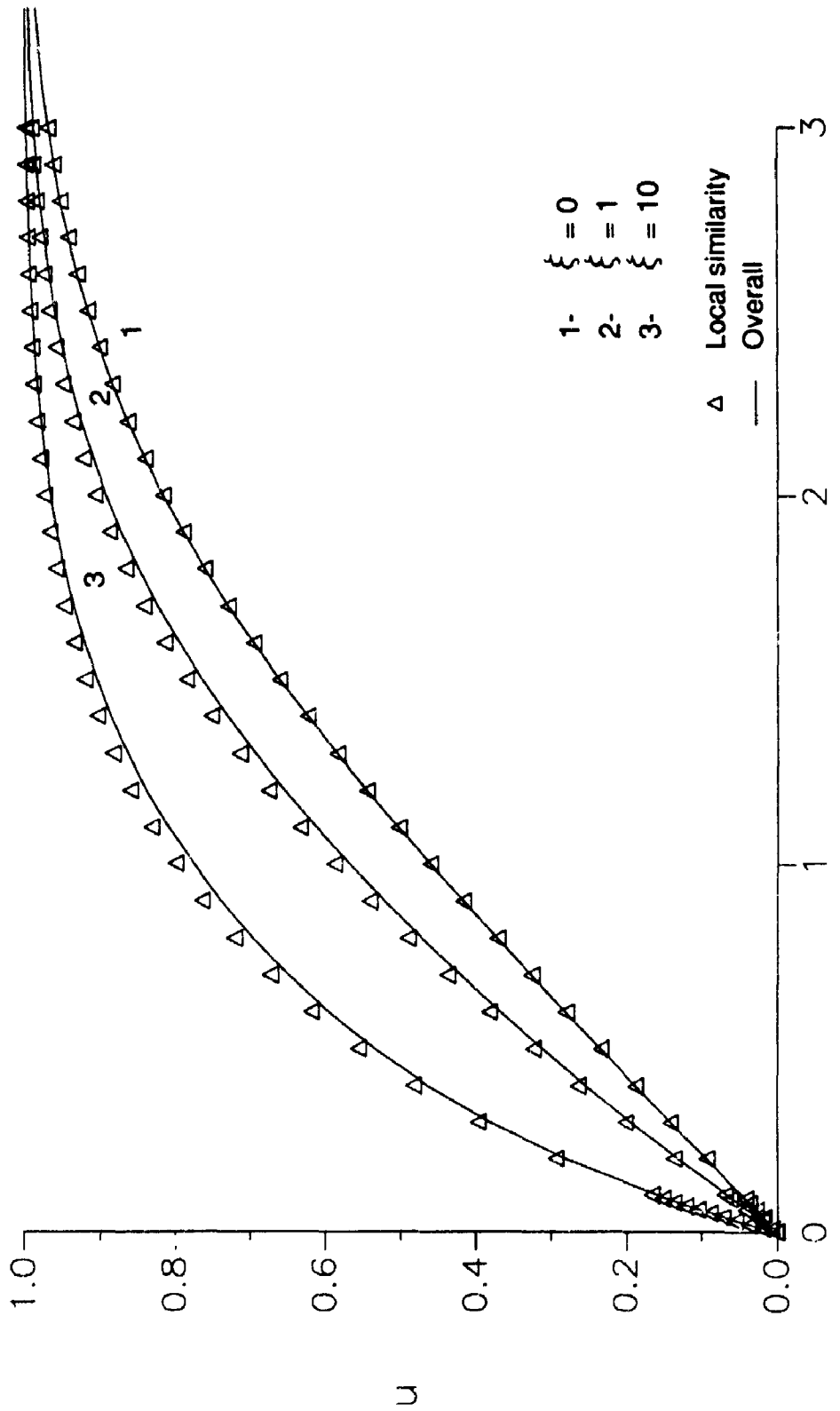


Figure 5.3.1 Comparison of axial velocity between the overall vs. the local similarity Keller Box solutions.

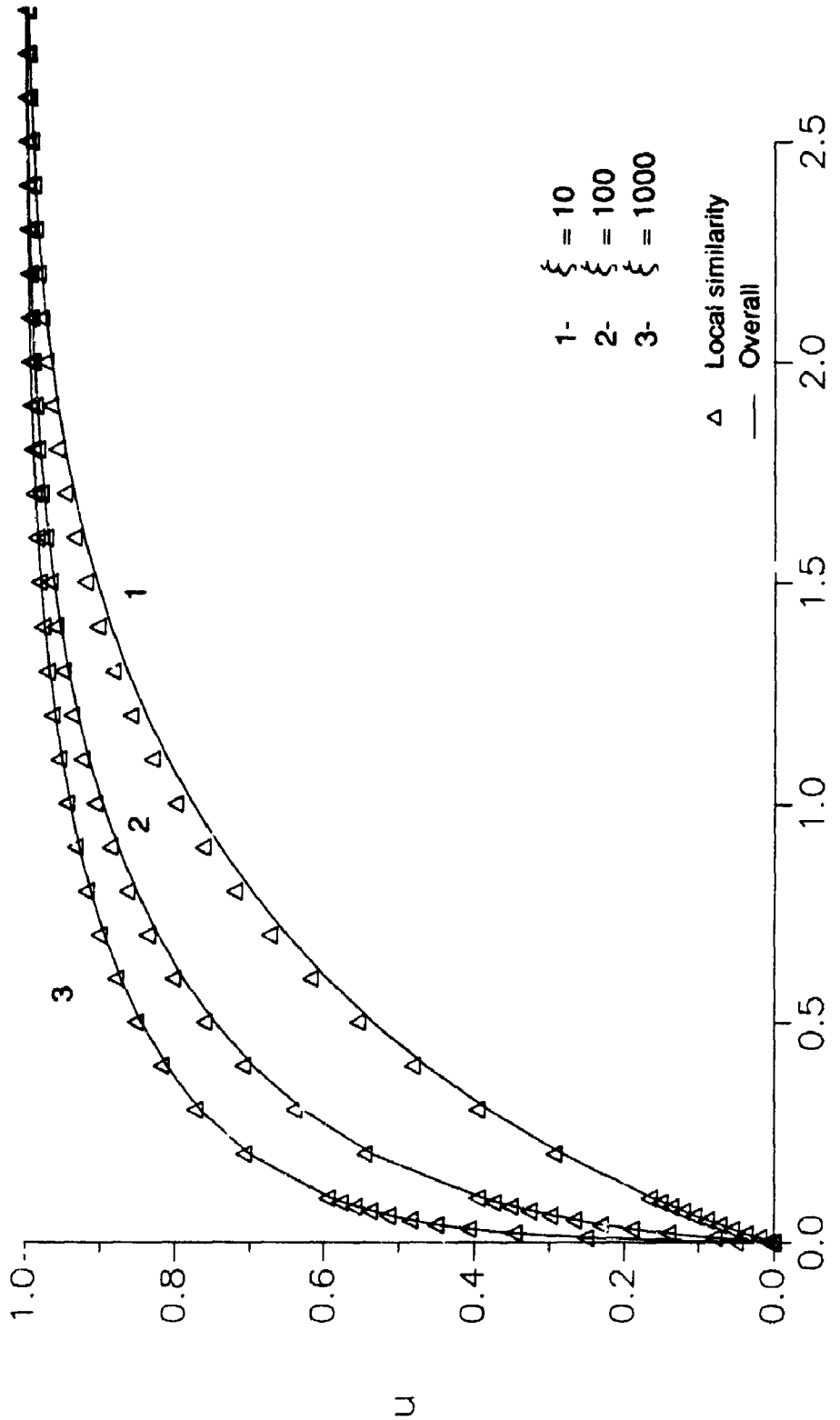


Figure 5.3.2 Comparison of axial velocity between overall vs. local local similarity Keller Box solutions.

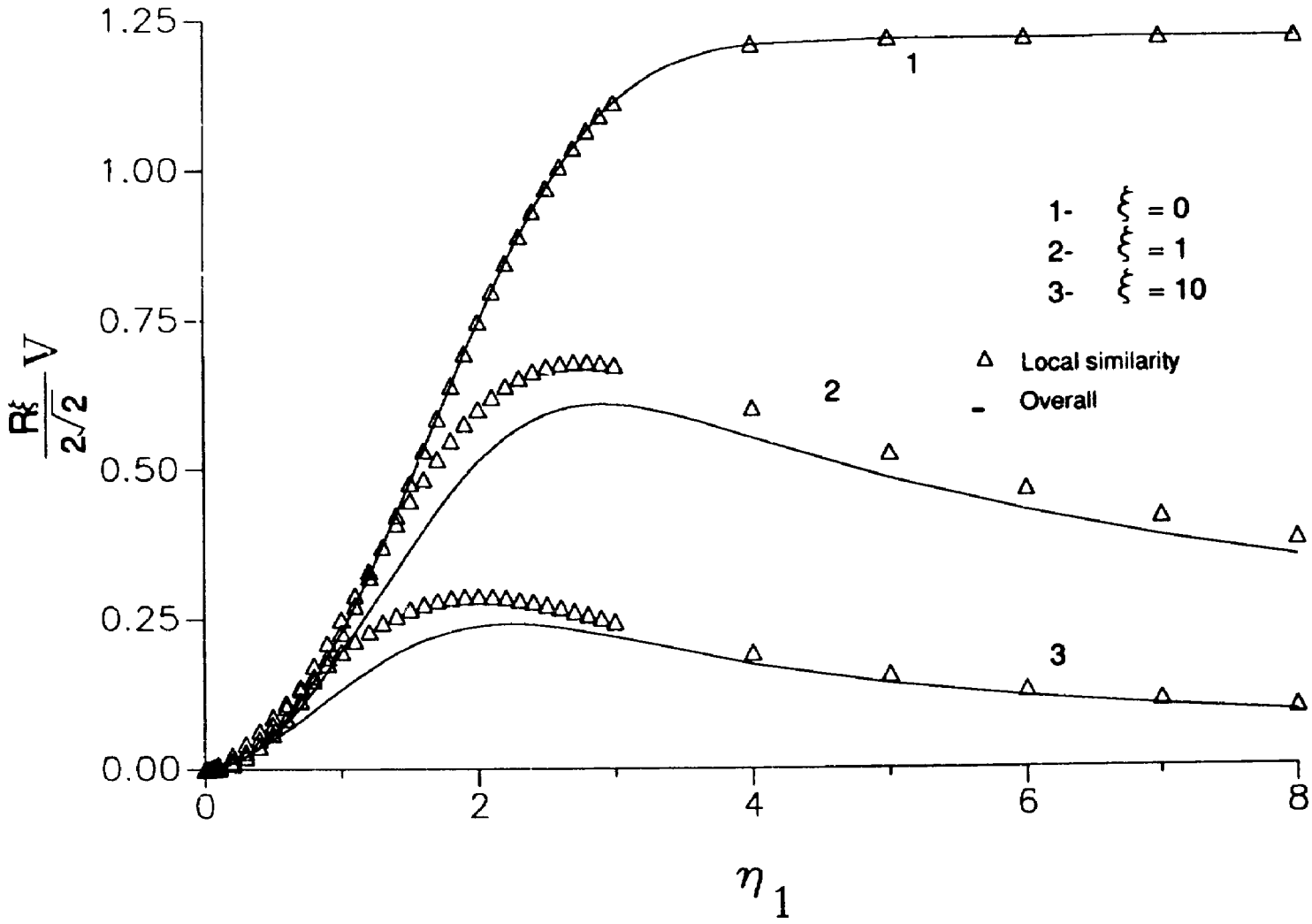


Figure 5.3.3 Comparison of radial velocity parameter between the overall vs. the local similarity Keller Box solutions.

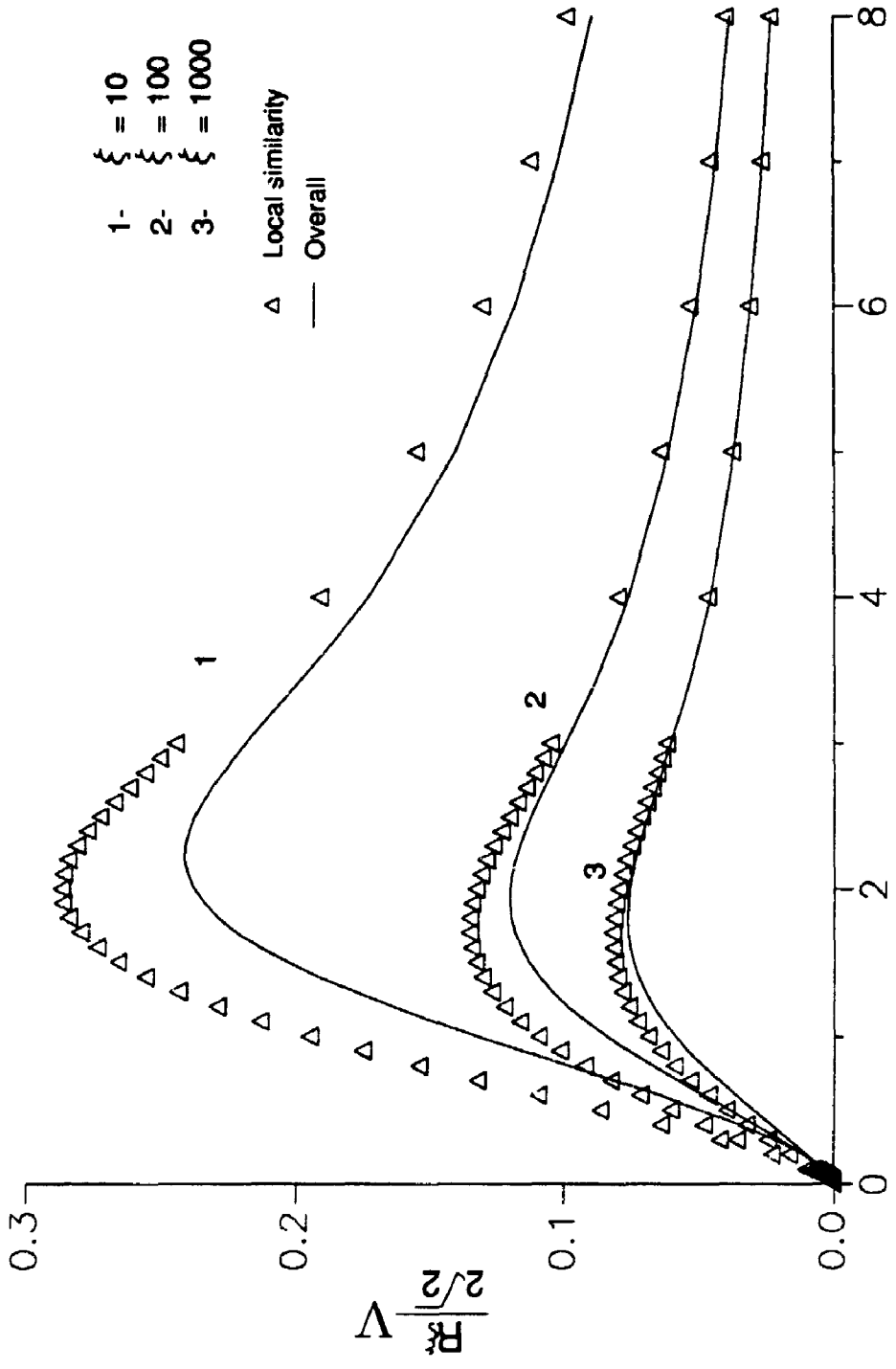


Figure 5.3.4 Comparison of radial velocity parameter between the overall vs. the local similarity Keller Box solutions.

# 6 RESULTS, DISCUSSIONS AND CONCLUSIONS

## 6.1 INTRODUCTION

Solutions have been obtained for the flow along a circular cylinder using the "overall" Keller's Box method in the range $\xi = 0$ to $\xi = 1000$. This range of $\xi$ considerably extends earlier results and connects the cylinder problem from the limit of very large radius (Blasius limit) to very small radius (needle limit). A special case of this method, the local similarity Keller's Box approach, extends the range even further from $\xi = 10^3$ to $\xi = 10^6$. Either method may, in principle, obtain solutions to a limitless range in $\xi$. However, practical considerations with respect to computer storage restrict this possibility.

'Quasi-similar' solutions have been obtained numerically using transformations based on obvious similarity variables. Near the Blasius limit, the solutions obtained using each transformation unexpectedly differ, while only the y-based transformation yields the proper solution in the Blasius limit. However, both solutions merge as we approach the needle limit. The validity of either solution appears to be in the range of $\xi \geq 1000$ with the exception of the y-based transformation which is also valid at the Blasius limit.

## 6.2 RESULTS

Final results obtained from the "overall" Keller's Box method using similarity coordinates, stretched coordinates, and results obtained from the local similarity Keller's Box method are presented. Richardson extrapolation has been applied in each case to maintain fourth order accuracy.

Velocity profiles and profiles of the shear stress parameter obtained from the "overall" Keller's Box method using similarity coordinates are presented in Figures 6.2.1-3. Results for the skin-friction coefficient, displacement and momentum thickness are presented in Figures 6.2.4a and 6.2.4b.

Velocity and shear stress parameter profiles obtained by the "overall" Keller's Box method using stretched coordinates are presented in Figure 6.2.5-10. The skin-friction, displacement and momentum thickness are presented in Figure 6.2.11.

Velocity and shear stress parameter profiles obtained by the local similarity Keller's Box method are presented in Figures 6.2.12-15.

## 6.3 COMPARISON WITH PREVIOUS RESULTS

Figures 6.3.1 and 6.3.2 compare the skin-friction and displacement thickness parameters obtained by the "overall" Keller's Box solution and the local similarity Keller's Box solution to the series solutions. A log-log graph is used for comparison.

The "overall" Keller's Box solution covers the entire range and fills the 'gap' created where each series solution begins to deviate. Solutions within the range of the 'gap' have been obtained by previous authors, but no extension was made into the so-called region of validity of the asymptotic series solution. The range of the present solution goes well beyond this region and widely overlaps with the region of validity

of the asymptotic solution. The range of the local similarity Keller's Box solution proceeds further, where the "overall" solution stops, even though the "overall" Keller's Box method could continue, in principle.

Table 6.3.1 compares the skin-friction coefficient obtained by the "overall" Keller's Box method with the series expansion methods. Percentage differences with respect to the series expansion and the numerical solution increase for increasing $\xi$. They begin at approximately 0 % at $\xi = 0$ and proceed to less than 3 % at $\xi = 1$. . . Percentage differences with respect to the asymptotic solution and the numerical solution decrease with increasing $\xi$. Beginning at $\xi = 10$, the percentage difference is approximately 1 % and it increases to a peak difference of less than 3 % at approximately $\xi = 20$. The differences then steadily decrease to less than 0.5 % at $\xi = 1000$.

Table 6.3.2 shows comparisons of the displacement thickness for the "overall" Keller's Box solution with the series expansion for small $\xi$ and with the asymptotic expansion for large $\xi$. The percentage differences start at approximately 0 % at $\xi = 0$ and gradually increase to less than 3 % at $\xi = 1$. The percentage differences obtained for the comparison with the asymptotic solution fluctuate beneath 8.5 % in the range of $10 \leq \xi \leq 60$, after which it decreases from approximately 5 % to less than 3 % at $\xi = 1000$.

If a percentage difference of one percent is tolerated with respect to the skin-friction coefficient, then the range of validity of the series expansion appears to be within $0 \leq \xi \leq 0.7$. With a similar criterion, the range of validity of the asymptotic expansion appears to be $\xi \geq 200$. Although, establishing the region of validity of solutions from either expansion depends upon the accuracy one chooses to match with

numerical solution. The criterion we have chosen, considered to be reasonable, decreases the range of validity of the asymptotic expansion suggested by Glauert and Lighthill (1954) from $\xi \geq 40$ to $\xi \geq 200$. Quantities obtained from the asymptotic solution should be given a liberal leeway, since error estimates are vague.

A comparison of velocity profiles obtained from the numerical solutions with those obtained from the asymptotic expansion is made in Figures 6.3.3-6. Velocity profiles from the asymptotic solution are inaccurate near the surface of the cylinder and also near the boundary layer edge as indicated in the figures. However, as was previously mentioned, more terms in the expansion would improve the accuracy of the solution, but these are difficult to obtain. Figure 6.3.3 and 6.3.4 show that at $\xi = 100$, the axial velocity obtained from the asymptotic expansion is still inaccurate. This is also reflected in the results given by Figures 6.3.5 and 6.3.6 with respect to the radial velocity parameter and by Figures 6.3.7 and 6.3.8 regarding the shear stress parameters. At $\xi = 1000$, agreement becomes good throughout, although the axial velocity is still negative at the surface and the profiles of the radial velocity and shear stress parameter do not match completely. This is shown in Figures 6.3.4, 6.3.6 and 6.3.9 respectively. The local similarity Keller's Box solution is compared at $\xi = 10^6$ and even at this point, the asymptotic axial velocity is negative at the surface and still not in agreement near the surface. Thus, these comparisons indicate that the asymptotic solution appears to have a smaller range of validity, when the velocity and shear stress parameter profiles are taken into account.

The local similarity Keller's Box approach obtains results which match with the "overall" Keller's Box solution in the approximate range of $\xi \geq 100$, as is shown in Chapter 5. The solutions match the 'quasi-similar' solutions obtained in Chapter 2 at

$\xi = 0$ (except the r-based transformation solution) and in the approximate range $\xi \geq 400$, as has been shown in Figures 5.3.5-7. The comparison in Table 6.3.1 of the local similarity skin-friction coefficient with that of the asymptotic solution shows excellent agreement, where percentage differences start at less than 0.5 % at $\xi = 10^4$ and tend to less than 0.2 % at $\xi = 10^6$. Table 6.3.2 comparing displacement thickness shows percentage difference of less than 5 % to approximately 3 % in the same range. Figures 6.3.10 and 6.3.11 comparing the velocity components at $\xi = 10^6$ shows good agreement over most of the profile, except near the surface of the cylinder, where the asymptotic solution is inaccurate. This method obtains velocity components more accurately than the asymptotic solution, especially near the surface of the cylinder. Thus, it may be more advantageous to generate solutions using the local similarity method than the asymptotic expansions, especially if velocity and shear stress profiles are required.

Numerical results of previous authors, namely Cebeci (1968), Cebeci (1970), and Cebeci and Smith (1974), and Jaffe and Okamura (1968), have compared very well with solutions obtained using the present methods in this thesis. This is established in Tables 4.9.4-6 dealing with the results of Jaffe and Okamura (1968), and the "overall" solutions using either similarity or stretched coordinates. Also, Figure 4.5.2 demonstrates the close match in skin-friction coefficient from results of Cebeci (1970), Cebeci and Smith (1974) and the "overall" solution. Figure 6.3.12, compares the skin-friction coefficient from the "overall" Keller's Box solution with that obtained by Cebeci and Smith (1974). We see that the range of the "overall" present solution is much larger than that of Cebeci and Smith (1974), whose range extends the furthest of past numerical solutions.

The "overall" solution and the local similarity solution cover a large range of the flow along a circular cylinder in axial flow. These methods have the possibility of proceeding further to approach the needle limit even more closely. The solutions match very well with the series expansion for small $\xi$, numerical solutions of other authors for increasing values of $\xi$, and with the asymptotic solution for large $\xi$. Velocity profiles obtained are more accurate than those obtained by the asymptotic expansion. Thus, the "overall" Keller's Box solution, which is very accurate, can, in principle, cover the full range of the problem.

## 6.4 COMPARISON AND DISCUSSION OF DIFFERENT METHODS

Both analytical and numerical methods have been used in order to solve the boundary layer equations 1.2.6-7. The series expansion for small $\xi$ and, especially, the asymptotic solution for large $\xi$, have guided the solution of the problem numerically.

The 'quasi-similar' solutions which are obtained by solving either the ordinary differential equation 2.2.22 or 2.3.18 numerically with the parameter $\eta_0$ use a standard Runge-Kutta shooting method described in chapter 2. The solution is obtained at one location in $\xi$ only. Thus, computer storage of previous solutions is not required. This numerical integration method is accurate to 4th order and does not need to be extrapolated for further accuracy, although stability and consistency problems may arise if the step size or domain of integration is inappropriate. It is a self starting step-by-step method in the cross-stream direction that can easily employ a variable grid if desired. Even though an efficient shooting algorithm is used with the Runge-Kutta procedure, shooting itself draws on more computer time because it is an

iterative process. Both similarity transformations yield solutions which appear to be valid for $\xi \geq 1000$, while only the solution obtained from the y-based transformation is valid at $\xi = 0$.

Jaffe and Okamura (1968) used a least squares approximation in the stream-wise direction, while using a Runge-Kutta shooting method in the cross-stream direction. Because of the least squares approach, much computer memory is required to store the solutions obtained at three previous location in $\xi$. Again, the iterations brought about by shooting slow down the process of marching downstream at each step of $\xi$. The shooting procedure may become complicated because stretched coordinates are used and these promote the enlargement of the numerical grid that deal with the growth of the boundary layer as one moves downstream. The inefficiency of this method, which is due to the requirement of large amounts of computer storage, may have prevented further progression in $\xi$, i.e., beyond $\xi = 40$.

The implicit finite difference method used by Cebeci (1970) requires computer storage of 2 previous steps in $\xi$. It also uses 5 points for the discretization in the cross-stream direction, which complicates the numerical formulae used, when combined with a variable grid. Stretched coordinates are used, again, promoting the growing numerical grid as one moves downstream in $\xi$. This exhausts more computer time, since the iteration at a particular step must be repeated until the asymptotic conditions are satisfied within the larger grid.

Cebeci and Smith (1974) used a stream function formulation in conjunction with the Keller's Box method which uses arbitrary step sizes and needs to store solutions at one previous step in $\xi$ only. Thus, a variable grid is easily implemented and the solution, accurate to second order, may be extrapolated via Richardson extrapolation

to 4th order. This implicit method is stable. Usually, 3 iterations are required at each step in $\xi$, only. Increase in computer time at each step in $\xi$ is due to the progressive lengthening of the numerical grid, again, due the use of stretched coordinates. The application of Richardson extrapolation is more complicated because the individual solutions obtained for different mesh sizes, do not all end at a common value of the boundary layer edge.

The "overall" Keller's Box method used in this thesis uses primitive variables and similarity coordinates. It has the same advantages as stated in the method used by Cebeci and Smith (1974), i.e., arbitrary step sizes, variable grid, computer storage at only one previous location, stability , second order accuracy with possibility of using Richardson extrapolation, and only 3 iterations required per step in $\xi$. However, the enlarging of the numerical grid is eliminated because of using similarity coordinates, which scale down the growth of the boundary layer as we move downstream. In fact, the edge of the boundary layer can remain at a constant value of 8. Thus, fewer discretized points are needed, which access less computer memory. Also, the extra computational time required, which is due to the iterations required to satisfy the asymptotic conditions for an enlarged computational grid at a particular step in $\xi$, is eliminated.

The "overall" Keller's Box method using primitive variables and stretched coordinates is similar to the method using similarity coordinates. The major difference is that the growth of the boundary layer as one moves downstream must be taken into account because of using stretched coordinates. The computational grid must be enlarged to accommodate the boundary layer growth. Starting with a value of 8 for the edge of the boundary layer at $\xi = 0$, the grid grows quickly as we advance in

values of $\xi$. At $\xi = 40$, $\xi = 100$, and $\xi = 1000$, the numerical grid is enlarged, such that values of the boundary layer edge increase to approximately 80, 200, and 1850, respectively. Thus, at an early stage in computation, many more points are added to the grid. More computer time is involved for each step in $\xi$ that the numerical grid must be enlarged in order to satisfy the asymptotic conditions for the new domain, i.e., computations are repeated at the same step in $\xi$, but for a larger grid. As mentioned earlier, the asymptotic condition 4.4.7 must be tightened to obtain accurate values of the displacement and momentum thickness. This tightening causes even more computer time to be spent per step in $\xi$.

The advantages of using similarity coordinates over that of stretched coordinates is obvious when the question of the lengthening of the computational grid is raised. However, stretched coordinates, as the name implies, stretches or magnifies the domain of the boundary layer, whereas, similarity coordinates do the opposite of stretched coordinates, i.e., they compress the domain. Near the surface of the cylinder, where rapid changes occur in axial velocity and shear stress profiles as we move downstream, larger step sizes for computation may be taken with stretched coordinates than with similarity coordinates to obtain the same accuracy. This is advantageous because fewer discretized points are required within the numerical grid near the surface of the cylinder. However, we believe that approximately the same number of discretized points would be required to obtain equivalent accuracy regardless of coordinates that are used. This would only apply if a different variable grid is used in each case, which is optimal with respect to the number of discretized points required to maintain similar accuracy. Of course, in each case the spacing of the points within the grid would occur at different locations away from the cylinder,

i.e., the case using similarity coordinates would have more points concentrated near the wall and fewer near the edge of the boundary layer, while the case of stretched coordinates would involve fewer points concentrated near the wall and more near the boundary layer edge.

The local similarity Keller's Box method using primitive variables with similarity coordinates solves at one station of $\xi$ only, therefore, not needing to store solutions at any previous steps. It has the same advantages as the "overall" Keller's Box method using similarity coordinates described above. Only 3 to 4 iterations are, usually, required at any value of $\xi$ provided the estimates of the initial profiles are reasonable. Only two solutions are needed to apply Richardson extrapolation to obtain fourth order accuracy. Interpolation schemes are not required to obtain values for a more concentrated numerical grid because from the very beginning of the computation, the number of points within the grid can be increased and we need only to provide the usual estimates of the initial profiles. The validity of the solutions, however, are limited to $\xi = 0$ and for $\xi \geq 100$, as was pointed out in Chapter 5.

Out of all of the numerical methods described, it appears as though the "overall" Keller's Box method using primitive variables with similarity coordinates is the most efficient single method obtaining accurate results for a large range in $\xi$, namely, $0 \leq \xi \leq 1000$. Again, in principle, this method may proceed further in $\xi$. However, the local similarity Keller's Box method using primitive variables with similarity coordinates, which is also very efficient and requires no storage of previous solutions, obtains accurate results for the latter parts of this range and may be used at even larger values of $\xi$, i.e., further downstream. The velocity profiles it produces are easier to obtain and more accurate than those obtained by the asymptotic solution for very large

values of $\xi$.

## 6.5 PROPERTIES AT THE TWO LIMITS

From the "overall" and local similarity Keller's Box solutions, we describe the boundary layer along the semi-infinite circular cylinder in axial flow.

Two extreme situations arise which are reflected in the solutions obtained. At $\xi = 0$ or $\lambda = 0$, we have the flow along a cylinder with very large radius or the flow is in the region near (but not at) the front end of the cylinder. This is the Blasius limit, where similarity exists. As $\xi \to \infty$ or $\lambda \to \infty$, we approach the flow along a very thin needle or we are in the region of flow very far downstream. This is in the region near the needle limit, where a different similarity is approached. Between these two limiting cases, nonsimilar flows exist that start at the Blasius limit and gradually approach the needle limit.

At the Blasius limit $\xi = 0$ or $\lambda = 0$, velocity and shear stress profiles, skin-friction, displacement and momentum thickness are obtained that match with those of the Blasius solution.

As we proceed downstream or to cylinders of progressively smaller radii, the nonsimilar flows can be described as proceeding through a transition which starts with the Blasius limit. The growth of the boundary layer begins. Axial velocity profiles become different from that of the Blasius, while more rapid change occur near the surface of the cylinder. The radial velocity parameter deviates from that of the Blasius by becoming smaller in magnitude "overall" and developing a hump in between, which decays to the boundary layer edge. The shear stress changes more

rapidly near the surface of the cylinder and vanishes more quickly when approaching the boundary layer edge. The skin-friction coefficient steadily begins to increase as does the displacement and momentum thickness.

As $\xi \to \infty$ or $\lambda \to \infty$, the needle limit is being approached. The boundary layer thickness with respect to the radius of the cylinder is very large and is still growing. In fact, it grows without bound as it approaches the needle limit. The axial velocity changes very rapidly nearer to the surface of the cylinder and appears to approach a profile resembling a square in which most of the boundary layer is unity, except near the surface, where it rapidly changes from 0 to 1. The closer one approaches the needle limit, the nearer the changes occur to the surface and these changes become more rapid. The radial velocity parameter still exhibits the hump but the overall magnitude of the entire profile decreases even further. The shear stresses change more quickly near the wall, rapidly vanishing away from it. These changes become more extreme, as we more closely approach the needle limit. The skin-friction coefficient keeps increasing on to infinity, as do the displacement and momentum thickness.

The analytical and numerical results suggest the following description of the needle case. The axial velocity profile would be such that the overall flow would be that of the mainstream velocity except for an infinitesimal region near the surface of the cylinder, where an extremely sharp fluctuation occurs from zero at the surface of the cylinder to the value of the mainstream infinitesimally away from the surface, i.e., no-slip is just satisfied. The radial velocity parameter would vanish everywhere. The

shear stress would do the same, except for the skin-friction coefficient which would be infinite. The displacement and momentum thickness would, also, be infinite. The profiles vary more slowly the further we move downstream.

## 6.6 CONCLUSIONS

The solution to this seemingly simple axisymmetric boundary layer problem has been difficult to obtain due to complexities arising from the imposed boundary conditions and the transverse curvature term. These difficulties lead to the general nonsimilarity of the problem, although, similarity misleadingly appears to exist. The problem becomes more involved, however, because similarity does exist locally at the Blasius limit and another similarity, is approached, i.e., the needle limit.

The implication of similarity gives rise to the similarity methods of Chapter 2, while the solutions obtained are 'quasi-similar'. The two transformations using seemingly valid similarity variables obtain results at and near the Blasius limit, which numerically and analytically differ from each other. At $\xi = 0$, the r-based transformation gives a deceptive axial velocity profile which is shifted by a factor of $\sqrt{2}$ in the independent variable and radial velocity components that are one order of magnitude larger than expected. On the other hand, the y-based transformation gives the expected Blasius solution. Both solutions merge on approaching the needle case.

The "overall" Keller's Box method, can be used to solve the full range of the problem, in principle. Capable of handling the nonsimilarity of the problem, solutions are obtained from the Blasius limit to the needle limit. Solutions are obtained that greatly extend the range in $\xi$ that others have solved towards. These accurate solutions overlap much of the range of validity of the asymptotic solution, while obtaining more accurate velocity profiles.

Primitive variables and similarity coordinates are used, which have the advantage of compressing the cross-stream domain of the problem such that the boundary layer edge can remain fixed. We know that the commonly used stretched coordinates for the numerical solution of axially symmetric flows require the computational grid to be lengthened in order to handle the growth of the boundary layer.

However, we applied the efficient Keller's Box method using primitive variables with the stretched coordinates and the solution obtained covered the same range, i.e., $0 \leq \xi \leq 1000$. Solutions obtained using the "overall" Keller's Box method using either coordinates agree very well with both series solutions and past numerical solutions

An understanding of the flow for the full range is obtained, complete with velocity and shear stress profiles, skin-friction, displacement and momentum thickness. Finally, one simple method is used that efficiently and accurately obtains solutions from one end of the problem to the other, i.e. the Blasius limit to the needle case.

Another method, the local similarity Keller's Box method can solve at any fixed $\xi$ and is successful in obtaining valid results for the Blasius limit and larger $\xi$. The solutions match very well with the "overall" solution and the asymptotic solution for large values of $\xi$. Again, velocity profiles are obtained which are more accurate than that obtained by the asymptotic expansion.

It is this complete and accurate solution of the flow along a semi-infinite circular cylinder along with that of the flow past a semi-infinite flat plate which will aid in the study of the fully three dimensional problem of the boundary layer along a semi-infinite elliptical cylinder.

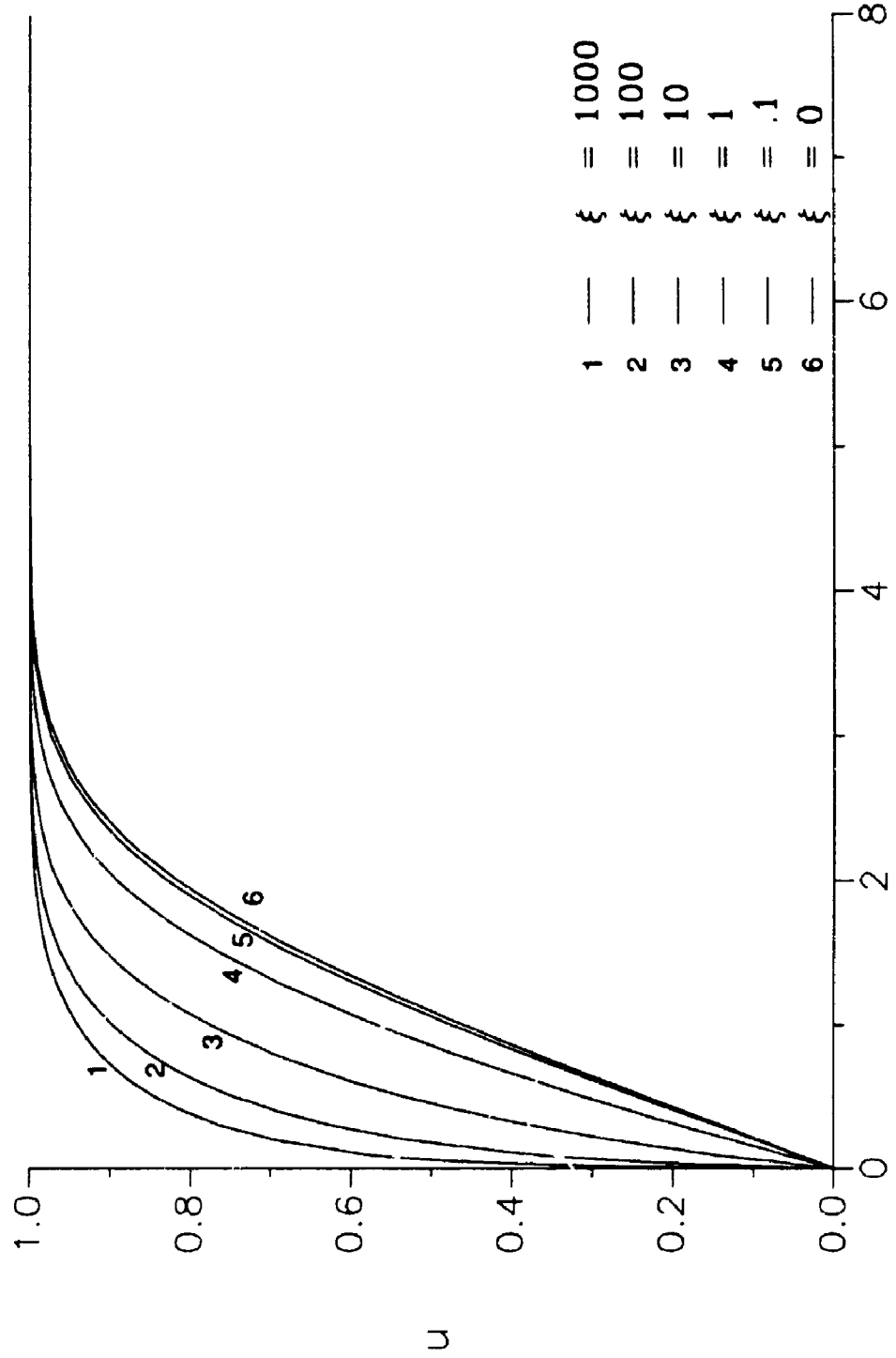


Figure 6.2.1 Axial velocity obtained by overall Keller Box method using similarity coordinates.

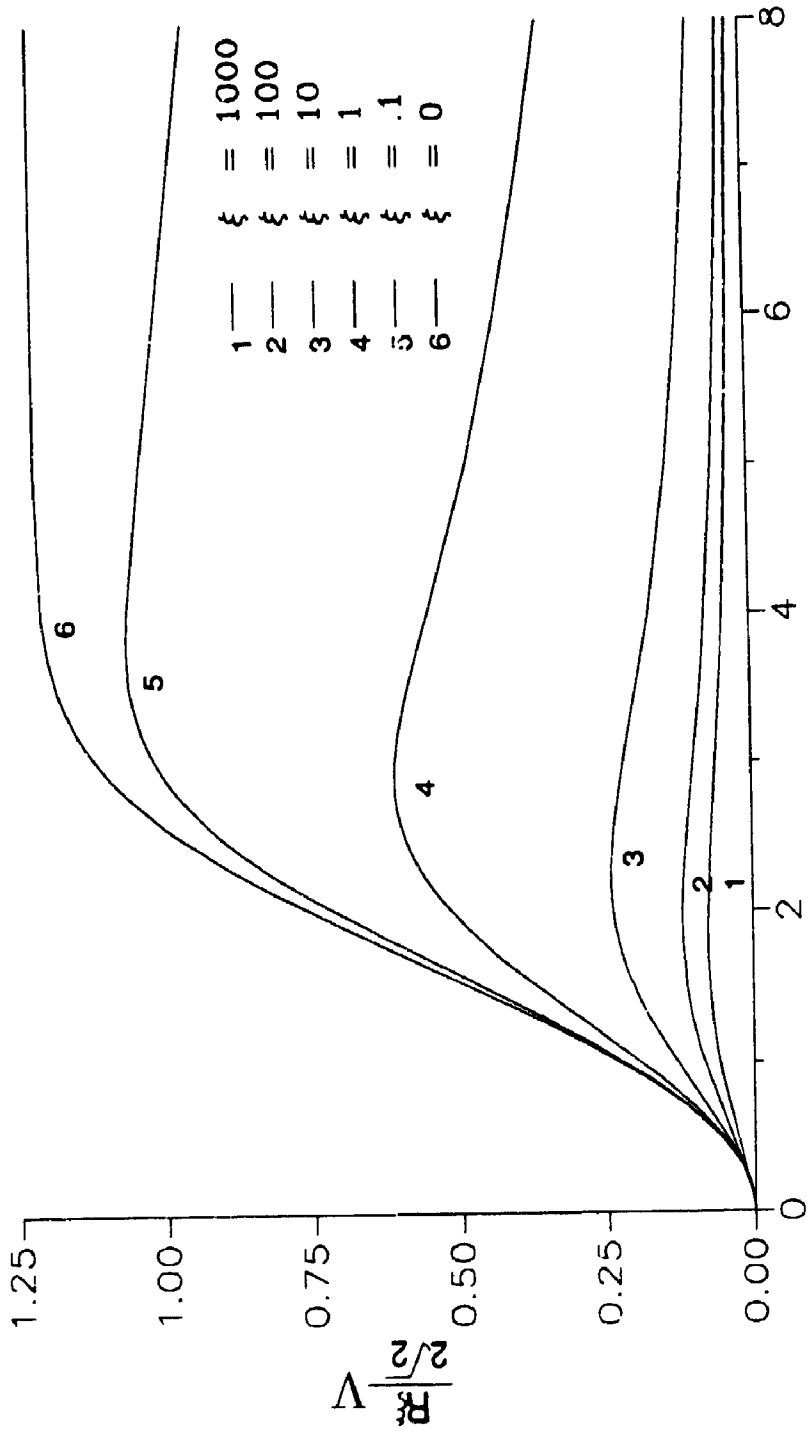


Figure 6.2.2 Radial velocity parameter obtained by overall Keller Box method using similarity coordinates.

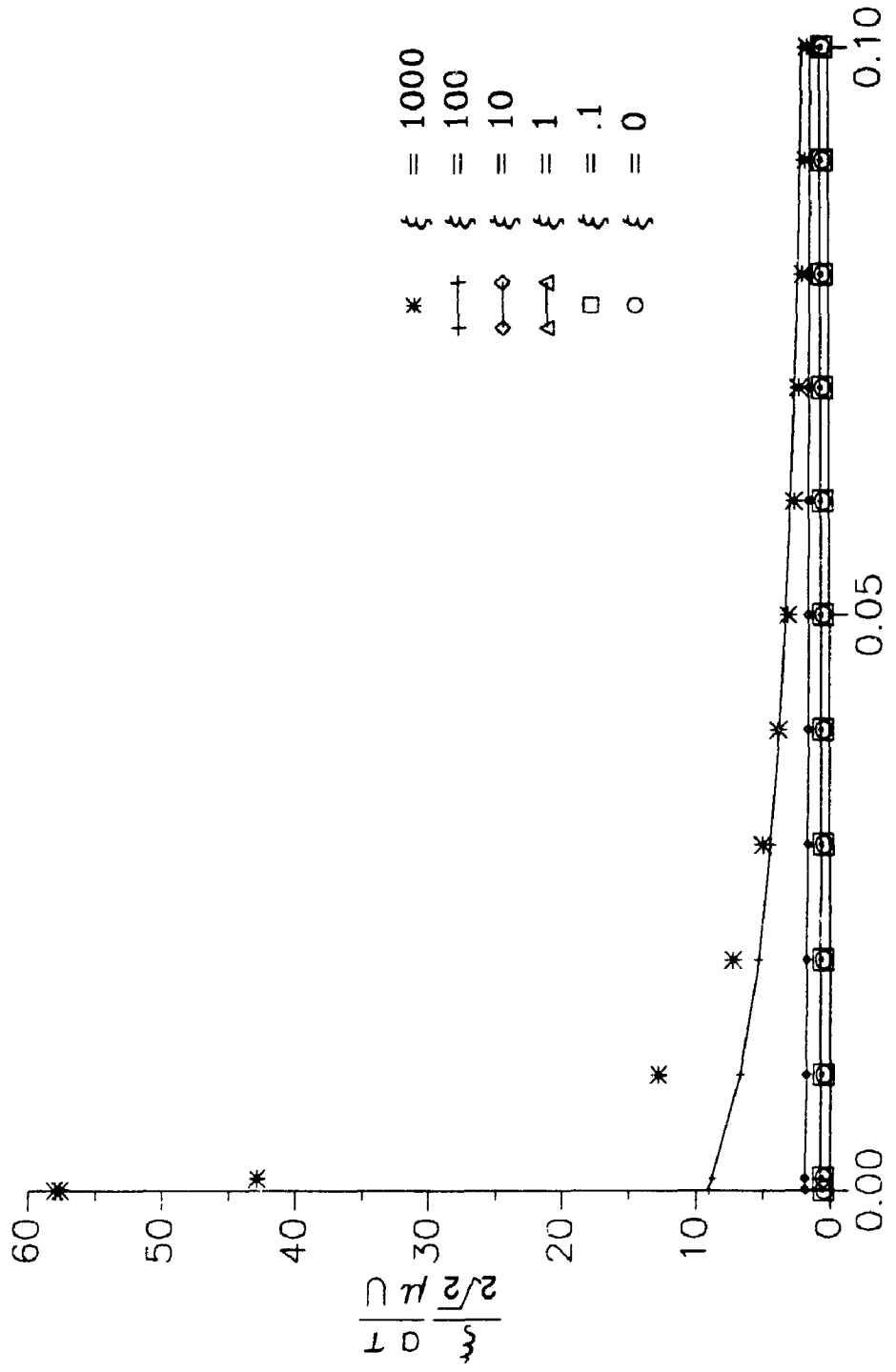


Figure 6.2.3 Shear stress parameter obtained by the overall Keller Box method using similarity coordinates.

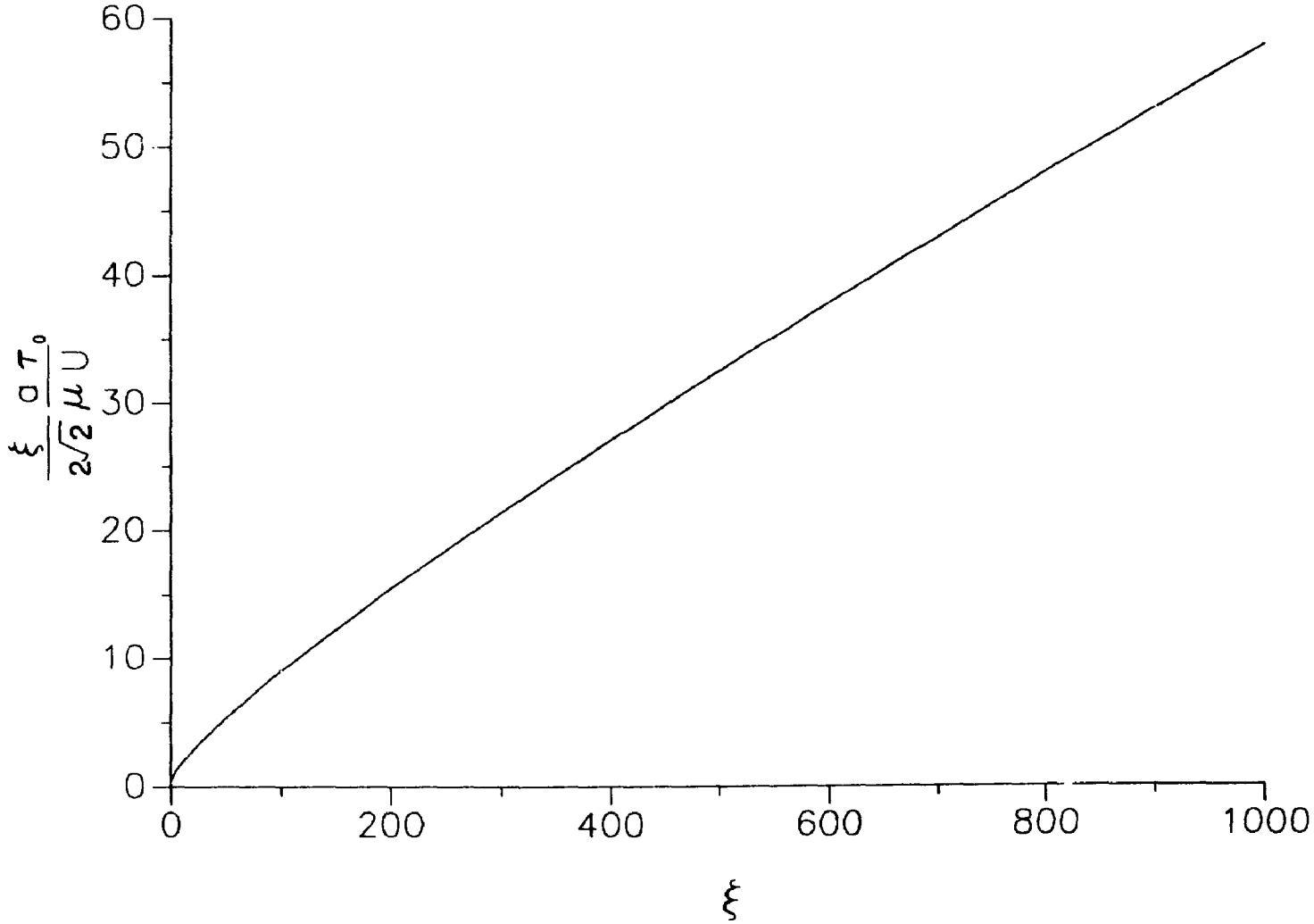


Figure 6.2.4a Skin-friction coefficient obtained by overall Keller Box method using similarity coordinates.

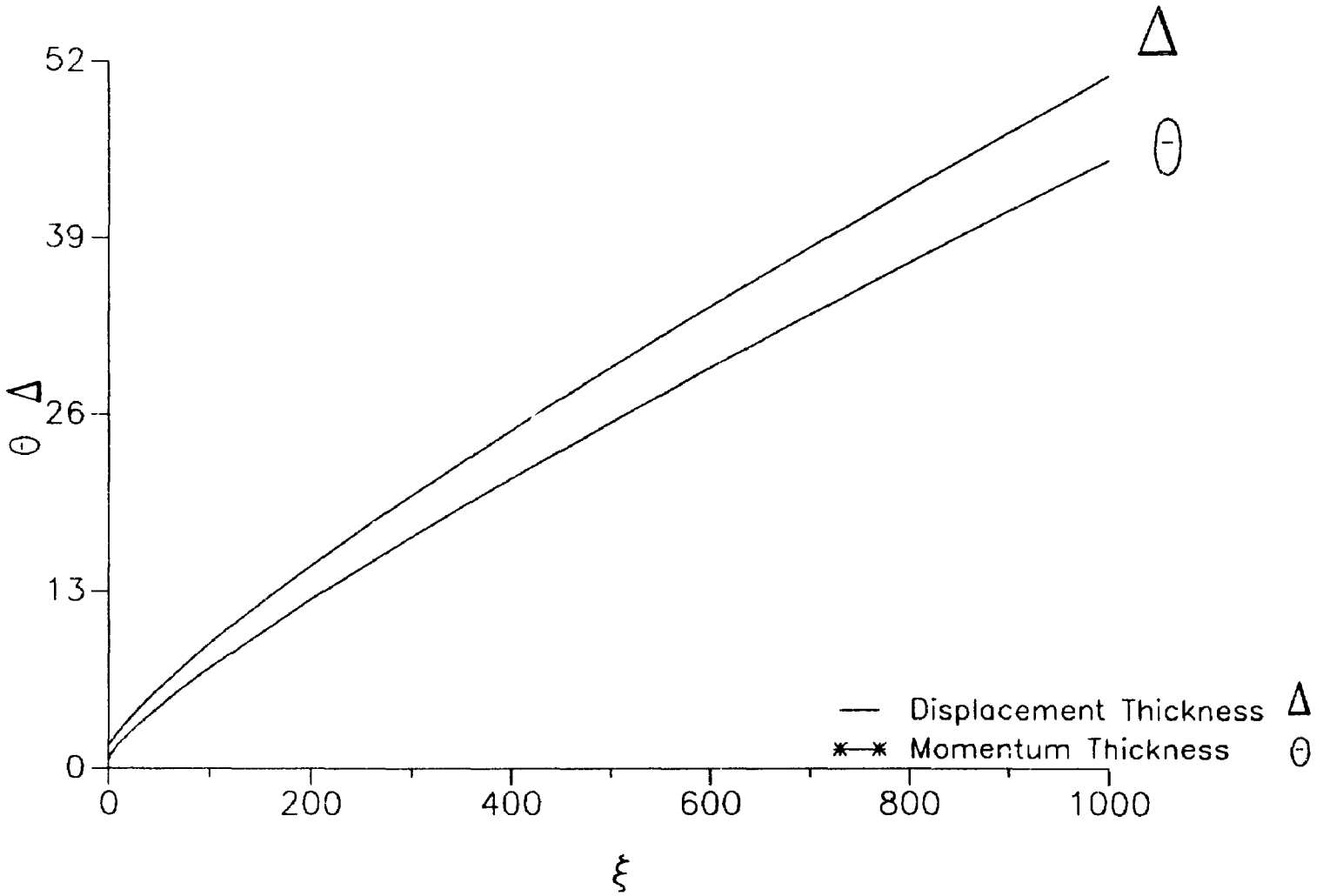


Figure 6.2.4b Displacement and momentum thicknesses obtained by overall Keller Box method using similarity coordinates.

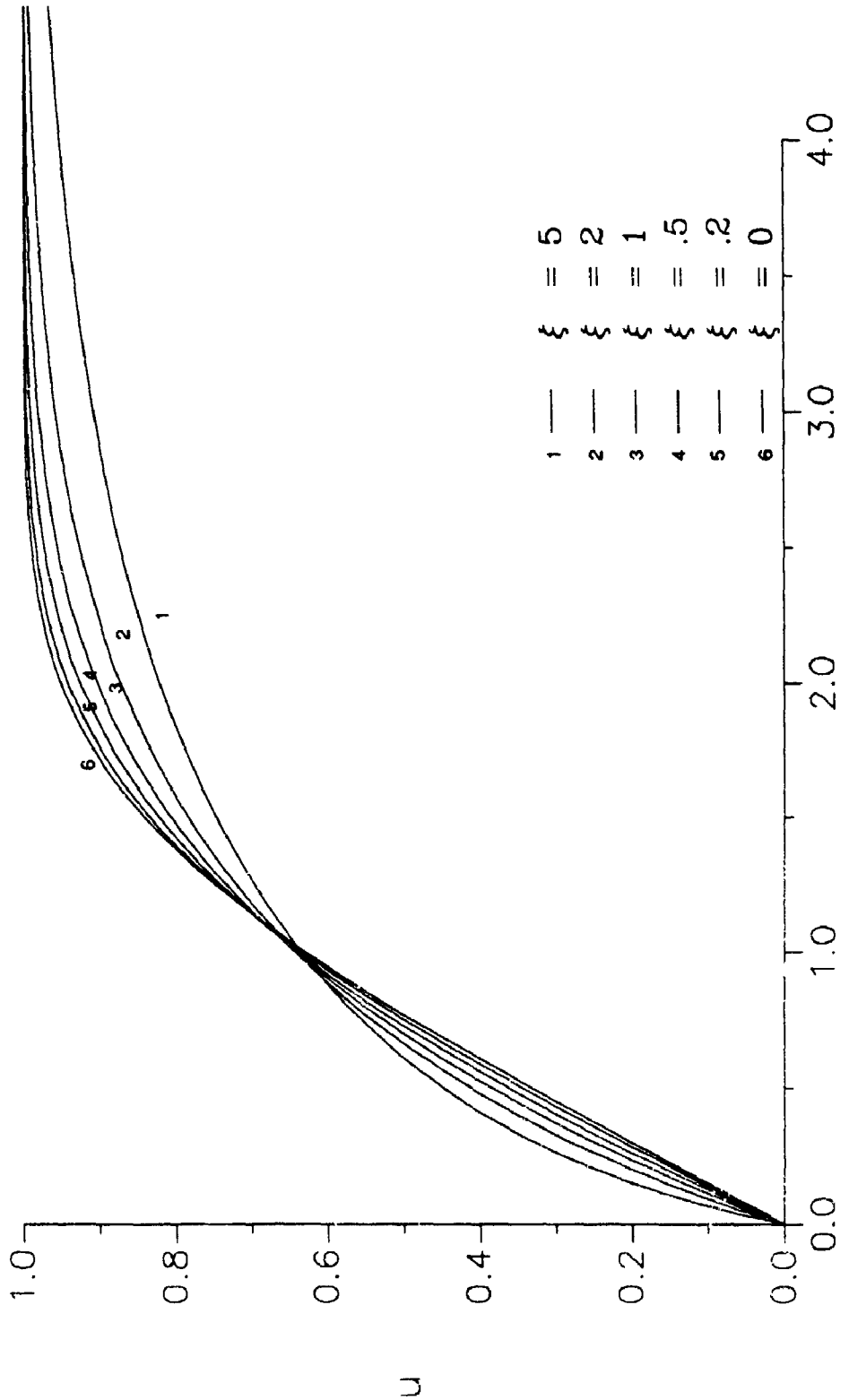


Figure 6.2.5 Axial velocity obtained by overall Keller Box method using stretched coordinates.

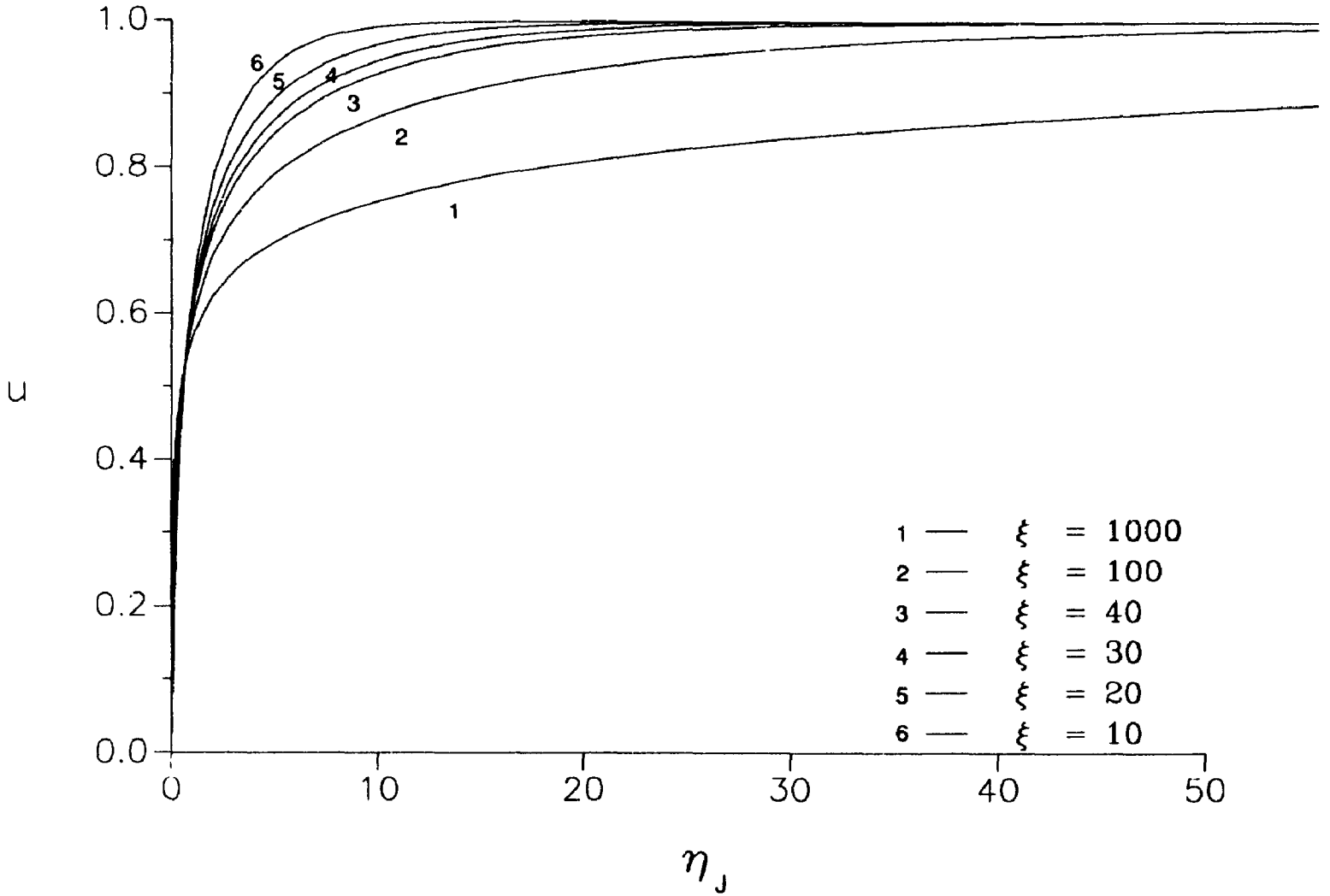


Figure 6.2.6 Axial velocity obtained from overall Keller Box method using stretched coordinates.

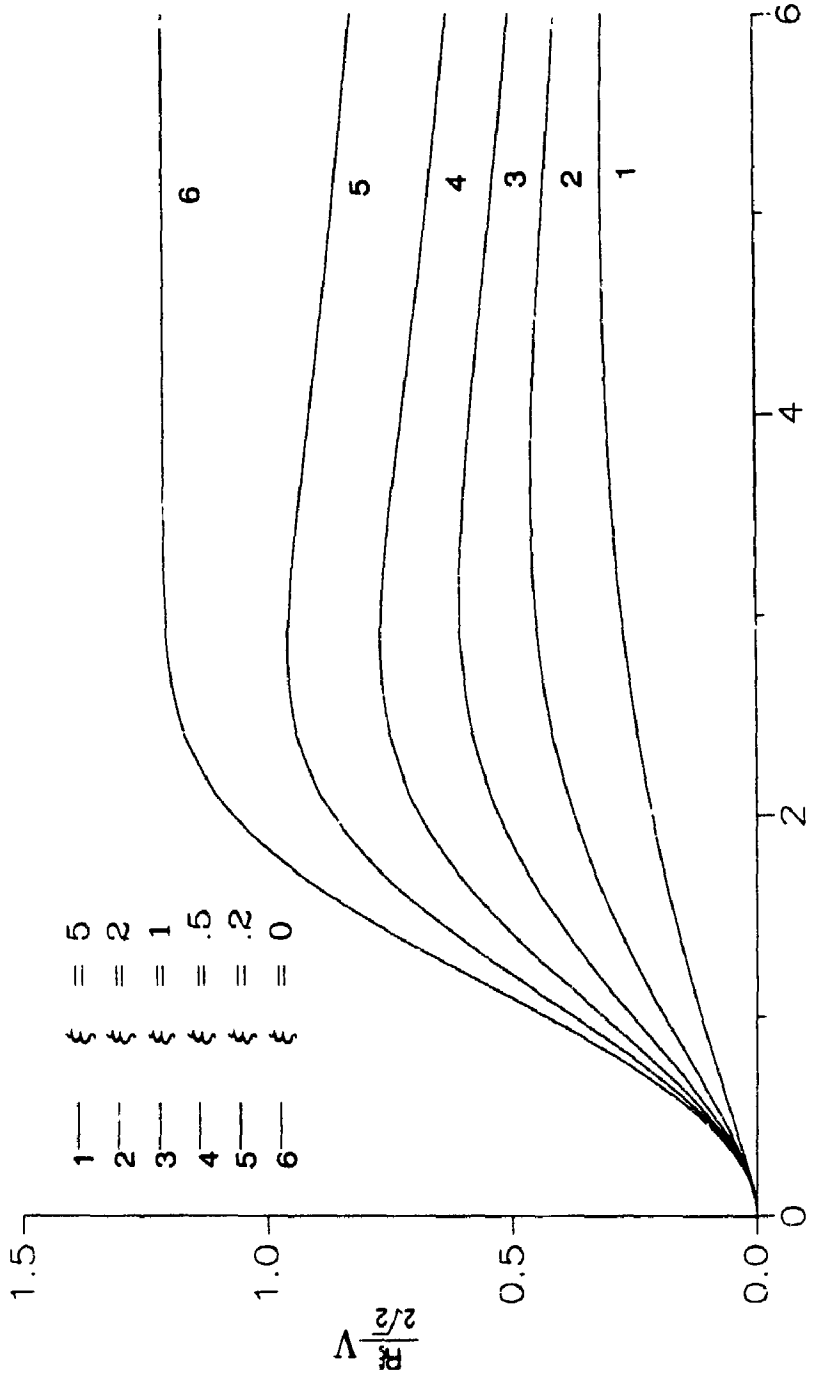


Figure 6.2.7 Radial velocity parameter obtained by overall Keller Box method using stretched coordinates.

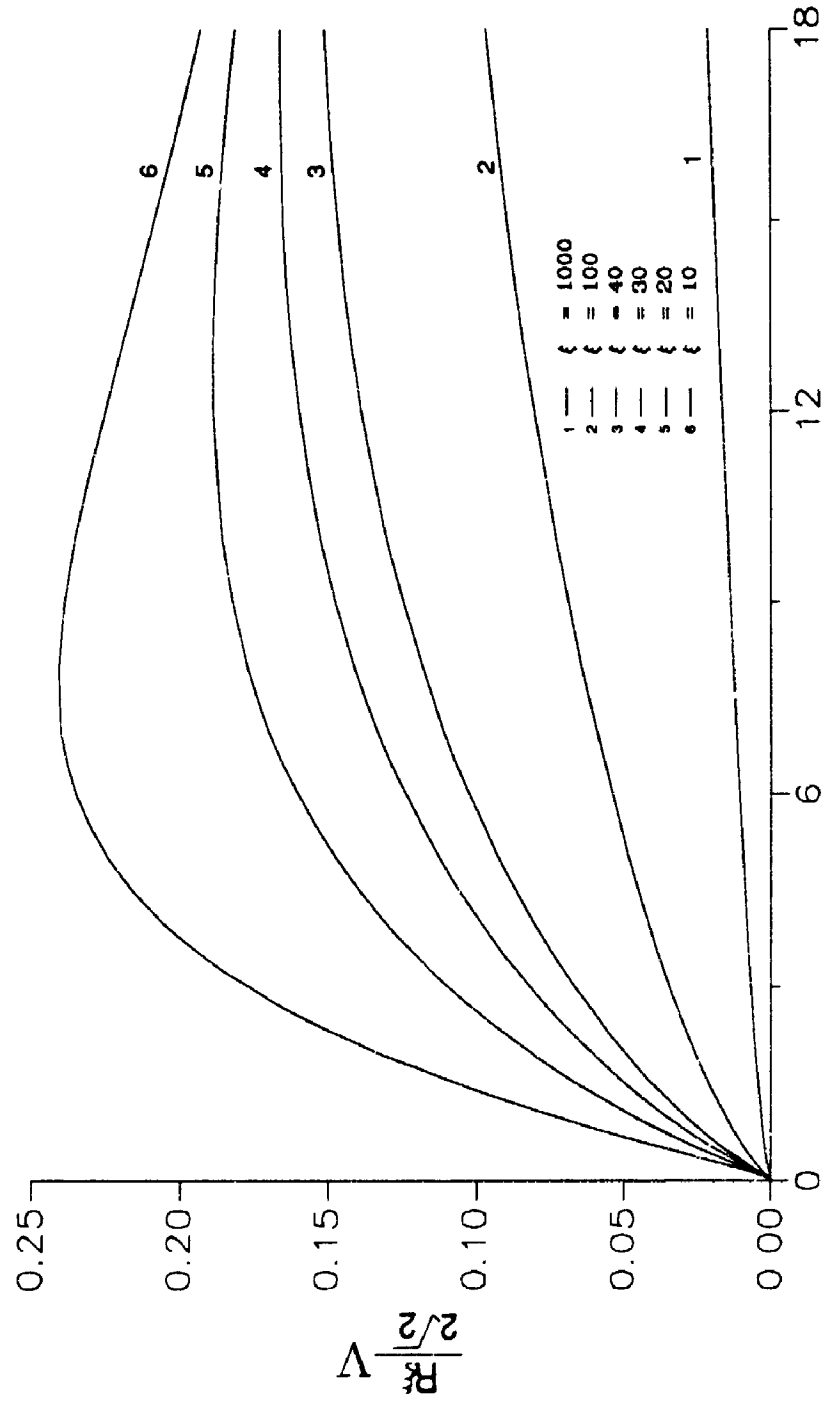


Figure 6.2.8 Radial velocity parameter obtained from overall Keller Box method using stretched coordinates.

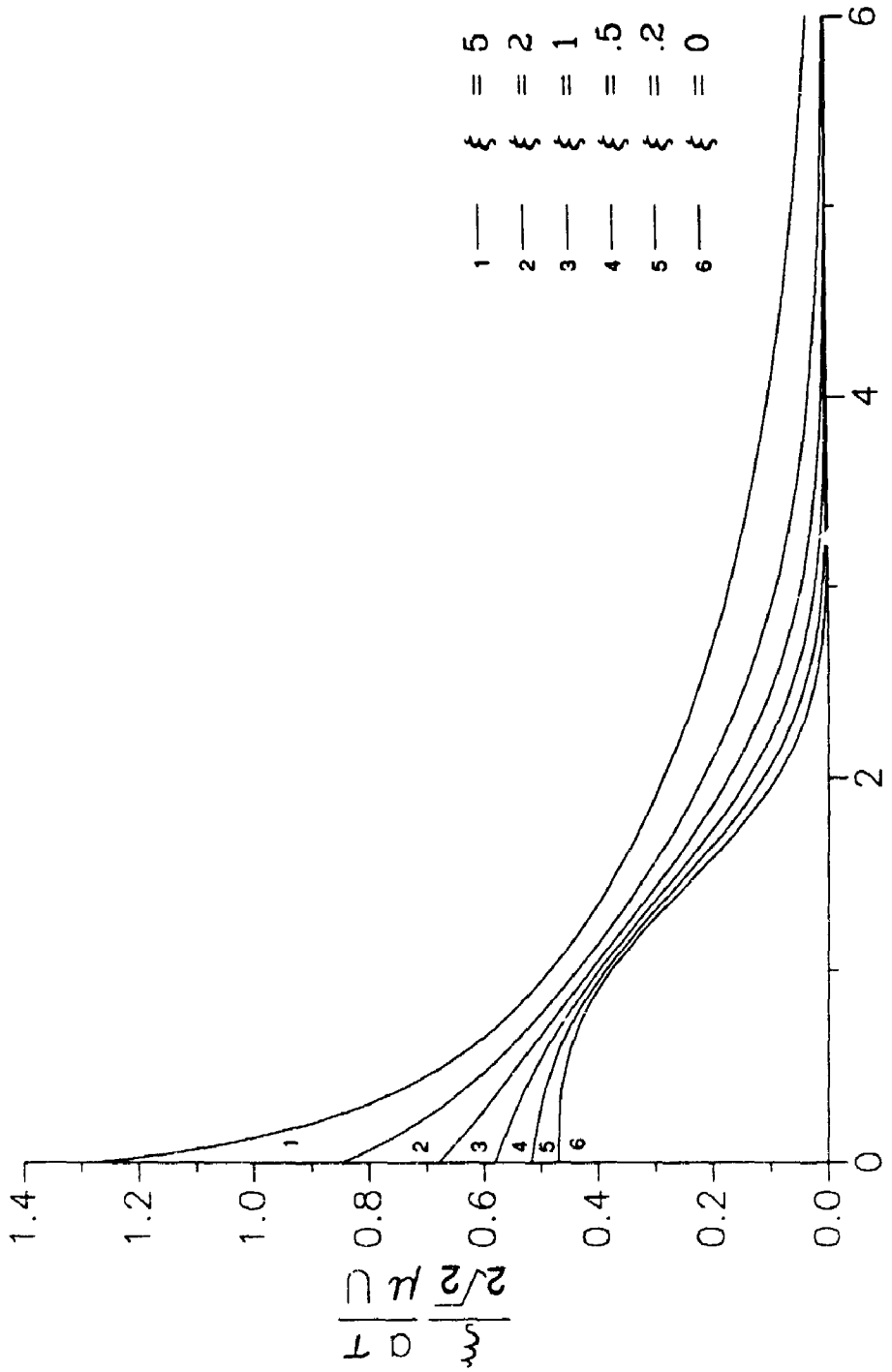


Figure 6.2.9 Shear stress parameter obtained by overall Keller Box method using stretched coordinates.

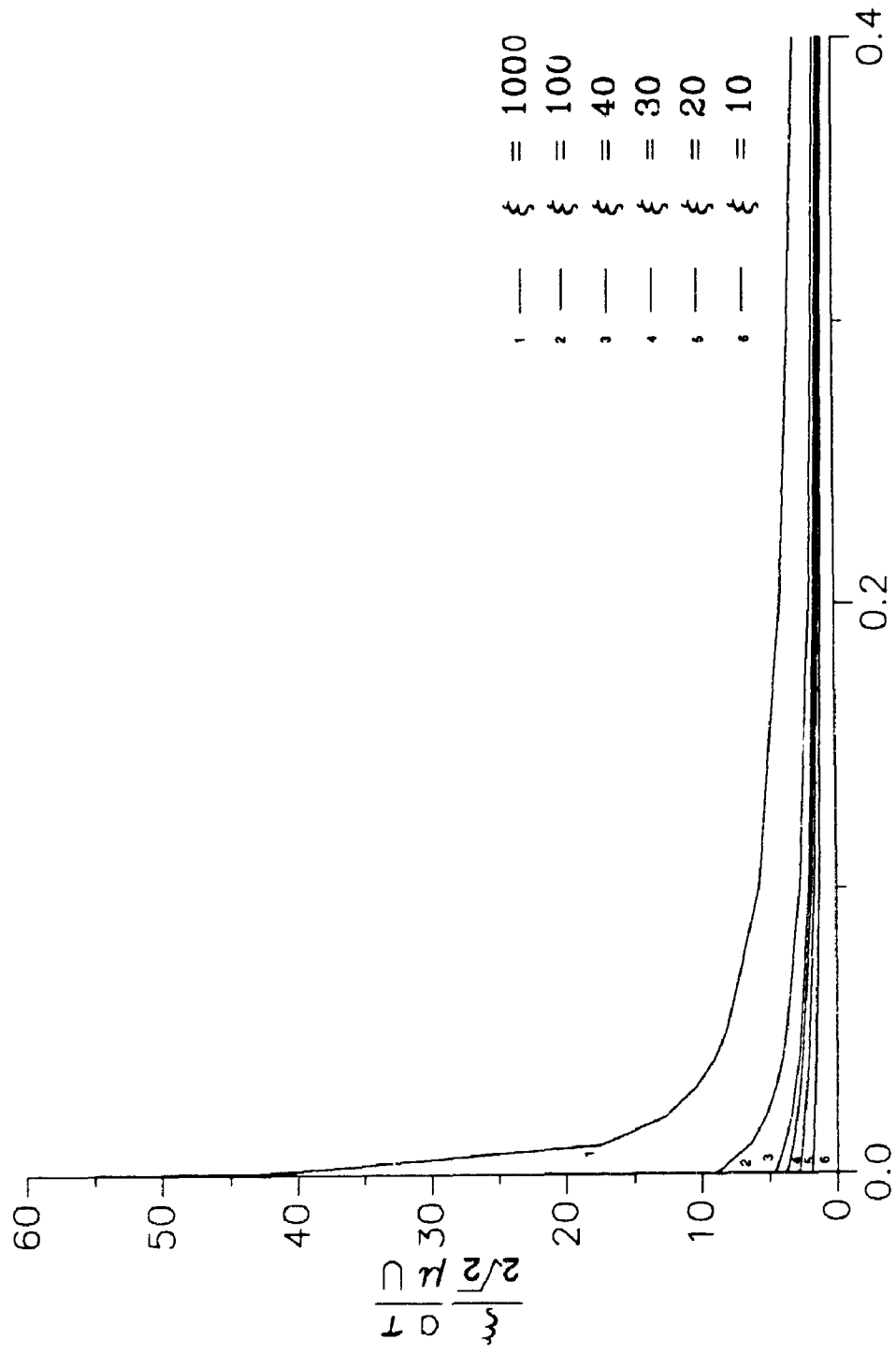


Figure 6.2.10 Shear stress parameter obtained by overall Keller Box method using stretched coordinates.

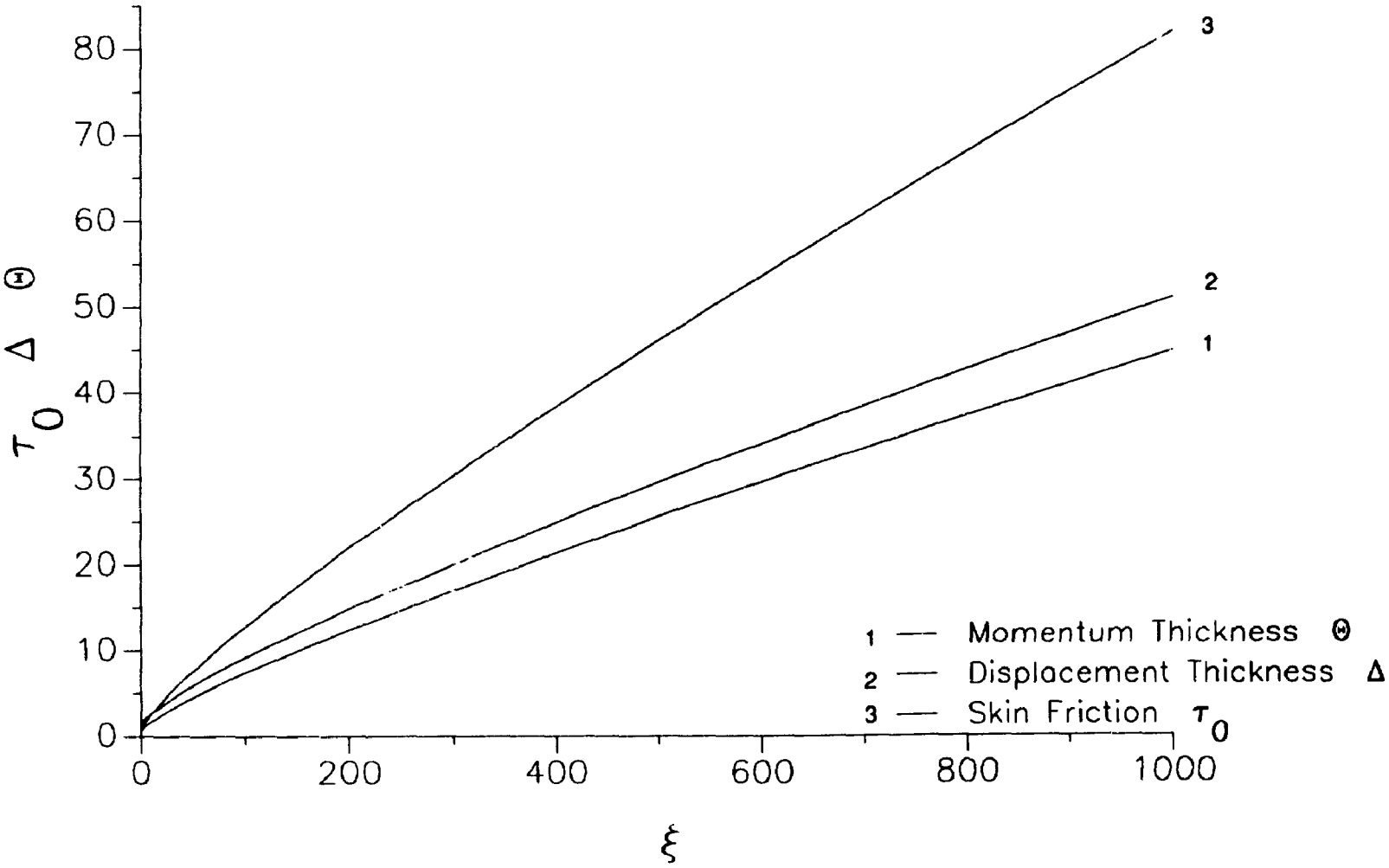


Figure 6.2.11 Skin-friction coefficient, displacement and momentum thicknesses obtained by Keller Box method using stretched coordinates.

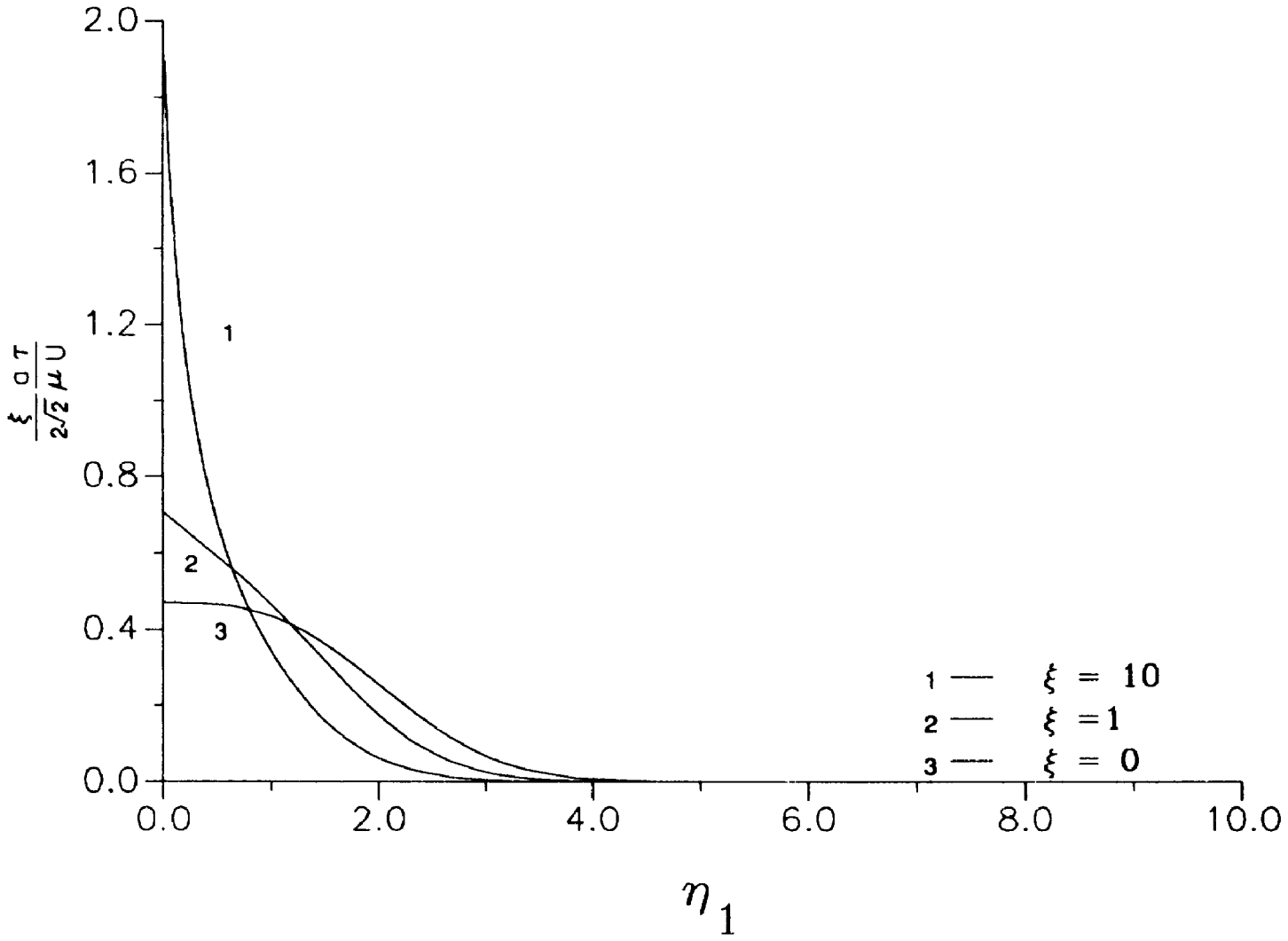


Figure 6.2.14 Shear stress parameter obtained by local similarity Keller Box method.

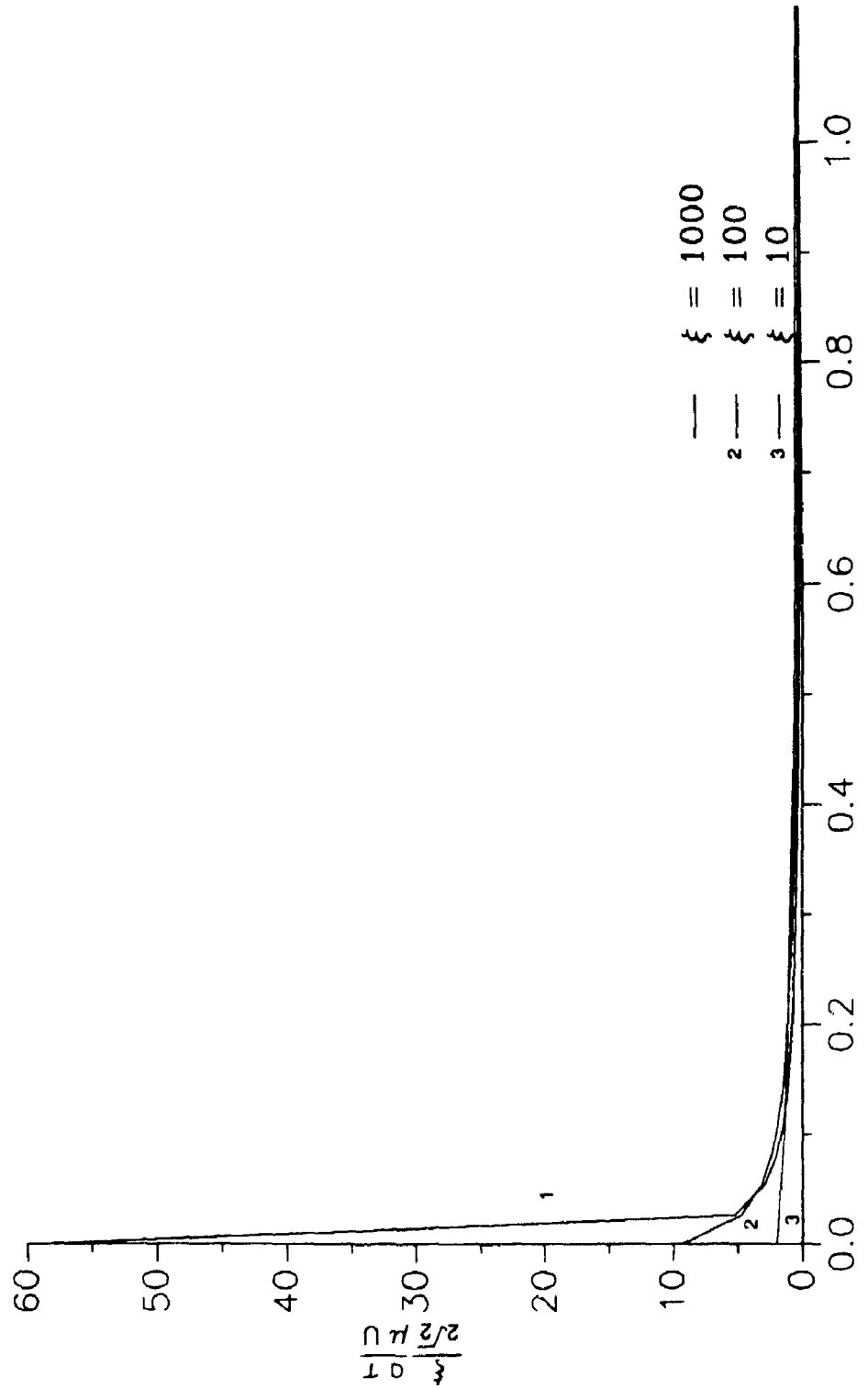


Figure 6.2.15 Shear stress parameter obtained by local similarity Keller Box method.

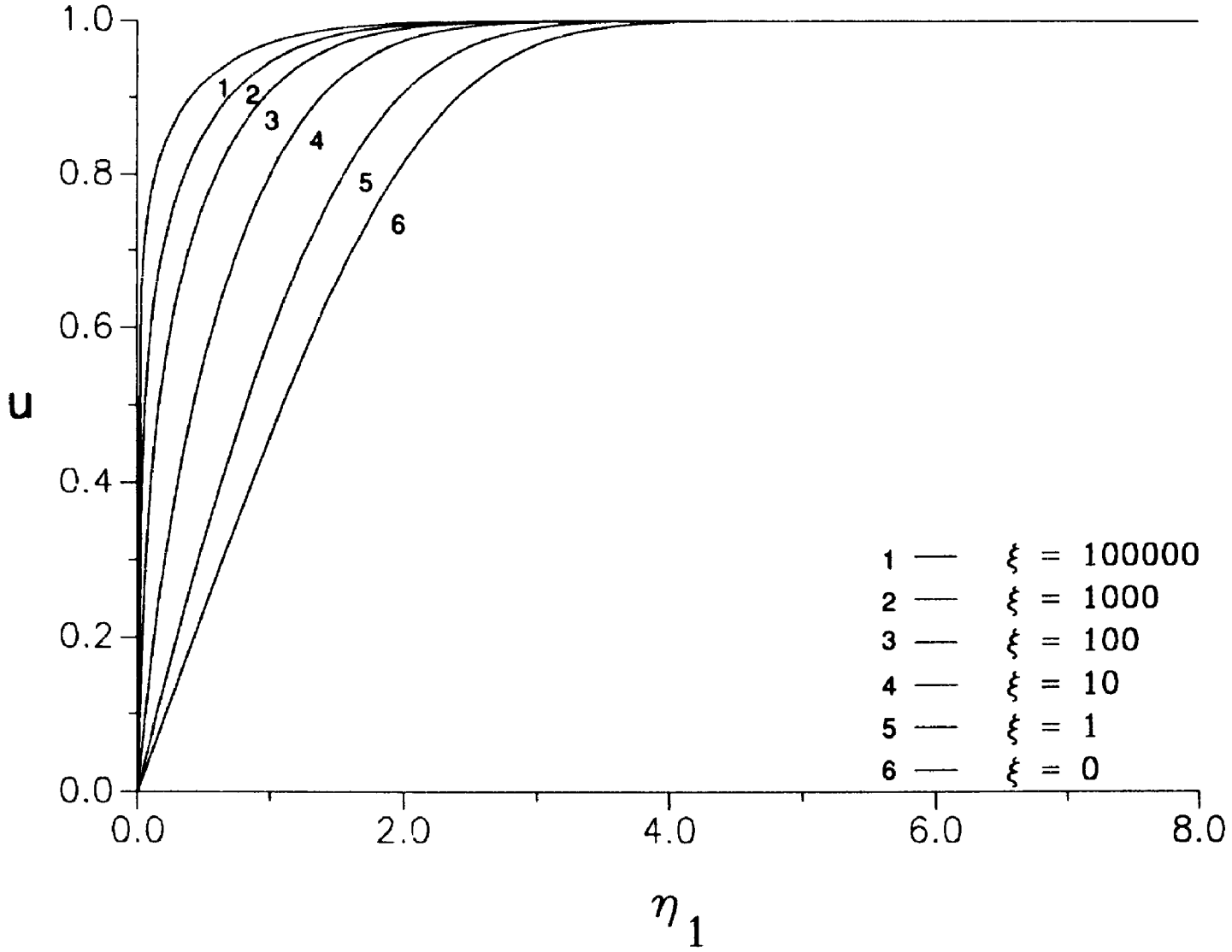


Figure 6.2.12 Axial velocity obtained by local similarity Keller Box method.

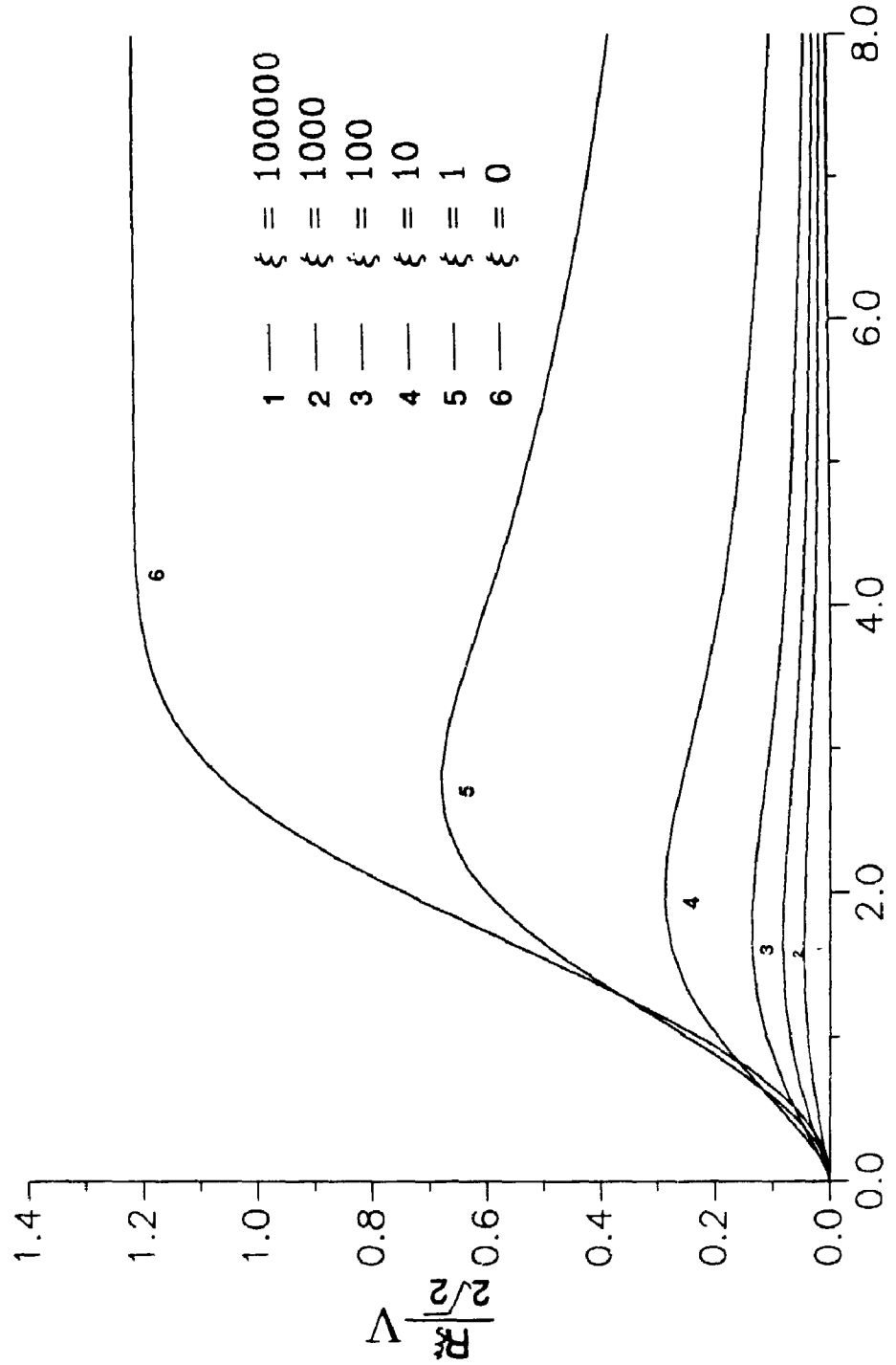


Figure 6.2.13 Radial velocity parameter obtained by local similarity Keller Box method.

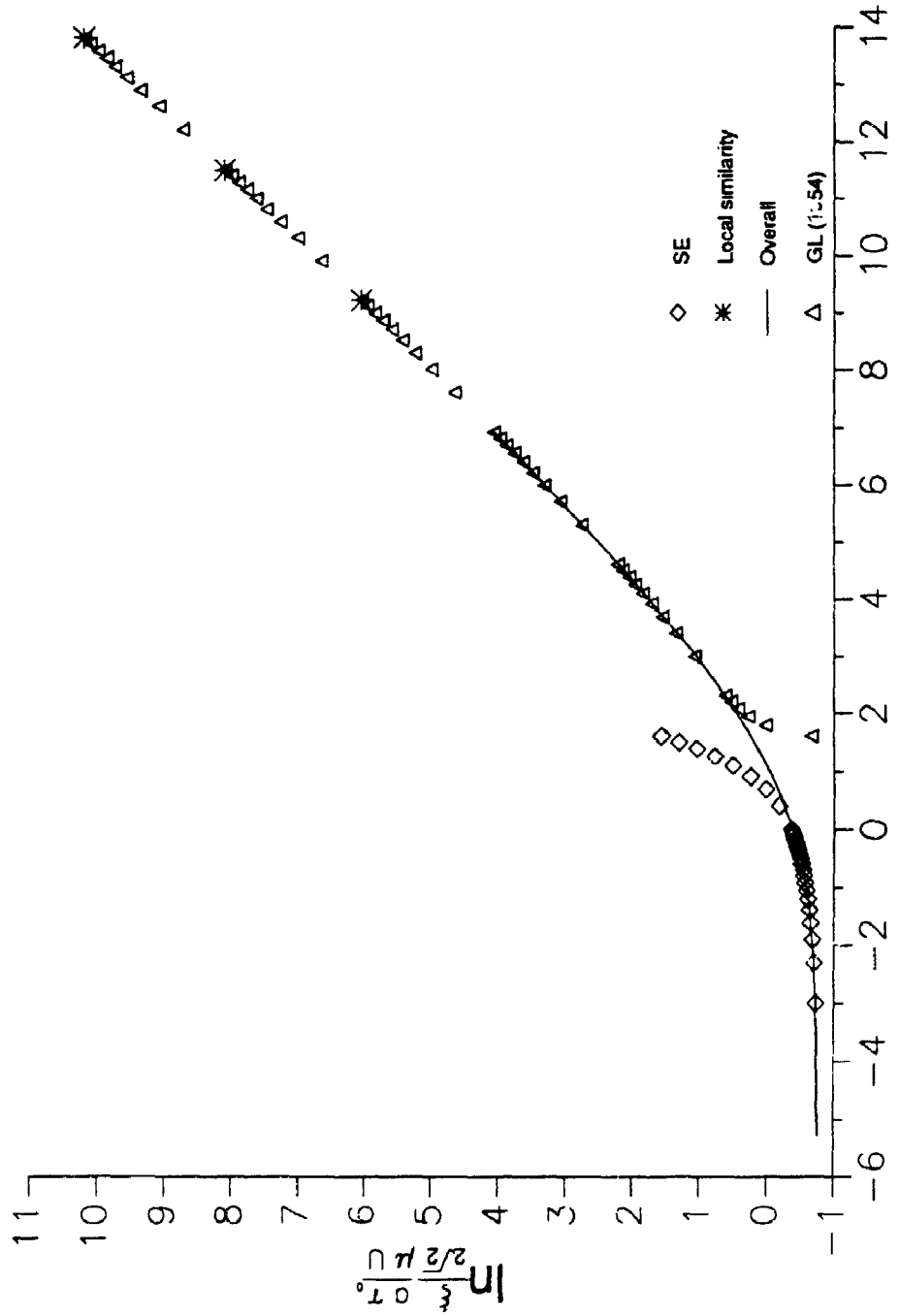


Figure 6.3.1 Comparison of skin-friction coefficient of overall and local similarity Keller Box solution vs. series expansion (SE) and asymptotic solution of Glauert and Lighthill (1954) (GL).

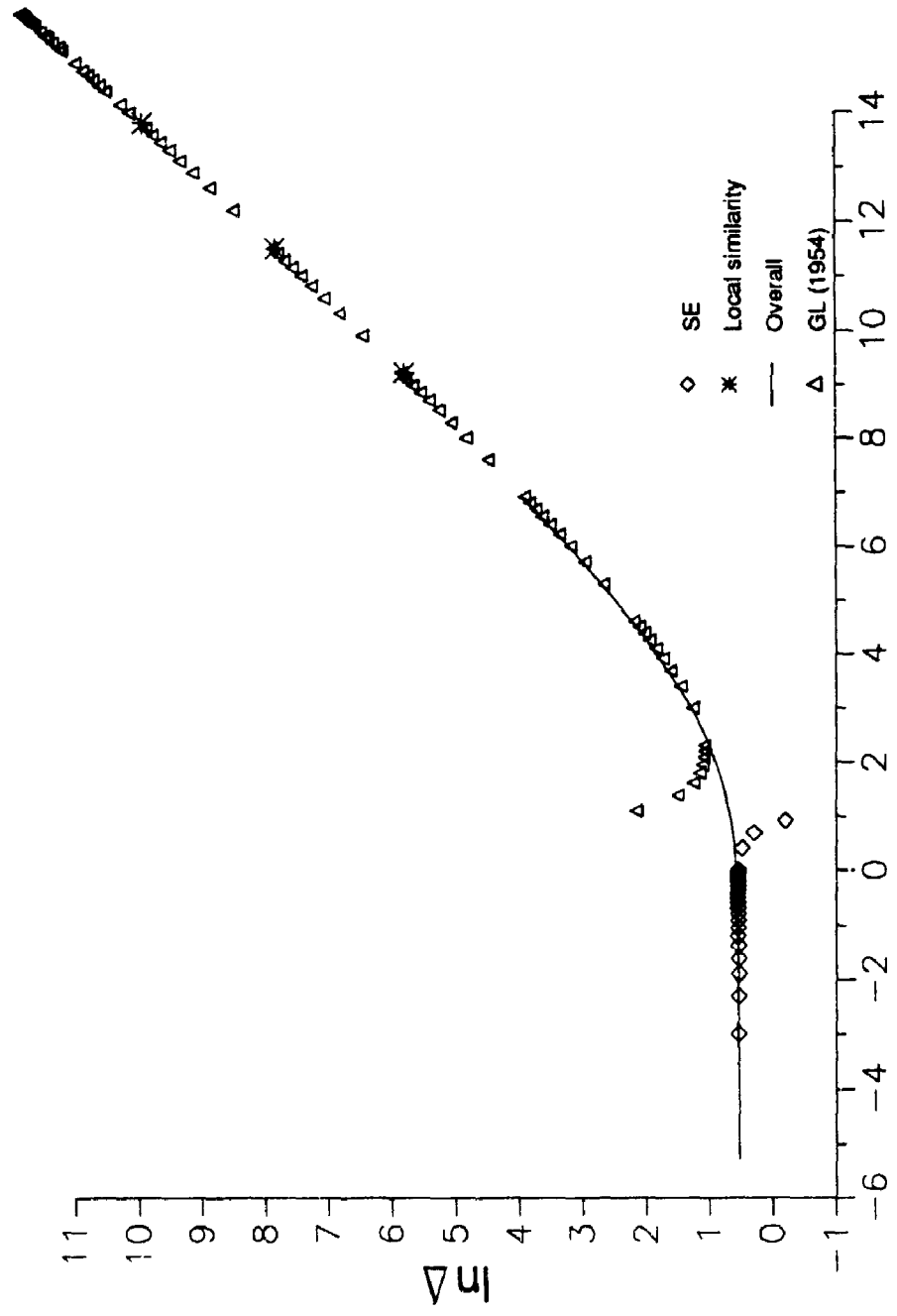


Figure 6.3.2 Comparison of displacement thickness of the overall and local similarity Keller Box solutions vs. the series expansion (SE) and the asymptotic solution of Glauert and Lighthill (1954) (GL).

| | $\frac{\xi \, a\tau_1}{2\sqrt{2}\,\mu U}$ | | | | | |
|---|---|---|---|---|---|---|
| $\xi$ | GL (1954) | Overall | % | SE | LS | % |
| 0.000 | | 0.46959999 | 0.001 | 0.46960000 | | |
| 0.050 | | 0.48173322 | 0.001 | 0.48173303 | | |
| 0.100 | | 0.49360110 | 0.001 | 0.49360287 | | |
| 0.200 | | 0.51662389 | 0.007 | 0.51666072 | | |
| 0.300 | | 0.53881807 | 0.031 | 0.53898901 | | |
| 0.400 | | 0.56028460 | 0.092 | 0.56080323 | | |
| 0.500 | | 0.58112207 | 0.205 | 0.58231883 | | |
| 0.600 | | 0.60139830 | 0.391 | 0.60375130 | | |
| 0.700 | | 0.62117561 | 0.666 | 0.62531611 | | |
| 0.800 | | 0.64050179 | 1.050 | 0.64722873 | | |
| 0.900 | | 0.65942026 | 1.559 | 0.66970464 | | |
| 1.000 | | 0.67796572 | 2.211 | 0.69295930 | | |
| 2.000 | | 0.84815952 | | | | |
| 3.000 | | 1.02000031 | | | | |
| 4.000 | | 1.14036703 | | | | |
| 5.000 | | 1.27270049 | | | | |
| 10.000 | 1.84426434 | 1.86279121 | 1.004 | | | |
| 14.000 | 2.32969474 | 2.28500414 | 1.918 | | | |
| 18.000 | 2.74878356 | 2.68094183 | 2.468 | | | |
| 20.000 | 2.94605603 | 2.87157226 | 2.528 | | | |
| 24.000 | 3.32460604 | 3.24123318 | 2.507 | | | |
| 28.000 | 3.68733649 | 3.59818404 | 2.417 | | | |
| 30.000 | 3.86405165 | 3.77266300 | 2.365 | | | |
| 34.000 | 4.20981598 | 4.11476272 | 2.257 | | | |
| 38.000 | 4.54687995 | 4.44887716 | 2.155 | | | |
| 40.000 | 4.71258788 | 4.61329320 | 2.107 | | | |
| 44.000 | 5.03902421 | 4.93740605 | 2.016 | | | |
| 48.000 | 5.35952831 | 5.25585419 | 1.934 | | | |
| 50.000 | 5.51777659 | 5.41314768 | 1.896 | | | |
| 60.000 | 6.29169560 | 6.18281300 | 1.730 | | | |
| 70.000 | 7.04137378 | 6.92861010 | 1.598 | | | |
| 80.000 | 7.77140625 | 7.65551583 | 1.491 | | | |
| 90.000 | 8.48502127 | 8.36604846 | 1.402 | | | |
| 100.000 | 9.18460267 | 9.06272953 | 1.326 | | | |
| 200.000 | 15.67968185 | 15.53403022 | 0.928 | | | |
| 300.000 | 21.64537519 | 21.48068881 | 0.760 | | | |
| 400.000 | 27.30884112 | 27.12760065 | 0.663 | | | |
| 500.000 | 32.76549523 | 32.56933001 | 0.598 | | | |
| 600.000 | 38.06717865 | 37.85727105 | 0.551 | | | |
| 700.000 | 43.24612839 | 43.02338901 | 0.515 | | | |
| 800.000 | 48.32416683 | 48.08932591 | 0.485 | | | |
| 900.000 | 53.31696011 | 53.07062068 | 0.462 | | | |
| 1000.000 | 58.23625132 | 57.97892267 | 0.441 | | | |
| 10000.000 | 424.13519870 | | | | 425.92115936 | 0.421 |
| 100000.000 | 3330.25353165 | | | | 3339.60642956 | 0.280 |
| 1000000.000 | 27397.67274930 | | | | 27451.32127265 | 0.195 |

Table 6.3.1 Comparison of skin-friction coefficient obtained from the overall and local similarity (LS) Keller Box solutions with the Glauert and Lighthill (1954) (GL) asymptotic and the series expansion (SE) solutions. Percentage differences (%) between the numerical vs. the corresponding series solutions are presented.

| | Δ | | | | | |
|---|---|---|---|---|---|---|
| $\xi$ | GL (1954) | Overall | % | SE | LS | % |
| 0.000 | | 1.72082086 | 0.016 | 1 72109791 | | |
| 0.050 | | 1.72196839 | 0.015 | 1.72224275 | | |
| 0.100 | | 1.72357246 | 0.015 | 1.72383605 | | |
| 0.200 | | 1.72791746 | 0.008 | 1.72806074 | | |
| 0.300 | | 1.73350480 | 0.020 | 1.73315735 | | |
| 0.400 | | 1.74006935 | 0.089 | 1.73851125 | | |
| 0.500 | | 1.74740560 | 0.223 | 1.74350781 | | |
| 0.600 | | 1.75536896 | 0.446 | 1.74753243 | | |
| 0.700 | | 1.76384311 | 0.786 | 1.74997045 | | |
| 0.800 | | 1.77273877 | 1.270 | 1.75020727 | | |
| 0.900 | | 1.78196359 | 1.927 | 1.74762826 | | |
| 1.000 | | 1.79151997 | 2.785 | 1.74161879 | | |
| 2.000 | | 1.89560738 | | | | |
| 3.000 | | 2.00509106 | | | | |
| 4.000 | | 2.11452606 | | | | |
| 5.000 | | 2.22239838 | | | | |
| 10.000 | 2.98344244 | 2.73205314 | 8.426 | | | |
| 14.000 | 3.16826039 | 3.10954636 | 1.853 | | | |
| 18.000 | 3.42918563 | 3.46714612 | 1.106 | | | |
| 20.000 | 3.56885404 | 3.63992185 | 1.991 | | | |
| 24.000 | 3.85439529 | 3.97547179 | 3.141 | | | |
| 28.000 | 4.14174377 | 4.29969473 | 3.813 | | | |
| 30.000 | 4.28490970 | 4.45815149 | 4.043 | | | |
| 34.000 | 4 56917701 | 4.76867364 | 4.366 | | | |
| 38.000 | 4.85008034 | 5.07164631 | 4.568 | | | |
| 40.000 | 4.98917072 | 5.22060547 | 4.638 | | | |
| 44.000 | 5.26456180 | 5.51396814 | 4.736 | | | |
| 48.000 | 5.53639221 | 5.80181121 | 4.794 | | | |
| 50.000 | 5.67097473 | 5.94384265 | 4.811 | | | |
| 60.000 | 6.33155052 | 6.63740675 | 4.830 | | | |
| 70.000 | 6.97356156 | 7.30740686 | 4.787 | | | |
| 80.000 | 7.59949800 | 7.95805263 | 4.718 | | | |
| 90.000 | 8.21144345 | 8.59238309 | 4.639 | | | |
| 100.000 | 8.81110298 | 9.21269426 | 4.557 | | | |
| 200.000 | 14.35081610 | 14.91228436 | 3.912 | | | |
| 300.000 | 19.39457630 | 20.07915374 | 3.529 | | | |
| 400.000 | 24.15229430 | 24.94353439 | 3.276 | | | |
| 500.000 | 28.71438540 | 29.60222405 | 3.091 | | | |
| 600.000 | 33.13024210 | 34.10764140 | 2.950 | | | |
| 700.000 | 37.43060390 | 38.49225729 | 2.836 | | | |
| 800.000 | 41.63626360 | 42.77797040 | 2.742 | | | |
| 900.000 | 45.76212740 | 46.98044679 | 2.662 | | | |
| 1000.000 | 49.81935080 | 51.11139189 | 2.593 | | | |
| 10000.000 | 344.58893741 | | | | 329.527886 | 4.370 |
| 100000.000 | 2627.01487735 | | | | 2530.689761 | 3.666 |
| 1000000.000 | 21202.70319614 | | | | 20535.037208 | 3.148 |

Table 6.3.2 Comparison of displacement thickness for overall and local similarity (LS) Keller Box solution with series expansion (SE) and Glauert and Lighthill (1954) (GL) asymptotic solution. Percentage differences (%) between the numerical vs. series and asymptotic solutions are presented.

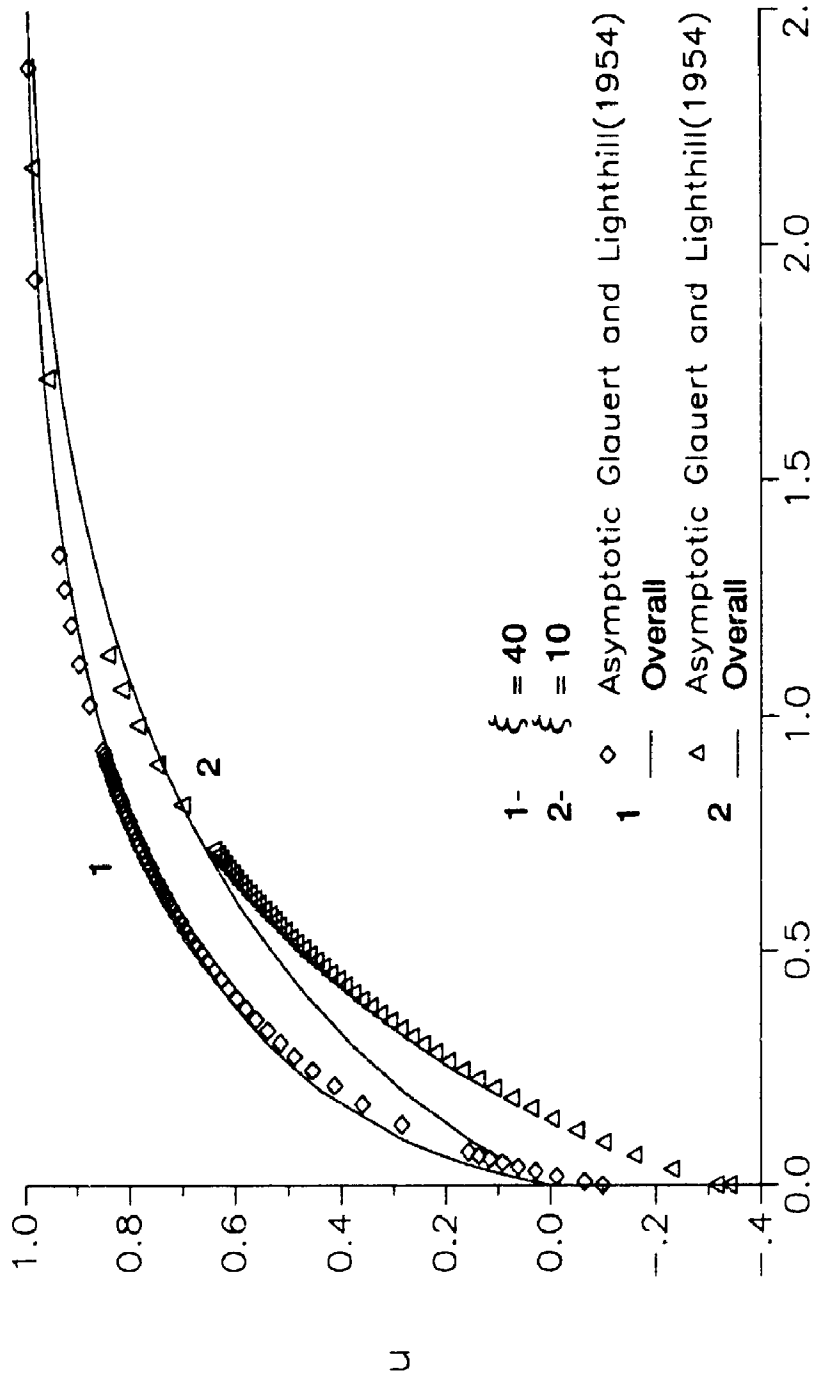


**Figure 6.3.3 Axial velocity comparison between overall Keller Box solution vs. asymptotic solution of Glauert and Lighthill (1954).**

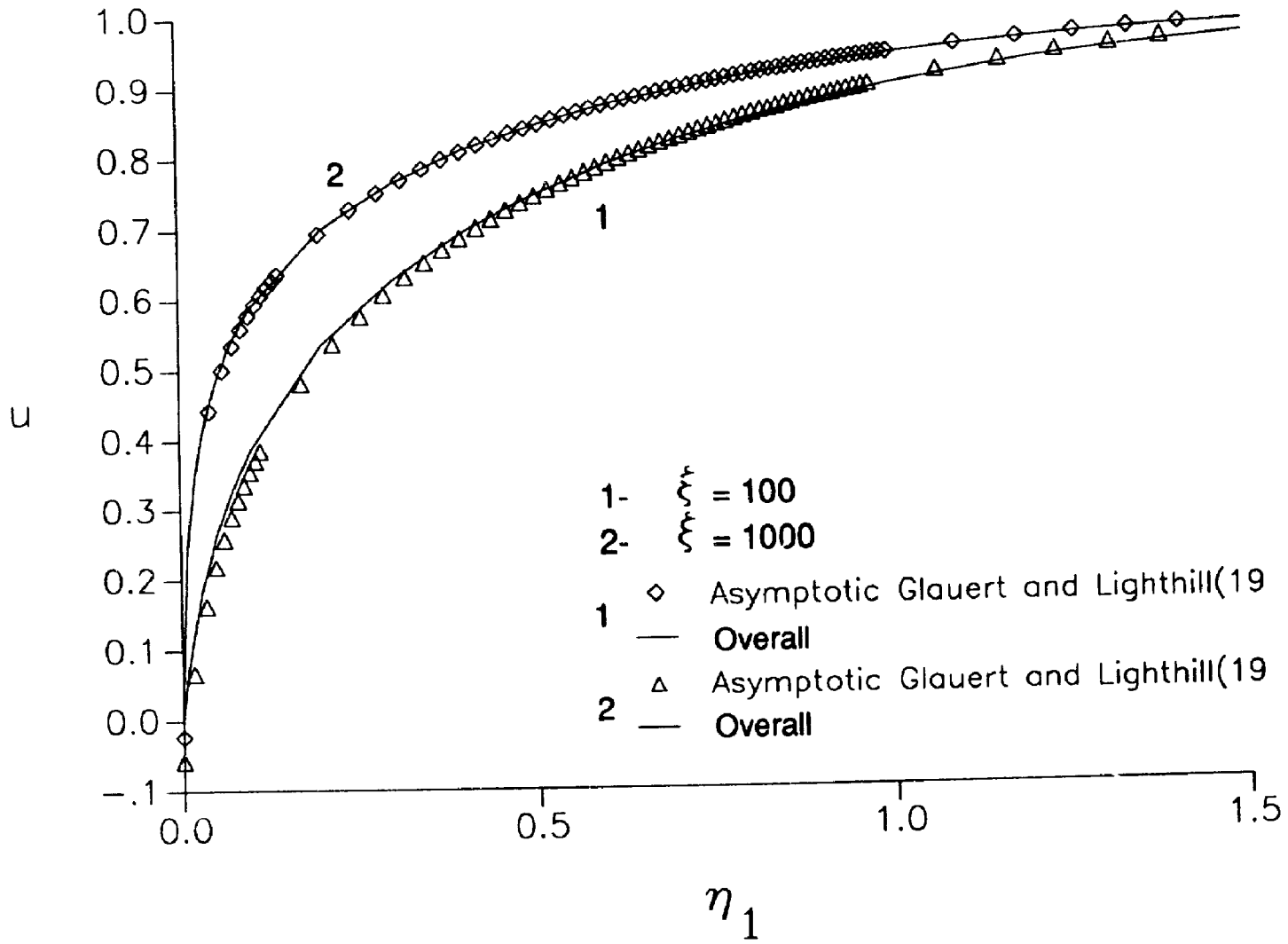


Figure 6.3.4 Axial velocity comparison between overall Keller Box solution vs. asymptotic solution of Glauert and Lighthill (1954).

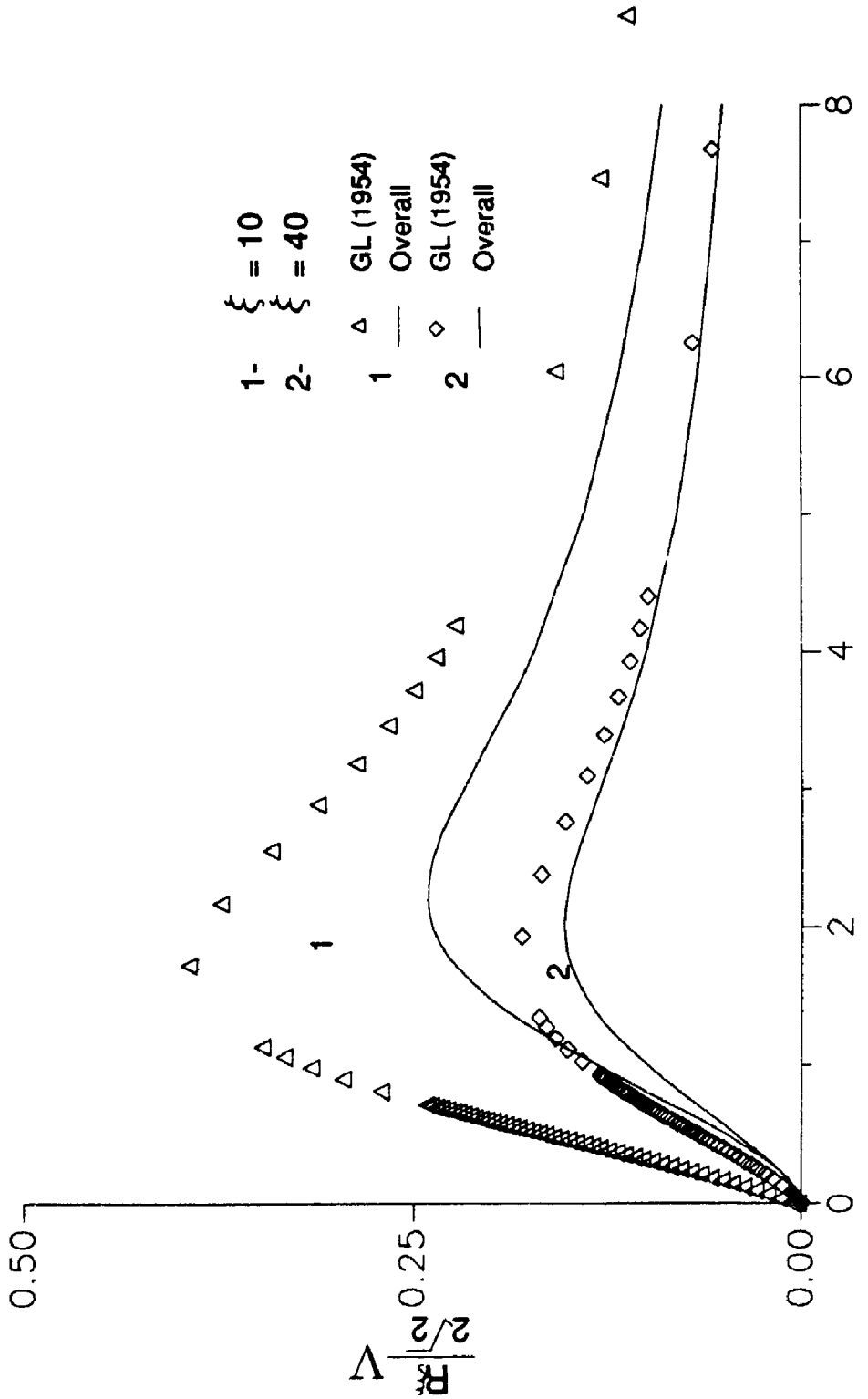


Figure 6.3.5 Comparison of radial velocity parameter from overall Keller Box solution vs. asymptotic solution of Glauert and Lighthill (1954).

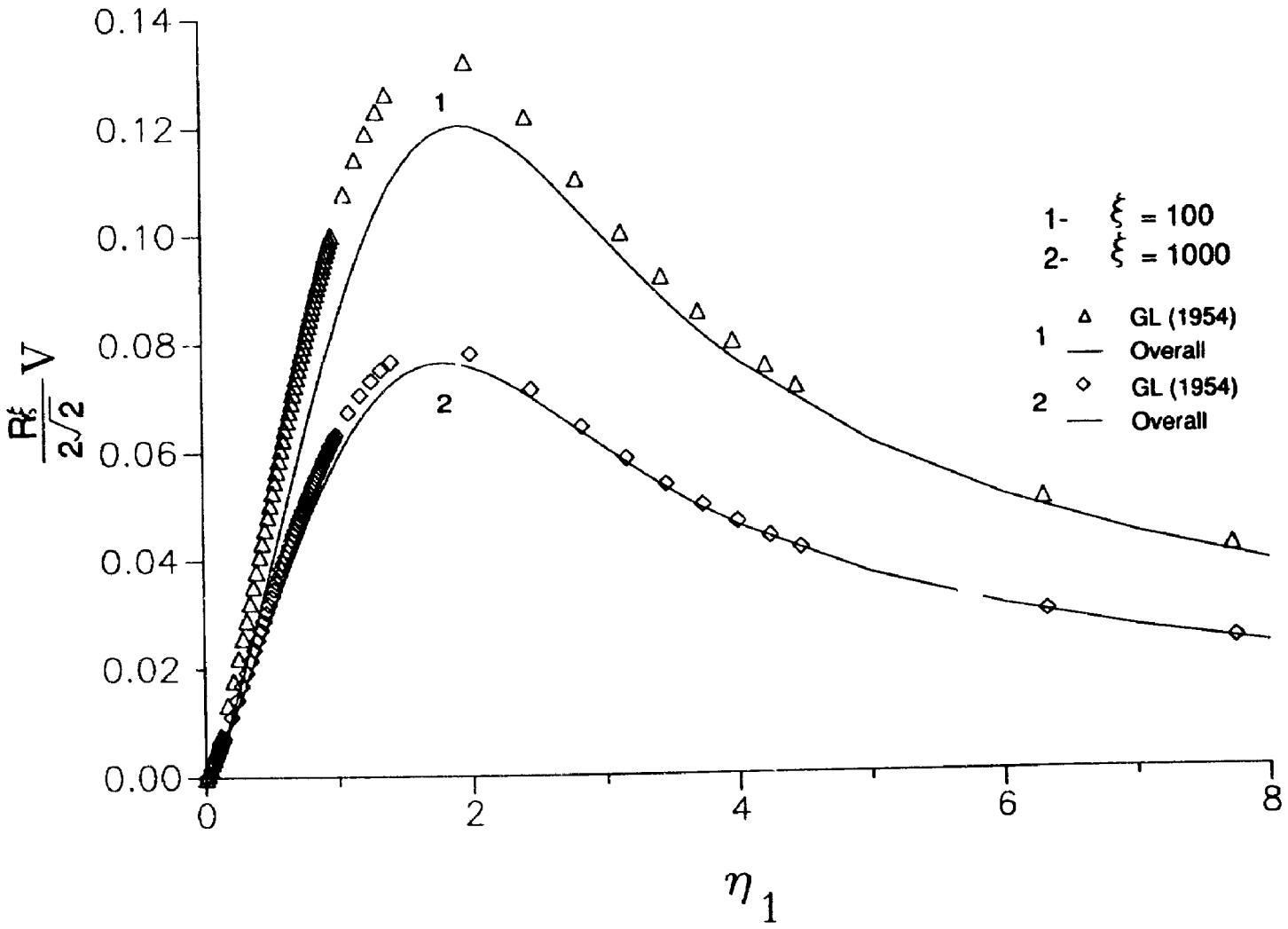


Figure 6.3.6 Comparison of radial velocity parameter from overall Keller Box solution vs. asymptotic solution of Glauert and Lighthill (1954).

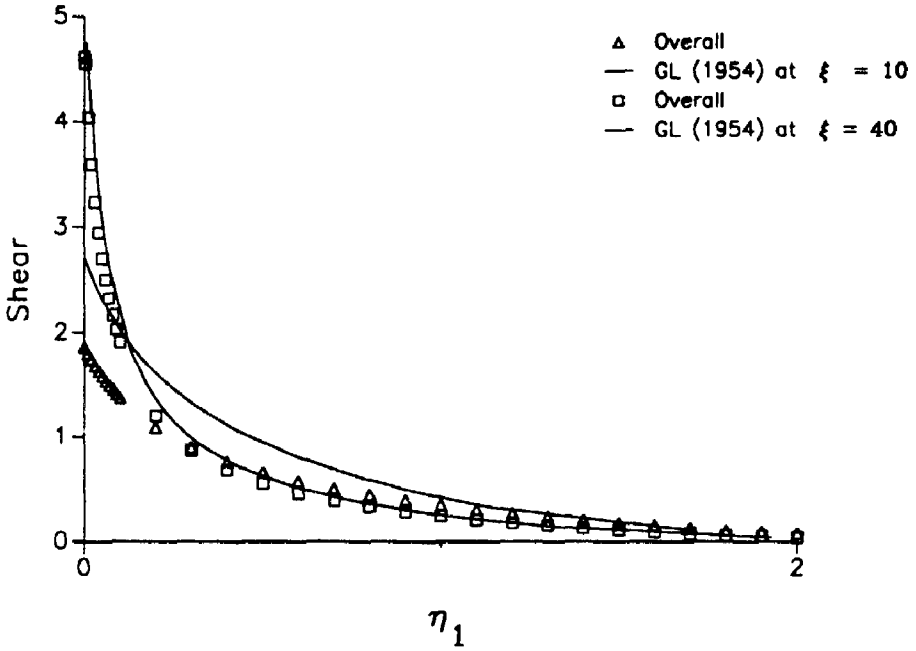


Figure 6.3.7 Comparison of shear stress parameter obtained from overall Keller Box vs. asymptotic solution of Glauert and Lighthill (1954).

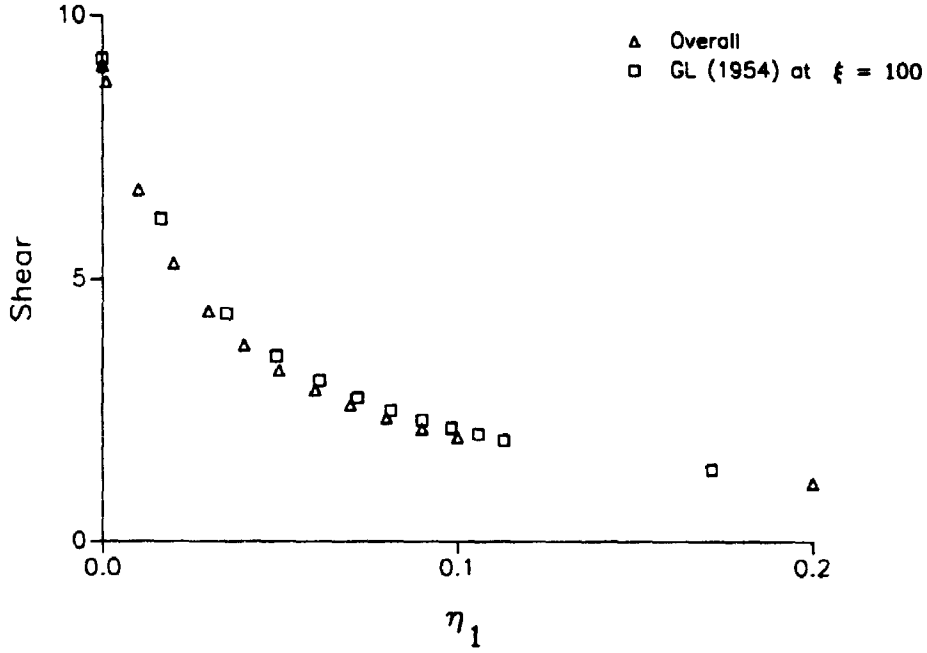


Figure 6.3.8 Comparison of shear stress parameter obtained from overall Kellert Box vs. asymptotic solution of Glauert and Lighthill (1954).

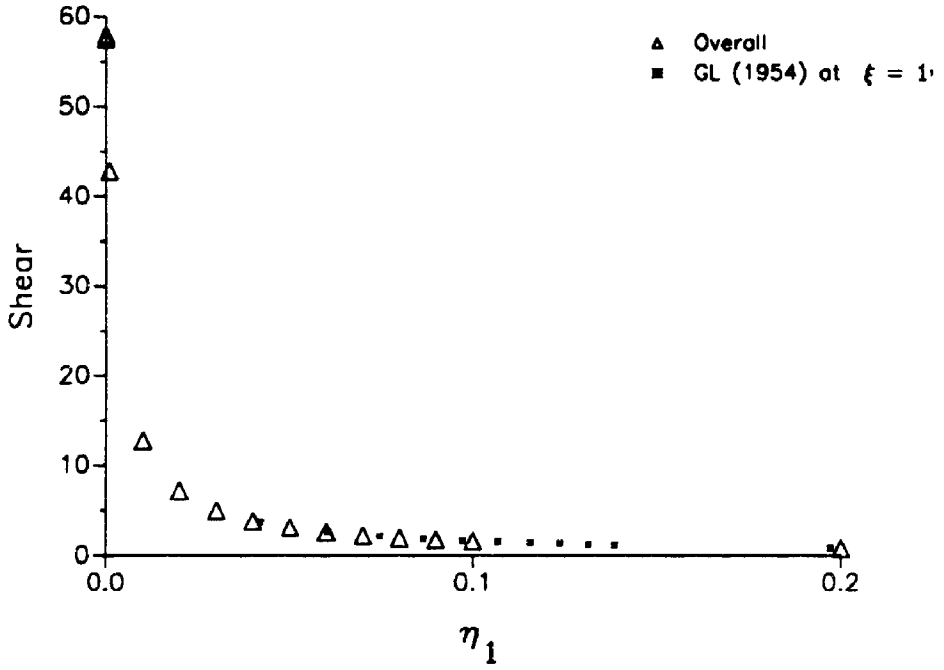


Figure 6.3.9 Comparison of shear stress parameter obtained from overall Keller Box vs asymptotic solution of Glauert and Lighthill (1954).

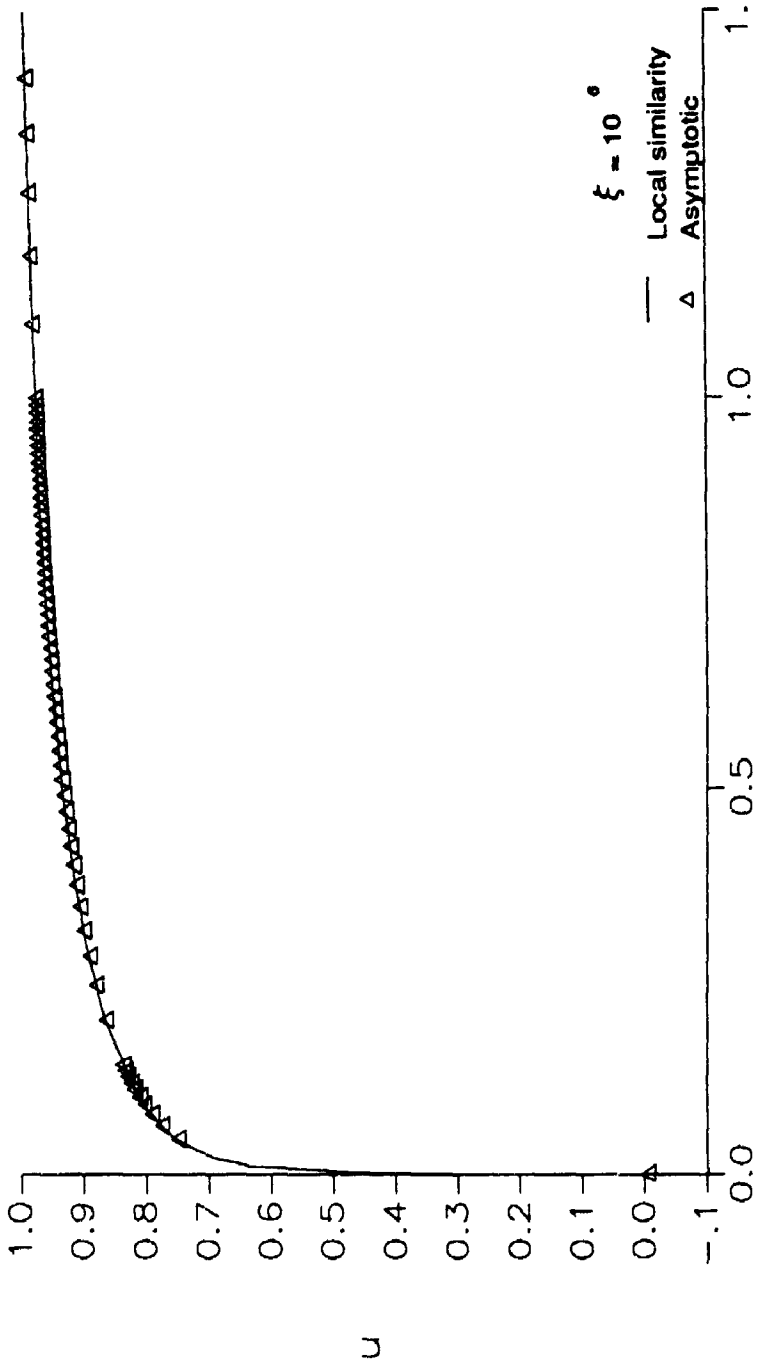


Figure 6.3.10 Comparison of axial velocity profile from local similarity Keller Box solution to Glauert and Lighthill (1954) asymptotic solution.

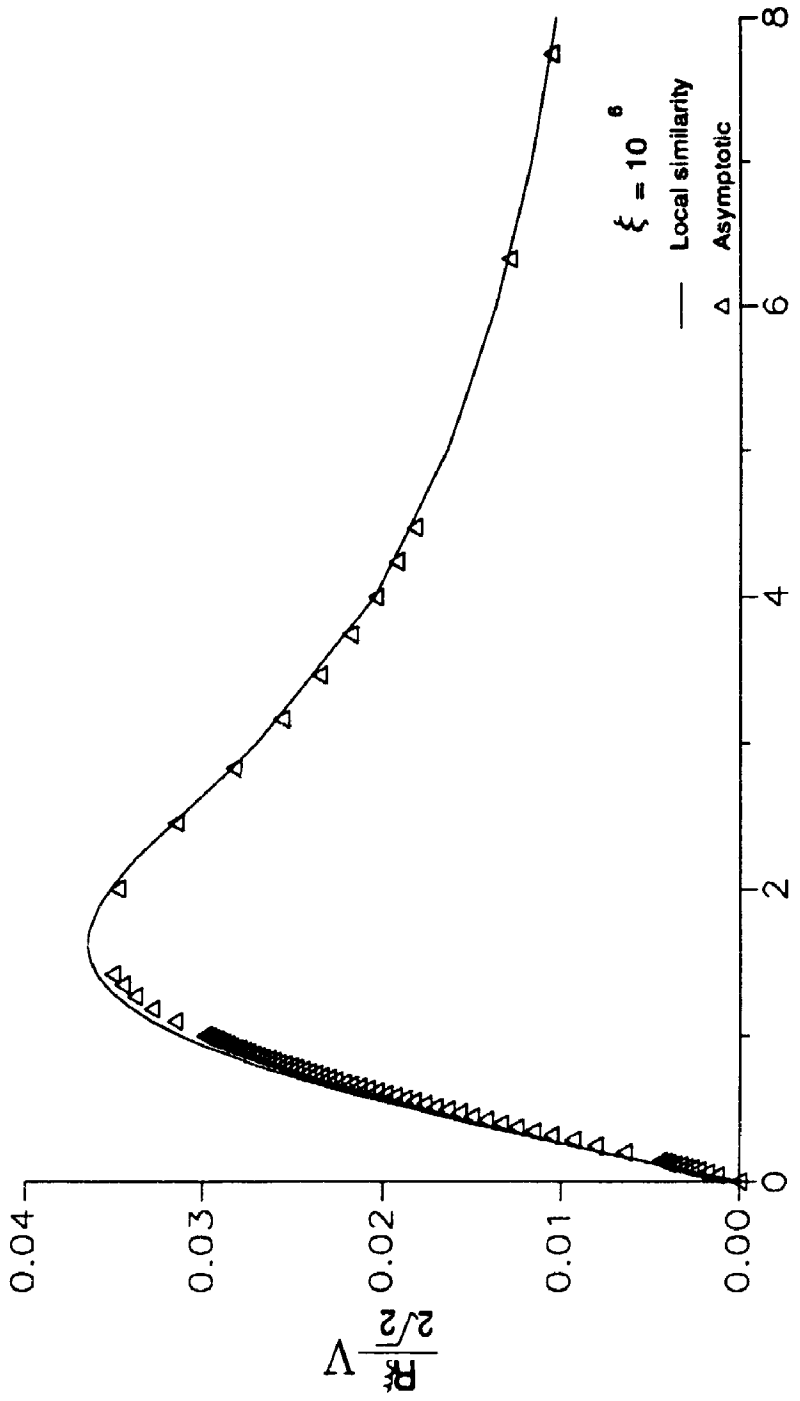


Firgure 6.3.11 Comparison of radial velocity parameter for local similarity Keller Box solution with Glauert and Lighthill (1954) asymptotic solution.

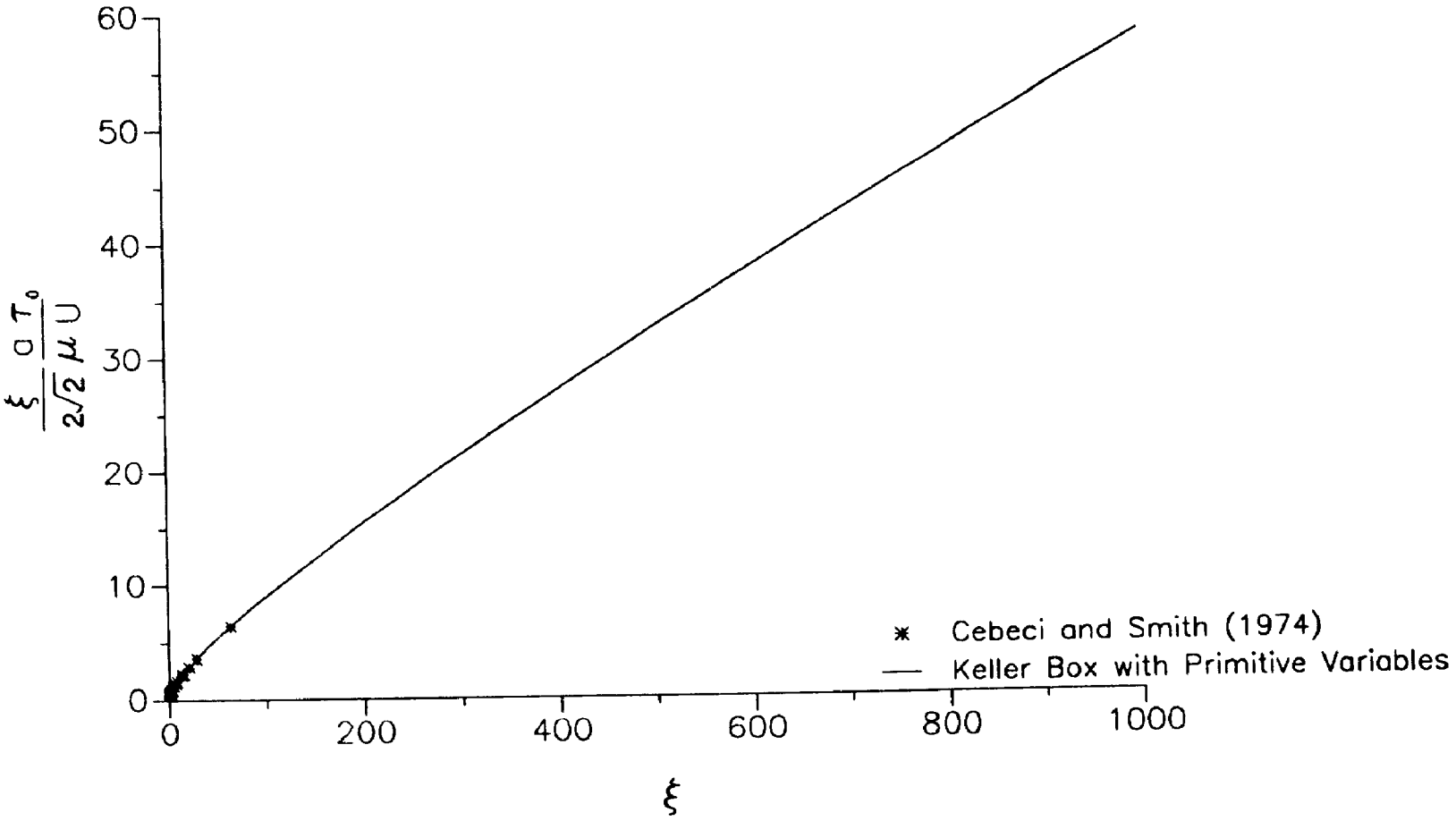


Figure 6.3.12 Comparing the skin-friction parameter from the overall solution obtained by the Keller Box method with the results of Cebeci and Smith (1974) indicates the range of each solution.

# APPENDIX A: INTEGRATING $f_2'(\xi_G)$

In this appendix, we present the exponential integrals which are not given in the paper by Glauert and Lighthill (1954), but are used to generate their asymptotic solution. We also integrate $f_2'(\xi_G)$ from (1.3.16) to obtain $f_2(\xi_G)$.

The exponential integrals are given by :

$$\int_{\infty}^{\xi_G} Ei(-t)dt = \xi_G Ei(-\xi_G) + e^{-\xi_G},$$

$$\int_{\infty}^{\xi_G} Ei(-2t)dt = \xi_G Ei(-2\xi_G) + \frac{e^{-2\xi_G}}{2},$$

$$\int_{\infty}^{\xi_G} EI(-t)dt = \xi_G EI(-\xi_G) - \xi_G Ei(-\xi_G) - e^{-\xi_G},$$

$$\int_{\infty}^{\xi_G} Ei(-t)Ei(-t)dt = \xi_G Ei(-\xi_G)Ei(-\xi_G) + 2e^{-\xi_G} Ei(-\xi_G) - 2Ei(-\xi_G),$$

$$\int_{\infty}^{\xi_G} \ln(t)Ei(-t)dt = \left(\xi_G Ei(-\xi_G) + e^{-\xi_G}\right)\ln(\xi_G) - \xi_G Ei(-\xi_G) - e^{-\xi_G} - Ei(-\xi_G),$$

$$\int_{\infty}^{\xi_G} e^{-t} Ei(-t)dt = -e^{-\xi_G} Ei(-\xi_G) + Ei(-2\xi_G),$$

The method of integration by parts is used to obtain the above.

Thus, $f_2'$, given by (1.3.16), can be integrated to obtain :

$$f_2(\xi_G) = \int_{-\infty}^{\xi_G} f_2'(t)dt$$

$$= \int_{-\infty}^{\xi_G} \{2e^{-t}Ei(-t) - 4Ei(-2t) - Ei(-t)Ei(-t) + 4\ln(t)Ei(-t) - 6EI(-t) + (2+6\gamma)Ei(-t)\}\,dt$$

$$= Ei(-\xi_G)\left[-4e^{-\xi_G} - \xi_G Ei(-\xi_G) + 4\xi_G \ln(\xi_G) + (4+6\gamma)\xi_G - 4\right]$$

$$+4Ei(-\xi_G)(1-\xi_G) + e^{-\xi_G}\left(-2e^{-\xi_G} + 4\ln(\xi_G) + 4 + 6\gamma\right) - 6\xi_G EI(-\xi_G) + C$$

The asymptotic forms of the functions Ei and EI given in the Glauert and Lighthill paper, are:

$$Ei(-\xi_G) \sim \ln(\xi_G) + \gamma$$

and

$$EI(-\xi_G) \sim \frac{1}{2}(\ln(\xi_G) + \gamma)^2 + \frac{\pi^2}{12}$$

Applying the asymptotic forms as $\xi_G \to 0$ and $f_20$ gives:

$$f_2 \sim (\ln(\xi_G) + \gamma)(4-4) + 4(\ln(2\xi_G) + \gamma) + 4\ln(\xi_G) + 2 + 6\gamma - 6\xi_G\left(\frac{1}{2}(\ln(\xi_G) + \gamma)^2 + \frac{\pi^2}{12}\right) + C = 0,$$

i.e.,

$$C = -4\ln 2 - 2\gamma - 2.$$

Therefore,

$$f_2(\xi_G) = Ei(-\xi_G)\left[-4e^{-\xi_G} - \xi_G Ei(-\xi_G) + 4\xi_G \ln(\xi_G) + (4+6\gamma)\xi_G - 4\right]$$

$$+ 4Ei(-\xi_G)(1-\xi_G) + e^{-\xi_G}\left(-2e^{-\xi_G} + 4\ln(\xi_G) + 4 + 6\gamma\right) - 6\xi_G EI(-\xi_G) \pm 4\ln 2 - 2\gamma - 2.$$

Glauert and Lighthill use this result to obtain the second term in the displacement thickness, i.e., they found $f_2(\infty)$.

Note that calculations include obtaining expansion formula for the Ei(-x) function from Abromowitz and Stegun (1965) and that the EI(-x) function is calculated using the fourth order Simpson's rule.

# APPENDIX B: SERIES EXPANSION OF F

In order to obtain the coefficients for the series expansions originating from the r-based similarity transformation, 8 ordinary differential equations obtained by differentiating ordinary differential equation 2.2.22 with respect to $\eta$ are needed. The series expansion is then used to obtain the expansions of the individual terms of the Navier-Stokes equations, 1.2.3-5, and Cooke's equations, 1.2.6-7.

The 8 equations obtained by differentiating (2.2.22) are :

$$\eta^3 F^{IV} + 5\eta^2 F^{III} + 3\eta F^{II} - 2FF + 2\eta^2 F^I F^I + 8\eta^2 F F^{II} + 2\eta^3 F^I F^{II} + 2\eta^3 F F^{III}, \qquad (B.1)$$

$$\eta^3 F^V + 8\eta^2 F^{IV} + 13\eta F^{III} + 3F^{II} - 4FF^I + 4\eta F^I F^I + 18\eta^2 F^I F^{II} + 16\eta F F^{II}$$
$$+14\eta^2 F F^{III} + \eta^3\{2F^{II}F^{II} + 4F^I F^{III} + 2FF^{IV}\} = 0, \qquad (B.2)$$

$$\eta^3 F^{VI} + 11\eta^2 F^V + 29\eta F^{IV} + 16F^{III} + 12FF^{II} + \eta\{60F^I F^{II} + 44FF^{III}\}$$
$$+\eta^2\{24F^{II}F^{II} + 44F^I F^{III} + 20FF^{IV}\} + \eta^3\{8F^{II}F^{III} + 6F^I F^{IV} + 2FF^V\} = 0, \qquad (B.3)$$

$$\eta^3 F^{VII} + 14\eta^2 F^{VI} + 51\eta F^V + 45F^{IV} + 72F^I F^{II} + 56FF^{III} + \eta\{108F^{II}F^{II}$$
$$+192F^I F^{III} + 84FF^{IV}\} + \eta^2\{116F^{II}F^{III} + 82F^I F^{IV} + 26FF^V\} + \eta^3\{8F^{III}F^{III}$$
$$+14F^{II}F^{IV} + 8F^I F^V + 2FF^{VI}\} = 0, \qquad (B.4)$$

$$\eta^3 F^{VIII} + 17\eta^2 F^{VII} + 79\eta F^{VI} + 96F^{V} + 180F^{II}F^{II} + 320F^{I}F^{III} + 140FF^{IV}$$
$$+\eta\{640F^{II}F^{III} + 440F^{I}F^{IV} + 136FF^{V}\} + \eta^2\{140F^{III}F^{III} + 240F^{II}F^{IV}$$
$$+132F^{I}F^{V} + 32FF^{VI}\} + \eta^3\{30F^{III}F^{IV} + 22F^{II}F^{V} + 10F^{I}F^{VI} + 2FF^{VII}\} = 0, \qquad (B.5)$$

$$\eta^3 F^{\cdot} + 20\eta^2 F^{VIII} + 113\eta F^{VII} + 175F^{VI} + 1320F^{II}F^{III} + 900F^{I}F^{IV} + 276FF^{V}$$
$$+\eta\{920F^{III}F^{III} + 1560F^{II}F^{IV} + 840F^{I}F^{V} + 200FF^{VI}\} + \eta^2\{610F^{III}F^{IV} + 438F^{II}F^{V}$$
$$+194F^{I}F^{VI} + 38FF^{VII}\} + \eta^3\{30F^{IV}F^{IV} + 52F^{III}F^{V} + 32F^{II}F^{VI} + 12F^{I}F^{VII}$$
$$+2FF^{VIII}\} = 0, \qquad (B.6)$$

$$\eta^3 F^{X} + 23\eta^2 F^{IX} + 153\eta F^{VIII} + 288F^{VII} + 2240F^{III}F^{III} + 3780F^{II}F^{IV} + 2016F^{I}F^{V}$$
$$+476FF^{VI} + \eta\{4620F^{III}F^{IV} + 3276F^{II}F^{V} + 1428F^{I}F^{VI} + 276FF^{VII}\}$$
$$+\eta^2\{700F^{IV}F^{IV} + 1204F^{III}F^{V} + 728F^{II}F^{VI} + 268F^{I}F^{VII} + 44FF^{VIII}\} + \eta^3\{112F^{IV}F^{V}$$
$$+84F^{III}F^{VI} + 44F^{II}F^{VII} + 14F^{I}F^{VIII} + 2FF^{IX}\} = 0, \qquad (B.7)$$

$$\eta^3 F^{XI} + 26\eta^2 F^{X} + 199\eta F^{IX} + 441F^{VIII} + 12880F^{III}F^{IV} + 9072F^{II}F^{V} + 3920F^{I}F^{VI}$$
$$+752FF^{VII} + \eta\{6020F^{IV}F^{IV} + 10304F^{III}F^{V} + 6160F^{II}F^{VI} + 2240F^{I}F^{VII} + 364FF^{VIII}\}$$
$$+\eta^2\{2940F^{IV}F^{V} + 2184F^{III}F^{VI} + 1128F^{II}F^{VII} + 354F^{I}F^{V.III} + 50FF^{IX}\} + \eta^3\{112F^{V}F^{V}$$
$$+196F^{IV}F^{VI} + 128F^{III}F^{VII} + 58F^{II}F^{VIII} + 16F^{I}F^{IX} + 2FF^{X}\} = 0, \qquad (B.8)$$

The corresponding coefficients for the expansion of F are obtained by evaluating the above equations at $\eta = \eta_0$ and replacing known coefficients obtained in previous equations into the current equation being evaluated. Thus, evaluating equation 2.2.22 at $\eta = \eta_0$ gives :

$$F_0^{III} = -2\frac{F_0^{II}}{\eta_0} = -2\frac{\alpha_F}{\eta_0}, \tag{B.9}$$

where

$$\alpha_F \equiv F_0^{II} \tag{B.10}$$

Evaluating the next equations (B.1-8) in order and using previously obtained coefficients gives :

$$F_0^{IV} = 7\frac{\alpha_F}{\eta_0^2}, \tag{B.11}$$

$$F_0^{V} = -33\frac{\alpha_F}{\eta_0^3} - 2\alpha_F^2, \tag{B.12}$$

$$F_0^{VI} = 192\frac{\alpha_F}{\eta_0^4} + 14\frac{\alpha_F^2}{\eta_0}, \tag{B.13}$$

$$F_0^{VII} = -1320\frac{\alpha_F}{\eta_0^5} - 100\frac{\alpha_F^2}{\eta_0^2}, \tag{B.14}$$

$$F_0^{VIII} = 10440\frac{\alpha_F}{\eta_0^6} + 792\frac{\alpha_F^2}{\eta_0^3} + 44\alpha_F^3, \tag{B.15}$$

$$F_0^{IX} = -93240\frac{\alpha_F}{\eta_0^7} - 7002\frac{\alpha_F^2}{\eta_0^4} - 660\frac{\alpha_F^3}{\eta_0}, \tag{B.16}$$

$$F_0^{X} = 927360\frac{\alpha_F}{\eta_0^{8}} + 68706\frac{\alpha_F^{2}}{\eta_0^{5}} + 8312\frac{\alpha_F^{3}}{\eta_0^{2}}, \qquad (B.17)$$

$$F_0^{XI} = -10160640\frac{\alpha_F}{\eta_0^{9}} - 742374\frac{\alpha_F^{2}}{\eta_0^{6}} - 103904\frac{\alpha_F^{3}}{\eta_0^{3}} - 3000\alpha_F^{4}. \qquad (B.18)$$

Series expansions of individual terms from the boundary layer equations of Cooke, 1.2.6-7, and of individual terms from the Navier-Stokes equations, 1.2.3-5, have been obtained by applying the resulting series expansion for F and its derivatives to the corresponding terms.

Series expansions of individual terms from the momentum equation 1.2.6 are given by :

$$u\frac{\partial u}{\partial x} = \frac{1}{R}\{\eta_0^{3}\left[-\alpha_F^{2}\eta_1 + 10\alpha_F^{3}\frac{\eta_1^{4}}{4!} - 492\alpha_F^{4}\frac{\eta_1^{7}}{7!} + O(\eta_1^{10})\right]$$

$$+\eta_0^{2}\left[\alpha_F^{2}\frac{\eta_1^{2}}{2} - 52\alpha_F^{3}\frac{\eta_1^{5}}{5!} + 6216\alpha_F^{4}\frac{\eta_1^{8}}{8!} + O(\eta_1^{11})\right] + \eta_0\left[-2\alpha_F^{2}\frac{\eta_1^{3}}{3!} + 298\alpha_F^{3}\frac{\eta_1^{6}}{6!} + O(\eta_1^{9})\right]$$

$$+3!\alpha_F^{2}\frac{\eta_1^{4}}{4!} - 1966\alpha_F^{3}\frac{\eta_1^{7}}{7!} + O(\eta_1^{10}) + \frac{1}{\eta_0}\left[-4!\alpha_F^{2}\frac{\eta_1^{5}}{5!} + 14810\alpha_F^{3}\frac{\eta_1^{8}}{8!} + O(\eta_1^{11})\right]$$

$$+\frac{1}{\eta_0^{2}}\left[5!\alpha_F^{2}\frac{\eta_1^{6}}{6!} + O(\eta_1^{9})\right] + \frac{1}{\eta_0^{3}}\left[-6!\alpha_F^{2}\frac{\eta_1^{7}}{7!} + O(\eta_1^{10})\right] + \frac{1}{\eta_0^{4}}\left[7!\alpha_F^{2}\frac{\eta_1^{8}}{8!} + O(\eta_1^{11})\right] + \ldots\}, \qquad (B.19)$$

$$\nu\frac{\partial u}{\partial r} = \frac{1}{R}\{\eta_0^{3}\left[\alpha_F^{2}\eta_1 - 10\alpha_F^{3}\frac{\eta_1^{4}}{4!} + 492\alpha_F^{4}\frac{\eta_1^{7}}{7!} + O(\eta_1^{10})\right]$$

$$+\eta_0^{2}\left[-3\alpha_F^{2}\frac{\eta_1^{2}}{2} + 96\alpha_F^{3}\frac{\eta_1^{5}}{5!} - 9216\alpha_F^{4}\frac{\eta_1^{8}}{8!} + O(\eta_1^{11})\right] + \eta_0\left[12\alpha_F^{2}\frac{\eta_1^{3}}{3!} - 870\alpha_F^{3}\frac{\eta_1^{6}}{6!} + O(\eta_1^{9})\right]$$

$$-60\alpha_F^{2}\frac{\eta_1^{4}}{4!} + 8298\alpha_F^{3}\frac{\eta_1^{7}}{7!} + O(\eta_1^{10}) + \frac{1}{\eta_0}\left[360\alpha_F^{2}\frac{\eta_1^{5}}{5!} - 85194\alpha_F^{3}\frac{\eta_1^{8}}{8!} + O(\eta_1^{11})\right]$$

$$+\frac{1}{\eta_0^2}\left[-2520\alpha_F^2\frac{\eta_1^6}{6!}+O(\eta_1^9)\right]+\frac{1}{\eta_0^3}\left[20160\alpha_F^2\frac{\eta_1^7}{7!}+O(\eta_1^{10})\right]+\frac{1}{\eta_0^4}\left[-181440\alpha_F^2\frac{\eta_1^8}{8!}+O(\eta_1^{11})\right]+\ldots\},$$

(*B*.20)

$$\frac{1}{R}\frac{\partial^2 u}{\partial r^2}=\frac{1}{R}\{\eta_0^2\left[-\alpha_F^2\eta_1^2+44\alpha_F^3\frac{\eta_1^5}{5!}-3000\alpha_F^4\frac{\eta_1^8}{8!}+O(\eta_1^{11})\right]$$

$$+\eta_0\left[-\alpha_F+12\alpha_F^2\frac{\eta_1^3}{3!}-616\alpha_F^3\frac{\eta_1^6}{6!}+O(\eta_1^9)\right]+2\alpha_F\eta_1-74\alpha_F^2\frac{\eta_1^4}{4!}+7256\alpha_F^3\frac{\eta_1^7}{7!}+O(\eta_1^{10})]$$

$$+\frac{1}{\eta_0}\left[-6\alpha_F\frac{\eta_1^2}{2}+510\alpha_F^2\frac{\eta_1^5}{5!}-85032\alpha_F^3\frac{\eta_1^8}{8!}+O(\eta_1^{11})\right]+\frac{1}{\eta_0^2}\left[4!\alpha_F\frac{\eta_1^3}{3!}-3954\alpha_F^2\frac{\eta_1^6}{6!}+O(\eta_1^9)\right]$$

$$+\frac{1}{\eta_0^3}\left[-5!\alpha_F\frac{\eta_1^4}{4!}+34272\alpha_F^2\frac{\eta_1^7}{7!}+O(\eta_1^{10})\right]+\frac{1}{\eta_0^4}\left[6!\alpha_F\frac{\eta_1^5}{5!}-329328\alpha_F^2\frac{\eta_1^8}{8!}+O(\eta_1^{11})\right]+\ldots\},$$

(*B*.21)

$$\frac{1}{Rr}\frac{\partial u}{\partial r}=\frac{1}{R}\{\eta_0\left[\alpha_F-2\alpha_F^2\frac{\eta_1^3}{3!}+44\alpha_F^3\frac{\eta_1^6}{6!}+O(\eta_1^9)\right]-2\alpha_F\eta_1+20\alpha_F^2\frac{\eta_1^4}{4!}-924\alpha_F^3\frac{\eta_1^7}{7!}+O(\eta_1^{10})$$

$$+\frac{1}{\eta_0}\left[3!\alpha_F\frac{\eta_1^2}{2}-174\alpha_F^2\frac{\eta_1^5}{5!}+14648\alpha_F^3\frac{\eta_1^8}{8!}+O(\eta_1^{11})\right]+\frac{1}{\eta_0^2}\left[-4!\alpha_F\frac{\eta_1^3}{3!}+1554\alpha_F^2\frac{\eta_1^6}{6!}+O(\eta_1^9)\right]$$

$$+\frac{1}{\eta_0^3}\left[5!\alpha_F\frac{\eta_1^4}{4!}-14832\alpha_F^2\frac{\eta_1^7}{7!}+O(\eta_1^{10})\right]+\frac{1}{\eta_0^4}\left[-6!\alpha_F\frac{\eta_1^5}{5!}+152928\alpha_F^2\frac{\eta_1^8}{8!}+O(\eta_1^{11})\right]+\ldots\}.$$

(*B*.22)

Series expansions of neglected terms from the Navier-Stokes equations, due to boundary layer approximation are given by :

$$\frac{1}{R}\frac{\partial^2 u}{\partial x^2}=\frac{1}{R^3}\{\eta_0^6\left[-2\alpha_F^2\frac{\eta_1^2}{2}+44\alpha_F^3\frac{\eta_1^5}{5!}-3000\alpha_F^4\frac{\eta_1^8}{8!}+O(\eta_1^{11})\right]$$

$$+\eta_0^5\left[2\alpha_F-6\alpha_F^2\frac{\eta_1^3}{3!}+44\alpha_F^3\frac{\eta_1^6}{6!}+O(\eta_1^9)\right]+\eta_0^4\left[10\alpha_F^2\frac{\eta_1^4}{4!}-444\alpha_F^3\frac{\eta_1^7}{7!}+O(\eta_1^{10})\right]+\ldots\},$$

(*B*.23)

$$u\frac{\partial v}{\partial x}=\frac{1}{R^2}\{\eta_0^5\left[-\alpha_F^2\eta_1+10\alpha_F^3\frac{\eta_1^4}{4!}-492\alpha_F^4\frac{\eta_1^7}{7!}+O(\eta_1^{10})\right]$$

$$+\eta_0^4\left[-\alpha_F^2\frac{\eta_1^2}{2}-2\alpha_F^3\frac{\eta_1^5}{5!}+2280\alpha_F^4\frac{\eta_1^8}{8!}+O(\eta_1^{11})\right]$$

$$+\eta_0^3\left[\alpha_F^2\frac{\eta_1^3}{3!}-14\alpha_F^3\frac{\eta_1^6}{6!}-12752\alpha_F^4\frac{\eta_1^9}{9!}+O(\eta_1^{12})\right]+\ldots\},\qquad(B.24)$$

$$v\frac{\partial v}{\partial r}=\frac{1}{R^2}\{\eta_0^5\left[\alpha_F^2\eta_1-10\alpha_F^3\frac{\eta_1^4}{4!}+492\alpha_F^4\frac{\eta_1^7}{7!}+O(\eta_1^{10})\right]$$

$$+\eta_0^4\left[-3\alpha_F^2\frac{\eta_1^2}{2}+66\alpha_F^3\frac{\eta_1^5}{5!}-6264\alpha_F^4\frac{\eta_1^8}{8!}+O(\eta_1^{11})\right]$$

$$+\eta_0^3\left[15\alpha_F^2\frac{\eta_1^3}{3!}-546\alpha_F^3\frac{\eta_1^6}{6!}+79136\alpha_F^4\frac{\eta_1^9}{9!}+O(\eta_1^{12})\right]+\ldots\},\qquad(B.25)$$

$$\frac{1}{Rr}\frac{\partial v}{\partial r}=\frac{1}{R^2}\{\eta_0^3\left[\alpha_F-2\alpha_F^2\frac{\eta_1^3}{3!}+44\alpha_F^3\frac{\eta_1^6}{6!}-3000\alpha_F^4\frac{\eta_1^9}{9!}+O(\eta_1^{12})\right]$$

$$+\eta_0^2\left[-2\alpha_F\eta_1+14\alpha_F^2\frac{\eta_1^4}{4!}-660\alpha_F^3\frac{\eta_1^7}{7!}+O(\eta_1^{10})\right]$$

$$+\eta_0\left[7\alpha_F\frac{\eta_1^2}{2}-100\alpha_F^2\frac{\eta_1^5}{5!}+8312\alpha_F^3\frac{\eta_1^8}{8!}+O(\eta_1^{11})\right]+\ldots\},\qquad(B.26)$$

$$\frac{1}{R}\frac{\partial^2 v}{\partial r^2}=\frac{1}{R^2}\{\eta_0{}^4\left[-2\alpha_F{}^2\frac{\eta_1{}^2}{2}+44\alpha_F^3\frac{\eta_1^5}{5!}-3000\alpha_F^4\frac{\eta_1^8}{8!}+O(\eta_1{}^{11})\right]$$

$$+\eta_0{}^3\left[-\alpha_F+6\alpha_F{}^2\frac{\eta_1{}^3}{3!}-352\alpha_F^3\frac{\eta_1^6}{6!}+O(\eta_1{}^9)\right]$$

$$+\eta_0{}^2\left[3\alpha_F\eta_1-30\alpha_F{}^2\frac{\eta_1{}^4}{4!}+3032\alpha_F^3\frac{\eta_1^7}{7!}+O(\eta_1{}^{10})\right]+\ldots\}, \qquad (B.27)$$

$$\frac{1}{R}\frac{\partial^2 v}{\partial x^2}=\frac{1}{R^4}\{\eta_0{}^8\left[-2\alpha_F{}^2\frac{\eta_1{}^2}{2}+44\alpha_F^3\frac{\eta_1^5}{5!}-3000\alpha_F^4\frac{\eta_1^8}{8!}+O(\eta_1{}^{11})\right]$$

$$+\eta_0{}^7\left[4\alpha_F-16\alpha_F{}^2\frac{\eta_1{}^3}{3!}+396\alpha_F^3\frac{\eta_1^6}{6!}+O(\eta_1{}^9)\right]$$

$$+\eta_0{}^6\left[4\alpha_F\eta_1-22\alpha_F{}^2\frac{\eta_1{}^4}{4!}-136\alpha_F^3\frac{\eta_1^7}{7!}+O(\eta_1{}^{10})\right]+\ldots\}, \qquad (B.28)$$

$$\frac{v}{Rr^2}=\frac{1}{R^2}\{\eta_0{}^2\left[\alpha_F\eta_1-2\alpha_F^2\frac{\eta_1^4}{4!}+44\alpha_F^3\frac{\eta_1^7}{7!}+O(\eta_1{}^{10})\right]$$

$$+\eta_0\left[-5\alpha_F\frac{\eta_1^2}{2}+26\alpha_F^2\frac{\eta_1^5}{5!}-1056\alpha_F^3\frac{\eta_1^8}{8!}+O(\eta_1{}^{11})\right]$$

$$+27\alpha_F\frac{\eta_1^3}{3!}-282\alpha_F^2\frac{\eta_1^6}{6!}+18872\alpha_F^3\frac{\eta_1^9}{9!}+O(\eta_1{}^{12})+\ldots\}. \qquad (B.29)$$

Series expansions of individual terms from continuity equation 1.2.7 are given by :

$$\frac{\partial u}{\partial x}=\frac{1}{R}\{\eta_0^3\left[-\alpha_F+2\alpha_F^2\frac{\eta_1^3}{3!}-44\alpha_F^3\frac{\eta_1^6}{6!}+3000\alpha_F^4\frac{\eta_1^9}{9!}+O(\eta_1^{12})\right]$$

$$+\eta_0^2\left[-4\alpha_F^2\frac{\eta_1^4}{4!}+308\alpha_F^3\frac{\eta_1^7}{7!}+O(\eta_1^{10})\right]+\eta_0\left[14\alpha_F^2\frac{\eta_1^5}{5!}-2328\alpha_F^3\frac{\eta_1^8}{8!}+O(\eta_1^{11})\right]$$

$$-66\alpha_F^2\frac{\eta_1^6}{6!}+19728\alpha_F^3\frac{\eta_1^9}{9!}+O(\eta_1^{12})+\frac{1}{\eta_0}\left[384\alpha_F^2\frac{\eta_1^7}{7!}+O(\eta_1^{10})\right]$$

$$+\frac{1}{\eta_0^2}\left[-2640\alpha_F^2\frac{\eta_1^8}{8!}+O(\eta_1^{11})\right]+\frac{1}{\eta_0^3}\left[20880\alpha_F^2\frac{\eta_1^9}{9!}+O(\eta_1^{121})\right]+\ldots\}, \qquad (B.30)$$

$$\frac{\partial v}{\partial r}=\frac{1}{R}\{\eta_0^3\left[\alpha_F-2\alpha_F^2\frac{\eta_1^3}{3!}+44\alpha_F^3\frac{\eta_1^6}{6!}-3000\alpha_F^4\frac{\eta_1^9}{9!}+O(\eta_1^{12})\right]$$

$$+\eta_0^2\left[-\alpha_F\eta_1+6\alpha_F^2\frac{\eta_1^4}{4!}-352\alpha_F^3\frac{\eta_1^7}{7!}+O(\eta_1^{10})\right]$$

$$+\eta_0\left[3\alpha_F\frac{\eta_1^2}{2}-30\alpha_F^2\frac{\eta_1^5}{5!}+3032\alpha_F^3\frac{\eta_1^8}{8!}+O(\eta_1^{11})\right]$$

$$-12\alpha_F\frac{\eta_1^3}{3!}+192\alpha_F^2\frac{\eta_1^6}{6!}-29096\alpha_F^3\frac{\eta_1^9}{9!}+O(\eta_1^{12})$$

$$+\frac{1}{\eta_0}\left[60\alpha_F\frac{\eta_1^4}{4!}-1458\alpha_F^2\frac{\eta_1^7}{7!}+O(\eta_1^{10})\right]+\frac{1}{\eta_0^2}\left[-360\alpha_F\frac{\eta_1^5}{5!}+12690\alpha_F^2\frac{\eta_1^8}{8!}+O(\eta_1^{11})\right]$$

$$+\frac{1}{\eta_0^3}\left[2520\alpha_F\frac{\eta_1^6}{6!}-124020\alpha_F^2\frac{\eta_1^9}{9!}+O(\eta_1^{12})\right]+\ldots\}, \qquad (B.31)$$

$$\frac{\nu}{r}=\frac{1}{R}\{\eta_0^2\left[\alpha_F\eta_1-2\alpha_F^2\frac{\eta_1^4}{4!}+44\alpha_F^3\frac{\eta_1^7}{7!}+O(\eta_1^{10})\right]$$

$$+\eta_0\left[-3\alpha_F\frac{\eta_1^2}{2}+16\alpha_F^2\frac{\eta_1^5}{5!}-704\alpha_F^3\frac{\eta_1^8}{8!}+O(\eta_1^{11})\right]+12\alpha_F\frac{\eta_1^3}{3!}-126\alpha_F^2\frac{\eta_1^6}{6!}+9368\alpha_F^3\frac{\eta_1^9}{9!}+O(\eta_1^{12})$$

$$+\frac{1}{\eta_0}\left[-60\alpha_F\frac{\eta_1^4}{4!}+1074\alpha_F^2\frac{\eta_1^7}{7!}+O(\eta_1^{10})\right]+\frac{1}{\eta_0^2}\left[360\alpha_F\frac{\eta_1^5}{5!}-10050\alpha_F^2\frac{\eta_1^8}{8!}+O(\eta_1^{11})\right]$$

$$+\frac{1}{\eta_0^3}\left[-2520\alpha_F\frac{\eta_1^6}{6!}+103140\alpha_F^2\frac{\eta_1^9}{9!}+O(\eta_1^{12})\right]+\ldots\}. \qquad (B.32)$$

# APPENDIX C: SERIES EXPANSION OF G

In order to obtain the coefficients for the series expansions originating from the y-based similarity transformation, 8 ordinary differential equations obtained by differentiating ordinary differential equation 2.3.18 with respect to $\eta_1$ are required. The series expansion is then used to obtain the expansions for the individual terms of the Navier-Stokes equations, 1.2.3-5, and Cooke's equations, 1.2.6-7.

The 8 ordinary differential equations obtained by differentiating equation 2.3.18 with respect to $\eta_1$ are given by :

$$(\eta_1+\eta_0)^3G^{IV}+5(\eta_1+\eta_0)^2G^{III}+3(\eta_1+\eta_0)G^{II}-2GG-2\eta_0GG^I+2\eta_1(\eta_1+\eta_0)G^IG^I$$
$$+(8\eta_1+4\eta_0)(\eta_1+\eta_0)GG^{II}+(2\eta_1+\eta_0)(\eta_1+\eta_0)^2\{GG^{III}+G^IG^{II}\},$$
$$(C.1)$$

$$(\eta_1+\eta_0)^3G^{V}+8(\eta_1+\eta_0)^2G^{IV}+13(\eta_1+\eta_0)G^{III}+3G^{II}-4GG^I+4\eta_1G^IG^I$$
$$+(16\eta_1+10\eta_0)GG^{II}+2(9\eta_1+4\eta_0)(\eta_1+\eta_0)G^IG^{II}+(14\eta_1+8\eta_0)(\eta_1+\eta_0)GG^{III}$$
$$+(2\eta_1+\eta_0)(\eta_1+\eta_0)^2\{GG^{IV}+G^IG^{III}+G^{II}G^{II}\}=0,$$
$$(C.2)$$

$$(\eta_1+\eta_0)^3G^{VI}+11(\eta_1+\eta_0)^2G^{V}+29(\eta_1+\eta_0)G^{IV}+16G^{III}+12GG^{II}$$
$$+(60\eta_1+36\eta_0)G^IG^{II}+(44\eta_1+32\eta_0)GG^{III}+(24\eta_1^2+36\eta_0\eta_1+12\eta_0^2)G^{II}G^{II}$$
$$+(44\eta_1^2+68\eta_1\eta_0+24\eta_0^2)G^IG^{III}+(20\eta_1^2+32\eta_0\eta_1+12\eta_0^2)GG^{IV}+(2\eta_1^3$$
$$+5\eta_0\eta_1^2+4\eta_0^2\eta_1+\eta_0^3)\{4G^{II}G^{III}+3G^IG^{IV}+GG^{V}\}=0,$$
$$(C.3)$$

$$(\eta_1+\eta_0)^3G^{VII}+14(\eta_1+\eta_0)^2G^{VI}+51(\eta_1+\eta_0)G^{V}+45G^{IV}+72G^{I}G^{II}+56GG^{III}$$
$$+(108\eta_1+72\eta_0)G^{II}G^{II}+(192\eta_1+136\eta_0)G^{I}G^{III}+(84\eta_1+64\eta_0)GG^{IV}$$
$$+(116\eta_1^2+180\eta_0\eta_1+64\eta_0^2)G^{II}G^{III}+(82\eta_1^2+130\eta_0\eta_1+48\eta_0^2)G^{I}G^{IV}$$
$$+(26\eta_1^2+42\eta_0\eta_1+16\eta_0^2)GG^{V}+(2\eta_1^3+5\eta_0\eta_1^2+4\eta_0^2\eta_1+\eta_0^3)\{4G^{III}G^{III}$$
$$+7G^{II}G^{IV}+4G^{I}G^{V}+GG^{VI}\}=0,$$

(C.4)

$$(\eta_1+\eta_0)^3G^{VIII}+17(\eta_1+\eta_0)^2G^{VII}+79(\eta_1+\eta_0)G^{VI}+96G^{V}+180G^{II}G^{II}+320G^{I}G^{III}$$
$$+140GG^{IV}+(640\eta_1+460\eta_0)G^{II}G^{III}+(440\eta_1+330\eta_0)G^{I}G^{IV}+(136\eta_1+106\eta_0)GG^{V}$$
$$+(140\eta_1^2+220\eta_0\eta_1+80\eta_0^2)G^{III}G^{III}+(240\eta_1^2+380\eta_0\eta_1+140\eta_0^2)G^{II}G^{IV}$$
$$+(132\eta_1^2+212\eta_0\eta_1+80\eta_0^2)G^{I}G^{V}+(32\eta_1^2+52\eta_0\eta_1+20\eta_0^2)GG^{VI}$$
$$+(2\eta_1^3+5\eta_0\eta_1^2+4\eta_0^2\eta_1+\eta_0^3)\{15G^{III}G^{IV}+11G^{II}G^{V}+5G^{I}G^{VI}+GG^{VII}\}=0,$$

(C.5)

$$(\eta_1+\eta_0)^3G^{IX}+20(\eta_1+\eta_0)^2G^{VIII}+113(\eta_1+\eta_0)G^{VII}+175G^{VI}+1320G^{II}G^{III}$$
$$+900G^{I}G^{IV}+276GG^{V}+(920\eta_1+680\eta_0)G^{III}G^{III}+(1560\eta_1+1170\eta_0)G^{II}G^{IV}$$
$$+(840\eta_1+648\eta_0)G^{I}G^{V}+(200\eta_1+158\eta_0)GG^{VI}+(610\eta_1^2+970\eta_0\eta_1+360\eta_0^2)G^{III}G^{IV}$$
$$+(438\eta_1^2+702\eta_0\eta_1+264\eta_0^2)G^{II}G^{V}+(194\eta_1^2+314\eta_0\eta_1+120\eta_0^2)G^{I}G^{VI}+(38\eta_1^2$$
$$+62\eta_0\eta_1+24\eta_0^2)GG^{VII}+(2\eta_1^3+5\eta_0\eta_1^2+4\eta_0^2\eta_1+\eta_0^3)\{15G^{IV}G^{IV}+26G^{III}G^{V}$$
$$+16G^{II}G^{VI}+6G^{I}G^{VII}+GG^{VIII}\}=0,$$

(C.6)

$$(\eta_1+\eta_0)^3G^{X}+23(\eta_1+\eta_0)^2G^{IX}+153(\eta_1+\eta_0)G^{VIII}+288G^{VII}+2240G^{III}G^{III}$$
$$+3780G^{II}G^{IV}+2016G^{I}G^{V}+476GG^{VI}+(4620\eta_1+3500\eta_0)G^{III}G^{IV}+(3276\eta_1$$
$$+2520\eta_0)G^{II}G^{V}+(1428\eta_1+1120\eta_0)G^{I}G^{VI}+(276\eta_1+220\eta_0)GG^{VII}+(700\eta_1^2$$
$$+1120\eta_0\eta_1+420\eta_0^2)G^{IV}G^{IV}+(1204\eta_1^2+1932\eta_0\eta_1+728\eta_0^2)G^{III}G^{V}+(728\eta_1^2$$
$$+1176\eta_0\eta_1+448\eta_0^2)G^{II}G^{VI}+(268\eta_1^2+436\eta_0\eta_1+168\eta_0^2)G^{I}G^{VII}+(44\eta_1^2$$
$$+72\eta_0\eta_1+28\eta_0^2)GG^{VIII}+(2\eta_1^3+5\eta_0\eta_1^2+4\eta_0^2\eta_1+\eta_0^3)\{56G^{IV}G^{V}$$
$$+42G^{III}G^{VI}+22G^{II}G^{VII}+7G^{I}G^{VIII}+GG^{IX}\}=0,$$

(C.7)

$$(\eta_1+\eta_0)^3G^{XI}+26(\eta_1+\eta_0)^2G^{X}+199(\eta_1+\eta_0)G^{IX}+441G^{VIII}+12880G^{III}G^{IV}$$
$$+9072G^{II}G^{V}+3920G^{I}G^{VI}+752GG^{VII}+(6020\eta_1+4620\eta_0)G^{IV}G^{IV}+(10304\eta_1$$
$$+7952\eta_0)G^{III}G^{V}+(6160\eta_1+4816\eta_0)G^{II}G^{VI}+(2240\eta_1+1776\eta_0)G^{I}G^{VII}+(364\eta_1$$
$$+292\eta_0)GG^{VIII}+(2940\eta_1^2+4732\eta_0\eta_1+1792\eta_0^2)G^{IV}G^{V}+(2184\eta_1^2+3528\eta_0\eta_1$$
$$+1344\eta_0^2)G^{III}G^{VI}+(1128\eta_1^2+1832\eta_0\eta_1+704\eta_0^2)G^{II}G^{VII}+(354\eta_1^2+578\eta_0\eta_1$$
$$+224\eta_0^2)G^{I}G^{VIII}+(50\eta_1^2+82\eta_0\eta_1+32\eta_0^2)GG^{IX}+(2\eta_1^3+5\eta_0\eta_1^2+4\eta_0^2\eta_1$$
$$+\eta_0^3)\{56G^{V}G^{V}+98G^{IV}G^{VI}+64G^{III}G^{VII}+29G^{II}G^{VIII}+8G^{I}G^{IX}+GG^{X}\}=0, \qquad (C.8)$$

Evaluating the equation 2.3.18 at $\eta_1 = 0$ gives

$$G_0^{III}=-2\frac{G_0^{II}}{\eta_0}=-2\frac{\alpha_G}{\eta_0}, \qquad (C.9)$$

where

$$\alpha_G \equiv G_0^{II} \qquad (C.10)$$

Evaluating the next equations (C.1-8) in order and using previously obtained coefficients gives :

$$G_0^{IV}=7\frac{\alpha_G}{\eta_0^2}, \qquad (C.11)$$

$$G_0^{V}=-33\frac{\alpha_G}{\eta_0^3}-\alpha_G^2, \qquad (C.12)$$

$$G_0^{VI}=192\frac{\alpha_G}{\eta_0^4}+7\frac{\alpha_G^2}{\eta_0}, \qquad (C.13)$$

$$G_0^{VII}=-1320\frac{\alpha_G}{\eta_0^5}-56\frac{\alpha_G^2}{\eta_0^2}, \qquad (C.14)$$

$$G_0^{VIII}=10440\frac{\alpha_G}{\eta_0^6}+508\frac{\alpha_G^2}{\eta_0^3}+11\alpha_G^3, \qquad (C.15)$$

$$G_0^{IX} = -93240\frac{\alpha_G}{\eta_0^7} - 5098\frac{\alpha_G^2}{\eta_0^4} - 120\frac{\alpha_G^3}{\eta_0}, \qquad (C.16)$$

$$G_0^{X} = 927360\frac{\alpha_G}{\eta_0^8} + 55858\frac{\alpha_G^2}{\eta_0^5} + 1217\frac{\alpha_G^3}{\eta_0^2}, \qquad (C.17)$$

$$G_0^{XI} = -10160640\frac{\alpha_G}{\eta_0^9} - 663110\frac{\alpha_G^2}{\eta_0^6} - 12771\frac{\alpha_G^3}{\eta_0^3} - 375\alpha_G^4. \qquad (C.18)$$

Series expansions of individual terms from the boundary layer equations of Cooke, 1.2.6-7, and of individual terms from the Navier-Stokes equations, 1.2.3-5, have been obtained by applying the series expansion of G and its derivatives to the corresponding terms.

Series expansions of individual terms from momentum equation 1.2.6 are given by :

$$u\frac{\partial u}{\partial x} = \frac{1}{R}\{\eta_0^2\left[-2\alpha_G^2\frac{\eta_1^2}{2} + 25\alpha_G^3\frac{\eta_1^5}{5!} - 984\alpha_G^4\frac{\eta_1^8}{8!} + O(\eta_1^{11})\right]$$

$$+\eta_0\left[12\alpha_G^2\frac{\eta_1^3}{3} - 327\alpha_G^3\frac{\eta_1^6}{6!} + 19818\alpha_G^4\frac{\eta_1^9}{9!} + O(\eta_1^{12})\right]$$

$$-82\alpha_G^2\frac{\eta_1^4}{4!} + 4039\alpha_G^3\frac{\eta_1^7}{7!} + O(\eta_1^{10}) + \frac{1}{\eta_0}\left[645\alpha_G^2\frac{\eta_1^5}{5!} - 52378\alpha_G^3\frac{\eta_1^8}{8!} + O(\eta_1^{11})\right]$$

$$+\frac{1}{\eta_0^2}\left[-5537\alpha_G^2\frac{\eta_1^6}{6!} + O(\eta_1^9)\right] + \frac{1}{\eta_0^3}\left[56231\alpha_G^2\frac{\eta_1^7}{7!} + O(\eta_1^{10})\right] + \frac{1}{\eta_0^4}\left[-607204\alpha_G^2\frac{\eta_1^8}{8!} + O(\eta_1^{11})\right]$$

$$+\ldots\}, \qquad (C.19)$$

$$\nu\frac{\partial u}{\partial y}=\frac{1}{R}\{\eta_0^2\left[\alpha_G^2\frac{\eta_1^2}{2}-14\alpha_G^3\frac{\eta_1^5}{5!}+609\alpha_G^4\frac{\eta_1^8}{8!}+O(\eta_1^{11})\right]$$

$$+\eta_0\left[-7\alpha_G^2\frac{\eta_1^3}{3!}+229\alpha_G^3\frac{\eta_1^6}{6!}+O(\eta_1^9)\right]+49\alpha_G^2\frac{\eta_1^4}{4!}-3227\alpha_G^3\frac{\eta_1^7}{7!}+O(\eta_1^{10})$$

$$+\frac{1}{\eta_0}\left[-377\alpha_G^2\frac{\eta_1^5}{5!}+45500\alpha_G^3\frac{\eta_1^8}{8!}+O(\eta_1^{11})\right]+\frac{1}{\eta_0^2}\left[-3222\alpha_G^2\frac{\eta_1^6}{6!}+O(\eta_1^9)\right]$$

$$+\frac{1}{\eta_0^3}\left[-30474\alpha_G^2\frac{\eta_1^7}{7!}+O(\eta_1^{10})\right]+\frac{1}{\eta_0^4}\left[316872\alpha_G^2\frac{\eta_1^8}{8!}+O(\eta_1^{11})\right]+\ldots\}, \qquad (.20)$$

$$\frac{1}{R}\frac{\partial^2 u}{\partial y^2}=\frac{1}{R}\{\eta_0^2\left[-\alpha_G^2\frac{\eta_1^2}{2}+11\alpha_G^3\frac{\eta_1^5}{5!}-375\alpha_G^4\frac{\eta_1^8}{8!}+O(\eta_1^{11})\right]$$

$$+\eta_0\left[-\alpha_G+6\alpha_G^2\frac{\eta_1^3}{3!}-109\alpha_G^3\frac{\eta_1^6}{6!}+O(\eta_1^9)\right]+2\alpha_G\eta_1-43\alpha_G^2\frac{\eta_1^4}{4!}+998\alpha_G^3\frac{\eta_1^7}{7!}+O(\eta_1^{10})]$$

$$+\frac{1}{\eta_0}\left[-6\alpha_G\frac{\eta_1^2}{2}+361\alpha_G^2\frac{\eta_1^5}{5!}-9364\alpha_G^3\frac{\eta_1^8}{8!}+O(\eta_1^{11})\right]$$

$$+\frac{1}{\eta_0^2}\left[4!\alpha_G\frac{\eta_1^3}{3!}-3414\alpha_G^2\frac{\eta_1^6}{6!}+O(\eta_1^9)\right]+\frac{1}{\eta_0^3}\left[-5!\alpha_G\frac{\eta_1^4}{4!}+35604\alpha_G^2\frac{\eta_1^7}{7!}+O(\eta_1^{10})\right]$$

$$+\frac{1}{\eta_0^4}\left[6!\alpha_G\frac{\eta_1^5}{5!}-404712\alpha_G^2\frac{\eta_1^8}{8!}+O(\eta_1^{11})\right]+\ldots\}, \qquad (C.21)$$

$$\frac{1}{R(1+y)}\frac{\partial u}{\partial y}=\frac{1}{R}\{\eta_0\left[\alpha_G-\alpha_G^2\frac{\eta_1^3}{3!}+11\alpha_G^3\frac{\eta_1^6}{6!}+O(\eta_1^9)\right]$$

$$-2\alpha_G\eta_1+10\alpha_G^2\frac{\eta_1^4}{4!}-186\alpha_G^3\frac{\eta_1^7}{7!}+O(\eta_1^{10})$$

$$+\frac{1}{\eta_0}\left[3!\alpha_G\frac{\eta_1^2}{2}-93\alpha_G^2\frac{\eta_1^5}{5!}+2486\alpha_G^3\frac{\eta_1^8}{8!}+O(\eta_1^{11})\right]$$

$$+\frac{1}{\eta_0^2}\left[-4!\alpha_G\frac{\eta_1^3}{3!}+919\alpha_G^2\frac{\eta_1^6}{6!}+O(\eta_1^9)\right]+\frac{1}{\eta_0^3}\left[5!\alpha_G\frac{\eta_1^4}{4!}-9847\alpha_G^2\frac{\eta_1^7}{7!}+O(\eta_1^{10})\right]$$

$$+\frac{1}{\eta_0^4}\left[-6!\alpha_G\frac{\eta_1^5}{5!}+114380\alpha_G^2\frac{\eta_1^8}{8!}+O(\eta_1^{11})\right]+\ldots\}. \qquad (C.22)$$

Series expansion of neglected individual terms from the Navier-Stokes equations are given by :

$$\frac{1}{R}\frac{\partial^2 u}{\partial x^2}=\frac{1}{R^3}\{\eta_0^4\left[3\alpha_G\eta_1-4!\alpha_G^2\frac{\eta_1^4}{4!}+693\alpha_G^3\frac{\eta_1^7}{7!}-45000\alpha_G^4\frac{\eta_1^{10}}{10!}+O(\eta_1^{13})\right]$$

$$+\eta_0^3\left[-13\alpha_G\frac{\eta_1^2}{2}+221\alpha_G^2\frac{\eta_1^5}{5!}+-3147\alpha_G^3\frac{\eta_1^8}{8!}+O(\eta_1^{11})\right]$$

$$+\eta_0^2\left[80\alpha_G\frac{\eta_1^3}{3!}-2299\alpha_G^2\frac{\eta_1^6}{6!}+105636\alpha_G^3\frac{\eta_1^9}{9!}+O(\eta_1^{12})\right]+\ldots\}, \qquad (C.23)$$

$$u\frac{\partial v}{\partial x}=\frac{1}{R^2}\{\eta_0^3\left[-9\alpha_G^2\frac{\eta_1^3}{3!}+189\alpha_G^3\frac{\eta_1^6}{6!}-10449\alpha_G^4\frac{\eta_1^9}{9!}+O(\eta_1^{12})\right]$$

$$+\eta_0^2\left[82\alpha_G^2\frac{\eta_1^4}{4!}-3157\alpha_G^3\frac{\eta_1^7}{7!}+250758\alpha_G^4\frac{\eta_1^{10}}{10!}+O(\eta_1^{13})\right]$$

$$+\eta_0\left[-745\alpha_G^2\frac{\eta_1^5}{5!}+47390\alpha_G^3\frac{\eta_1^8}{8!}-4958547\alpha_G^4\frac{\eta_1^{11}}{11!}+O(\eta_1^{14})\right]+\ldots\}, \qquad (C.24)$$

$$v\frac{\partial v}{\partial y}=\frac{1}{R^2}\{\eta_0^3\left[3\alpha_G^2\frac{\eta_1^3}{3!}-84\alpha_G^3\frac{\eta_1^6}{6!}+5481\alpha_G^4\frac{\eta_1^9}{9!}+O(\eta_1^{11})\right]$$

$$+\eta_0^2\left[-40\alpha_G^2\frac{\eta_1^4}{4!}+1876\alpha_G^3\frac{\eta_1^7}{7!}-168300\alpha_G^4\frac{\eta_1^{10}}{10!}+O(\eta_1^{13})\right]$$

$$+\eta_0\left[475\alpha_G^2\frac{\eta_1^5}{5!}-34440\alpha_G^3\frac{\eta_1^8}{8!}+3998511\alpha_G^4\frac{\eta_1^{11}}{11!}+O(\eta_1^{14})\right]+\ldots\},\qquad (C.25)$$

$$\frac{1}{R(1+y)}\frac{\partial v}{\partial y}=\frac{1}{R^2}\{\eta_0^2\left[\alpha_G\eta_1-4\alpha_G^2\frac{\eta_1^4}{4!}+77\alpha_G^3\frac{\eta_1^7}{7!}-3750\alpha_G^4\frac{\eta_1^{10}}{10!}+O(\eta_1^{13})\right]$$

$$+\eta_0\left[-6\alpha_G\frac{\eta_1^2}{2}+55\alpha_G^2\frac{\eta_1^5}{5!}-1576\alpha_G^3\frac{\eta_1^8}{8!}+O(\eta_1^{11})\right]$$

$$+39\alpha_G\frac{\eta_1^3}{3!}-666\alpha_G^2\frac{\eta_1^6}{6!}+25137\alpha_G^3\frac{\eta_1^9}{9!}+O(\eta_1^{12})]+\ldots\},\qquad (C.26)$$

$$\frac{1}{R}\frac{\partial^2 v}{\partial y^2}=\frac{1}{R^2}\{\eta_0^3\left[\alpha_G-4\alpha_G^2\frac{\eta_1^3}{3!}+77\alpha_G^3\frac{\eta_1^6}{6!}-3750\alpha_G^4\frac{\eta_1^9}{9!}+O(\eta_1^{12})\right]$$

$$+\eta_0^2\left[-4\alpha_G\eta_1+35\alpha_G^2\frac{\eta_1^4}{4!}-960\alpha_G^3\frac{\eta_1^7}{7!}+O(\eta_1^{10})\right]$$

$$+\eta_0\left[21\alpha_G\frac{\eta_1^2}{2}-336\alpha_G^2\frac{\eta_1^5}{5!}+10953\alpha_G^3\frac{\eta_1^8}{8!}+O(\eta_1^{11})\right]+\ldots\},\qquad (C.27)$$

$$\frac{1}{R}\frac{\partial^2 v}{\partial x^2}=\frac{1}{R^4}\{\eta_0^5\left[15\alpha_G\frac{\eta_1^2}{2}-192\alpha_G^2\frac{\eta_1^5}{5}+7623\alpha_G^3\frac{\eta_1^8}{8!}-630000\alpha_G^4\frac{\eta_1^{11}}{11!}+O(\eta_1^{14})\right]$$

$$+\eta_0^4\left[-96\alpha_G\frac{\eta_1^3}{3!}+2205\alpha_G^2\frac{\eta_1^6}{6!}-115200\alpha_G^3\frac{\eta_1^9}{9!}+O(\eta_1^{12})\right]$$

$$+\eta_0^3\left[735\alpha_G\frac{\eta_1^4}{4!}-26880\alpha_G^2\frac{\eta_1^7}{7!}+1566279\alpha_G^3\frac{\eta_1^{10}}{10!}+O(\eta_1^{13})\right]+\ldots\},\qquad (C.28)$$

$$\frac{v}{R(1+y)^2}=\frac{1}{R^2}\{\eta_0\left[\alpha_G\frac{\eta_1^2}{2}-4\alpha_G^2\frac{\eta_1^5}{5!}+77\alpha_G^3\frac{\eta_1^8}{8!}+O(\eta_1{}^{11})\right]-10\alpha_G\frac{\eta_1^3}{3!}+83\alpha_G^2\frac{\eta_1^6}{6!}-2346\alpha_G^3\frac{\eta_1^9}{9!}$$

$$+O(\eta_1{}^{12})+\frac{1}{\eta_0}\left[89\alpha_G\frac{\eta_1^4}{4!}-1330\alpha_G^2\frac{\eta_1^7}{7!}+50943\alpha_G^3\frac{\eta_1^{10}}{10!}+O(\eta_1{}^{13})+\ldots\right]\}. \qquad (C.29)$$

Series expansions of individual terms from continuity equation 1.2.7 are given by :

$$\frac{\partial u}{\partial x}=\frac{1}{R}\{\eta_0{}^2\left[-\alpha_G\eta_1+4\alpha_G^2\frac{\eta_1^4}{4!}-77\alpha_G^3\frac{\eta_1^7}{7!}+3750\alpha_G^4\frac{\eta_1^{10}}{10!}+O(\eta_1{}^{13})\right]$$

$$+\eta_0\left[3\alpha_G\frac{\eta_1^2}{2}-31\alpha_G^2\frac{\eta_1^5}{5!}+883\alpha_G^3\frac{\eta_1^8}{8!}+O(\eta_1{}^{11})\right]-14\alpha_G\frac{\eta_1^3}{3!}+277\alpha_G^2\frac{\eta_1^6}{6!}-9300\alpha_G^3\frac{\eta_1^9}{9!}+O(\eta_1{}^{12})]$$

$$+\frac{1}{\eta_0}\left[83\alpha_G\frac{\eta_1^4}{4!}-2807\alpha_G^2\frac{\eta_1^7}{7!}+100227\alpha_G^3\frac{\eta_1^{10}}{10!}+O(\eta_1{}^{13})\right]+\frac{1}{\eta_0^2}\left[-583\alpha_G\frac{\eta_1^5}{5!}+31236\alpha_G^2\frac{\eta_1^8}{8!}+O(\eta_1{}^{11})\right]$$

$$+\frac{1}{\eta_0^3}\left[4698\alpha_G\frac{\eta_1^6}{6!}-376006\alpha_G^2\frac{\eta_1^9}{9!}+O(\eta_1{}^{12})\right]+\frac{1}{\eta_0^4}\left[-42606\alpha_G\frac{\eta_1^7}{7!}+4861218\alpha_G^2\frac{\eta_1^{10}}{10!}+O(\eta_1{}^{13})\right]$$

$$+\frac{1}{\eta_0^5}\left[429048\alpha_G\frac{\eta_1^8}{8!}+O(\eta_1{}^{11})\right]+\frac{1}{\eta_0^6}\left[-4748472\alpha_G\frac{\eta_1^9}{9!}+O(\eta_1{}^{12})\right]+\frac{1}{\eta_0^7}\left[57282480\alpha_G\frac{\eta_1^{10}}{10!}+O(\eta_1{}^{13})\right]$$

$$+\ldots\}, \qquad (C.30)$$

$$\frac{\partial v}{\partial y}=\frac{1}{R}\{\eta_0^2\left[\alpha_G\eta_1-4\alpha_G^2\frac{\eta_1^4}{4!}+77\alpha_G^3\frac{\eta_1^7}{7!}-3750\alpha_G^4\frac{\eta_1^{10}}{10!}+O(\eta_1^{13})\right]$$

$$+\eta_0\left[-4\alpha_G\frac{\eta_1^2}{2}+35\alpha_G^2\frac{\eta_1^5}{5!}-960\alpha_G^3\frac{\eta_1^8}{8!}+O(\eta_1^{11})\right]+21\alpha_G\frac{\eta_1^3}{3!}-336\alpha_G^2\frac{\eta_1^6}{6!}+10953\alpha_G^3\frac{\eta_1^9}{9!}+O(\eta_1^{12})$$

$$+\frac{1}{\eta_0}\left[-132\alpha_G\frac{\eta_1^4}{4!}+3556\alpha_G^2\frac{\eta_1^7}{7!}-127710\alpha_G^3\frac{\eta_1^{10}}{10!}+O(\eta_1^{13})\right]$$

$$+\frac{1}{\eta_0^2}\left[960\alpha_G\frac{\eta_1^5}{5!}-40784\alpha_G^2\frac{\eta_1^8}{8!}+O(\eta_1^{11})\right]+\frac{1}{\eta_0^3}\left[-7920\alpha_G\frac{\eta_1^6}{6!}+502722\alpha_G^2\frac{\eta_1^9}{9!}+O(\eta_1^{12})\right]$$

$$+\frac{1}{\eta_0^4}\left[73080\alpha_G\frac{\eta_1^7}{7!}-6631100\alpha_G^2\frac{\eta_1^{10}}{10!}+O(\eta_1^{13})\right]+\frac{1}{\eta_0^5}\left[-745920\alpha_G\frac{\eta_1^8}{8!}+O(\eta_1^{11})\right]$$

$$+\frac{1}{\eta_0^6}\left[8346240\alpha_G\frac{\eta_1^9}{9!}+O(\eta_1^{12})\right]+\frac{1}{\eta_0^7}\left[-101606400\alpha_G\frac{\eta_1^{10}}{10!}+O(\eta_1^{13})\right]+\ldots\},\qquad(C.31)$$

$$\frac{v}{(1+y)}=\frac{1}{R}\{\eta_0\left[\alpha_G\frac{\eta_1^2}{2}-4\alpha_G^2\frac{\eta_1^5}{5!}+77\alpha_G^3\frac{\eta_1^8}{8!}+O(\eta_1^{11})\right]$$

$$-7\alpha_G\frac{\eta_1^3}{3!}+59\alpha_G^2\frac{\eta_1^6}{6!}-1653\alpha_G^3\frac{\eta_1^9}{9!}+O(\eta_1^{12})+\frac{1}{\eta_0}\left[49\alpha_G\frac{\eta_1^4}{4!}-749\alpha_G^2\frac{\eta_1^7}{7!}+27483\alpha_G^3\frac{\eta_1^{10}}{10!}+O(\eta_1^{13})\right]$$

$$+\frac{1}{\eta_0^2}\left[-377\alpha_G\frac{\eta_1^5}{5!}+9548\alpha_G^2\frac{\eta_1^8}{8!}+O(\eta_1^{11})\right]+\frac{1}{\eta_0^3}\left[3222\alpha_G\frac{\eta_1^6}{6!}-126716\alpha_G^2\frac{\eta_1^9}{9!}+O(\eta_1^{12})\right]$$

$$+\frac{1}{\eta_0^4}\left[-30474\alpha_G\frac{\eta_1^7}{7!}+1769882\alpha_G^2\frac{\eta_1^{10}}{10!}+O(\eta_1^{13})\right]+\frac{1}{\eta_0^5}\left[316872\alpha_G\frac{\eta_1^8}{8!}+O(\eta_1^{11})\right]$$

$$+\frac{1}{\eta_0^6}\left[-3597768\alpha_G\frac{\eta_1^9}{9!}+O(\eta_1^{12})\right]+\frac{1}{\eta_0^7}\left[44323920\alpha_G\frac{\eta_1^{10}}{10!}+O(\eta_1^{13})\right]+\ldots\}.\qquad(C.32)$$

# APPENDIX D: SERIES EXPANSION OF H AND OF $f_B$

The series expansions of H are obtained by differentiating equation 2.6.18 with respect to s in order to obtain 8 ordinary differential equations, which when evaluated at $s_0$ yield the coefficients for the expansions. Then series expansions of individual terms from the governing equations 1.2.6-7 and those neglected from the Navier-Stokes equations 1.2.3-5 are then obtained.

The resulting series expansions for the individual terms of the two dimensional boundary layer equations are also ob ned in this appendix. Those of individual terms neglected from the two dimensional Navier-Stokes equations are also presented.

The 8 ordinary differential equations obtained by differentiating equation 2.6.18 with respect to $s$ are given by :

$$s^3H^{IV} + 5s^2H^{III} + 3sH^{II} - HH + s^2H^IH^I + 4s^2HH^{II} + s^3H^IH^{II} + s^3HH^{III}, \qquad (D.1)$$

$$s^3H^V + 8s^2H^{IV} + 13sH^{III} + 3H^{II} - 2HH^I + 2sH^IH^I + 9s^2H^IH^{II} + 8sHH^{II}$$

$$+7s^2HH^{III} + s^3\{H^{II}H^{II} + 2H^IH^{III} + HH^{IV}\} = 0, \qquad (D.2)$$

$$s^3H^{VI} + 11s^2H^V + 29sH^{IV} + 16H^{III} + 6HH^{II} + s\{30H^IH^{II} + 22HH^{III}\}$$

$$+s^2\{12H^{II}H^{II} + 22H^IH^{III} + 10HH^{IV}\} + s^3\{4H^{II}H^{III} + 3H^IH^{IV} + HH^V\} = 0, \qquad (D.3)$$

$$s^3H^{VII}+14s^2H^{VI}+51sH^{V}+45H^{IV}+36H^{I}H^{II}+28HH^{III}+s\{54H^{II}H^{II}$$
$$+96H^{I}H^{III}+42HH^{IV}\}+s^2\{58H^{II}H^{III}+41H^{I}H^{IV}+13HH^{V}\}+s^3\{4H^{III}H^{III}$$
$$+7H^{II}H^{IV}+4H^{I}H^{V}+HH^{VI}\}=0, \qquad (D.4)$$

$$s^3H^{VIII}+17s^2H^{VII}+79sH^{VI}+96H^{V}+90H^{II}H^{II}+160H^{I}H^{III}+70HH^{IV}$$
$$+s\{320H^{II}H^{III}+220H^{I}H^{IV}+68HH^{V}\}+s^2\{70H^{III}H^{III}+120H^{II}H^{IV}$$
$$+66H^{I}H^{V}+16HH^{VI}\}+s^3\{15H^{III}H^{IV}+11H^{II}H^{V}+5H^{I}H^{VI}+HH^{VII}\}=0, \qquad (D.5)$$

$$s^3H^{IX}+20s^2H^{VIII}+113sH^{VII}+175H^{VI}+660H^{II}H^{III}+450H^{I}H^{IV}+138HH^{V}$$
$$+s\{460H^{III}H^{III}+780H^{II}H^{IV}+420H^{I}H^{V}+100HH^{VI}\}+s^2\{305H^{III}H^{IV}+219H^{II}H^{V}$$
$$+97H^{I}H^{VI}+19HH^{VII}\}+s^3\{15H^{IV}H^{IV}+26H^{III}H^{V}+16H^{II}H^{VI}+6H^{I}H^{VII}$$
$$+HH^{VIII}\}=0, \qquad (D.6)$$

$$s^3H^{X}+23s^2H^{IX}+153sH^{VIII}+288H^{VII}+1120H^{III}H^{III}+1890H^{II}H^{IV}+1008H^{I}H^{V}$$
$$+238HH^{VI}+s\{2310H^{III}H^{IV}+1638H^{II}H^{V}+714H^{I}H^{VI}+138HH^{VII}\}$$
$$+s^2\{350H^{IV}H^{IV}+602H^{III}H^{V}+364H^{II}H^{VI}+134H^{I}H^{VII}+22HH^{VIII}\}+s^3\{56H^{IV}H^{V}$$
$$+42H^{III}H^{VI}+22H^{II}H^{VII}+7H^{I}H^{VIII}+HH^{IX}\}=0, \qquad (D.7)$$

$$s^3H^{XI}+26s^2H^{X}+199sH^{IX}+441H^{VIII}+6440H^{III}H^{IV}+4536H^{II}H^{V}+1960H^{I}H^{VI}$$

$$+376HH^{VII}+s\{3010H^{IV}H^{IV}+5152H^{III}H^{V}+3080H^{II}H^{VI}+1120H^{I}H^{VII}+182HH^{VIII}\}$$

$$+s^2\{1470H^{IV}H^{V}+1092H^{III}H^{VI}+564H^{II}H^{VII}+177H^{I}H^{VIII}+25HH^{IX}\}+s^3\{56H^{V}H^{V}$$

$$+98H^{IV}H^{VI}+64H^{III}H^{VII}+29H^{II}H^{VIII}+8H^{I}H^{IX}+HH^{X}\}=0, \qquad (D.8)$$

Evaluating equation 2.6.18 at $s=s_0$ gives

$$H_0^{III}=-2\frac{H_0^{II}}{s_0}=-2\frac{\alpha_H}{s_0}, \qquad (D.9)$$

where

$$\alpha_H \equiv H_0^{II} \qquad (D.10)$$

Evaluating the next equations (D.1-8) in order and using previously obtained coefficients gives the following coefficients for the series expansion of H :

$$H_0^{IV}=7\frac{\alpha_H}{s_0^2}, \qquad (D.11)$$

$$H_0^{V}=-33\frac{\alpha_H}{s_0^3}-\alpha_H^2, \qquad (D.12)$$

$$H_0^{VI}=192\frac{\alpha_H}{s_0^4}+7\frac{\alpha_H^2}{s_0}, \qquad (D.13)$$

$$H_0^{VII}=-1320\frac{\alpha_H}{s_0^5}-50\frac{\alpha_H^2}{s_0^2}, \qquad (D.14)$$

$$H_0^{VIII}=10440\frac{\alpha_H}{s_0^6}+396\frac{\alpha_H^2}{s_0^3}+11\alpha_H^3, \qquad (D.15)$$

$$H_0^{IX} = -93240\frac{\alpha_H}{s_0^{7}} - 3501\frac{\alpha_H^2}{s_0^{4}} - 165\frac{\alpha_H^3}{s_0}, \tag{D.16}$$

$$H_0^{X} = 927360\frac{\alpha_H}{s_0^{8}} + 34353\frac{\alpha_H^2}{s_0^{5}} + 2078\frac{\alpha_H^3}{s_0^{2}}, \tag{D.17}$$

$$H_0^{XI} = -10160640\frac{\alpha_H}{s_0^{9}} - 371187\frac{\alpha_H^2}{s_0^{6}} - 25976\frac{\alpha_H^3}{s_0^{3}} - 375\alpha_H^4. \tag{D.18}$$

The velocity components obtained from the series expansion for H are given by :

$$u = \alpha_H s_1 - \frac{\alpha_H}{2s_0}s_1^{2} + 2\frac{\alpha_H}{s_0^{2}}\frac{s_1^{3}}{3!} - \left(3!\frac{\alpha_H}{s_0^{3}} + \alpha_H^{2}\right)\frac{s_1^{4}}{4!} + \left(4!\frac{\alpha_H}{s_0^{4}} + 6\frac{\alpha_H^2}{s_0}\right)\frac{s_1^{5}}{5!}$$

$$-\left(5!\frac{\alpha_H}{s_0^{5}} + 37\frac{\alpha_H^2}{s_0^{2}}\right)\frac{s_1^{6}}{6!} + \left(6!\frac{\alpha_H}{s_0^{6}} + 255\frac{\alpha_H^2}{s_0^{3}} + 11\alpha_H^{3}\right)\frac{s_1^{7}}{7!} - (7!\frac{\alpha_H}{s_1^{7}} + 1977\frac{\alpha_H^2}{s_0^{4}}$$

$$+154\frac{\alpha_H^3}{s_0})\frac{s_1^{8}}{8!} + \left(8!\frac{\alpha_H}{s_0^{8}} + 17136\frac{\alpha_H^2}{s_0^{5}} + 1814\frac{\alpha_H^3}{s_0^{2}}\right)\frac{s_1^{9}}{9!} - (9!\frac{\alpha_H}{s_0^{9}} + 164664\frac{\alpha_H^2}{s_0^{6}}$$

$$+21258\frac{\alpha_H^3}{s_0^{3}} + 375\alpha_H^{4})\frac{s_1^{10}}{10!} + O(s_1^{11}), \tag{D.19}$$

$$v=\frac{1}{2R}\{s_0{}^2\alpha_H s_1-s_0\frac{\alpha_H}{2}s_1{}^2+3\alpha_H\frac{s_1{}^3}{3!}-\left(12\frac{\alpha_H}{s_0}+s_0{}^2\alpha_H^2\right)\frac{s_1{}^4}{4!}+\left(60\frac{\alpha_H}{s_0{}^2}+3s_0\alpha_H^2\right)\frac{s_1{}^5}{5!}$$

$$-\left(360\frac{\alpha_H}{s_0{}^3}+15\alpha_H^2\right)\frac{s_1{}^6}{6!}+\left(2520\frac{\alpha_H}{s_0{}^4}+96\frac{\alpha_H^2}{s_0}+11s_0{}^2\alpha_H^3\right)\frac{s_1{}^7}{7!}-(20160\frac{\alpha_H}{s_0{}^5}+729\frac{\alpha_H^2}{s_0{}^2}$$

$$+88s_0\alpha_H^3)\frac{s_1{}^8}{8!}+\left(181440\frac{\alpha_H}{s_0{}^6}+6345\frac{\alpha_H^2}{s_0{}^3}+758\alpha_H^3\right)\frac{s_1{}^9}{9!}-(1814400\frac{\alpha_H}{s_0{}^7}+62010\frac{\alpha_H^2}{s_0{}^4}$$

$$+7274\frac{\alpha_H^3}{s_0}+375s_0{}^2\alpha_H^4)\frac{s_1{}^{10}}{10!}+O(s_1{}^{11})\}. \qquad (D.20)$$

The series expansions of the individual terms of momentum equation 1.2.6 are given by :

$$u\frac{\partial u}{\partial x}=\frac{1}{2R}\{s_0{}^3\left[-\alpha_H^2 s_1+5\alpha_H^3\frac{s_1^4}{4!}-123\alpha_H^4\frac{s_1^7}{7!}+O(s_1{}^{10})\right]$$

$$+s_0{}^2\left[\alpha_H^2\frac{s_1^2}{2}-26\alpha_H^3\frac{s_1^5}{5!}+1554\alpha_H^4\frac{s_1^8}{8!}+O(s_1{}^{11})\right]$$

$$+s_0\left[-2\alpha_H^2\frac{s_1^3}{3!}+149\alpha_H^3\frac{s_1^6}{6!}+O(s_1{}^9)\right]+3!\alpha_H^2\frac{s_1^4}{4!}-983\alpha_H^3\frac{s_1^7}{7!}+O(s_1{}^{10})$$

$$+\frac{1}{s_0}\left[-4!\alpha_H^2\frac{s_1^5}{5!}+7405\alpha_H^3\frac{s_1^8}{8!}+O(s_1{}^{11})\right]+\frac{1}{s_0^2}\left[5!\alpha_H^2\frac{s_1^6}{6!}+O(s_1{}^9)\right]$$

$$+\frac{1}{s_0^3}\left[-6!\alpha_H^2\frac{s_1^7}{7!}+O(s_1{}^{10})\right]+\frac{1}{s_0^4}\left[7!\alpha_H^2\frac{s_1^8}{8!}+O(s_1{}^{11})\right]+\ldots), \qquad (D.21)$$

$$\nu\frac{\partial u}{\partial r}=\frac{1}{2R}\{s_0^3\left[\alpha_H^2 s_1-5\alpha_H^3\frac{s_1^4}{4!}+123\alpha_H^4\frac{s_1^7}{7!}+O(s_1^{10})\right]$$

$$+s_0^2\left[-3\alpha_H^2\frac{s_1^2}{2}+48\alpha_H^3\frac{s_1^5}{5!}-2304\alpha_H^4\frac{s_1^8}{8!}+O(s_1^{11})\right]$$

$$+s_0\left[12\alpha_H^2\frac{s_1^3}{3!}-435\alpha_H^3\frac{s_1^6}{6!}+O(s_1^9)\right]-60\alpha_H^2\frac{s_1^4}{4!}+4149\alpha_H^3\frac{s_1^7}{7!}+O(s_1^{10})$$

$$+\frac{1}{s_0}\left[360\alpha_H^2\frac{s_1^5}{5!}-42597\alpha_H^3\frac{s_1^8}{8!}+O(s_1^{11})\right]+\frac{1}{s_0^2}\left[-2520\alpha_H^2\frac{s_1^6}{6!}+O(s_1^9)\right]$$

$$+\frac{1}{s_0^3}\left[20160\alpha_H^2\frac{s_1^7}{7!}+O(s_1^{10})\right]+\frac{1}{s_0^4}\left[-181440\alpha_H^2\frac{s_1^8}{8!}+O(s_1^{11})\right]+\ldots), \qquad (D.22)$$

$$\frac{1}{R}\frac{\partial^2 u}{\partial r^2}=\frac{1}{2R}\{s_0^2\left[-\alpha_H^2 s_1^2+22\alpha_H^3\frac{s_1^5}{5!}-750\alpha_H^4\frac{s_1^8}{8!}+O(s_1^{11})\right]$$

$$+s_0\left[-2\alpha_H+12\alpha_H^2\frac{s_1^3}{3!}-308\alpha_H^3\frac{s_1^6}{6!}+O(s_1^9)\right]+4\alpha_H s_1-74\alpha_H^2\frac{s_1^4}{4!}+3628\alpha_H^3\frac{s_1^7}{7!}+O(s_1^{10})]$$

$$+\frac{1}{s_0}\left[-3!\alpha_H s_1^2+510\alpha_H^2\frac{s_1^5}{5!}-42516\alpha_H^3\frac{s_1^8}{8!}+O(s_1^{11})\right]$$

$$+\frac{1}{s_0^2}\left[24!\alpha_H\frac{s_1^3}{3!}-3954\alpha_H^2\frac{s_1^6}{6!}+O(s_1^9)\right]+\frac{1}{s_0^3}\left[-25!\alpha_H\frac{s_1^4}{4!}+34272\alpha_H^2\frac{s_1^7}{7!}+O(s_1^{10})\right]$$

$$+\frac{1}{s_0^4}\left[6!\alpha_H\frac{s_1^5}{5!}-329328\alpha_H^2\frac{s_1^8}{8!}+O(s_1^{11})\right]+\ldots), \qquad (D.23)$$

$$\frac{1}{Rr}\frac{\partial u}{\partial r}=\frac{1}{R}\{s_0\left[\alpha_H-\alpha_H^2\frac{s_1^3}{3!}+11\alpha_H^3\frac{s_1^6}{6!}+O(s_1{}^9)\right]-2\alpha_H s_1+10\alpha_H^2\frac{s_1^4}{4!}-231\alpha_H^3\frac{s_1^7}{7!}+O(s_1{}^{10})$$

$$+\frac{1}{s_0}\left[3!\alpha_H\frac{s_1^2}{2}-87\alpha_H^2\frac{s_1^5}{5!}+3662\alpha_H^3\frac{s_1^8}{8!}+O(s_1{}^{11})\right]$$

$$+\frac{1}{s_0^2}\left[-4!\alpha_H\frac{s_1^3}{3!}+777\alpha_H^2\frac{s_1^6}{6!}+O(s_1{}^9)\right]+\frac{1}{s_0^3}\left[5!\alpha_H\frac{s_1^4}{4!}-7416\alpha_H^2\frac{s_1^7}{7!}+O(s_1{}^{10})\right]$$

$$+\frac{1}{s_0^4}\left[-6!\alpha_H\frac{s_1^5}{5!}+76464\alpha_H^2\frac{s_1^8}{8!}+O(s_1{}^{11})\right]+\ldots). \qquad (D.24)$$

The series expansions of individual terms from continuity equation 1.2.7 are given by :

$$\frac{\partial u}{\partial x}=\frac{1}{2R}\{s_0{}^3\left[-\alpha_H+\alpha_H^2\frac{s_1^3}{3!}-11\alpha_H^3\frac{s_1^6}{6!}+375\alpha_H^4\frac{s_1^9}{9!}+O(s_1{}^{12})\right]$$

$$+s_0{}^2\left[-2\alpha_H^2\frac{s_1^4}{4!}+77\alpha_H^3\frac{s_1^7}{7!}+O(s_1{}^{10})\right]+s_0\left[7\alpha_H^2\frac{s_1^5}{5!}-582\alpha_H^3\frac{s_1^8}{8!}+O(s_1{}^{11})\right]$$

$$-33\alpha_H^2\frac{s_1^6}{6!}+4932\alpha_H^3\frac{s_1^9}{9!}+O(s_1{}^{12})+\frac{1}{s_0}\left[192\alpha_H^2\frac{s_1^7}{7!}+O(s_1{}^{10})\right]$$

$$+\frac{1}{s_0^2}\left[-1320\alpha_H^2\frac{s_1^8}{8!}+O(s_1{}^{11})\right]+\frac{1}{s_0^3}\left[10440\alpha_H^2\frac{s_1^9}{9!}+O(s_1{}^{121})\right]+\ldots), \qquad (D.25)$$

$$\frac{\partial v}{\partial r}=\frac{1}{2R}\{s_0^3\left[\alpha_H-\alpha_H^2\frac{s_1^3}{3!}+11\alpha_H^3\frac{s_1^6}{6!}-375\alpha_H^4\frac{s_1^9}{9!}+O(s_1^{12})\right]$$

$$+s_0^2\left[-\alpha_H s_1+3\alpha_H^2\frac{s_1^4}{4!}-88\alpha_H^3\frac{s_1^7}{7!}+O(s_1^{10})\right]$$

$$+s_0\left[3\alpha_H\frac{s_1^2}{2}-15\alpha_H^2\frac{s_1^5}{5!}+758\alpha_H^3\frac{s_1^8}{8!}+O(s_1^{11})\right]-12\alpha_H\frac{s_1^3}{3!}+96\alpha_H^2\frac{s_1^6}{6!}-7274\alpha_H^3\frac{s_1^9}{9!}+O(s_1^{12})]$$

$$+\frac{1}{s_0}\left[60\alpha_H\frac{s_1^4}{4!}-729\alpha_H^2\frac{s_1^7}{7!}+O(s_1^{10})\right]+\frac{1}{s_0^2}\left[-360\alpha_H\frac{s_1^5}{5!}+6345\alpha_H^2\frac{s_1^8}{8!}+O(s_1^{11})\right]$$

$$+\frac{1}{s_0^3}\left[2520\alpha_H\frac{s_1^6}{6!}-62010\alpha_H^2\frac{s_1^9}{9!}+O(s_1^{12})\right]+\ldots), \qquad (D.26)$$

$$\frac{v}{r}=\frac{1}{2R}\{s_0^2\left[\alpha_H s_1-\alpha_H^2\frac{s_1^4}{4!}+11\alpha_H^3\frac{s_1^7}{7!}+O(s_1^{10})\right]$$

$$+s_0\left[-3\alpha_H\frac{s_1^2}{2}+8\alpha_H^2\frac{s_1^5}{5!}-176\alpha_H^3\frac{s_1^8}{8!}+O(s_1^{11})\right]+12\alpha_H\frac{s_1^3}{3!}-63\alpha_H^2\frac{s_1^6}{6!}$$

$$+2342\alpha_H^3\frac{s_1^9}{9!}+O(s_1^{12})+\frac{1}{s_0}\left[-60\alpha_H\frac{s_1^4}{4!}+537\alpha_H^2\frac{s_1^7}{7!}+O(s_1^{10})\right]$$

$$+\frac{1}{s_0^2}\left[360\alpha_H\frac{s_1^5}{5!}-5025\alpha_H^2\frac{s_1^8}{8!}+O(s_1^{11})\right]+\frac{1}{s_0^3}\left[-2520\alpha_H\frac{s_1^6}{6!}+51570\alpha_H^2\frac{s_1^9}{9!}+O(s_1^{12})\right]+\ldots)(D.27)$$

The series expansion of individual terms for the two dimensional boundary layer equations and the two dimensional Navier-Stokes equations follow.

The series expansions of individual terms from the two dimensional momentum equation are given by :

$$u_B\frac{\partial u_B}{\partial x_B}=\frac{\eta_L^2}{R_L}\left[-2\alpha_B^2\frac{\eta_B^2}{2}25\alpha_B^3\frac{\eta_B^5}{5!}-984\alpha_B^4\frac{\eta_B^8}{8!}+85305\alpha_B^5\frac{\eta_B^{11}}{11!}+O(\eta_B^{14})\right]+\ldots\}, \qquad (D.28)$$

$$v_B \frac{\partial u_B}{\partial y_B} = \frac{\eta_L^2}{R_L}\left[\alpha_B^2 \frac{\eta_B^2}{2} - 14\alpha_B^3 \frac{\eta_B^5}{5!} + 609\alpha_B^4 \frac{\eta_B^8}{8!} - 57408\alpha_B^5 \frac{\eta_B^{11}}{11!} + O(\eta_B^{14})\right], \qquad (D.29)$$

$$\frac{1}{R_L}\frac{\partial^2 u_B}{\partial y_B^2} = \frac{\eta_L^2}{R_L}\left[-\alpha_B^2 \frac{\eta_B^2}{2} + 11\alpha_B^3 \frac{\eta_B^5}{5!} - 375\alpha_B^4 \frac{\eta_B^8}{8!} + O(\eta_B^{11})\right], \qquad (D.30)$$

The series expansions of individual terms from the two dimensional continuity equation are given by :

$$\frac{\partial u_B}{\partial x_B} = \frac{\eta_L^2}{R_L}\left[-\alpha_B \eta_B + 4\alpha_B^2 \frac{\eta_B^4}{4!} - 77\alpha_B^3 \frac{\eta_B^7}{7!} + 3750\alpha_B^4 \frac{\eta_B^{10}}{10!} + O(\eta_B^{13})\right], \qquad (D.31)$$

$$\frac{\partial v_B}{\partial y_B} = \frac{\eta_L^2}{R_L}\left[\alpha_B \eta_B - 4\alpha_B^2 \frac{\eta_B^4}{4!} + 77\alpha_B^3 \frac{\eta_B^7}{7!} - 3750\alpha_B^4 \frac{\eta_B^{10}}{10!} + O(\eta_B^{13})\right], \qquad (D.32)$$

The series expansion of neglected individual terms of the two dimensional Navier-Stokes equations are given by :

$$\frac{1}{R_L}\frac{\partial^2 u_B}{\partial x_B^2} = \frac{\eta_L^4}{R_L^2}\left[3\alpha_B \eta_B - 24\alpha_B^2 \frac{\eta_B^4}{4!} + 693\alpha_B^3 \frac{\eta_B^7}{7!} - 45000\alpha_B^4 \frac{\eta_B^{10}}{10!} + O(\eta_B^{13})\right], \qquad (D.33)$$

$$u_B \frac{\partial v_B}{\partial x_B} = \frac{\eta_L^3}{R_L^2}\left[-9\alpha_B^2 \frac{\eta_B^3}{3!} + 189\alpha_B^3 \frac{\eta_B^6}{6!} - 10449\alpha_B^4 \frac{\eta_B^9}{9!} + 1166373\alpha_B^5 \frac{\eta_B^{12}}{12!} + O(\eta_B^{15})\right], \qquad (D.34)$$

$$v_B \frac{\partial v_B}{\partial y_B} = \frac{\eta_L^3}{R_L^2}\left[3\alpha_B^2 \frac{\eta_B^3}{3!} - 84\alpha_B^3 \frac{\eta_B^6}{6!} + 5481\alpha_B^4 \frac{\eta_B^9}{9!} - 688896\alpha_B^5 \frac{\eta_B^{12}}{12!} + O(\eta_B^{15})\right], \qquad (D.35)$$

$$\frac{1}{R_L}\frac{\partial^2 v_B}{\partial y_B^2} = \frac{\eta_L^3}{R_L^2}\left[\alpha_B - 4\alpha_B^2 \frac{\eta_B^3}{3!} + 77\alpha_B^3 \frac{\eta_B^6}{6!} - 3750\alpha_B^4 \frac{\eta_B^9}{9!} + O(\eta_B^{12})\right], \qquad (D.36)$$

$$\frac{1}{R_L}\frac{\partial^2 v_B}{\partial x_B^2} = \frac{\eta_L^5}{R_L^4}\left[15\alpha_B \frac{\eta_B^2}{2} - 192\alpha_B^2 \frac{\eta_B^5}{5!} + 7623\alpha_B^3 \frac{\eta_B^8}{8!} - 630000\alpha_B^4 \frac{\eta_B^{11}}{11!} + O(\eta_B^{14})\right], \qquad (D.37)$$

## APPENDIX E: SOLVING THE BLOCK TRIDIAGONAL SYSTEM

The system (4.3.9) or (4.3.10) is solved by a block tridiagonal factorization procedure, which is described in this appendix.

A factorization for the matrix $\overline{A}_{(i)}$ of the form

$$\overline{A} = LU, \tag{E.1}$$

where $L = \begin{bmatrix} \alpha_{(i)}^1 & & & & & & \\ B_{(i)}^2 & \alpha_{(i)}^2 & & & & 0 & \\ & \ddots & \ddots & & & & \\ & & \ddots & \ddots & & & \\ & & & B_{(i)}^J & \alpha_{(i)}^J & & \end{bmatrix}$,

and $U = \begin{bmatrix} I & \Omega_{(i)}^1 & & & & & \\ & I & \Omega_{(i)}^2 & & & 0 & \\ & & \ddots & \ddots & & & \\ & & & \ddots & \ddots & & \\ & & & & I & \Omega_{(i)}^J & \\ & 0 & & & & \ddots & \ddots \\ & & & & & & I \end{bmatrix}$,

is employed.

In the large matrices L and U, the $I^j$ are identity matrices of 3rd order and the $\alpha^j$ and $\Omega^j$ are $3 \times 3$ matrices. Equation E.1 reduces to :

$$\alpha^1_{(i)} = A^1_{(i)}, \quad \alpha^j_{(i)}\Omega^j_{(i)} = C^j_{(i)}, \quad 1 \le j \le J-1, \tag{E.2a}$$

and

$$\alpha^j_{(i)} = A^j_{(i)} - B^j_{(i)}\Omega^{j-1}_{(i)} \quad 2 \le j \le J, \tag{E.2b}$$

when compared with matrix $\overline{A}_{(i)}$ in equation 4.3.11a.

The unknown matrices $\alpha^j_{(i)}$ and $\Omega^j_{(i)}$ can be calculated from equations E.2, i.e., $\Omega^1_{(i)}$ is obtained from E.2a and with it $\alpha^2_{(i)}$ from E.2b. Substituting $\alpha^2_{(i)}$ into E.2a, $\Omega^2_{(i)}$ can be calculated. Using $\Omega^2_{(i)}$ in E.2b yields $\alpha^3_{(i)}$ etc.. Defining

$$\Omega^j_{(i)} \equiv \begin{bmatrix} & 0 & 0 \\ \omega^j_{(i)} & 0 & 0 \\ & 0 & 0 \end{bmatrix}, \text{ and } \omega^j_{(i)} \equiv \begin{bmatrix} d^j_{(i)} \\ e^j_{(i)} \\ g^j_{(i)} \end{bmatrix},$$

equation E.2a at j = 1 can be written as :

$$\alpha^1_{(i)}\Omega^1_{(i)} = C^1_{(i)},$$

but

$$\alpha^1_{(i)} = A^1_{(i)}.$$

Therefore,

$$\begin{bmatrix} 0 & 1 & 0 \\ \beta^1_{(i)} & \theta^1_{(i)} & \beta^1_{(i)} \\ -\dfrac{h_1}{2} & 0 & -\dfrac{h_1}{2} \end{bmatrix} \begin{bmatrix} d^1_{(i)} \\ e^1_{(i)} \\ g^1_{(i)} \end{bmatrix} = \begin{bmatrix} FAC^1_{(i)} \\ \gamma^1_{(i)} \\ 1 \end{bmatrix}.$$

Solving for $d^1_{(i)}$, $e^1_{(i)}$, $g^1_{(i)}$, gives :

$$d^1_{(i)} = \frac{1}{\beta^1_{(i)} - \beta^1_{(i)}}\left(\gamma^1_{(i)} - \theta^1_{(i)} FAC^1_{(i)} + \frac{2}{h_1}\beta^1_{(i)}\right), \qquad (E.3\,a)$$

$$e^1_{(i)} = FAC^1_{(i)} \qquad (E.3\,b)$$

$$\text{and } g^1_{(i)} = -\left(\frac{2}{h_1} + d^1_{(i)}\right), \qquad (E.3\,c)$$

Defining

$$\alpha^j_{(i)} \equiv \begin{bmatrix} (\alpha_{11})^j & (\alpha_{12})^j & (\alpha_{13})^j \\ (\alpha_{21})^j & (\alpha_{22})^j & (\alpha_{23})^j \\ (\alpha_{31})^j & (\alpha_{32})^j & (\alpha_{33})^j \end{bmatrix},$$

equation E.2b can be written as

$$\begin{bmatrix} (\alpha_{11})^j & (\alpha_{12})^j & (\alpha_{13})^j \\ (\alpha_{21})^j & (\alpha_{22})^j & (\alpha_{23})^j \\ (\alpha_{31})^j & (\alpha_{32})^j & (\alpha_{33})^j \end{bmatrix} = \begin{bmatrix} FAC^j_{(i)} & 1 & 0 \\ \gamma^j_{(i)} & \theta^j_{(i)} & \beta^j_{(i)} \\ -1 & 0 & -\frac{h_j}{2} \end{bmatrix} - \begin{bmatrix} 0 & -1 & 0 \\ 0 & \theta^j_{(i)} & \beta^j_{(i)} \\ 0 & 0 & -\frac{h_j}{2} \end{bmatrix} \begin{bmatrix} d^{j-1}_{(i)} \\ e^{j-1}_{(i)} \\ g^{j-1}_{(i)} \end{bmatrix}.$$

Hence,

$$\alpha^j_{(i)} = \begin{bmatrix} e^{j-1}_{(i)} + FAC^j_{(i)} & 1 & 0 \\ \gamma^j_{(i)} - \theta^j_{(i)} e^{j-1}_{(i)} - \beta^j_{(i)} g^{j-1}_{(i)} & \theta^j_{(i)} & \beta^j_{(i)} \\ -1 + \frac{h_j}{2} g^{j-1}_{(i)} & 0 & -\frac{h_j}{2} \end{bmatrix}, \quad 2 \le j \le J.$$

$$(E.4)$$

Matrix $\Omega^j_{(i)}$ can be calculated for $j \ge 2$ from (E.2a) after obtaining $\alpha^j_{(i)}$ as above. Using (E.4) we rewrite (E.2a) as :

$$\begin{bmatrix} (\alpha_{11})^j & 1 & 0 \\ (\alpha_{21})^j & \theta^j_{(i)} & \beta^j_{(i)} \\ (\alpha_{31})^j & 0 & -\frac{h_j}{2} \end{bmatrix} \begin{bmatrix} d^j_{(i)} \\ e^j_{(i)} \\ g^j_{(i)} \end{bmatrix} = \begin{bmatrix} FAC^j_{(i)} \\ \gamma^j_{(i)} \\ 1 \end{bmatrix}.$$

Solving for $d^j_{(i)}, e^j_{(i)}$, and $g^j_{(i)}$ gives :

$$d^j_{(i)} = \frac{h_j/2(\gamma^j_{(i)} - FAC^j_{(i)}\theta^j_{(i)}) + \beta^j_{(i)}}{\Delta^j}, \qquad (E.5\,a)$$

$$e^j_{(i)} = FAC^j_{(i)} - (\alpha_{11})^j d^j_{(i)}, \quad 2 \le j \le J-1, \qquad (E.5\,b)$$

$$\text{and } g^j_{(i)} = \frac{2}{h_j}((\alpha_{31})^j d^j_{(i)} - 1), \qquad (E.5\,c)$$

where elements of $\alpha^j_{(i)}$ matrix are given in (E.4) and

$$\Delta^j \equiv \frac{h_j}{2}(\alpha_{21})^j - \frac{h_j}{2}\theta^j_{(i)}(\alpha_{11})^j + \beta^j_{(i)}(\alpha_{31})^j. \qquad (E.6)$$

To summarize the calculation of $\Omega^j_{(i)}$ and $\alpha^j_{(i)}$ matrices, we first calculate $\omega^1_{(i)}$ from (E.3), then $\alpha^j_{(i)}$ from (E.4) for j = 2, then $\omega^j_{(i)}$ from (E.5) for j = 2, etc..

The system (4.3.9) or (4.3.10) with (E.1) can be rewritten as $LU z^j_{(i)} = s^j_{(i)}$.

Let $U z^j_{(i)} = w^j_{(i)}$, which gives $L w^j_{(i)} = s^j_{(i)}$, or

$$\begin{bmatrix} \alpha_{(i)}^1 & & & & & & & \\ B_{(i)}^2 & \alpha_{(i)}^2 & & & & & 0 & \\ & \ddots & \ddots & & & & & \\ & & \ddots & \ddots & & & & \\ & & & B_{(i)}^j & \alpha_{(i)}^j & & & \\ & & & & \ddots & \ddots & & \\ & & & & & \ddots & \ddots & \\ & 0 & & & & & B_{(i)}^J & \alpha_{(i)}^J \end{bmatrix} \begin{bmatrix} w_{(i)}^1 \\ w_{(i)}^2 \\ \vdots \\ w_{(i)}^j \\ \vdots \\ w_{(i)}^J \end{bmatrix} = \begin{bmatrix} s_{(i)}^1 \\ s_{(i)}^2 \\ \vdots \\ s_{(i)}^j \\ \vdots \\ s_{(i)}^J \end{bmatrix}. \qquad (E.7)$$

From (E.7) it follows that :

$$\alpha_{(i)}^1 w_{(i)}^1 = s_{(i)}^1, \quad \alpha_{(i)}^j w_{(i)}^j = s_{(i)}^j - B_{(i)}^j w_{(i)}^{j-1} \equiv n_{(i)}^j, \quad 2 \le j \le J, \qquad (E.8)$$

where

$$n_{(i)}^j = \begin{bmatrix} (bb)_{(i)}^j \\ (nn)_{(i)}^j \\ (pp)_{(i)}^j \end{bmatrix}. \qquad (E.9)$$

Rewriting $U z_{(i)}^j = w_{(i)}^j$, as :

$$\begin{bmatrix} I & \Omega_{(i)}^1 & & & & & & \\ & I & \Omega_{(i)}^2 & & & & 0 & \\ & & \ddots & \ddots & & & & \\ & & & \ddots & \ddots & & & \\ & & & & I & \Omega_{(i)}^j & & \\ & & & & & \ddots & \ddots & \\ & & & & & & \ddots & \ddots \\ & 0 & & & & & & I \end{bmatrix} \begin{bmatrix} z_{(i)}^1 \\ z_{(i)}^2 \\ \vdots \\ z_{(i)}^j \\ \vdots \\ z_{(i)}^J \end{bmatrix} = \begin{bmatrix} w_{(i)}^1 \\ w_{(i)}^2 \\ \vdots \\ w_{(i)}^j \\ \vdots \\ w_{(i)}^J \end{bmatrix}. \qquad (E.10)$$

gives : $z_{(i)}^{J} = w_{(i)}^{J}$, and $z_{(i)}^{j} = w_{(i)}^{j} - \Omega_{(i)}^{j} z_{(i)}^{j+1}, \quad 2 \le j \le J-1.$ (*E*.11)

The components of vectors $w_{(i)}^{j}$ and $z_{(i)}^{j}$ are calculated in the following manner.

First, $w_{(i)}^{j} \equiv \begin{bmatrix} x_{(i)}^{j} \\ y_{(i)}^{j} \\ Z_{(i)}^{j} \end{bmatrix}$.

Then from (E.8) at j = 1,

$$\begin{bmatrix} 0 & 1 & 0 \\ \tilde{\beta}_{(i)}^{1} & \theta_{(i)}^{1} & \beta_{(i)}^{1} \\ -\frac{h_1}{2} & 0 & -\frac{h_1}{2} \end{bmatrix} \begin{bmatrix} x_{(i)}^{1} \\ y_{(i)}^{1} \\ Z_{(i)}^{1} \end{bmatrix} = \begin{bmatrix} m_{(i)}^{1} \\ t_{(i)}^{1} \\ l_{(i)}^{1} \end{bmatrix}.$$

Solving for $x_{(i)}^{1}$, $y_{(i)}^{1}$, $Z_{(i)}^{1}$, yields

$$x_{(i)}^{1} = \frac{t_{(i)}^{1} - \theta_{(i)}^{1} m_{(i)}^{1} + 2/h_1 l_{(i)}^{1} \beta_{(i)}^{1}}{(\tilde{\beta}_{(i)}^{1} - \beta_{(i)}^{1})}, \qquad (E.12\,a)$$

$$y_{(i)}^{1} = m_{(i)}^{1}, \qquad (E.12\,b)$$

and

$$Z_{(i)}^{1} = -\frac{2}{h_1}\left(l_{(i)}^{1} + \frac{h_1}{2} x_{(i)}^{1}\right). \qquad (E.12\,c)$$

The components of $n_{(i)}^{j}$, for $2 \le j \le J$, from (E.8) are given by :

$$(bb)_{(i)}^{j} = m_{(i)}^{j} + y_{(i)}^{j-1}, \qquad (E.13\,a)$$

$$(nn)_{(i)}^{j} = t_{(i)}^{j} - \theta_{(i)}^{j} y_{(i)}^{j-1} - \tilde{\beta}_{(i)}^{j} Z_{(i)}^{j-1}, \qquad (E.13\,b)$$

and

$$(pp)^{j}_{(i)} = l^{j}_{(i)} + \frac{h_j}{2} Z^{j-1}_{(i)}. \qquad (E.13c)$$

The quantities $x^{j}_{(i)}$, $y^{j}_{(i)}$, and $Z^{j}_{(i)}$ can be obtained for $2 \le j \le J$ from the latter part of (E.8), i.e.,

$$x^{j}_{(i)} = \frac{(h_j/2)\left((nn)^{j}_{(i)} - \theta^{j}_{(i)}(bb)^{j}_{(i)}\right) + \beta^{j}_{(i)}(pp)^{j}_{(i)}}{\Delta^{j}}, \qquad (E.14a)$$

$$y^{j}_{(i)} = (bb)^{j}_{(i)} - (\alpha_{11})^{j} x^{j}_{(i)}, \qquad (E.14b)$$

and

$$Z^{j}_{(i)} = \frac{2}{h_j}\left((\alpha_{31})^{j} x^{j}_{(i)} - (pp)^{j}_{(i)}\right). \qquad (E.14c)$$

Note that $\Delta^{j}$ is given in (E.6).

Now the components of $z^{j}_{(i)}$ defined by (4.3.11) can be calculated from (E.11).

For j = J, the components of $z^{J}_{(i)}$ are given by :

$$\delta P^{J-1}_{(i)} = x^{J}_{(i)},\ \delta\bar{Q}^{J}_{(i)} = y^{J}_{(i)},\ \text{and}\ \delta\bar{\bar{R}}^{J}_{(i)} = Z^{J}_{(i)}, \qquad (E.15)$$

For $2 \le j \le J-1$, the components of $z^{j}_{(i)}$ are given by :

$$\begin{bmatrix} \delta P^{j-1}_{(i)} \\ \delta\bar{Q}^{j}_{(i)} \\ \delta\bar{\bar{R}}^{j}_{(i)} \end{bmatrix} = \begin{bmatrix} x^{j}_{(i)} \\ y^{j}_{(i)} \\ Z^{j}_{(i)} \end{bmatrix} - \begin{bmatrix} d^{j}_{(i)} & 0 & 0 \\ e^{j}_{(i)} & 0 & 0 \\ g^{j}_{(i)} & 0 & 0 \end{bmatrix} \begin{bmatrix} \delta P^{j}_{(i)} \\ \delta\bar{Q}^{j+1}_{(i)} \\ \delta\bar{\bar{R}}^{j+1}_{(i)} \end{bmatrix},$$

or $\delta P^{j-1}_{(i)} = x^{j}_{(i)} - d^{j}_{(i)}\delta P^{j}_{(i)}$, $\delta\bar{Q}^{j}_{(i)} = y^{j}_{(i)} - e^{j}_{(i)}\delta P^{j}_{(i)}$, and $\delta\bar{\bar{R}}^{j}_{(i)} = Z^{j}_{(i)} - g^{j}_{(i)}\delta P^{j}_{(i)}$, $\qquad (E.16)$

Since, $z_{(i)}^{1} = \begin{bmatrix} \delta\overline{R}_{(i)}^{0} \\ \delta\bar{Q}_{(i)}^{1} \\ \delta\overline{R}_{(i)}^{1} \end{bmatrix}$,

then, $\delta\overline{R}_{(i)}^{0} = x_{(i)}^{1} - a_{(.)}^{'1}\delta P_{(i)}^{1}$, $\delta\bar{Q}_{(i)}^{1} = y_{(i)}^{1} - e_{(i)}^{1}\delta P_{(i)}^{1}$ and $\delta\overline{R}_{(i)}^{1} = Z_{(i)}^{1} - g_{(i)}^{1}\delta P_{(i)}^{1}$, (*E*.17)

# APPENDIX F: RICHARDSON EXTRAPOLATION

In this appendix we derive the expressions for Richardson extrapolation that apply to three numerical solutions of a two dimensional problem and two numerical solutions to a one dimensional problem. In applying the extrapolation an estimate of the asymptotic expansion of the solution is used which is in terms of the computational mesh sizes.

Richardson extrapolation or deferred approach to the limit in two dimensions requires three solutions each at a different mesh size in order to increase accuracy to the next level. Using central differences in discretization allows a leap frogging of orders of truncation errors, i.e. the truncated error terms in the series expansion go from second order to fourth order etc..

Three solutions of the form :

$$U - u_1 = Ah_1^2 + Bk_1^2 + Ch_1^4 + Dk_1^4 + O(h_1^6 + k_1^6),$$

$$U - u_2 = Ah_2^2 + Bk_2^2 + Ch_2^4 + Dk_2^4 + O(h_2^6 + k_2^6),$$

$$U - u_3 = Ah_3^2 + Bk_3^2 + Ch_3^4 + Dk_3^4 + O(h_3^6 + k_3^6), \qquad (F.1)$$

where U is the true solution, the $u_i$ are the ith numerical solutions using i different nets, and the A, B. C, and D are assumed constants of order one.

Eliminating A from equations F.1 yields :

$$h_2^2(U - u_1) - h_1^2(U - u_2) = B\beta + Ch_1^2h_2^2(h_1^2 - h_2^2) + D(h_2^2k_1^4 - h_1^2k_2^4) \qquad (F.2)$$

and

$$h_2^2(U-u_3)-h_3^2(U-u_2)=B\alpha+Ch_2^2h_3^2(h_3^2-h_2^2)+D(h_2^2k_3^4-h_3^2k_2^4), \qquad (F.3)$$

where $\alpha \equiv k_3^2h_2^2-k_2^2h_3^2$ and $\beta \equiv k_1^2h_2^2-k_2^2h_1^2$.

Eliminating B from equations F.2 and F.3 gives :

$$\{\alpha(h_2^2-h_1^2)+\beta(h_3^2-h_2^2)\}U=\alpha h_2^2u_1-\beta h_2^2u_3+(\beta h_3^2-\alpha h_1^2)u_2+Ch_2^2\{\alpha h_1^2(h_1^2-h_2^2)$$

$$-\beta h_3^2(h_3^2-h_2^2)\}+D\{\alpha(h_2^2k_1^4-h_1^2k_2^4)-\beta(h_2^2k_3^4-h_3^2k_2^4)\}. \qquad (F.4)$$

Rearranging equation F.4 establishes:

$$U=\frac{1}{k_1^2(h_3^2-h_2^2)+k_2^2(h_1^2-h_3^2)+k_3^2(h_2^2-h_1^2)}\{(k_3^2h_2^2-k_2^2h_3^2)u_1+(h_1^2k_2^2-h_2^2k_1^2)u_3$$

$$+(h_3^2k_1^2-h_1^2k_3^2)u_2+C(h_1^2h_2^2k_3^2(h_1^2-h_2^2)+h_2^2h_3^2k_1^2(h_2^2-h_3^2)+h_1^2h_3^2k_2^2(h_3^2-h_1^2))$$

$$+D(h_1^2k_2^2k_3^2(k_3^3-k_2^2)+h_2^2k_1^2k_3^2(k_1^2-k_3^2)+h_3^2k_1^2k_2^2(k_2^2-k_1^2))\}. \qquad (F.5)$$

In one dimension, two solutions are required with expansions of the form (F.1).

Neglecting $u_3$ and setting B and D to zero, equation F.2 becomes :

$$h_2^2(U-u_1)-h_1^2(U-u_2)=Ch_1^2h_2^2(h_1^2-h_2^2). \qquad (F.6)$$

Rearranging (F.6) yields :

$$U=\frac{1}{h_2^2-h_1^2}(h_2^2u_1-h_1^2u_2-Ch_1^2h_2^2). \qquad (F.7)$$

# APPENDIX G: SOME SERIES EXPANSIONS USED IN DISCRETIZATION

In this appendix we obtain the series expansions of $\bar{Q}$ about $(\eta_1'^{-1/2}, \xi_{n-1/2})$ used for numerical discretization in Chapter 4 to obtain expression 4.2.15.

The individual series expansions are given by :

$$\bar{Q}_n' = \bar{Q}_{n-1/2}^{J-1/2} + \frac{h_J}{2}\bar{Q}_{\eta_1} + \frac{k_n}{2}\bar{Q}_{\xi} + \frac{h_J^2}{8}\bar{Q}_{\eta_1\eta_1} + \frac{h_J k_n}{4}\bar{Q}_{\eta_1\xi} + \frac{k_n^2}{8}\bar{Q}_{\xi\xi} + \frac{h_J^3}{48}\bar{Q}_{\eta_1\eta_1\eta_1} + \frac{h_J^2 k_n}{24}\bar{Q}_{\eta_1\eta_1\xi}$$

$$+\frac{h_J k_n^2}{24}\bar{Q}_{\eta_1\xi\xi} + \frac{k_n^3}{48}\bar{Q}_{\xi\xi\xi} + \frac{h_J^4}{384}\bar{Q}_{\eta_1\eta_1\eta_1\eta_1} + \frac{h_J^3 k_n}{96}\bar{Q}_{\eta_1\eta_1\eta_1\xi} + \frac{h_J^2 k_n^2}{64}\bar{Q}_{\eta_1\eta_1\xi\xi} + \frac{h_J k_n^3}{96}\bar{Q}_{\eta_1\xi\xi\xi} + \frac{k_n^4}{384}\bar{Q}_{\xi\xi\xi\xi},$$

$$\bar{Q}_n'^{-1} = \bar{Q}_{n-1/2}^{J-1/2} - \frac{h_J}{2}\bar{Q}_{\eta_1} + \frac{k_n}{2}\bar{Q}_{\xi} + \frac{h_J^2}{8}\bar{Q}_{\eta_1\eta_1} - \frac{h_J k_n}{4}\bar{Q}_{\eta_1\xi} + \frac{k_n^2}{8}\bar{Q}_{\xi\xi} - \frac{h_J^3}{48}\bar{Q}_{\eta_1\eta_1\eta_1} + \frac{h_J^2 k_n}{24}\bar{Q}_{\eta_1\eta_1\xi}$$

$$-\frac{h_J k_n^2}{24}\bar{Q}_{\eta_1\xi\xi} + \frac{k_n^3}{48}\bar{Q}_{\xi\xi\xi} + \frac{h_J^4}{384}\bar{Q}_{\eta_1\eta_1\eta_1\eta_1} - \frac{h_J^3 k_n}{96}\bar{Q}_{\eta_1\eta_1\eta_1\xi} + \frac{h_J^2 k_n^2}{64}\bar{Q}_{\eta_1\eta_1\xi\xi} - \frac{h_J k_n^3}{96}\bar{Q}_{\eta_1\xi\xi\xi} + \frac{k_n^4}{384}\bar{Q}_{\xi\xi\xi\xi},$$

$$\bar{Q}_{n-1}'^{-1} = \bar{Q}_{n-1/2}^{J-1/2} - \frac{h_J}{2}\bar{Q}_{\eta_1} - \frac{k_n}{2}\bar{Q}_{\xi} + \frac{h_J^2}{8}\bar{Q}_{\eta_1\eta_1} + \frac{h_J k_n}{4}\bar{Q}_{\eta_1\xi} + \frac{k_n^2}{8}\bar{Q}_{\xi\xi} - \frac{h_J^3}{48}\bar{Q}_{\eta_1\eta_1\eta_1} - \frac{h_J^2 k_n}{24}\bar{Q}_{\eta_1\eta_1\xi}$$

$$-\frac{h_J k_n^2}{24}\bar{Q}_{\eta_1\xi\xi} - \frac{k_n^3}{48}\bar{Q}_{\xi\xi\xi} + \frac{h_J^4}{384}\bar{Q}_{\eta_1\eta_1\eta_1\eta_1} + \frac{h_J^3 k_n}{96}\bar{Q}_{\eta_1\eta_1\eta_1\xi} + \frac{h_J^2 k_n^2}{64}\bar{Q}_{\eta_1\eta_1\xi\xi} + \frac{h_J k_n^3}{96}\bar{Q}_{\eta_1\xi\xi\xi} + \frac{k_n^4}{384}\bar{Q}_{\xi\xi\xi\xi},$$

and

$$\tilde{Q}^{j}_{n-1} = \tilde{Q}^{j-1/2}_{n-1/2} + \frac{h_j}{2}\tilde{Q}_{\eta_1} - \frac{k_n}{2}\tilde{Q}_{\xi} + \frac{h_j^2}{8}\tilde{Q}_{\eta_1\eta_1} - \frac{h_j k_n}{4}\tilde{Q}_{\eta_1\xi} + \frac{k_n^2}{8}\tilde{Q}_{\xi\xi} + \frac{h_j^3}{48}\tilde{Q}_{\eta_1\eta_1\eta_1} - \frac{h_j^2 k_n}{24}\tilde{Q}_{\eta_1\eta_1\xi}$$

$$+\frac{h_j k_n^2}{24}\tilde{Q}_{\eta_1\xi\xi} - \frac{k_n^3}{48}\tilde{Q}_{\xi\xi\xi} + \frac{h_j^4}{384}\tilde{Q}_{\eta_1\eta_1\eta_1\eta_1} - \frac{h_j^3 k_n}{96}\tilde{Q}_{\eta_1\eta_1\eta_1\xi} + \frac{h_j^2 k_n^2}{64}\tilde{Q}_{\eta_1\eta_1\xi\xi} - \frac{h_j k_n^3}{96}\tilde{Q}_{\eta_1\xi\xi\xi} + \frac{k_n^4}{384}\tilde{Q}_{\xi\xi\xi\xi}.$$

# REFERENCES


Abromowitz, M. and Stegun, I. (1965). Handbook of Mathematical Functions. Dover New York. 228-231.

Blottner, F. G. (1975). Computational Techniques For Boundary Layers. For AGARD Lecture Series 73 on "Computational Methods for Inviscid and Viscous Two- and Three-Dimensional Flow Fields."

Cebeci, T., Wogulis, E. R., and Partin, R. D. (1968). Effect of Transverse Curvature on Skin Friction and Heat Transfer in Laminar Flows Past Slender Circular Cylinders. J. Heat Transfer.

Cebeci, T. (1970). Laminar and Turbulent Incompressible Boundary Layers on Slender Bodies of Revolution in Axial Flow. J. Basic Eng. **92**, 545.

Cebeci, T. and Smith, A. M. O. (1974). Analysis of Turbulent Boundary Layers. Academic Press. New York.

Glauert M. B. and Lighthill M. J. (1954). The Axisymmetric Boundary Layer on a Long Thin Cylinder. Proceedings of the Royal Society, London, **230**. 189-203.

Hayes, W. D. and Probstein, R. F. (1959). Hypersonic Flow Theory. Academic Press, New York and London. 290.

Jaffe, N. A., and Okamura, T. T. (1968). The Transverse Curvature Effect of the Incompressible Boundary Layer for Longitudinal Flow Over a Cylinder. Z. Angew. Math. Phys. **19**, fasc. 4, 564.

Keller, H. B. (1975). Some Computational Problems in Boundary-Layer Flows. Proc. Int. Conf. Numer. Meth. Fluid Dyn. 4th. 1-21.

Keller, H. B. (1978). Numerical Methods in Boundary-Layer Theory. Ann. Rev. Fluid Mech. **10**. 417-433.

Keller, H. B., and Cebeci, T. (1971). Accurate Numerical Methods For Boundary Layer Flows, I: Two-Dimensional Lamainar Flows. Proc. Int. Conf. Numer. Meth. Fluid Dyn. 2nd. Berkeley, Calif. 1970. Lect. Notes in Phys. 8:92-100. Berlin: Springer 462.

Keller, H. B., and Cebeci, T. (1972a). An Inverse Problem in Boundary Layer Flows: Numerical Determination of Pressure Gradient for a Given Wall Shear. J. Comput. Phys. **10**. 151-61.

Keller, H. B., and Cebeci, T. (1972b). Accurate Numerical Methods For Boundary Layer Flows, II: Two-Dimensional Turbulent Flows. AIAA J. **10**. 1193-99

Kelly H. R. (1954). A Note on the Laminar Boundary Layer on a Circular Cylinder in Axial Incompressible Flow. J. Aero. Sci., **21**, 634.

Lees, L , (1956). Laminar Heat Transfer Over Blunt-Nosed Bodies at Hypersonic Flight Speeds. Jet Propulsion, **26** No. 4, 259-269.

Prandtl, L., (1904). UberFlussigkeitsbe wegung bei sehr kleiner Reibung. Proc. Third Intern. Math. Congress, Heidelberg. 484-491

Probstein, R. F., and Elliott, D. (1956). The Transverse Curvature Effect in Compressible Axially Symmetric Laminar Boundary-Layer Flow. Journal of the Aeronautical Sciences, 208-223.

Rosenhead L. (1963). Laminar Boundary Layers. The Clarendon Press. 446-452.

Sawchuk, S. P., (1985). Boundary Layer on a Circular Cylinder in Axial Flow. M. Sc. Thesis, University of Western Ontario. 21-28

Seban , R. A. and Bond, R. (1952). Skin Friction and Heat Transfer Characteristics of a Laminar Boundary Layer on a Circular Cylinder in Axial Incompressible Flow. J. Aero. Sci. **18**, 671-675.

Sowerby L. and Cooke, J.C., 1953. The Flow of Fluid Along Corners and Edges. Quart. J. Mech. Appl. Math. **6**, 53-54.

Stewartson K., (1955). The Asymptotic Boundary Layer On a Circular Cylinder in Axial Incompressible Flow. Quart. Appl. Math. **8**, 113-122.

Weyl, H., (1942). On the differential equations of the simplest boundary layer problems. Ann. Math. **43**, 381-407.